



**HAL**  
open science

# Couplage entre tomographies hydrauliques et mesures hydrodynamique pour la caractérisation du champ de perméabilité de réservoirs géologiques hétérogènes : mise en œuvre en contexte sédimentaire côtier.

Mohammed Aliouache

## ► To cite this version:

Mohammed Aliouache. Couplage entre tomographies hydrauliques et mesures hydrodynamique pour la caractérisation du champ de perméabilité de réservoirs géologiques hétérogènes : mise en œuvre en contexte sédimentaire côtier.. Autre. Université Montpellier, 2021. Français. NNT : 2021MONTG092 . tel-03615691

**HAL Id: tel-03615691**

**<https://theses.hal.science/tel-03615691>**

Submitted on 21 Mar 2022

**HAL** is a multi-disciplinary open access archive for the deposit and dissemination of scientific research documents, whether they are published or not. The documents may come from teaching and research institutions in France or abroad, or from public or private research centers.

L'archive ouverte pluridisciplinaire **HAL**, est destinée au dépôt et à la diffusion de documents scientifiques de niveau recherche, publiés ou non, émanant des établissements d'enseignement et de recherche français ou étrangers, des laboratoires publics ou privés.

# THÈSE POUR OBTENIR LE GRADE DE DOCTEUR DE L'UNIVERSITÉ DE MONTPELLIER

École doctorale GAIA (N°584)

Filière Sciences de la Terre et de l'Eau

Unité de recherche HydroSciences Montpellier (HSM), UMR 5151 UM-CNRS-IRD

**Couplage entre tomographies hydrauliques et mesures hydrodynamiques pour la caractérisation du champ de perméabilité de réservoirs géologiques hétérogènes.  
Mise en œuvre en contexte sédimentaire côtier.**

Présentée par Mohammed ALIOUACHE

Le 17 Décembre 2021

Devant le jury composé de

Philippe RENARD, Professeur, Université de Neuchâtel, Suisse

Abderrahim JARDANI, Maitre de conférences HDR, Université de Rouen Normandie, France

Christian LEDUC, Directeur de recherche, Institut de Recherche pour le Développement, France

Véronique LEONARDI, Maitre de conférences, Université de Montpellier, France

Xiaoguang WANG, Professeur, Université de Technologie de Chengdu, Chine

Hervé JOURDE, Professeur, Université de Montpellier, France

Jean-Louis LESUEUR, Ingénieur, TotalEnergies CSTJF-PAU, France

Gerard MASSONNAT, Ingénieur, TotalEnergies CSTJF-PAU, France

Rapporteur

Rapporteur

Président du jury

Examinatrice

Examineur

Directeur de thèse

Invité

Invité



UNIVERSITÉ  
DE MONTPELLIER



Coupling hydraulic tomography with hydrodynamic measurements  
for the characterization of the permeability field of heterogeneous  
geological reservoirs.  
Application to coastal sedimentary deposits.

by

**Mohammed ALIOUACHE**

Thesis manuscript for the obtention of the Doctor of Philosophy (PhD) degree in the specialty  
**Water and Earth Sciences**

Thesis prepared at Université de Montpellier

2021



## ABSTRACT

The permeability of sedimentary rocks can be estimated in situ through hydraulic tests allowing access to an equivalent permeability of the investigated medium. However, this permeability can locally exhibit significant differences due to heterogeneity and the scale of investigation associated with the tests.

This PhD proposes a methodology for a spatial characterization of the permeability field of sedimentary rocks. It is based on the development of numerical models through hydraulic tomography integrating geological, geophysical, petrophysical and hydraulic data acquired at different scales. These models aim to image the spatial distribution of hydrodynamic properties, constrained by the distribution of sedimentary facies at the scale of the geological reservoir.

The proposed approach is firstly tested on synthetic models in order to assess their performance and limitations, then applied to an experimental site, located in coastal sediments. The drawdown data of pumping tests, that provide information about the horizontal distribution of hydraulic properties, are considered together with flux measurements in boreholes that provide information about the vertical distribution in order to estimate the permeability field in 3D. The results obtained are compared with petrophysical measurements (permeability and porosity) carried out on the various cored wells of the experimental site. The good match between the models and the field measurements validates the proposed approach as an efficient and economical way to characterize the permeability field in 3D.

Hydraulic tomography applications using transient hydrodynamic responses showed numerical instabilities. In fact, the inverse modelling approach can suffer from ill-posedness and non-uniqueness of the solution. A study investigating these instabilities is carried out using different approaches which show that the late time hydraulic responses are not only controlled by the boundary conditions of the system but also by the surrounding heterogeneities. A more numerically stable inversion method integrating heterogeneities at different resolutions is thus proposed.



## RESUME

La perméabilité des milieux matriciels sédimentaires peut être estimée in situ par l'intermédiaire d'essais hydrauliques permettant d'accéder à une perméabilité équivalente du milieu investigué. Cette perméabilité peut localement présenter des différences importantes du fait de l'hétérogénéité du milieu et de l'échelle d'investigation associée aux essais.

Le présent travail de doctorat propose une méthodologie de caractérisation spatiale du champ de perméabilité en contexte sédimentaire, basée sur la mise en place de modèles numériques par tomographies hydrauliques intégrant des données géologiques, géophysiques, pétrophysiques et hydrauliques, acquises à différentes échelles spatio-temporelles. Ces modèles visent in fine à imager la distribution spatiale des propriétés hydrodynamiques, contrainte par la distribution des faciès sédimentaires à l'échelle du réservoir géologique.

L'approche proposée est tout d'abord mise en œuvre sur des modèles synthétiques afin d'en apprécier les performances et les limites, puis appliquée à un site expérimental, situé en contexte de plate-forme carbonatée. Les données de rabattements acquises lors d'essais de pompages, renseignent sur l'organisation horizontale du champ de perméabilité. Elles sont complétées par des mesures de débitmètre le long des forages qui permettent de préciser la distribution verticale des perméabilités. Les résultats obtenus sont comparés aux mesures des propriétés pétrophysiques réalisées sur les différents puits carottés du site expérimental. La bonne adéquation entre les modèles et les mesures de terrain valide l'approche proposée comme un moyen efficace et économique pour caractériser le champ de perméabilités en 3D.

L'application de cette approche à des réponses hydrodynamiques en domaine transitoire s'accompagne d'instabilités numériques du problème inverse, l'inversion étant assujettie à des problématiques de non-unicité de solution. Une étude investiguant ces instabilités est réalisée au moyen de différentes approches qui montrent que les réponses hydrauliques pour les temps longs sont contrôlées par les conditions aux limites du système mais également par l'hétérogénéité à méso-échelle, et notamment la géométrie des dunes carbonatées. Une méthode d'inversion plus stable sur le plan numérique et intégrant l'hétérogénéité à différentes échelles est ainsi proposée.



## ACKNOWLEDGEMENTS

Firstly, I would like to thank my supervisor, Hervé Jourde that took me as a PhD student and gave me the chance to achieve this work. I thank him for his big support and guidance during the last three years. I also want to thank him for providing anything that made this thesis take place in the best conditions. As well as the trust he put on me. I would also like to thank Xiaoguang Wang for introducing me into the world of research and for his guidance.

I would also like to thank “TotalEnergies” and “Occitanie Region” for providing the funding for this PhD and made it possible. I also want to thank the colleagues from TotalEnergies for providing valuable expertise.

Many thanks to all the laboratory staff that know how to keep positive energy around the lab and thanks to the different PhD students and interns that were involved in the team. They surely were of a big help in one way or another. Also, many thanks to the field team in the lab that responded positively to all demands and prepared the necessary material for the field trips that allowed to acquire data that is very valuable for the achievement of the different studies during this thesis. Thanks also to the administrative team of the laboratory that provide all necessary material for better environment.

I would like to thank my parents and all my family for all the support that they gave me for my whole life. Thanks to all my friends that show support whenever needed.

I would also like to thank all the jury members that accepted to read my manuscript and attended my presentation in order to give beneficial feedback for future perspectives. It will surely help me a lot in the future that awaits me.



# TABLE OF CONTENT

<b>Résumé étendu de la thèse .....</b>	<b>1</b>
<i>Objectif de la thèse .....</i>	<i>4</i>
<i>Organisation de la thèse .....</i>	<i>7</i>
<i>Résultats Principaux.....</i>	<i>8</i>
<i>Conclusion et perspectives .....</i>	<i>10</i>
<i>Références.....</i>	<i>12</i>
<b>1. Heterogeneity of aquifers and reservoirs .....</b>	<b>13</b>
<i>1.1 Aquifers and depositional environments.....</i>	<i>16</i>
1.1.1 Continental deposits .....	17
1.1.2 Transitional environments .....	18
1.1.3 Marine environments.....	19
<i>1.2 Carbonate rocks .....</i>	<i>19</i>
1.2.1 Classification of carbonate rocks.....	20
1.2.1.1 Classification according to rock fabrics and pore size and shape.....	20
1.2.1.2 Classification according to the age of carbonate rocks .....	21
1.2.2 Carbonate facies and depositional environments.....	22
1.2.2.1 Basin and deep water deposits .....	22
1.2.2.2 Reefs and organic buildups.....	23
1.2.2.3 Sand bodies and shoals .....	26
1.2.2.4 Lagoons and tidal flats.....	28
1.2.3 Types of carbonate platforms .....	30
1.2.4 Diagenesis of carbonate rocks.....	32
1.2.4.1 Dolomitization .....	33
1.2.4.2 Dissolution and Karstification .....	34
1.2.4.3 Cementation and compaction .....	34
<i>1.3 Siliciclastic rocks .....</i>	<i>35</i>
1.3.1 Classification of siliciclastic rocks .....	35
1.3.2 Depositional environments of siliciclastic rocks.....	37
1.3.2.1 Fluvial Systems: .....	37
Meandering river facies.....	41
Braided-stream facies .....	41
Straight river .....	42
Anastomosing rivers .....	42
1.3.2.2 Alluvial fans systems.....	43
1.3.2.3 Deltas.....	43
<i>1.4 Sequence stratigraphy .....</i>	<i>45</i>

1.5 Influence of geological structure and processes.....	48
1.5.1 Fractures .....	49
1.5.2 Faults.....	49
1.5.3 Folds.....	51
1.5.4 Dissolution and karst systems.....	52
1.6 Geological heterogeneities and flow .....	53
1.6.1 Importance of the scale .....	53
1.6.2 Heterogeneity .....	54
1.6.3 Anisotropy.....	54
1.6.4 Connectivity .....	55
References .....	56
<b>2. Experimental site and data (mollusc shell limestone context).....</b>	<b>59</b>
2.1 Experimental site in mollusc shell limestones context (Font d'Armand).....	62
2.3.1 Localization and set up .....	62
2.3.2 Geological history of study area .....	63
2.2 Available data of the experimental site.....	68
2.2.1 Large scale .....	70
2.2.1.1 Regional model of the valley.....	70
2.2.1.2 Electrical Resistivity profiles.....	72
2.2.2 Medium scale.....	73
2.2.2.1 Pumping tests.....	74
2.2.2.2 Slug tests .....	75
2.2.2.3 Geo-Radar .....	76
2.2.3 Small scale.....	78
2.2.3.1 Cores and laboratory measurements.....	78
2.2.3.2 Well loggings .....	78
2.2.3.3 Flowmeter survey .....	80
2.2.3.4 Petrography .....	81
2.2.3.5 CT-Scan.....	82
2.3 Numerical modelling.....	83
2.4 Conclusion.....	84
References .....	85
<b>3. State of the art of techniques for the hydraulic characterization and modelling of aquifers and reservoirs</b>	<b>89</b>
3.1 Groundwater hydraulic basics .....	92
3.1.1 Simplified classification of hydraulic aquifers.....	92
3.1.2 Aquifer hydraulic properties.....	94
3.1.2.1 Porosity .....	94
3.1.2.2 Permeability .....	95

3.1.2.3 Hydraulic conductivity .....	95
3.1.2.4 Transmissivity .....	96
3.1.2.5 Storage coefficients .....	96
3.1.3 Darcy's law .....	97
3.2 Heterogeneity of aquifers and scale of investigation.....	97
3.3 In-situ evaluation techniques of aquifer hydraulic properties.....	100
3.3.1 Indirect estimation of hydraulic conductivity .....	102
3.3.2 Tiny/Mini permeameter measurements .....	103
3.3.3 Well cuttings and coring.....	105
3.3.4 Well logging.....	106
3.3.5 Flowmeter measurements .....	107
3.3.5.1 Spinner flowmeter.....	107
3.3.6 Pumping tests.....	109
3.3.7 Slug tests .....	110
3.3.8 Packer tests .....	111
3.4 Tools and models for the interpretation of hydraulic data and estimation of hydraulic properties .....	112
3.4.1 Estimation of effective hydraulic properties.....	112
3.4.2 Analytical methods for the interpretation of hydraulic tests.....	114
3.4.2.1 Thiem model.....	115
3.4.2.2 Theis equation .....	115
3.4.2.3 Cooper-Jacob solution .....	117
3.4.2.4 Partially penetrating wells.....	119
3.4.2.5 Hantush-Walton method for leaky aquifers.....	120
3.4.2.6 Neuman method for unconfined aquifers.....	121
3.4.3 Pressure transient and pressure derivative analysis .....	123
3.4.4 Inverse Modeling approach.....	125
3.4.5.1 Classification .....	126
3.4.5.2 Inverse modelling and hydrology .....	127
3.4.5.3 Hydraulic tomography .....	130
Background .....	130
Forward model .....	134
Sensitivity (Jacobean) matrix.....	134
Covariance matrix.....	135
Quasi Linear Geostatistical Approach.....	136
Successive linear estimator .....	138
Principal component geostatistical approach .....	140
Reduced order successive linear estimator .....	143
Synthetic example .....	146
Flexibility of HT to incorporate geological data .....	146
3.4.5 Review of analytical and numerical methods for anisotropy characterization of hydraulic properties	148
3.4.5.1 Abstract .....	150
3.4.5.2 Introduction.....	150

3.4.5.3 Methods.....	154
Papadopulos (1965): .....	155
Distance drawdown analysis .....	156
Spatial moments analysis .....	156
Graphical and Wang et al. methods.....	157
3.4.5.4 Results and discussion.....	158
3.4.5.5 Conclusion.....	165
<i>References</i> .....	166
<b>4. An inverse approach integrating flowmeter and pumping test data for three dimensional aquifer characterization.....</b>	<b>183</b>
4.1 Abstract .....	188
4.2 Introduction .....	188
4.3 Methodology .....	190
4.3.1 Groundwater flow model .....	191
4.3.2 Flowmeter analysis .....	192
4.3.3 Principal component geostatistical approach.....	194
4.3.4 Prior information .....	196
4.4 Validation of concept.....	197
4.4.1 2D synthetic case .....	197
4.4.2 3D synthetic case .....	201
4.5 Application.....	206
4.5.1 Flowmeter implementation and analysis .....	207
4.5.2 Pumping tests data .....	207
4.5.3 Hydraulic tomography .....	207
4.6 Discussion .....	209
4.7 Summary and conclusions .....	212
<i>References</i> .....	213
<i>Appendix</i> .....	218
<b>5. Hydraulic tomography considering regional heterogeneities through late time pumping tests data .....</b>	<b>225</b>
5.1 Abstract .....	230
5.2 Introduction .....	230
5.3 Methodology .....	232
5.3.1 Groundwater flow equations.....	233
5.3.2 Forward model description.....	234
5.3.3 Inverse model description .....	234
5.3.4 Model setup and input parameters .....	235
5.4 Results and discussion .....	237

5.4.1 Inversion using a buffer zone (Inversion 1, 2 and 3) .....	237
5.4.1.1 Use of a buffer area to reduce the effect of the boundary conditions .....	237
5.4.1.2 Use of early part of drawdown curve only .....	238
5.4.1.3 Hydraulic property of the buffer area is added as an unknown to HT .....	239
5.4.2 Multi-level grid inversion (Inversion 4 and 5) .....	240
5.4.2.1 Synthetic case .....	241
5.4.2.2 Application to real field data .....	242
5.4.2.3 Prediction .....	245
5.4.3 Comparison of different solutions .....	247
<i>5.5 Summary and conclusions</i> .....	249
<i>References</i> .....	251
<b>Conclusion</b> .....	<b>257</b>



## LIST OF FIGURES

<b>Figure 01:</b> Distribution des réserves d'eau dans le monde et l'origine de l'eau douce (d'après U.S. Geological Survey, 1993). .....	2
<b>Figure 02:</b> Workflow général de la technique d'inversion utilisée dans ce manuscrit pour les applications de la tomographie hydrauliques. ....	6
<b>Figure 1.1:</b> Main depositional environments. (from Wikipedia commons). ....	17
<b>Figure 1.2:</b> Carbonates classification according to rock texture and fabrics: Left) Folk's 1959, right) Dunham 1962. ....	21
<b>Figure 1.3:</b> Reef environments and its equivalent facies. ....	24
<b>Figure 1.4:</b> Types of reefs according to water agitation form quiet to rough waters. (Maliva 2016). ....	25
<b>Figure 1.5:</b> Classification of main organic reefs and carbonate mud mounds and its link to the main processes and structural support. ....	26
<b>Figure 1.6:</b> Sand shoals' environments and the main observed facies. ....	27
<b>Figure 1.7:</b> Lagoonal and tidal flat environments and its main equivalent facies. ....	29
<b>Figure 1.8:</b> Lagoonal environment and its main deposits showing the type of grains (Nichols 2013). ....	30
<b>Figure 1.9:</b> classification of carbonate platforms and the types of produced sediments (Pomar, 2001). ....	32
<b>Figure 1.10:</b> Sandstones classification (Dott 1964). ....	36
<b>Figure 1.11:</b> Sandstones classification (Folk 1974). ....	37
<b>Figure 1.12:</b> Classification of channels (Makaske 2001). ....	39
<b>Figure 1.13:</b> The major architectural elements (After Miall 1985). ....	40
<b>Figure 1.14:</b> Meandering river facies (Selly, 2000). ....	41
<b>Figure 1.15:</b> Braided stream facies (Selly, 2000). ....	42
<b>Figure 1.16:</b> Alluvial-fan cross section (After Rust and Koster 1984). ....	43
<b>Figure 1.17:</b> (a,c) wave dominated deltas, (b) river dominated delta, (d) tide dominated delta (Nichols, 2009). ....	44
<b>Figure 1.18:</b> Three basic styles of basin-filling and their resultant bedding geometries and vertical textural sequences. (Galloway and Hobday, 1983). ....	46
<b>Figure 1.19:</b> Schematic time-distance diagram illustrating the temporal and spatial relationships of a depositional episode and the phases of its component depositional events (Frazier, 1974). ....	47
<b>Figure 1.20:</b> Basic sequence stratigraphy diagram. A) Lowstand system tract (LST) offlaps on the sequence boundary. B) Transgressive system tract (TST) onlaps the sequence boundary. Its upper boundary is the maximum flooding surface (MFS), which is the surface of deposition at its maximum landward position (i.e., time of maximum transgression). C) Highstand systems tract (HST) marks return of progradation with the offlap of strata on the MFS (Maliva 2016). ....	48
<b>Figure 1.21:</b> Example of a highly fractured rock showing two fractures sets (from shutterstock.com). ....	49
<b>Figure 1.22:</b> Different types of faults. ....	50
<b>Figure 1.23:</b> Some physical properties of fault zones related to their structure (damage zone and fault core). (a) Single fault core and (b) multiple fault core, which illustrates the resulting complexity in characterizing the resultant properties (Faulkner 2010). ....	51

<b>Figure 1.24:</b> Example of a fold forming a syncline in Interstate 68 road cut in Sideling Hill in western Maryland (Wikipedia commons).....	52
<b>Figure 1.25:</b> Conceptual model of a karst system including all characteristic karst processes; dark green and red dashed lines represent the soil/epikarst and the groundwater subsystems (Hartmann et al. 2014).....	53
<b>Figure 2.1:</b> Geolocalization of the study area. A) Geo-relief map of France (from world maps online). B) zoom in of Montpellier region (from google maps). C) geological map showing the study area and its position compared to the city of Montpellier (from Infoterre; m: Miocene). .....	62
<b>Figure 2.2:</b> Localization of the experimental site in the Castries incised valley (geological map from infoterre; m:Miocene) and the distribution of the wells on top of a satellite view (google maps). The red circles refer to a fully cored wells. PZ0 to PC12 are drilled during the first phase. PZ13 to PC16 are drilled during the second phase. ....	63
<b>Figure 2.3:</b> Paleo-geographic map of the Miocene Rhodano-Provencal Basin showing the upper Burdigalian sea and the different documented incised valley of the area (from Rubino et al. 1990). ..	64
<b>Figure 2.4:</b> paleo-geographic map of the gulf of lion at lower Burdigalian period (Seranne, 2012). 65	
<b>Figure 2.5:</b> Distribution of A) energy types, B) morphological elements in plan view, and C) sedimentary facies in longitudinal section within an idealized tide-dominated estuary. URF = upper flow regime; M.H.T. = mean high tide. The section in C is taken along the axis of the channel and does not show the marginal mudflat and salt marsh facies; it illustrates the onset of progradation following transgression, the full extent of which is not shown (from Dalrymple et al. 1992). ....	66
<b>Figure 2.6:</b> Schematic section along the axis of a tide-dominated estuary, showing the distribution of litho-facies resulting from transgression of the estuary, followed by estuary filling and progradation of sand bars or tidal flats. The amount of the transgressive succession preserved depends on the relative rates of sea-level rise and head-ward translation of the thalweg or the tidal channels (after Dalrymple, 1992).....	67
<b>Figure 2.7:</b> Geological map of Castries incised valley (modified from BERGA Sud) with the localization of the experimental site. ....	71
<b>Figure 2.8:</b> Regional facies model of Castries incised valley; It is built based on the available well logs in the area provided by BRGM and Berga Sud. ....	72
<b>Figure 2.9:</b> A) Localization of the electrical resistivity profiles, B) Example of electrical resistivity dipole-dipole result from profile 1 (P. BRUNET). ....	73
<b>Figure 2.10:</b> Conceptual facies model of the experimental site (conceptualized based on the observations on the cored wells of the site).....	74
<b>Figure 2.11:</b> Drawdown response of different observation wells to a constant-rate pumping test performed in PC6.....	74
<b>Figure 2.12:</b> Hydrodynamic behavior of the aquifer in the experimental site. a) fitting the drawdown curve of pumping in PC6 to the theoretical Theis type curve. b) Plot of pressure transient derivative using drawdown response of PC6 to pumping in the same well (black) and equivalent drawdown response converted from PC6 slug test using Peres et al. method (red) (X. WANG). ....	75
<b>Figure 2.13:</b> Drawdown response of different wells to a slug test performed in PZ3.....	76
<b>Figure 2.14:</b> A) localization of the four transects of georadar. B) Example of results from transect n°4 at 250MHz. C) Example of results from transect n°4 at 100MHz (D. ROUSSET and G. SENECHAL). ....	77

<b>Figure 2.15:</b> Tiny-Perm measurements log in wells PC8, PC6, PC15 and PC16, and the corresponding litho-facies models. ....	78
<b>Figure 2.16:</b> List of the performed logs in each borehole. The measurements displayed in this figure as an example are obtained from well PC12. ....	80
<b>Figure 2.17:</b> Example of flowmeter data and its conversion into hydraulic conductivity gathered from the flowmeter survey of the experimental site (the method used for the interpretation of flowmeter tests is detailed in chapter 3 and Chapter 4 of the thesis). ....	81
<b>Figure 2.18:</b> Thin slices petrography from the core of PC12 at different depth. ....	82
<b>Figure 2.19:</b> Extract of X-Ray imaging of PC12 at different depths. A) at depth=25m with fine sediments. B) at depth=15m which corresponds to the main permeable layer of the aquifer. ....	83
<b>Figure 2.20:</b> Different numerical modelling approaches to investigate the highly heterogeneous behavior of the studied aquifer. A) A 2D depth averaged model. B) A 2D vertical cross section. C) a 3D model. ....	84
<b>Figure 3.1:</b> Conceptual diagram of the main aquifer types and the relationship of their piezometric surface level and the water table. The potentiometric surface of semiconfined and confined aquifers may be positioned alternatively below the water table, particularly where the aquifers are heavily exploited (from Maliva 2016). ....	93
<b>Figure 3.2:</b> Approximate scale (radius of investigated volume) of techniques used to measure hydraulic conductivity (from Maliva 2016) ....	102
<b>Figure 3.3:</b> Principles of permeability measurements on plug samples: (A) Hassler cell, (B) mini-permeameter using air injection, and (C) mini-permeameter applying a vacuum. Note the difference in rock volume and flow trajectories in (A), (B), (C). Likewise, the difference in rock volume needs to be considered when conducting outcrop measurements = unconfined rock volume (D) (Filomena et al. 2014). ....	104
<b>Figure 3.4:</b> Flowmeter setup scheme with an interpretation example. $Q_{cum}$ is the cumulative flow rate and $K_{rel}$ is the interpreted relative permeability from flow log (Aliouache et al. 2021). ....	109
<b>Figure 3.5:</b> Typical well configuration for pumping test in non-leaky confined aquifer (from AQT SOLV). ....	110
<b>Figure 3.6:</b> Slug test set up (from Fileccia, 2015). ....	111
<b>Figure 3.7:</b> Conceptual diagram of a straddle-packer and single-packer test. ....	112
<b>Figure 3.8:</b> Example of match point method. Black dots on a black grid represent the time drawdown plot, the data are from a hydraulic pumping test. The red curve on a red grid is the Theis type curve (from Maliva 2016). ....	117
<b>Figure 3.9:</b> Application example of the Cooper and Jacob (1946) solution, (from AQT SOLV). Blue line is the matched straight line; its slope and intersection with time axis are used to estimate the effective transmissivity $T$ and the storage coefficient $S$ of the tested aquifer. ....	118
<b>Figure 3.10:</b> fully vs Partially penetrating wells. ....	119
<b>Figure 3.11:</b> Application example using Hantush–Walton curve match for pumping test data. ....	121
<b>Figure 3.12:</b> Neuman (1975) delayed-yield type curves, which consists of early and late Theis curves (red) and a series of b curves (blue). ....	123
<b>Figure 3.13:</b> typical drawdown behaviors – pressure transient interpretations (Renard, 2005). ....	124
<b>Figure 3.14:</b> Summary of published theoretical flow regimes and their associated flow dimensions, $n$ (from Ferroud et al. 2019 modified from Ehlig-Economides et al. 1994). ....	125

**Figure 3.15:** Main criteria for the classification of inverse modelling methods. Other secondary criteria can be added to the chart (preserve the prior structure or not, real time integration or not, multi-Gaussian or not, integration of data...) ..... 127

**Figure 3.16:** Inversion flowchart for hydraulic tomography applications. .... 134

**Figure 3.17:** Comparison of  $HQH^T$  group calculated from finite difference method (a) and estimated using PCGA approach with different truncation numbers (b, c, d and e). .... 140

**Figure 3.18:** Principal component Geostatistical Approach workflow..... 143

**Figure 3.19:**Results of HT synthetic example. A) true transmissivity field. B) inverted transmissivity field. C) data measurements fitting; true observations versus simulated observations..... 146

**Figure 3.20:**HT results comparing between a simple hydraulic tomography and a hydraulic tomography incorporating facies data. A) true transmissivity field. B) inverted transmissivity field using a simple hydraulic tomography. C) inverted transmissivity field using the two red rectangles as known prior facies. D) and e) are a scatter plot of inverted T versus true T for the two cases respectively. 147

**Figure 3.21:** Synthetic model used in simulation. .... 154

**Figure 3.22:** Validation case for the different methods. For each method, a tensor and its values are presented. .... 159

**Figure 3.23:** Plot of different tensors at different time steps (up right of the figure, the red tensor is the true). The plots (up left and down left) are the log-log and semi-log plots respectively of drawdown data and its derivative. The plot (down right) is the evolution of the spatial variance components calculated by the spatial moment method. .... 160

**Figure 3.24:** Case for showing the sensitivity of the elliptical regression to the initial guess. .... 161

**Figure 3.25:** Results of efficiency of the methods to the direction of the tensor. (A) all the wells are inside a domain with same anisotropy. (B) the wells cover the heterogeneity..... 162

**Figure 3.26:** Results of testing the efficiency of the methods to capture the tensor transmissivity values in case of heterogeneity presence. .... 163

**Figure 3.27:**Results of the synthetic study to investigate the scale effect on the characterization of the horizontal anisotropy. A) map of the principal component of transmissivity tensor. B) map of the minor component of transmissivity tensor. C) contour plot of drawdown caused by a pumping in P5. D) estimated transmissivity tensors using different combination of wells. E) estimated transmissivity tensor using all observation wells compared the geometric mean of the tensors estimated in D). .... 164

**Figure 4.1:** Data usage scheme. Red dashes correspond to flowmeter log data and green surface corresponds to cross-hole pumping tests data. The wells are open hole and the drawdowns are sampled at the green z-level ..... 191

**Figure 4.2:** Flowmeter setup scheme with an interpretation example.  $Q_{cum}$  is the cumulative flow rate and  $K_{rel}$  is the interpreted relative permeability from flow log. .... 193

**Figure 4.3:** Two-dimensional validation case – results of HT using different prior information. a) true hydraulic conductivity, d) interpreted hydraulic conductivity from flowmeter tests, b, c, e and f are inverted hydraulic conductivities using different prior models.  $K_i$  and  $Q_i$  correspond to the initial hydraulic conductivity and initial covariance matrix respectively, g) is the constructed facies from flowmeter analyses to use in order to construct the nested covariance..... 200

**Figure 4.4:** Scatterplots of true hydraulic conductivity versus estimated hydraulic conductivity for the different cases of the two-dimensional synthetic case. c) scatter plot of true K versus interpreted K

from flowmeter. a, b, d and e are scatter plots of true K versus inverted K using different prior models. ....	201
<b>Figure 4.5:</b> Three-dimensional validation case - results of HT using different prior information; b) interpreted hydraulic conductivity from flowmeter tests, c) true hydraulic conductivity, a, d and e are inverted hydraulic conductivities using different prior models. $K_i$ and $Q_i$ correspond to the initial hydraulic conductivity and initial covariance matrix respectively. ....	203
<b>Figure 4.6:</b> Hydraulic head response to simulated pumping tests in the new added well P6. Solid red, dotted and dashed black curves correspond to the simulated drawdowns using respectively the true conductivity, the hydraulic conductivity map obtained from hydraulic tomography and the hydraulic conductivity map obtained from the hydraulic tomography conditioned by flowmeter analysis data. ....	204
<b>Figure 4.7:</b> Two-dimensional validation case – scatterplots of true hydraulic conductivity versus estimated hydraulic conductivity for the different cases of the two-dimensional synthetic case. b) scatter plot of true K versus interpreted K from flowmeter. a, c and d are scatter plots of true K versus inverted K using different prior models. ....	205
<b>Figure 4.8:</b> Experimental site composed of a multilayered system. a) geo-localization map, b) well pattern, c) log of P6 obtained from the core analysis. ....	206
<b>Figure 4.9:</b> Inverted hydraulic conductivity map and observation data fitting results from hydraulic tomography of real-case experimental site. a) inverted hydraulic conductivity map obtained from classical HT, b) inverted hydraulic conductivity map obtained from HT conditioned by flowmeter data, c) hydraulic conductivity map obtained from flowmeter interpretation, d) data fitting for classical HT results, e) data fitting for HT conditioned by flowmeter data, f) data fitting for flowmeter interpretation. ....	209
<b>Figure 4.10:</b> Hydraulic conductivity profiles for wells PC6, PC8 and PC12 of the experimental site. Red dots are laboratory measurements. Grey solid line is extracted from THT results. Black solid line is extracted from THT integrating flowmeter analysis data results. Dashed line is from flowmeter interpretation. ....	211
<b>Figure 5.1:</b> Presentation of the experimental site. a) geo-localization of the site, b) well pattern, c) example of the hydrodynamics of the site through a response to a pumping test in P6. ....	233
<b>Figure 5.2:</b> Inversion results using a fixed constant hydraulic transmissivity for the buffer domain; conditioning measurements cover early and late times of the drawdown curves. a) Inverted $\text{Log}_{10}$ Transmissivity map. b) A scatter plot of simulated versus true observation data. ....	238
<b>Figure 5.3:</b> Inversion results using a fixed constant hydraulic transmissivity for the buffer domain; no conditioning measurements were sampled in the flattened part at late times. a) contour plot of the inverted $\text{log}_{10}$ (Transmissivity) map. b) scatter plot of simulated versus true observation data. ....	239
<b>Figure 5.4:</b> Inversion results using an unknown hydraulic transmissivity value for the buffer domain; conditioning measurements cover early and late times of the drawdown curves. a) Contour plot of the inverted $\text{log}_{10}$ (Transmissivity) map. b) scatter plot of simulated versus true observation data. ....	240
<b>Figure 5.5:</b> a) Inverted domain used in the HT and distribution of the multigrid refinement cells. b) Equivalent covariance model used for HT; the covariance model is used in domains $\Omega_1$ and $\Omega_2$ while the cells in $\Omega_3$ are not correlated. ....	241

**Figure 5.6:** Synthetic case results: inversion using a multiscale local grid refinement. a) True hydraulic transmissivity field. b) Inverted hydraulic transmissivity field using 2 grid levels. c) Inverted hydraulic transmissivity field using 3 grid levels. .... 242

**Figure 5.7:** Inversion results using multilevel local grid refinement approach for one cross hole pumping test; conditioning measurements cover early and late times. a) contour plot of the inverted  $\log_{10}$ (hydraulic transmissivity) map. b) scatter plot of simulated versus true observation..... 243

**Figure 5.8:** Plot of the normalized sensitivity of the different cells in the inverted domain for the pumping test in P6. .... 244

**Figure 5.9:** Inversion results using multilevel local grid refinement approach for one cross hole pumping test; conditioning measurements cover early and late times. a) plot of the inverted  $\log_{10}$ (hydraulic transmissivity) map. b) scatter plot of simulated versus true observation..... 245

**Figure 5.10:** Prediction of drawdowns at different wells (black dashed line) using the inverted hydraulic transmissivity field from inversion 5 and its comparison to real observed drawdowns (red line). Pumping at PZ3..... 246

**Figure 5.11:** True versus predicted observations for three different pumping tests (PZ3, PZ7 and PZ9). Dashed lines represent the linear regression of the scatter, solid lines represent 1:1 lines ..... 247

**Figure 5.12:** Comparison of different inverted transmissivity fields and their potential to fit the observed drawdowns and delineate the late time behavior. .... 248

## RESUME ETENDU DE LA THESE

Plus de 97 % des ressources en eau sur Terre se trouvent dans les océans ou sous forme d'eau salée, de telle sorte que moins de 3 % de l'eau sur Terre est de l'eau douce. En fait, la majeure partie de cette eau douce est inaccessible, piégée dans les glaciers, ou difficilement accessible car souterraine et emmagasinée dans des aquifères. Environ 1,2 % de cette eau douce est considérée comme accessible car en surface, ce qui est essentiel pour répondre aux besoins de la vie. Cependant, près de 70 % de cette « eau de surface » se trouve sous forme de glaciers ou de permafrost (voir Figure 1).

Lopez-Gunn and Ramón Llamas, (2008) ont passé en revue la rareté de l'eau douce à l'échelle de la planète et ont mis en évidence l'importance de la ressource en eau souterraine pour répondre à la majeure partie des besoins en eau douce. Ils ont estimé que d'ici 2030, plus de 60 % de la population vivra dans des zones urbaines qui seront alimentées principalement par des eaux souterraines, illustrant ainsi le rôle crucial des eaux souterraines dans l'approvisionnement public en eau potable. Les eaux souterraines fournissent globalement 25 à 40 % de l'eau potable mondiale (Morris et al., 2003) et plus de la moitié de la population mondiale dépend des eaux souterraines pour son approvisionnement en eau potable (Coughanowr, 1994). En 2004 par exemple, plus de 2 milliards de personnes dépendaient des eaux souterraines pour leur approvisionnement quotidien (Kemper, 2004). A l'échelle mondiale, les

eaux souterraines sont d'une importance cruciale dans les mégapoles du monde et des centaines d'autres grandes villes à grande consommation (Foster et al., 1998).

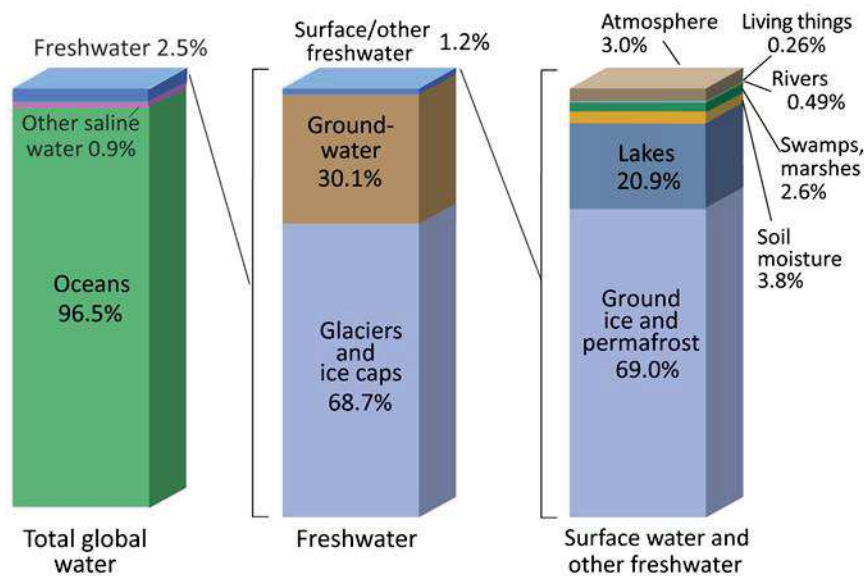


*Figure 01: Distribution des réserves d'eau dans le monde et l'origine de l'eau douce (d'après U.S. Geological Survey, 1993).*

Un aquifère (ou nappe phréatique) correspond généralement à une couche souterraine de roches perméables qui laisse facilement circuler de l'eau. Cette eau est la plupart du temps reconstituée ou rechargée par les précipitations et les eaux de surfaces qui s'infiltrent à travers le sol jusqu'à la nappe phréatique, considérée comme la fraction supérieure des eaux souterraines sous la surface du sol. Son niveau fluctue de façon saisonnière et d'année en année à mesure que les recharges et décharges varient. La profondeur de la nappe phréatique varie également selon sa localisation sur la planète, celle-ci pouvant être située à proximité de la surface terrestre dans les zones proches des plans d'eau de surface et dans les climats humides, ou à des centaines de mètres sous la surface terrestre dans les régions arides.

Les eaux souterraines se retrouvent en surface soit de manière naturelle à travers des sources, ou de manière artificielle via des puits d'exploitation. Les sources, souvent localisées là où la nappe phréatique rencontre la surface du sol, peuvent soutenir l'écoulement des cours d'eau ou encore la consommation locale des populations. Pour la production artificielle de cette eau, il est également fréquent de forer des puits qui traversent la nappe phréatique sur des profondeurs importantes afin de pomper l'eau en quantités suffisantes. Le pompage excessif des eaux souterraines peut par ailleurs entraîner un abaissement important de la nappe phréatique créant ainsi un déclin de production, localisé ou général. L'abaissement de la nappe phréatique peut aussi affecter les sources, qui passent de permanentes à temporaires ou s'assèchent parfois complètement, et par conséquent les rivières alimentées en partie

par ces eaux souterraines. La surexploitation des eaux souterraines peut être la conséquence d'études biaisées ou de l'utilisation d'un modèle de prédiction erroné ou non précis. Une petite erreur dans un modèle peut ainsi avoir des conséquences irréversibles alors qu'un modèle adapté pourra permettre d'économiser de grandes quantités d'eaux souterraines, en proposant un mode de gestion adapté.

L'exploitation de cette ressource en eau souterraine requiert par conséquent une bonne connaissance du fonctionnement hydrodynamique de la nappe phréatique, de l'aquifère, ou plus généralement du réservoir géologique contenant la ressource. Les propriétés hydrodynamiques du réservoir, telles que le champ de perméabilités (conductivités hydrauliques) et le champ de capacités de stockage (emmagasinement des roches constitutives de l'aquifère) doivent par conséquent être connues afin d'étudier la réponse du réservoir à des sollicitations diverses telles qu'une augmentation des prélèvements ou encore une modification de la recharge, au moyen de modèle numérique de simulation des écoulements. Ces propriétés hydrodynamiques sont en effet d'une importance majeure puisqu'elles contrôlent l'écoulement, mais également le transport et la migration d'éventuelles pollutions. Celles-ci peuvent être déterminées par le biais de mesures effectuées au laboratoire sur des carottes issues des forages. Néanmoins, le nombre de forages étant généralement relativement limité, ces mesures de perméabilité et porosité sur plugs (prélevés sur les carottes) ne donnent généralement qu'une information très locale sur les propriétés hydrodynamiques du réservoir géologique investigué. De ce fait, d'autres approches permettant d'estimer ces propriétés sont mises en œuvre, notamment via des mesures hydrauliques *in situ*, tels que les essais par pompages (test d'interférences), les slugs tests, ou encore la débitmétrie en forage. En effet, les réponses hydrauliques de l'aquifère sont gouvernées par les propriétés hydrauliques du réservoir géologique mais dépendent également de son hétérogénéité. Une fois les tests réalisés, différentes méthodes d'interprétation permettent de déterminer les propriétés effectives du milieu ou d'estimer la distribution spatiale de ces propriétés, notamment au moyen de « méthodes inverses ».

Un problème inverse est défini comme le processus qui, à partir d'un ensemble d'observations, permet d'identifier les différents facteurs contrôlant la variable mesurée (par exemple la charge hydraulique lorsque le problème inverse concerne les écoulements). Il comprend généralement un modèle initial, un modèle direct de simulation et un outil d'optimisation. Les problèmes inverses sont parmi les problèmes mathématiques les plus appliqués en sciences, et notamment en géosciences, car ils nous renseignent sur des paramètres que nous ne pouvons pas mesurer directement. L'inversion constitue par conséquent une étape clé pour répondre à des problématiques géophysiques ou hydrogéologiques, et plusieurs techniques d'inversion ont été développées au cours des dernières décennies pour la caractérisation des propriétés hydrodynamiques de réservoirs hétérogènes et la modélisation des écoulements souterrains.

Les étapes nécessaires pour résoudre un problème inverse peuvent être résumées comme suit (cf Figure 2):

- Acquérir les données qui dépendent du paramètre recherché
- Construire un modèle direct de simulation qui permette de simuler les données observées. Plus le modèle direct est proche du cas réel, meilleures sont les estimations du paramètre recherché (il est d'ailleurs préférable d'augmenter le coût en temps des simulations plutôt que d'augmenter le nombre d'hypothèses)
- Construire un modèle initial comprenant une information sur la distribution spatiale du paramètre recherché. Des estimations issues d'autres investigations peuvent être utilisées dans cette étape. Les propriétés hydrauliques effectives estimées au moyen de solutions analytiques peuvent par exemple être utilisées comme conditions initiales.
- Evaluer la sensibilité des inconnues sur les observations simulées (calcul de la matrice Jacobienne)
- Définir la fonction objectif à minimiser pour apprécier la différence entre données observées et simulées
- Utiliser un outil d'optimisation permettant de minimiser la fonction objectif retenue

Il est important de garder à l'esprit que les inversions sont des processus itératifs qui convergent vers une solution et s'arrêtent selon des critères définis. Il arrive donc parfois qu'une inversion ne soit pas en mesure de converger vers une solution satisfaisante.

Plusieurs méthodes ont été proposées pour résoudre le problème inverse et chaque méthode peut avoir ses propres avantages et inconvénients. L'un des avantages majeurs de l'inversion est qu'elle permet d'obtenir des solutions au problème posé, sans se soucier de la complexité ou de la non-linéarité du problème. Et, avec les progrès de l'informatique, le fardeau du temps de calcul s'estompe de plus en plus. L'inversion utilise par ailleurs des modèles numériques qui sont souvent flexibles et facilement ajustables à des cas particuliers. Un autre avantage des modèles inverses est la possibilité de fusion de différents jeux de données pour l'estimation de paramètres qui permettent de reproduire les différentes observations. Cependant, l'inversion peut aboutir à différentes solutions permettant de reproduire les observations (non unicité de la solution)

## Objectif de la thèse

L'objectif principal de la thèse est de proposer de nouvelles approches et techniques pour améliorer l'estimation du champ de perméabilité d'aquifères et réservoir sur la base de différentes données complémentaires. Ces données sont souvent associées à diverses échelles d'investigations et l'interprétation de ces données séparément peut conduire à des estimations différentes des propriétés

hydrauliques. Dans cette thèse, l'ensemble des informations obtenues à des échelles d'investigation différentes seront considérées pour l'estimation des propriétés hydrauliques du milieu, et des techniques à moindre coût tenant compte de données alternatives et complémentaires seront proposées.

Différentes méthodes inverses (e.g. Zimmerman et al., 1998, Hendricks Franssen et al., 2009, Zhou et al., 2014) sont tout d'abord passées en revue afin de comparer et d'évaluer leurs performances. Sur la base des travaux de Zhou et al. (2014), l'évolution des principales méthodes d'inversion utilisées en hydrogéologie est ensuite présentée. Parmi les méthodes inverses qui sont appliquées à l'hydrogéologie, on trouve la méthode du maximum de vraisemblance (Maximum Likelihood Estimation MLE), la méthode d'auto-calibration (Self-Calibration Method SCM), la méthode du point pilote (Pilot Points Method PiPM), Markov Chain Monte Carlo (MCMC) ou encore le Quasi-Linear Geostatistical Approach (QLGA), etc. Ces modèles inverses permettent d'estimer les propriétés hydrauliques de l'aquifère mais aussi la recharge ou encore les conditions aux limites.

Les méthodes analytiques traditionnellement utilisées pour la caractérisation des aquifères sont devenues insuffisantes car elles reposent sur des modèles conceptuels simplifiés qui ne capturent pas toute la complexité hydrogéologique du milieu investigué et ne fournissent qu'une estimation de certains paramètres effectifs. Ces méthodes analytiques sont en effet basées sur des hypothèses d'homogénéités, ce qui impliquent la considération de conditions idéales généralement non représentatives du milieu, qui peuvent par conséquent entraîner une estimation biaisée des paramètres. Par exemple, les réponses hydrodynamiques à un essai de pompage sont souvent analysées au moyen d'une solution analytique reposant sur l'hypothèse d'un milieu homogène et infini, ce qui est évidemment loin d'être vrai. La plupart des solutions analytiques supposent par exemple que l'aquifère est homogène infini, ce qui est rarement confirmé par des observations sur le terrain, et les solutions obtenues ne permettent de prédire les rabattements que sur un certain volume de l'aquifère, et de manière très approximative (Liu et al., 2007). Parmi les techniques de caractérisation alternatives, la tomographie hydraulique dispose d'un grand potentiel pour estimer les propriétés hydrauliques des aquifères à partir de réponses hydrauliques à des sollicitations diverses (Liu et al., 2007).

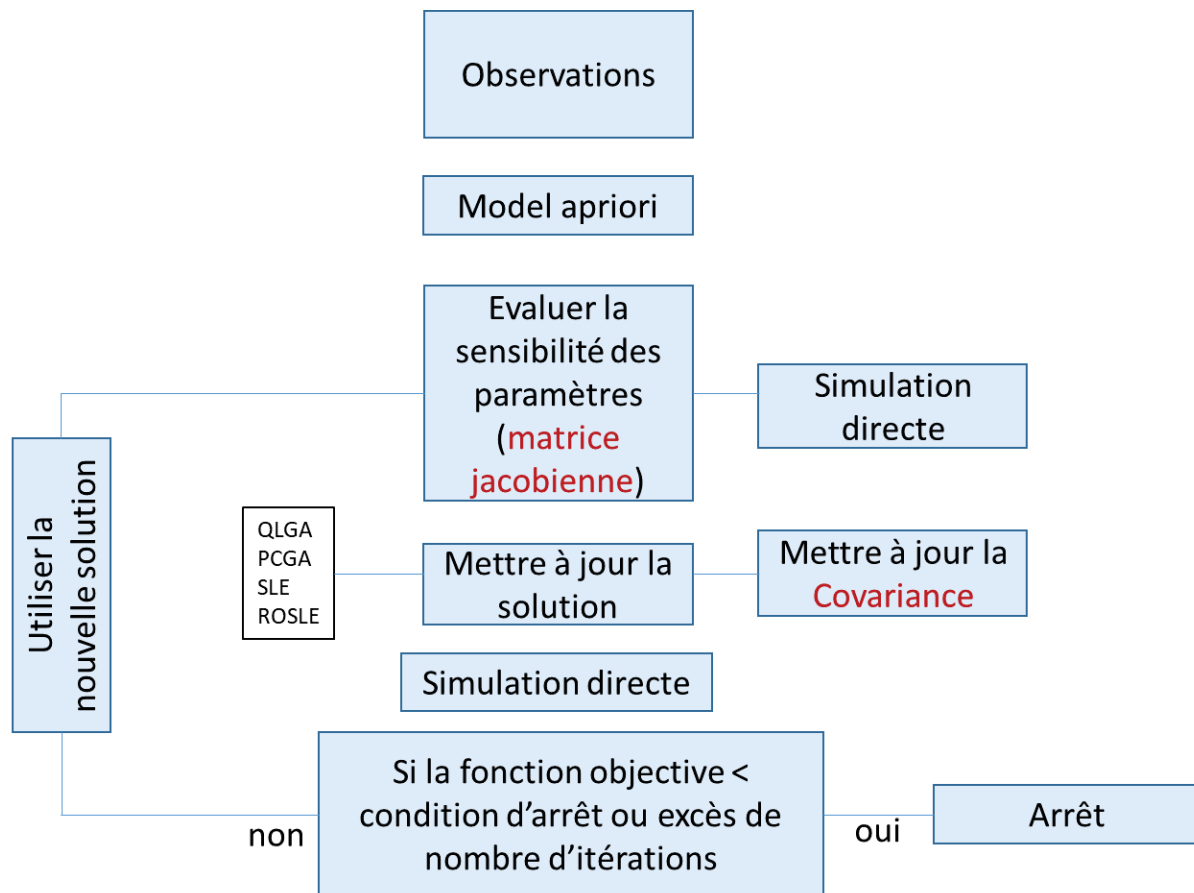


**Figure 02:** Workflow général de la technique d'inversion utilisée dans ce manuscrit pour les applications de la tomographie hydrauliques.

La tomographie hydraulique (HT) est une approche de caractérisation des aquifères qui a déjà montré son efficacité (Kitanidis 1995, Yeh et al. 1996, Yeh et Liu 2000). Elle permet de corrélérer spatialement les propriétés hydrauliques des milieux géologiques tels que conductivité hydraulique et coefficient d'emmagasinement spécifique qui sont deux paramètres importants et suffisants pour prédire correctement les écoulements et le transport de soluté. La tomographie hydraulique (HT) s'est plus particulièrement développée au cours des deux dernières décennies, au moyen de diverses techniques d'inversion. L'efficacité de la HT a été démontrée à l'échelle du laboratoire mais a également à l'échelle de sites expérimentaux au moyens de jeux de données réels. La tomographie hydraulique nécessite cependant plusieurs points d'observation à plusieurs endroits, et bien répartis, pour obtenir la distribution spatiale des propriétés hydrauliques de la zone investiguée. Les techniques d'inversion permettent d'accéder à la distribution spatiale des propriétés hydrauliques avec une résolution satisfaisante, mais l'absence d'informations *a priori* empêche parfois l'obtention d'une solution. En effet, un modèle initial mal renseigné peut avoir pour conséquence que l'inversion ne converge pas vers une solution unique, ou bien carrément diverge.

## Organisation de la thèse

Le présent manuscrit comporte 5 chapitres qui sont organisés comme suit :

- Le chapitre 1 passe en revue les différentes origines possibles de l'hétérogénéité des réservoirs géologiques, qui datent généralement des processus de sédimentation. Les sédiments, qui s'accumulent dans différents environnements de dépôts, sont en effet assujettis à différents phénomènes physiques et chimiques au cours des processus d'enfouissement ou encore de diagenèse, ce qui aboutit à l'obtention de roches sédimentaires hétérogènes et très différentes les unes des autres. Après avoir rappelé les différents environnements de dépôts, la sédimentation des carbonates et des silicates est passée en revue, et les phénomènes géologiques majeurs qui peuvent changer considérablement la structure des roches sont décrits, tout comme leurs conséquences sur l'hétérogénéité des réservoirs géologiques. Ce chapitre discute ainsi de l'importance de la reconstruction de l'histoire géologique du milieu étudié pour améliorer les modèles conceptuels, mais également apprécier les relations existantes entre propriétés géologiques (statiques) et hydrauliques (dynamiques).
- Le Chapitre 2 présente le site expérimental sur lequel les différentes approches et techniques développées dans cette thèse sont mises en œuvre. Il résume l'histoire géologique de la région et décrit les différentes données pétrophysiques, géologiques, géophysiques et hydrauliques acquises sur le site, en fonction de l'échelle d'investigation (échelle régionale, échelle du site expérimental, échelle des forages) ; ce chapitre pourra ultérieurement être valorisé sous la forme d'un 'Data Paper'.
- Le chapitre 3 propose un état de l'art des différentes techniques de caractérisation des propriétés hydrodynamiques des aquifères et réservoirs géologiques. Les différentes étapes nécessaires à cette caractérisation, basées sur la collecte de données à différentes échelles depuis la mise en place des forages jusqu'à la réalisation et l'interprétation des différents tests hydrauliques, sont ensuite abordées. Les principales méthodes d'analyses des données obtenues en réponses à différents tests hydrauliques sont présentées, notamment les méthodes analytiques qui reposent sur des hypothèses d'homogénéité, ainsi que celles qui permettent d'apprécier l'hétérogénéité du milieu. Sur la base de modèles synthétiques, les performances de 5 différentes méthodes d'estimation du tenseur de transmissivité sont ainsi comparées, et le potentiel de ces méthodes pour procéder au changement d'échelles (upscaling) des propriétés hydrauliques du milieu investigué est discuté. Finalement, des méthodes d'inversion utilisées en hydrogéologie sont présentées, avec un focus spécifique sur celles majoritairement utilisées pour l'estimation des propriétés hydrauliques au moyen de tomographies hydrauliques.
- Le chapitre 4 consiste en la mise en place de modèles numériques par tomographie hydraulique 3D intégrant des données géologiques, géophysiques, pétrophysiques et hydrauliques, acquises

sur le site expérimental à différentes échelles spatio-temporelles. Cette application intègre ainsi les données collectées à différentes échelles d'investigation et propose une solution alternative pour l'estimation de la distribution 3D du champ de perméabilité, en l'absence de données de pompages entre obturateurs (packers). Dans ce cas, les données de débitmétrie en forage, qui donnent une information sur les profils verticaux de perméabilité, viennent remplacer les données de pompages entre obturateurs (packers).

- Le chapitre 5 est une application de tomographie hydraulique en 2D à l'échelle du site expérimental. Dans ce chapitre, l'origine des instabilités associées aux différentes techniques d'inversion considérées pour réaliser une tomographie hydraulique est discutée. Il est par exemple montré que les réponses hydrodynamiques obtenues pour les temps longs peuvent être en conflit avec les conditions aux limites du modèle de simulation direct utilisé dans l'inversion. Des approches alternatives permettant de limiter ces instabilités et de stabiliser le système à inverser sont testées, et une approche constituée d'un maillage multi-niveau est finalement proposée.

## Résultats Principaux

Les modèles de faciès du site d'étude expérimental, réalisés sur la base des données géologiques et géophysiques, sont discutés au regard des solutions numériques pouvant être mises en œuvre pour l'interprétation des tomographies hydrauliques. Ces modèles, utilisés soit comme contrainte dans les techniques d'inversions, soit comme moyen de validation des résultats de ces inversions, visent *in fine* à imager la distribution spatiale des propriétés hydrodynamique du réservoir géologique.

Conventionnellement, afin de réaliser une tomographie hydraulique en 3D d'un aquifère, il est nécessaire d'être en possession de données de pompages type « packer tests » alors que les tests de pompage conventionnels contiennent une information utilisable seulement dans le cas de tomographie hydraulique en 2D. Les tests avec packers permettent en effet d'isoler différentes parties d'un forage et ainsi de réaliser différentes sollicitations hydrauliques (et mesures de pressions) suivant un profil vertical. Par contre, ce type de test est beaucoup plus coûteux qu'un simple pompage et très rarement mis en œuvre. Dans ce travail, nous explorons par conséquent le potentiel de combiner différentes données pour une caractérisation 3D de l'aquifère en l'absence de données issues de tests entre packers. Plus précisément, on propose une approche qui combine les données obtenues en réponse aux essais par pompage, à celles obtenues via les diagraphies de débit en forage, pour imager en 3D le champ de perméabilité du site investigué. Ainsi, les données de pompage fournissent des informations 2D sur les connectivités hydrauliques entre forages, tandis que les données de débitmétrie en forage contraignent la distribution des propriétés hydrauliques suivant un profil vertical 1D, au niveau des différents forages.

Afin d'améliorer les résultats de tomographie hydraulique, des données géologiques sont ensuite considérées dans l'inversion, en complément des données hydrauliques. Nous exploitons ainsi la

flexibilité offerte par chacune des techniques d'inversion pour remplacer l'information verticale pouvant être obtenue par des tests entre packers par un autre jeu de données qui donne une information équivalente. Le premier jeu de données considéré dans l'inversion correspond aux rabattements mesurés sur les différents forages lors des tests d'interférence, qui apporte des informations sur la variation latérale des propriétés hydrauliques. Le deuxième jeu de données consiste en des mesures de débit réalisés sur chacun des forages, qui renseignent la variation verticale des propriétés hydrauliques. Après avoir converti les mesures de débitmètrie en forage en profils de conductivité hydrauliques, ces profils sont interpolés afin d'obtenir une information continue dans l'espace, relative à la distribution 3D des conductivités hydrauliques, qui serve de base à la construction du modèle a priori. Ce modèle a priori, ainsi que les observations récoltées lors des essais par pompage, sont pris en compte dans l'inversion pour réaliser une tomographie hydraulique 3D de l'aquifère à l'échelle du site expérimental. La technique d'inversion utilisée pour estimer la distribution du champ de la conductivité hydraulique en 3D correspond à l'approche géostatistique en composantes principales (Principal Component Geostatistical Approach), qui permet une réduction notable des temps de calculs. L'approche PCGA est une procédure itérative déterministe qui réalise une mise à jour du paramètre recherché en faisant correspondre aux mieux les données du modèle aux données observées lors des essais par pompage afin de minimiser la fonction objectif.

L'approche proposée est validée à l'aide de deux modèles synthétiques : un modèle synthétique en 2D correspondant à une coupe transversale du milieu et un modèle synthétique en 3D. Nous l'appliquons ensuite sur des données d'un site expérimental qui ne dispose pas de tests type « packer » pour caractériser le champ de conductivité hydraulique en 3D. Les modèles synthétiques montrent bien la robustesse de la tomographie hydraulique et l'efficacité de l'approche proposée pour estimer le champ de conductivités hydrauliques en 3D. Les résultats obtenus sont confrontés aux données réelles, en considérant d'une part les prédictions des rabattements en réponse à un test hydraulique réalisé sur un forage (non considéré dans l'inversion), et d'autre part en comparant les valeurs de perméabilité estimées suivant un profil vertical à l'emplacement d'un forage, à celles mesurées sur des plugs prélevés sur le forage considéré, au moyen d'un perméamètre de laboratoire. Ces différentes comparaisons confirment la bonne adéquation entre le champ de conductivités hydrauliques estimées et les mesures de perméabilité sur carottes. La méthode proposée offre ainsi une approche efficace et peu coûteuse pour une évaluation rapide des propriétés hydrauliques en 3D et pourrait être extrapolée à d'autres applications sur le terrain.

Le passage de tests synthétiques à des applications utilisant des données d'observation est souvent accompagné d'instabilités numériques lorsque le modèle est mal posé ou qu'il manque d'informations. Ces instabilités, mentionnées à plusieurs reprises dans la littérature, sont généralement évitées ou éliminées au moyen de différentes approches (e.g. usage d'une région tampon dans les modèles, non-

usage des données acquises pour des temps longs) mais peu d'investigations relatives à l'analyse de ces instabilités ont été réalisées. Nous avons par conséquent proposé une approche permettant de limiter les instabilités d'inversion lors des applications sur des données réelles, sans pour autant éliminer les données qui peuvent être à l'origine de celles-ci. Les différentes approches utilisées montrent que les réponses hydrauliques sur les temps longs étaient contrôlées par les conditions aux limites du système mais également par la présence d'hétérogénéités à plus grande échelle (échelle régionale). Les résultats ont aussi montré que l'utilisation de différentes approches pour éliminer l'instabilité conduit à différentes solutions. Aussi, les résultats recommandent de placer les conditions aux limites du modèle loin des puits afin de retrouver la bonne stabilité du système inverse. L'approche proposée se base également sur l'éloignement des conditions aux limites et la discrétisation de la région tampon avec un raffinement graduel permettant d'éviter des temps de calculs prohibitifs. Des investigations supplémentaires ont permis de proposer une inversion, stable sur le plan numérique, et permettant également d'apprécier les propriétés hydrauliques associées aux hétérogénéités régionales.

## Conclusion et perspectives

Une méthodologie de caractérisation du champ de perméabilité en contexte sédimentaire, basée sur i) la réalisation de tomographies hydrauliques et de modèles à l'échelle des zones investiguées et ii) la prise en compte des données géologiques, géophysiques, pétrophysiques et hydrauliques, acquises à différentes échelles, a ainsi été proposée. Après avoir présenté les différents types d'hétérogénéité potentiellement présentes dans les réservoirs géologiques en fonction de l'environnement de dépôt (silicoclastique ou carbonaté) et les processus susceptibles de modifier ces hétérogénéités à l'échelle de temps géologiques, leur potentielle influence sur les écoulements souterrains a été discutée, au regard des spécificités du site expérimental situé en contexte sédimentaire côtier (calcaires coquillers) utilisé comme support à la méthodologie proposée.

Un état de l'art des différentes techniques hydrauliques permettant de caractériser l'hétérogénéité et l'anisotropie des réservoirs géologiques a ensuite été proposé avant de montrer comment la prise en compte de données complémentaires (données de pompages et données de débitmétrie en forages) dans l'interprétation des tomographies hydrauliques permettait d'aboutir à une caractérisation rapide (et à moindre coût) du champ de perméabilités en 3D.

Une approche permettant de limiter les instabilités associées aux inversions a enfin permis de montrer que les réponses hydrauliques sur les temps longs étaient contrôlées par les conditions aux limites du système mais également par la présence d'hétérogénéités à plus grande échelle (échelle régionale). Fort de ce constat, des investigations complémentaires ont permis de proposer une méthode d'inversion stable sur le plan numérique et permettant d'apprécier les propriétés hydrauliques associées aux hétérogénéités à l'échelle régionale.

A l'issue de ce travail, différentes perspectives peuvent d'ores et déjà être envisagées :

- L'intégration de différentes données mesurées à différentes échelles étant pertinente, il est recommandé de poursuivre cette démarche en intégrant d'avantage de jeu de données dans les inversions afin de construire un modèle non seulement en adéquation avec les différentes données, mais également qui présente un meilleur réalisme géologique.
- Les investigations relatives à la discrétisation des hétérogénéités, et donc à la prise en compte des modèles de faciès et de structures sédimentaires suivant leur environnement de dépôt, devront être poursuivies pour la caractérisation 3D des propriétés hydrodynamiques du milieu. L'objectif principal est d'obtenir des champs de propriétés hydrauliques qui présentent des structures similaires aux structures sédimentaires.
- Il sera également pertinent d'investiguer d'avantage l'anisotropie horizontale des propriétés des réservoirs géologiques, afin de proposer de nouvelles approches qui, en se basant sur des modèles synthétiques (pour la validation), permettront d'améliorer l'estimation des propriétés hydrodynamiques (par exemple, les tenseurs de perméabilité estimés en utilisant différentes combinaisons de réponses hydrauliques peuvent permettre de contraindre le champ de perméabilité estimé par des méthodes inverses).
- Avec l'abondance de données, l'intelligence artificielle peut constituer une piste prometteuse pour l'analyse et l'interprétation des réponses. En effet, il existe certains sites expérimentaux qui ont fait l'objet de multiple tests et interprétations. Ces sites sont souvent bien appréhendés et leurs propriétés hydrauliques sont bien estimées. Il serait par conséquent intéressant de tester des techniques, basées sur des modèles d'apprentissage sur les sites retenus, afin d'améliorer l'estimation des propriétés hydrauliques sur des sites semblables, où les données sont beaucoup plus rares.

## Références

- Coughanowr, C., 1994. Groundwater, Humid Tropics Program Series No. 8. Paris: UNESCO-IHP
- Foster, S. D., Hirata, R., & Howard, K. W. (2011). Groundwater use in developing cities: policy issues arising from current trends. *Hydrogeology Journal*, 19(2), 271-274.
- Hendricks Franssen, H. J., Alcolea, A., Riva, M., Bakr, M., Van der Wiel, N., Stauffer, F., & Guadagnini, A. (2009). A comparison of seven methods for the inverse modelling of groundwater flow. Application to the characterisation of well catchments. *Advances in Water Resources*, 32(6), 851-872.
- Kemper, K. E. (2004). Groundwater—from development to management. *Hydrogeology Journal*, 12(1), 3-5.
- Kitanidis, P. K. (1995), Quasi-Linear Geostatistical Theory for Inversing, *Water Resour. Res.*, 31( 10), 2411– 2419, doi:[10.1029/95WR01945](https://doi.org/10.1029/95WR01945).
- Liu, X., Illman, W. A., Craig, A. J., Zhu, J., and Yeh, T.-C. J. (2007), Laboratory sandbox validation of transient hydraulic tomography, *Water Resour. Res.*, 43, W05404, doi:[10.1029/2006WR005144](https://doi.org/10.1029/2006WR005144).
- Lopez-Gunn, E. and Ramón Llamas, M. (2008), Re-thinking water scarcity: Can science and technology solve the global water crisis?. *Natural Resources Forum*, 32: 228-238. <https://doi.org/10.1111/j.1477-8947.2008.00200.x>
- Morris, B. L., Lawrence, A. R., Chilton, P. J. C., Adams, B., Calow, R. C., & Klinck, B. A. (2003). Groundwater and its susceptibility to degradation: a global assessment of the problem and options for management.
- Wu, C.-M., Yeh, T.-C. J., Zhu, J., Lee, T. H., Hsu, N.-S., Chen, C.-H., and Sancho, A. F. (2005), Traditional analysis of aquifer tests: Comparing apples to oranges? *Water Resour. Res.*, 41, W09402, doi:[10.1029/2004WR003717](https://doi.org/10.1029/2004WR003717).
- Yeh, T.-C. J., and Liu, S. (2000), Hydraulic tomography: Development of a new aquifer test method, *Water Resour. Res.*, 36(8), 2095– 2105, doi:[10.1029/2000WR900114](https://doi.org/10.1029/2000WR900114).
- Yeh, T.-C. J., M. Jin, and S. Hanna (1996), An iterative stochastic inverse method: Conditional effective transmissivity and hydraulic head fields, *Water Resour. Res.*, 32(1), 85– 92, doi:[10.1029/95WR02869](https://doi.org/10.1029/95WR02869).
- Zhou, H., Gómez-Hernández, J. J., & Li, L. (2014). Inverse methods in hydrogeology: Evolution and recent trends. *Advances in Water Resources*, 63, 22-37.
- Zimmerman, D. A., et al. (1998), A comparison of seven geostatistically based inverse approaches to estimate transmissivities for modeling advective transport by groundwater flow, *Water Resour. Res.*, 34( 6), 1373– 1413, doi:[10.1029/98WR00003](https://doi.org/10.1029/98WR00003).

## CHAPTER 1

**Résumé :** Ce premier chapitre présente les différents types d'hétérogénéité potentiellement présentes dans les réservoirs géologiques et discute de leurs spécificités en fonction de l'environnement de dépôt (silicoclastique ou carbonaté), et des processus susceptibles de modifier ces hétérogénéités à l'échelle de temps géologiques. La potentielle influence de ces hétérogénéités sur les écoulements souterrains est finalement abordée, avec leurs conséquences sur l'anisotropie et la connectivité des réservoirs géologiques considérés.



## 1. HETEROGENEITY OF AQUIFERS AND RESERVOIRS

Geology is a science that investigate the earth and its constituents. It focuses on the type and structure of those constituents and study the different processes that impact them. Geology is also about the different organisms that lived in the planet through the passed ages. It tries to reconstruct the story of different processes that made earth we see nowadays. Multiple science branches that usually include earth materials (underground or surface) refer to geology and aim to link the modeled physics with reality and thus propose validations to the obtained results. Geology confirmed its major importance in different aspects; economically with the exploitation of the different resources (water, oil, gas...), scientifically with earth history reconstruction, physics modelling and physics predictions, technologically with the fast industry evolution that requires geological background, safety with the study of the natural disasters (earthquakes, volcanos, inundations,...). Geology has several branches; e.g. petrography that studies base materials that covers earth surface, stratigraphy that studies sedimentary rocks and layering, sedimentology for the processes that govern the deposit of sediments, hydrogeology for water resource exploitation, geochemistry, seismology, petro geology, and much more. Hydrogeology is the part of geology that tries to understand the behavior of underground water flow. Such behaviors are commonly complex and exhibit several challenges that researchers try to face and find a way to either bypass or solve them. The main objective of hydrogeology is to find a better way to enhance both the recovery and the quality of water and protect it from possible contaminations. As like in all branches that study earth crust, geology is fundamental. The knowledge of the geological history of a certain area allows us to reach a better model of the studied system in order to decrease the fear of the resource scarcity. The geologist uses a variety of techniques that allows him to better

comprehend earth's structure and evolution and how they impact several applications. Some techniques can be listed as: field experiments, rock analysis, geophysics, chemical analysis ...

## 1.1 Aquifers and depositional environments

Geologists have always been examining and describing aquifers and reservoirs by using characteristic features in order to interpret a sedimentary deposit and reconstruct the story behind its formation. A depositional environment is usually defined in terms of physical, biological, chemical or geomorphic variables. As a common definition, a depositional environment is a geomorphic unit in which deposition takes place. Different depositional environments have different set of processes operating at specified rates which makes it possible to characterize the produced sediments and deposits and distinguish the differences between them. Some depositional environments are rather complex where the physical, chemical and biological processes vary strongly in different places, such environments yield complex sedimentary rocks. Complex processes within a sedimentary environment can exhibit different sub-environments that makes the resulting sedimentary rock heterogeneous.

Ancient sediments are influenced by many physical factors, e.g. depositional medium, current and wave intensity and velocity, depth of water, climate, tectonics, etc. To which are added biological and chemical factors e.g. pH, salinity, etc. Combining different features and factors helps for a better description of the depositional environment. In fact, some structures can be seen in different environmental deposits and other clues from other features need to be gathered in order to provide more accurate interpretation.

The main types of depositional environments are continental, transitional and marine environments; the rest can be classified as other categories. Wilson 1975 categorized the depositional environments by dividing them into belts that extend from deep waters into terrestrial environments. Each of these categories can also be classified into further subcategories; continental deposits into alluvial, fluvial and lacustrine; transitional deposits into deltaic, lagoonal, tidal and beach environments; marine deposits into glacial, evaporitic ... Figure 1.1 summarizes different deposits environments.

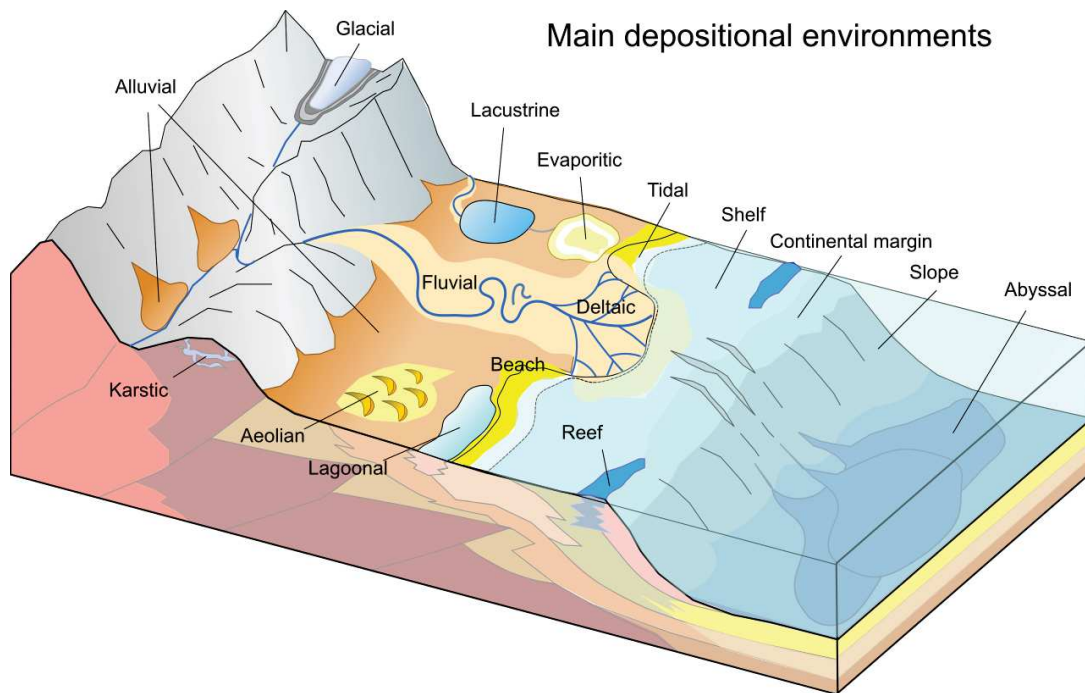


*Figure 1.1: Main depositional environments. (from Wikipedia commons).*

### 1.1.1 Continental deposits

The continental deposits occur on terrestrial plains of continents. They are mainly found on rivers, lakes, deserts, swamps ... those different places allow to classify the continental deposits into different sub-environments.

In the rivers, fluvial processes can be defined as the motion of the sediments erosion/deposition in the river bed. Sediments are transported in a different way according to their size; for example, big size sediments are transported close to the bed while finer sediments are carried in the water. Such process can already create different parts such as river channels that consist on coarse rounded gravel and sand, levees made of fine sand or silt, floodplains covered by silt and clay. Fluvial environments include braided and meandering river systems and are subdivided into coarse-grained channel deposits and fine-grained overbank sediments. At lower parts where the river overflows, alluvial deposits will also be found by forming floodplains and deltas. Alluvial deposits typically contain coarse boulders, gravels, sand and are poorly sorted.

In the lakes, incoming sediments fill the lacustrine plains which can lead into the draining of the lake leaving the deposited sediments behind. Over time, the lake can drain, evaporate or can be subject to a physical phenomenon that can cause its water to disappear. Lacustrine sediments contain valuable information about physical, chemical and biological changes on that environment. Two lakes can never be the same and their sedimentology processes differ, such variations can only lead into the creation of

a variety of deposits with heterogeneities that could be explained by the difference in sediments type and the difference in physical, chemical and biological processes that occurred during deposition.

In deserts, the wind can transport dust-sized particles and the gravel is left behind. The dust is lifted in the air and can be transported at large distances from its origin. Such hostile climate can also roll and windblown sand which forms dunes at large scales with well sorted sands. Eolian environments commonly result cross-bedding rocks.

Swamps are areas of standing water usually rich on vegetation and trees. Plants decay and its matter accumulates to form peat that can transform into coal. Paludal environments are known with their high biological activity and rocks with high organic content are thus abundant. Swamps deposition results are shale and sandstone deposits with high organic content or coal deposits.

### **1.1.2 Transitional environments**

Transitional or coastal environments are a transition between continental and marine environments and occur where the land meets the sea. They include a large variety of deposits environments: e.g. deltas, lagoons, beaches, tidal flats ... In this zone, there are both marine and non-marine influences. The non-marine influence increases in the landward direction, and the marine influence increases toward the shore zone.

Deltas are sediment accumulations that occur where a river empties into a large body of standing water. Deltas are largely studied and one of the most significant environments. The river carries sediments on its water and when it arrives to the shoreline, the mixture extends into the standing water as a sediment plume. Those sediments will either sink or ride up following the density of the mixture compared the seawater density. Also, for deltaic deposits, many factors can impact the sedimentation process; e.g. currents, waves, river features, tides, etc.

Lagoons are bodies of water separated from a larger body of water by barrier islands. They are protected from the effects of the larger body of water (waves) with their limited connection to each other. Lagoons develop generally along coasts where a wave-formed barrier is existent but also can be found behind reefs or in the center of atolls. A lagoonal succession is typically mudstone often organic-rich, with thin, wave-rippled sand beds.

Beaches are common transitions between continent and marine environments. They form where waves energy washes silt and clay and leaves larger sand particles behind. The silt and clay will then be deposited in another environment with lower energy. Beaches are exposed to wave energy, dominated by sand and commonly associated with tidal flat deposits.

Classified also as a transitional environment, an estuary is the marine influenced portion of a drowned valley. Estuaries are characterized by the mixing of fluvial and marine waters and the presence of energy gradients associated with wave, tide, and river processes.

### **1.1.3 Marine environments**

The marine depositional environments are mainly represented by seas and oceans. When the part gets further from the coast, some processes disappear and others appear. Marine environments mainly consist of shallow water environments and deep water environments.

Abyssal plains are classified as deep depositional environments and are usually situated at the base of the continental rise. They are the deepest part of the ocean floor lying at a couple kilometers deep. Abyssal deposits are alimented by organic debris and sediments and receive very little continental sediments. The abyssal plain sediments primarily consist of clay and shells of microscopic organisms and may include chalk, diatomite and shale.

Shallow water marine environment refers to the area that extends from the shore to deeper waters. This environment is characterized by oceanic geological and biological conditions. The water in this environment is shallow and clear, allowing the formation of different sedimentary structures, carbonate rocks, coral reefs, and allowing certain organisms to survive and become fossils. Overtime, this environment creates aquifers and reservoirs that are mainly carbonates that cover several sedimentary structures.

In this section, we will be focusing on the main depositional sedimentary environments that are relevant for water resource management. Aquifers are one of the most important fresh water supply and their exploitation are more or less easy according to their classification, depth, type of rock, hydraulic properties and many other attributes. Nowadays, most existing aquifers are classified into two main types according to their type of sedimentary rock:

- Carbonate rocks
- Siliciclastic rocks

## **1.2 Carbonate rocks**

Carbonate aquifers/reservoirs are mainly composed of calcite and dolomite and they are generally reactive under geochemical conditions at the near surface area. They consist of two main types of rocks: limestones which are composed of calcite and dolostones which are composed of dolomite. They are easily distinguished in the outcrop by comparing their solubility in acid (HCl). Limestone will instantly

react to the acid comparing to dolostone. Also, dolostone tends to weather into a brown color because of the replacement of the Mg by the Fe, while limestone tends to weather into white and grey colors

As for other rocks, carbonate rocks are also strongly controlled by the depositional environment and are also strongly altered by the age under physical and chemical diagenesis. Carbonate sediments and rocks are widely investigated and their heterogeneities remain important to characterize because carbonates reservoirs still contain a big amount of global oil reserves. Carbonate rocks are distinguished by their very high heterogeneity which makes their characterization even more challenging. Carbonate sediments consist mainly of calcium and carbonate forming the calcite and the polymorph aragonite. The classification of carbonate rocks according to the type of their grains and texture can already justify the very high heterogeneity and anisotropy that can be seen in these rocks, such variability in a microscopic content and texture affects greatly porosity and permeability of the system (F. Jerry Lucia 2007).

## **1.2.1 Classification of carbonate rocks**

### **1.2.1.1 Classification according to rock fabrics and pore size and shape**

Several classifications of carbonate rocks were proposed: Bramkamp and Powers (1959) classified carbonate rocks according to the original particle size; Leighton and Pendexter (1962) proposed basic textural elements of carbonate rocks; Plumley et al. (1962) classified on the basis of the energy of the environment in which carbonate sediments were deposited; Folk (1959) classified limestones on the basis of their clastic origin and grouped carbonate rocks into: intraclasts, pellets, fossils, oolites, micrite and calcite cement; Dunham (1962) (see Figure 1.2) grouped the carbonate rocks on the basis of the depositional fabrics and the relative proportion of coarse clastic particles (grains) and finer matrix or mud; Embry and Klovan (1971) and James (1984) proposed a modified version of Dunham (1962); Wright (1991) also proposed a revised classification of limestones; Lucia (1995) defined a classification on the basis of pore space instead of rock fabrics and modified the Dunham (1962) classification to adapt for pore space studies where he investigated the relations between pore space, porosity and capillary pressure; Maryam Mousavi (2012) proposed a new classification where he added subtypes using the pore-size distribution of Lonoy (2006). The two most widely used classifications are those proposed by Folk 1959 and Dunham 1962.



considerably decreased which makes the secondary hydraulic properties dominant when they appear (fractures and karstic systems).

Most carbonate rocks are susceptible to several alterations at any time from deposition: mineralogical and textural changes, cementation and dissolution. Most diagenetic changes affect the hydraulic properties of the rock. Hence, the classification according to the age and especially the Alteration history needs to be taken into consideration in addition to the classification according to rock fabrics in order to better characterize carbonate reservoirs/aquifers (Lucia et al. 2003, Perras and Diederichs 2011).

## **1.2.2 Carbonate facies and depositional environments**

Understanding the carbonates rocks properties extends when the depositional environment in which its sediments were deposited are characterized. Carbonate sediments deposit in different environments covering from terrestrial into marine depositional areas. However, some environments are known to be favorable to a rapid accumulation of carbonate sediments. Carbonate depositional environments were reviewed by Wilson (1975), Reading (1978), Tucker and Wright (1990), Scholle (2003). With intensive studies and exploration, carbonate depositional settings have become better known and different physical and chemical parameters are better explained and proved of how relevant they are on the sedimentation processes. Sea water level, waves, currents, chemistry, temperature, all affect the type of the formed carbonate. And diagenesis also alter them to become how we see them nowadays.

Most of carbonate sediments are formed in special depositional environments, warm, generally shallow, clear marine water (Wilson 1975). However, different areas that offer such conditions also have their own different conditions that make the deposited carbonate different one from another. The main depositional environments discussed in this section are:

- Basin and deep water deposits
- Reefs and buildups
- Sand shoals
- Lagoons and tidal flats

### **1.2.2.1 Basin and deep water deposits**

Sediments in this environment are usually referred as pelagic carbonates. Pelagic calcareous sediments are open marine deposits that are formed close to the surface. They are usually found at the seaward margins of shelves and platforms and extend basin-ward where the percentage of pelagic carbonates varies as a function of depth. Pelagic carbonates are composed mostly of the fossils of planktonic organisms that were deposited out of suspension and the texture of the fabric of the formed rock are categorized as mudstones and wackstones. They have very low matrix hydraulic properties due to their

very fine grain size. However, their aquifers may have well-developed secondary porosity and permeability. In between the organic sources of pelagic carbonates, we cite the most relevant: coccolithophores, planktic foraminifera and pteropods. Deep-sea sediments are however dominated by coccolith and foraminiferal carbonate, while shells of pteropods are highly susceptible to dissolution (Schiebel 2002).

Transported and reworked sediments issue from marginal platforms can also be transported to this area. They are referred as Turbidites and debris flows. The type of deposited carbonate depends on the type of the original source. Turbidites are sediments transported, usually for long distances, and redeposited by turbidity currents. Debris flow deposits are a mixture of angular fragments that have anomalously oriented stratification and the debris can get to several meters of diameter. Those mega-debris may float in terrigenous muds.

Changes in sea level have probably a big impact on the deposits occurring in basin slope to deep sea area. Changes in base level will often expose a carbonate basin margin which may lead to instability and to slope failure, generating then turbidity and flow debris.

#### **1.2.2.2 Reefs and organic buildups**

Reefs are carbonate build-ups of skeletal organisms that occur in topographically modified sea floor that are known to be wave resistant, hence, differ from banks (Selley 1985). Such conditions allow a quick deposition of organic sediments, however, different conditions affecting the deposition processes or alter them after deposition lead into a variety of reefs which makes Reefs and buildups very complex. Fossil reefs contains a big amount of oil and gas reserves which made them a target of intensive research and exploration in reservoir sedimentology. Reefs and organic buildups can form in shallow to slightly deep marine waters where a break on the sea floor slope exists. Reefs and buildups can have a variety of shapes but in general, two major forms are abundant: they can be either continuous elongate bodies with different lengths and directions or as a series of isolated buildups which may occur on either sides of the shelf break.

Carbonate reefs are commonly composed of large reef building organisms such as: corals, sponges, and rudists that are either bound together or transported, forming sediments composed of very large particles. Coral reefs often shelter a shallow-water lagoon from the open sea.

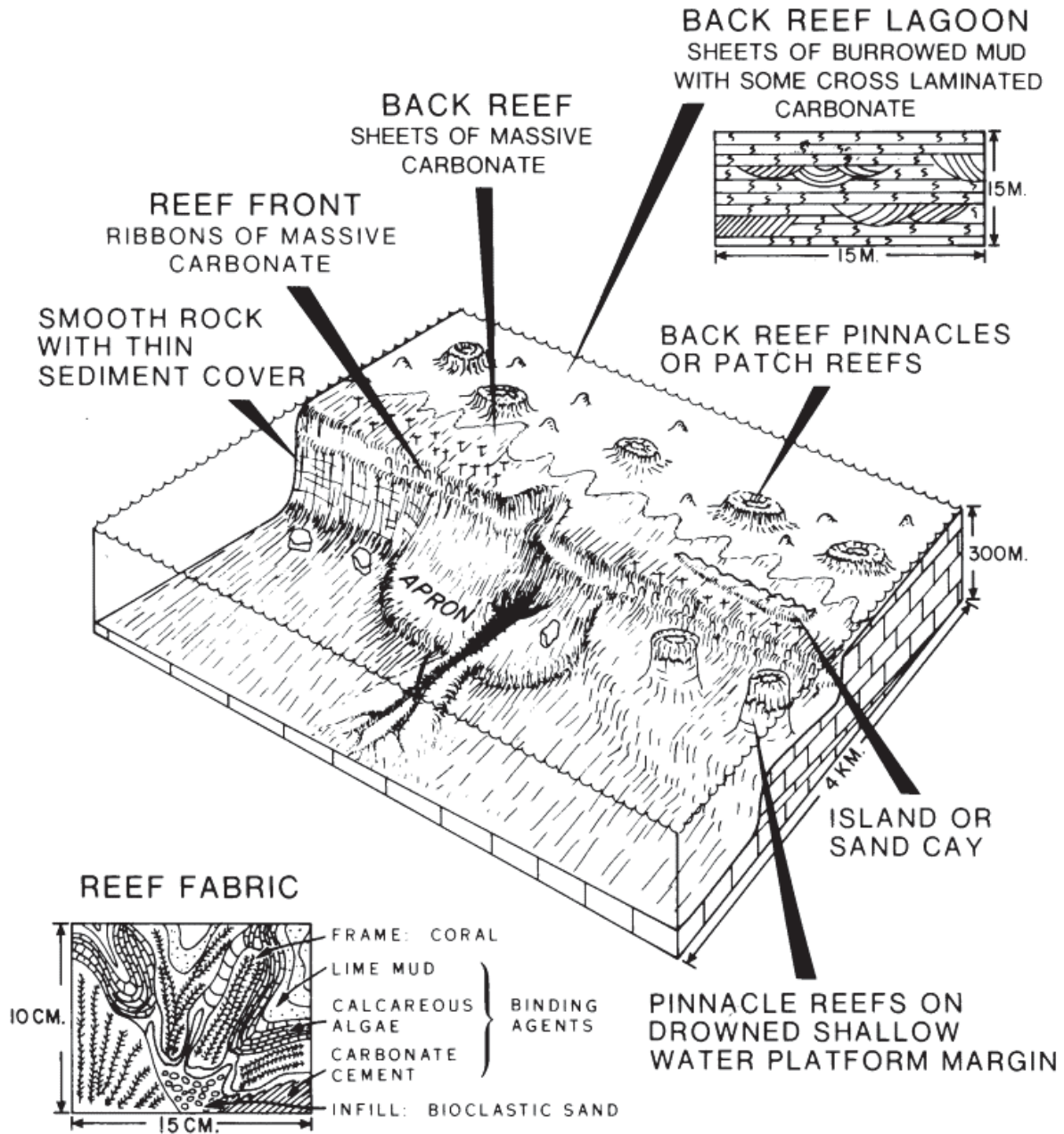
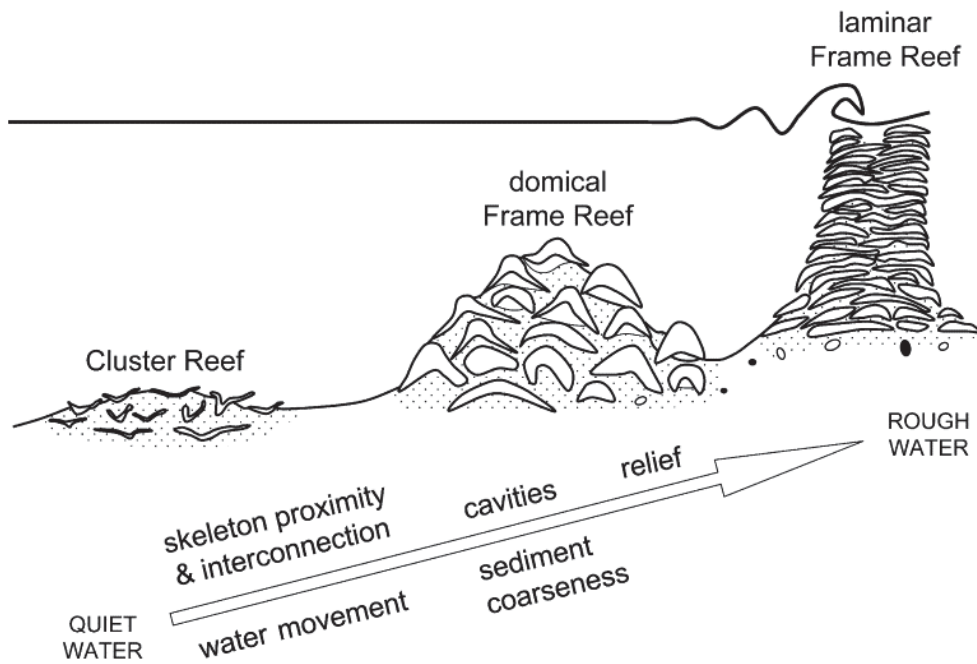


Figure 1.3: Reef environments and its equivalent facies.

Different classification of reefs and buildups exist according to their composition, structure and depositional conditions (Riding 2002, Maliva 2016). Riding 2002 presented a review of reefs and buildups and different classifications were shown. Maliva 2016 divided reefs into four main categories based on the relationship of the reef to the lagoon if present: 1) fringing reefs—linear along coast with no intervening lagoon, 2) barrier reefs—linear with lagoon, 3) atolls—sub-circular reefs enclosing lagoon from open water, 4) patch reefs—isolated reefs in lagoon behind barrier reefs and in atolls. Different attributes are commonly invoked to characterize reefs, some are objective (carbonate, organic

and skeletal composition, predominantly in place accumulation, etc.) and others are subjective (wave-resistance, primary relief, sources of carbonate sediment, energy (see Figure 1.4), etc.).



**Figure 1.4:** Types of reefs according to water agitation form quiet to rough waters. (Maliva 2016).

Riding 2001 presented a classification based on the structural support that englobes: 1) Matrix supported reefs, 2) skeleton supported reefs and 3) cement supported reefs.

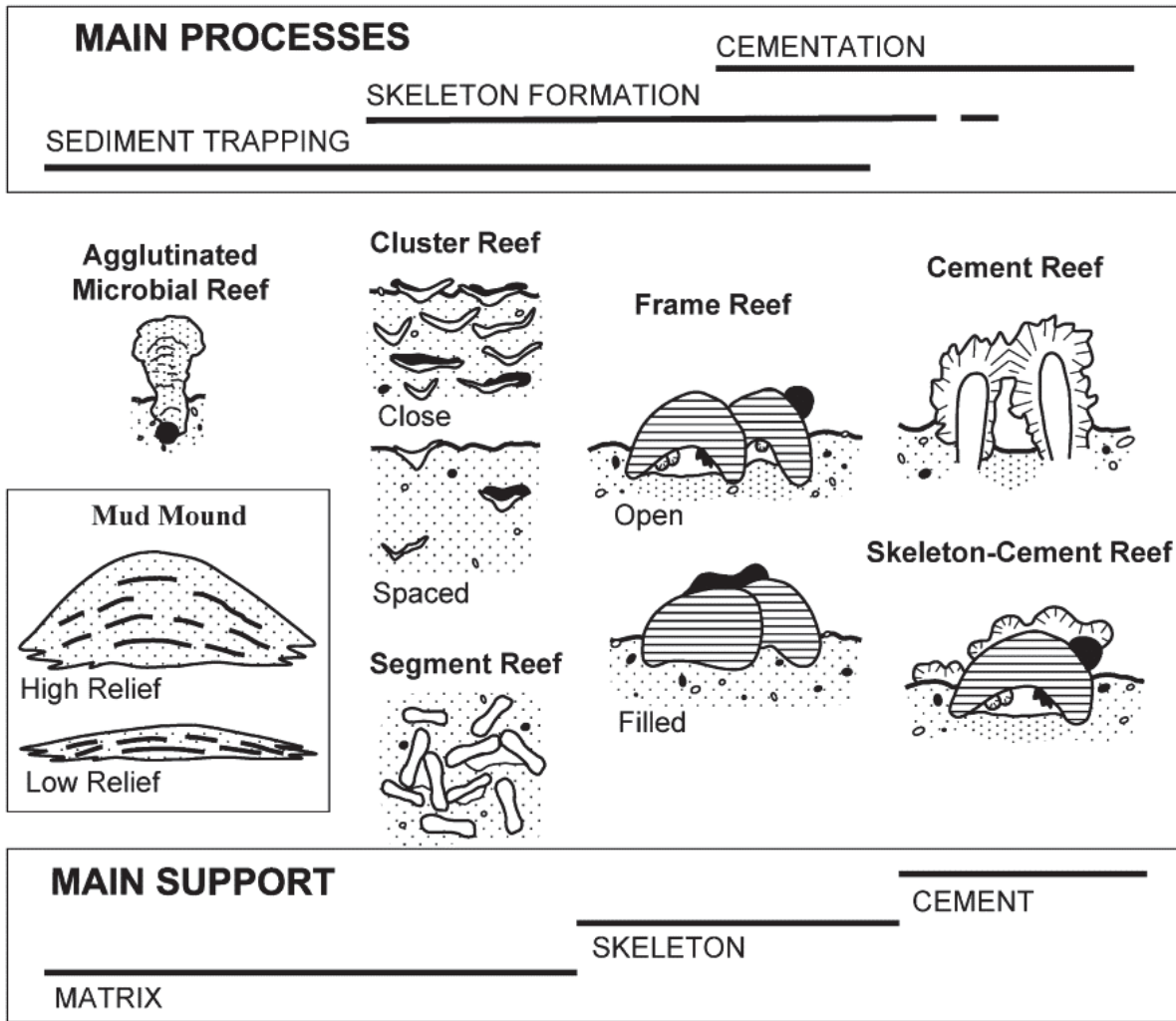


Figure 1.5: Classification of main organic reefs and carbonate mud mounds and its link to the main processes and structural support.

### 1.2.2.3 Sand bodies and shoals

Sand shoals cumulate along platform margins; they are also referred as carbonates factories of the shallow water deposits. Carbonate sand bodies have often high primary hydraulic properties and makes them very productive aquifers. They commonly occur in platforms, shelves and the edges of banks and much less in platform interiors or deep waters. The requirements for the formation of these sand bodies are often met where a change in shelf slope coincides with wave action or strong tidal currents.

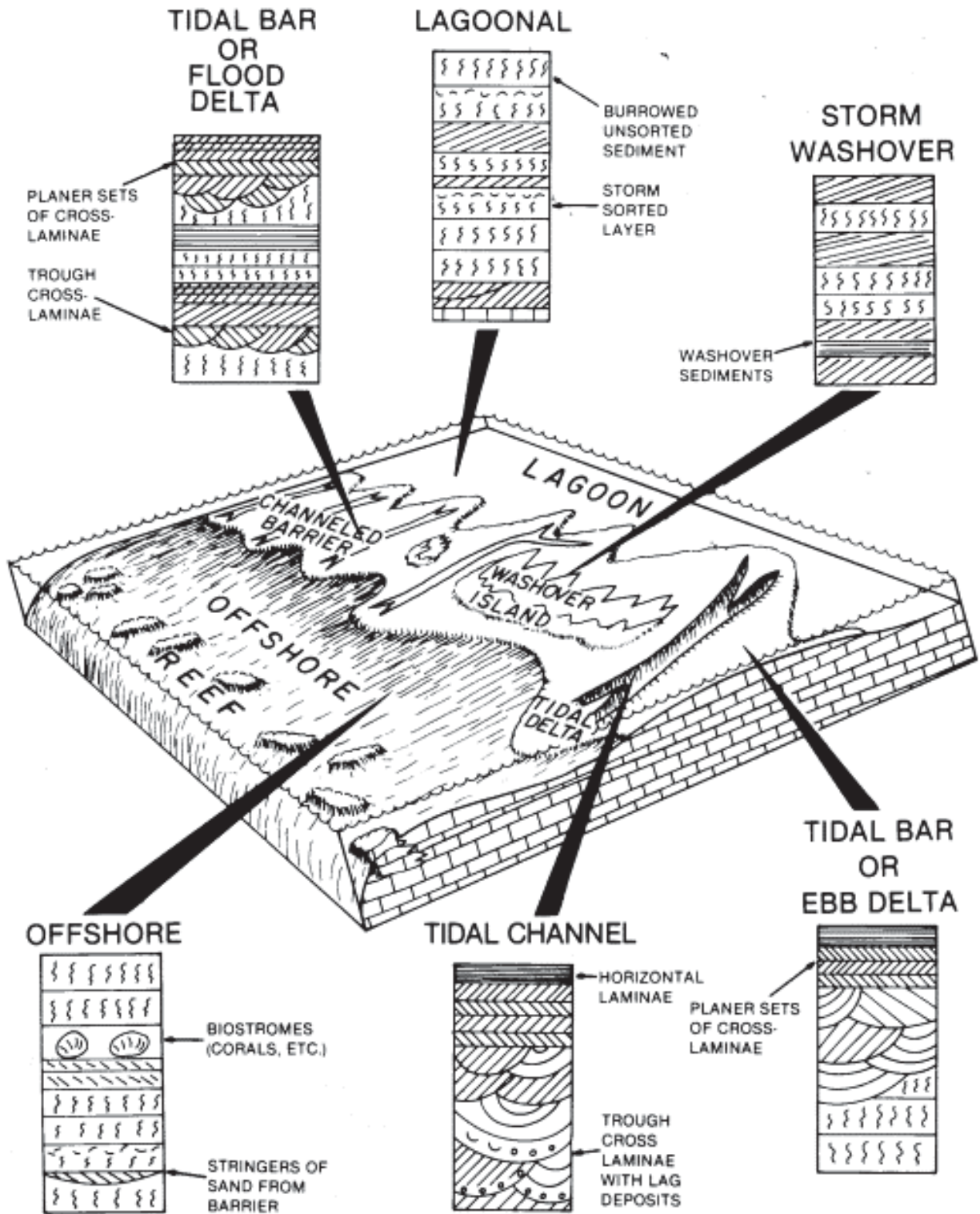


Figure 1.6: Sand shoals' environments and the main observed facies.

A variety of skeletal sand form along open platform margins where high energy dominates and the sediments transport toward the bank. If small islands exist, the gaps between them may be the site of

tidal deltas and the storms may enlarge the flood delta of the system and can also contribute on forming tidal bars.

Carbonate sands deposit in high-energy and shallow-water environments, in which current energy is sufficiently high to prevent deposition of finer sediments and carbonate muds. However, carbonate sands may also be transported into deeper-water environments or into sheltered lagoons that presents much lower energy. Carbonate sand can form thick, relatively homogenous limestone units with high hydraulic conductivities and porosities. The change of base water level affects the shoaling sequences and cyclic sedimentation beds are seen in ancient carbonate sands deposits. Carbonate sand bodies are not potential oil or gas reservoirs, which decreased the attention to them in this domain but usually become heterogeneous aquifers. What remains unclear are: the details of shoal evolution and how do shoals with different plan-view geometries arise, change, and evolve (Sparks et al. 2013).

Wilson (1975) in his characterization of carbonate rocks and their depositional environment where he divided the environments into different belts extending from the basin deep sea into the terrestrial land. He grouped the sands into a winnowed platform edge sands that englobes shoals, beaches, offshore, tidal bars and eolianite dune islands. Their grains are rounded and fairly well-sorted and construct a cross-bedded calcareous or dolomitic lime sand. These environments are well oxygenated and not hospitable for marine life.

#### **1.2.2.4 Lagoons and tidal flats**

Lagoons, epeiric seas and bays are protected by reefs, wide shallow seas or sand barriers. The water is shallow (few meters deep), the circulation is very limited to very moderate, the water conditions are favorable for organisms, the sediments texture can have a large variety but governed by lime muds. Water depth and current energy play roles on the texture and type of deposited sediments. The water at its deepest, marls and shales are most likely to be seen. And at shallower waters, where energy is only sufficient to winnow lime muds but not sand grains, sands can form. The restriction to the marine platforms increases the amount of fine sediments that will be deposited in the carbonate.

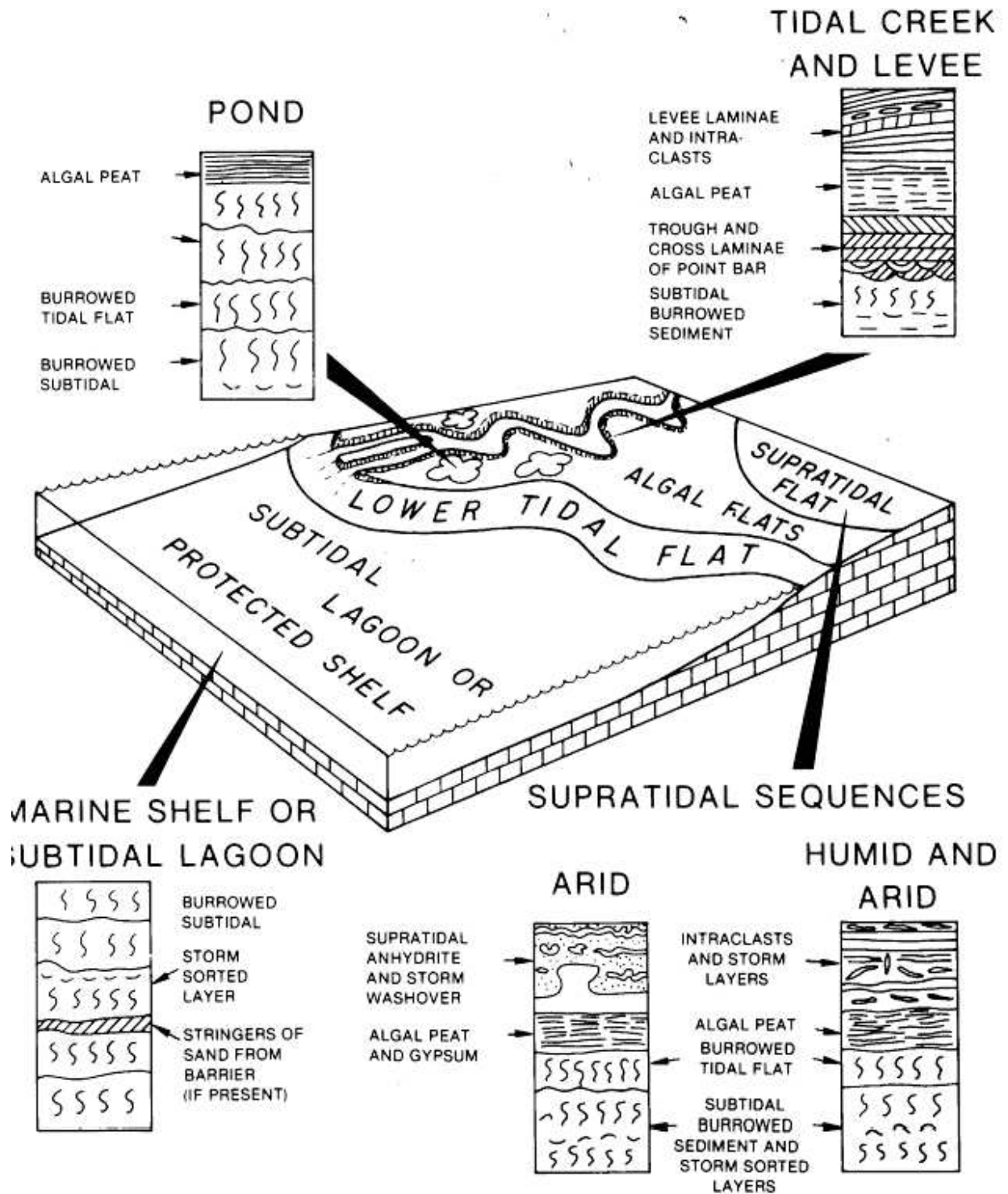
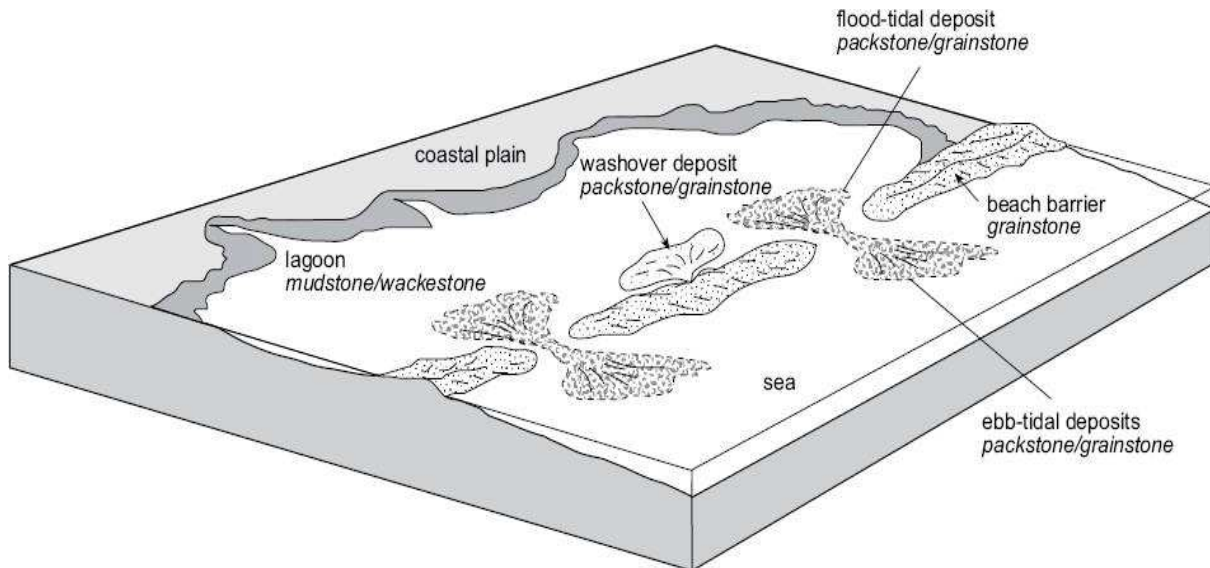


Figure 1.7: Lagoonal and tidal flat environments and its main equivalent facies.

Carbonate lagoons form along coastlines enclosed totally or partially by a barrier and its water is very shallow. Salinity of the water plays a big role in the nature of deposited sediments which is linked to the degree of connection to the opened sea and the climate. Carbonate lagoons are characterized by fine-grained sediments; they are mainly mudstone and wackestone. However, limited amount of grainstone and packstone are deposited as wash-overs near the barrier. The deposited fine-grained

carbonate sediments in lagoons are from calcareous algae and the coarser bioclastic detritus are from molluscs forming Pellets. In hot and dry climates, with the condition of the lagoon being poorly alimented by fresh water, water of lagoons is susceptible for high evaporation which increases the salinity in the remaining water and it becomes hypersaline. These conditions are favorable for the precipitation of evaporate minerals known as a saltern. Deposits are typically layered gypsum and/ or halite.



*Figure 1.8: Lagoonal environment and its main deposits showing the type of grains (Nichols 2013).*

Tidal flats are flooded by daily tides and the supratidal zone flooded by wind and spring tides. Sediments, sand and mud, can deposit in tidal flats and occur as widespread sheets that are often dissected by channels. Bedding is thin and even and contacts are sharp. Sediments deposited in supratidal flat vary according to the governing conditions. For instance, high salinities and magnesium concentrations lead into dolomitization. These environments known to have lime muds in levees, intertidal flats, ponds, and marshes. Coarser sediment exists in tidal channels and local beaches.

### 1.2.3 Types of carbonate platforms

Different types of carbonate platform with different morphologies are observed and the most widely explored and investigated are carbonate ramps and rimmed shelves. Ramps are gently sloping platforms and can be divided into two subcategories: homoclinal ramps and distally steepened ramps. Rimmed shelves are flat-topped platforms with shallow waters protected from the deep sea by a border or a barrier formed mainly by a reef; a carbonate sand shoal bordering the shelf may occur as well (see Figure 1.9). Pomar (2001) stated that it is very difficult to identify a particular type of a platform, especially recognize the different belts of the platform, with low uncertainty because of the fact that many types can occur within a carbonate rock succession. Some of these difficulties also may result

from defining the type of platform only from the facies array found from shore to basin. However, defining the type and understanding the conditions of the sedimentation greatly help improving models of carbonate platform development and evolution, hence, the aquifer/reservoir characterization. In any case, predictive efficiency of conceptual models depends on the degree of comprehension of the genetic factors controlling development distribution of the facies of different belts.

Carbonate ramps are gently sloping platforms characterized by the increase of water base level basinward. They are mainly developed in areas that don't meet the conditions of forming reefs. According to the base water level, tidal effect and storm process in inner, mid and outer ramp can be distinguished. In ramps, carbonate prograde which in overall results in a coarsening up from the outer to the inner ramp. Non rimmed carbonate shelves are flat topped with shallow marine environment and marked with a steepen slope at the outer shelf toward the deep water. They don't have a barrier which makes the shelf exposed to the deep ocean environment. Rimmed carbonate shelves have similar slope evolution toward the deep waters as in non-rimmed shelves, however, a barrier (usually reefs) in the outer shelf develop and decreases greatly the effect of ocean environment. Landward of the reef, lower energy shallow platforms are observed in the modern rimmed platforms.

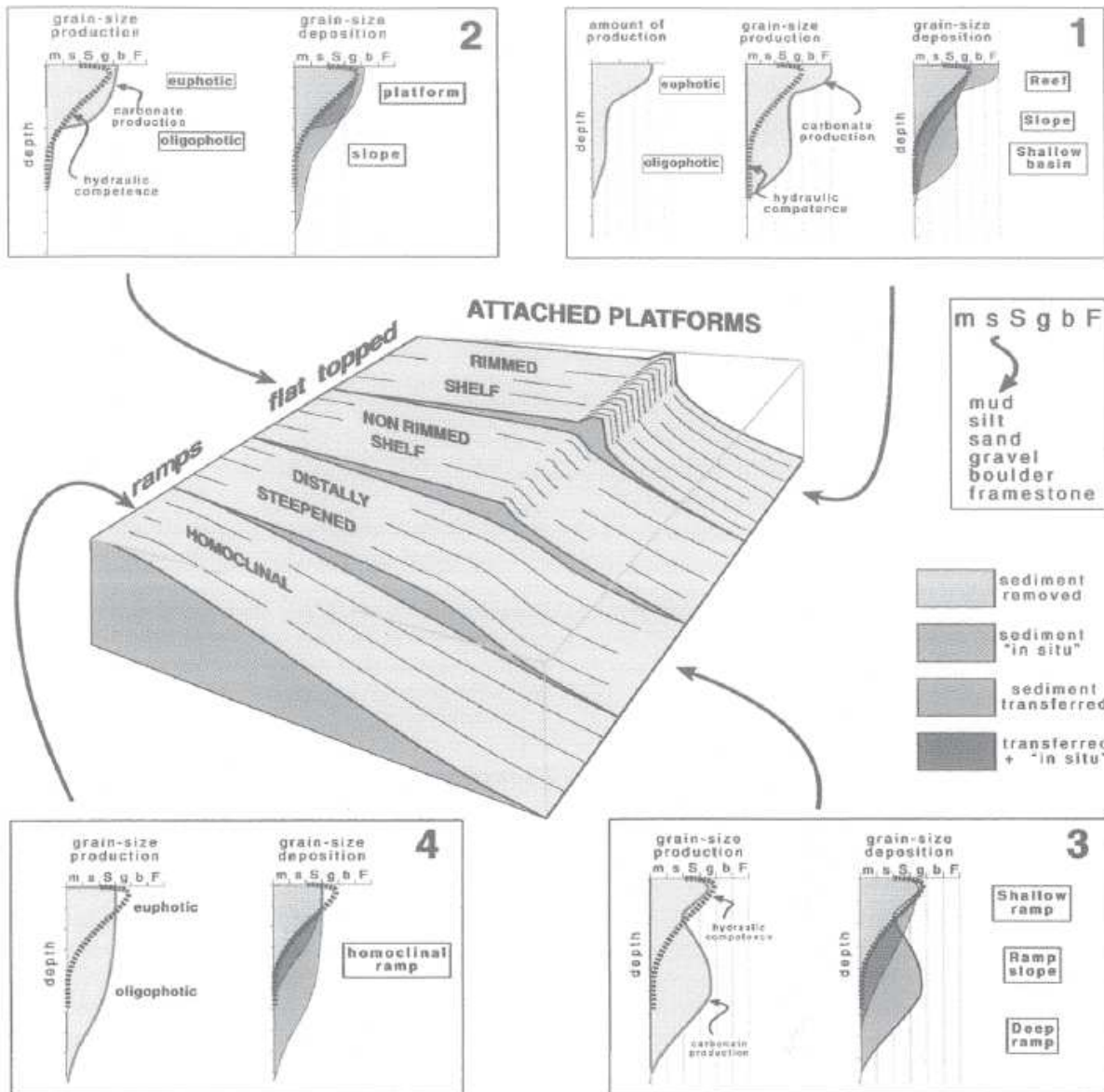


Figure 1.9: classification of carbonate platforms and the types of produced sediments (Pomar, 2001).

The progradation of the barrier in rimmed platforms results in steepening of the slope along the seaward margin. At the edge of the slope of rimmed platforms, carbonate may be redeposited in the form of debris flows in the upper part and turbidites on the lower part of the slope classified as pelagic deposits of the deep basin. In addition to the fact that these different platforms creates heterogeneities in the resulting carbonate rock, the base water level can change which makes the whole system change.

### 1.2.4 Diagenesis of carbonate rocks

Carbonate diagenesis is well documented because of how important the alterations are to understand the high heterogeneities and anisotropies of the formed aquifer/reservoir. Diagenesis can indeed

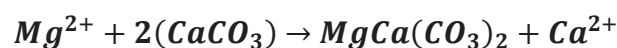
decrease the hydraulic properties of the rock but also create secondary flow-governing porosity and permeability that come and overwrite the primary properties. Carbonate rocks mainly pass through three different stages: the deposition, the burial and uplift. These stages are also referred as eogenetic, mesogenetic, and telogenetic (Choquette and Pray, 1970). And during the different stages, carbonates are susceptible to minor and major changes according to the governing conditions. They can change their texture and mineralogy, they can go through cementation processes, they can be subject to fracturing and they can dissolve to create big karstic systems. The different alterations have a great effect on changing the hydraulic properties of the rock and create highly heterogeneous aquifers and reservoirs. The main alteration of carbonates through diagenesis occur near the sedimentation surface and at shallow depths. In contrast, at deep burial stage, the carbonates are mostly stable but important alterations may occur. More detailed carbonate diagenesis overviews can be found in the works of, Bathurst (1971), Tucker and Bathurst (1990) and Moore (2001).

Eogenetic stage is usually very brief, it occurs while the sediments are still under the near-surface processes influence such as the influx of meteoric waters. Eogenetic stage can be of extreme importance because of the big change of hydraulic properties that can occur. Mesogenesis refers to the burial step of the sediments and highly related to compaction processes. Telogenesis refers to processes that occur upon the uplift and erosion of older rocks. Along the stage, it exists different processes that are relevant in aquifer characterization:

- Dolomitization
- Dissolution and Karstification
- Physical and chemical compaction

#### 1.2.4.1 Dolomitization

Dolomitization is a geological process that forms dolomite where the ions of calcium are replaced by ions of magnesium which also involves the recrystallization of the rock. Dolomitization is expressed by a replacement equation:



This process remains not fully explained and several theories arisen, Hardie (1987) reviewed several views of how dolomite were formed and he also stated that several current dolomitization models have high uncertainty. It does not inherently result in a change in porosity. However, dolomitization does change the texture of the rock and its permeability. The dolomite has also the potential for creating good porosity and permeability in originally tight limestones. In older (e.g., Mesozoic and Paleozoic) dolomites, entire formations can be found dolomitized at a regional scale.

#### 1.2.4.2 Dissolution and Karstification

Dissolution is the diagenetic process where minerals are dissolved and removed, thus creating and modifying pore space in reservoir rocks. Dissolution can be fabric selective and can form moldic pores and vugs or, not fabric selective and results in interconnected voids. The dissolution can involve the positive feedback loop by getting more water influx by the increase of permeability which leads into the increase of reaction rate and, thus, resulting on big conduits systems that will govern the flow.

Carbonates can already dissolve at early stages and the dissolved calcite plays a role in cementation processes. Some carbonates don't pass through the deep burial phase and remain close to the surface. These carbonates may be subject to dissolution and karstification. In the other hand, older limestones can uplift or their tops get eroded which makes them more susceptible to dissolution processes. These two different scenarios may form two different karsts classified as Eogenetic and Telogenetic karsts. The dissolution requires to meet some geochemical conditions where the rock being flushed with water. Dissolution models state that the dissolution rate depends on water saturation, carbonate minerals and the kinetics (Palmer 1991, Dreybrodt 1999, Hanna and Rajaram 1998). Dissolution processes tend to be initiated at discontinuities, such as fractures, joints, or bedding planes because of their higher exposure to water flow.

#### 1.2.4.3 Cementation and compaction

These process starts since the deposition of the sediments and remains active at different rates during the whole diagenesis. They reduce the intergranular pore space and they are both considered as phenomena that reduces the hydraulic properties of the carbonate rocks and can lead into the formation of tight limestones and very poor quality reservoirs. Cementation starts soon after deposition and requires a fluid flow that transport the cement. Early cementation in shallow burial environment results from marine water circulation, driven by tidal and wave energies, through very permeable deposited sediments. The cementation continues as the sediment is buried deeper however as for dolomitization, the burial cementation is still to be more explored. Cementation textures and fabrics are more discussed in Lucia (2007).

Compaction involves both physical and chemical processes and its effects are hard to distinguish from cementation effects. Compaction is caused by the increase of the overburden due to burial stages. Budd (2002) suggested that both cementation and compaction changes the pore size, decreasingly, in a different way. Such difference may have different impact on permeability and capillarity. The change of rock texture due to compaction can also involve grain deformation, grain breaking and fracturing.

### 1.3 Siliciclastic rocks

Siliciclastic rocks are the deposited sediments that were issue from the weathering of already existing rocks (terrigenous material). They are usually eroded and transported by wind or flowing water. Silicate sandstones can have a variety of colors due to the impurities transported with the sediments.

The hydraulic properties of siliciclastic rocks depend on their depositional texture (grain size, sorting, supporting matrix (clay and silt) content, mineralogy, ...etc.). The siliciclastic rocks highly depend on the source rock, weathering, transport processes and new depositional environment. Eroded sand is transported by rivers or by the wind to depositional environments. Continuous sedimentation leads into diagenesis that includes the compaction and the lithification of the sand. Early stages of diagenesis in shallow depths going to several meters favor mineralogical changes and are slightly compacted. At latter diagenesis after deep burial, the rock is subject to the most of compaction and lithification. Compaction is caused by the accumulation of overlying sediments that increases the pressure on the older sand. The compaction rearranges the grains and, thus, alter the hydraulic properties of the rock. In addition to this physical compaction, chemical compaction may take place via pressure solution. Lithification follows closely the compaction while cementation of the pores takes place when temperature increases. Sandstones also may develop secondary porosities at the late stages of the diagenesis.

#### 1.3.1 Classification of siliciclastic rocks

Silicate sandstones are mainly composed of Quartz, Feldspar and matrix (silt, clay). The quartz and the feldspar are the grains that are its main constituent because of their resistance to weathering in the terrigenous materials. The terms sand or clay refers to grain size that plays an important role on characterizing the hydraulic properties of the rock. Folk (1974) classified the grains of silicate sandstones (Table 1.1) according to their size range.

**Table 1.1:** Terminology of grains according to their size (After Folk 1974)

Terminology	Size or diameter (mm)
Pebble	4-64
Granule	2-4
Very coarse sand	1-2
Coarse sand	0.5-1
Medium sand	0.25-0.5
Fine sand	0.125-0.25
Very fine sand	0.0625-0.125
Silt	0.0039-0.0625
Clay	<0.0039

Dott (1964) and Folk (1974) classified the sandstones using a ternary diagram (see Figures 1.10 and Figure 1.11). The diagram gives different information to the geologist just by the position of a rock in this diagram. They used the main grain types quartz, feldspar, and rock fragments (lithic fragments) in the different angles of the diagram and the positioning of the rocks will depend on the percentage of these constituents. The triangle itself can be divided into different zones that allow to classify the different rocks into categories. The composition of sandstones is thus displayed using a ternary diagram based on their quartz-feldspar-lithic fragments ratio and percent matrix. As sand is transported and weathered, its composition approaches the quartz pole of the QFR diagram and is said to increase in compositional maturity.

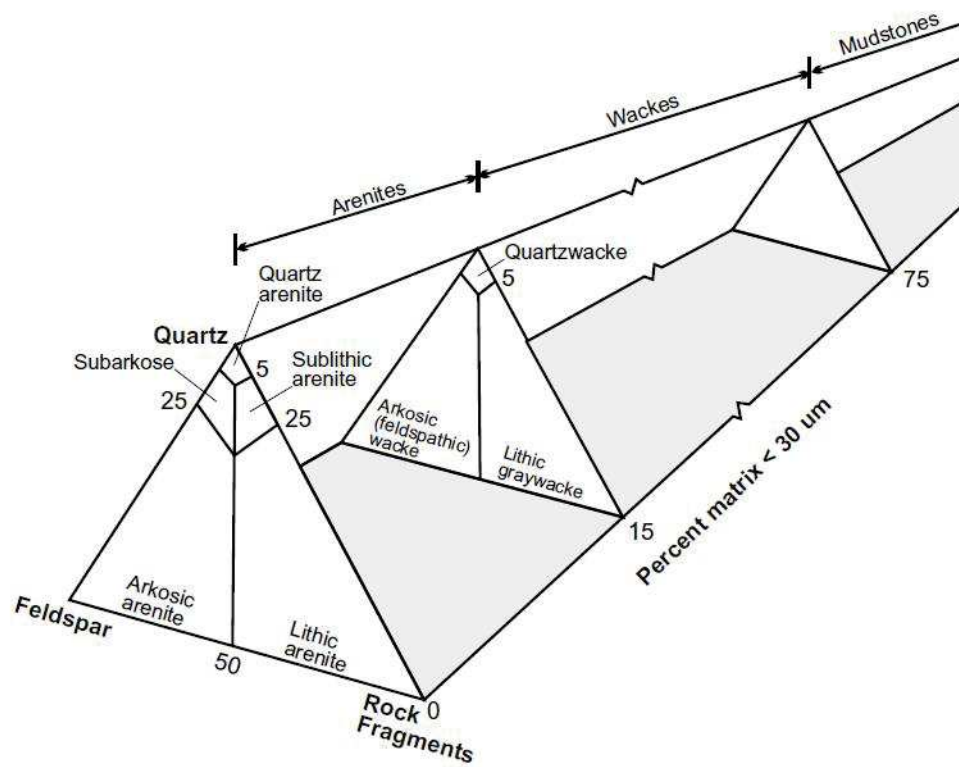


*Figure 1.10: Sandstones classification (Dott 1964).*

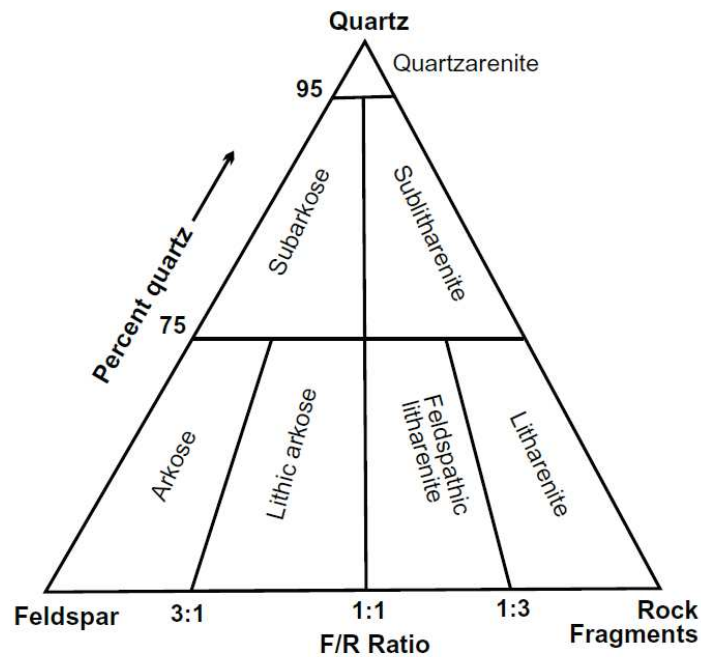


*Figure 1.11: Sandstones classification (Folk 1974).*

### 1.3.2 Depositional environments of siliciclastic rocks

Heterogeneity in siliciclastic aquifers/reservoirs depends on depositional and textural variations (i.e., differences in grain size and sorting). And the hydraulic properties are then altered by diagenesis. The texture of the rock is related to the depositional environment. The history of sedimentation and the depositional environment are very important in characterizing any aquifer/reservoir for better development of conceptual and numerical models of siliciclastic aquifers. The different depositional environment of terrigenous deposits are reviewed in Galloway and Hobday (1983). In this section, the following depositional environments are discussed:

- Fluvial systems
- Alluvial-fan systems
- Deltas

Terrigenous clastic sediments can also occur on estuarine, eolian, lacustrine and marine environments. Knowing the type of the of the rock and its depositional environment mainly allow to reconstruct the bedding and can provide an insight of the continuity of the different sand bodies and especially link in between the transmissive ones.

#### 1.3.2.1 Fluvial Systems:

Fluvial systems are represented by rivers or streams. In a more general term “alluvial” refers to the action of flowing water and the deposited fluvial material is called alluvium. Fluvial deposits are

characterized by different criteria: they can for example be classified following the main channel types into bed load, mixed load or suspended load. Also, the erosional or aggradational nature of the main stream (Schumm 1977; Galloway and Hobday 1996) allow a better understanding of the system and the resultant rock sequence. Rivers (channels) with one channel belt are divided into three main types: straight, meandering, and braided. The two most common types of rivers are meandering (high sinuosity) and braided (low sinuosity); a straight river at the scale of one channel belt can be defined as a low sinuosity with lateral stability. And, multiple channel belts rivers are called anastomosing (see Table 2, Figure 1.12).

**Table 1.2:** Classification of river types (Miall 1977)

Type	Morphology	Sinuosity	Load type	Bedload (%)	Width / Depth	Erosive Behavior	Depositional behavior
Meandering	Single channels	>1.3	Suspension or mixed load	<11	<40	Channel incision, meander widening	Point-bar formation
Braided	Two or more channels with bars and small islands	<1.3	Bedload	>11	>40	Channel widening	Channel aggradation, mid-channel bar formation
Straight	Single channel with pools and riffles, meandering thalweg	<1.5	Suspension, mixed or bedload	<11	<40	Minor channel widening and incision	Side-channel bar formation
Anastomosing	Two or more channels with large, stable islands	>2.0	Suspension load	<3	<10	Slow meander widening	Slow bank accretion

Makaske 2001 reviewed the classification of the anastomosing rivers and he redefined them according to the belt scale and he also pointed out the main characteristics of the multiple channel belts type. They can also be classified according to different variables including channel slope, water flow (average and flood), bank stability, sediment source, and sediment load (supply and grain size). Fluvial depositional systems are primarily aggradational but Localized progradation and lateral accretion occur within specific environments.

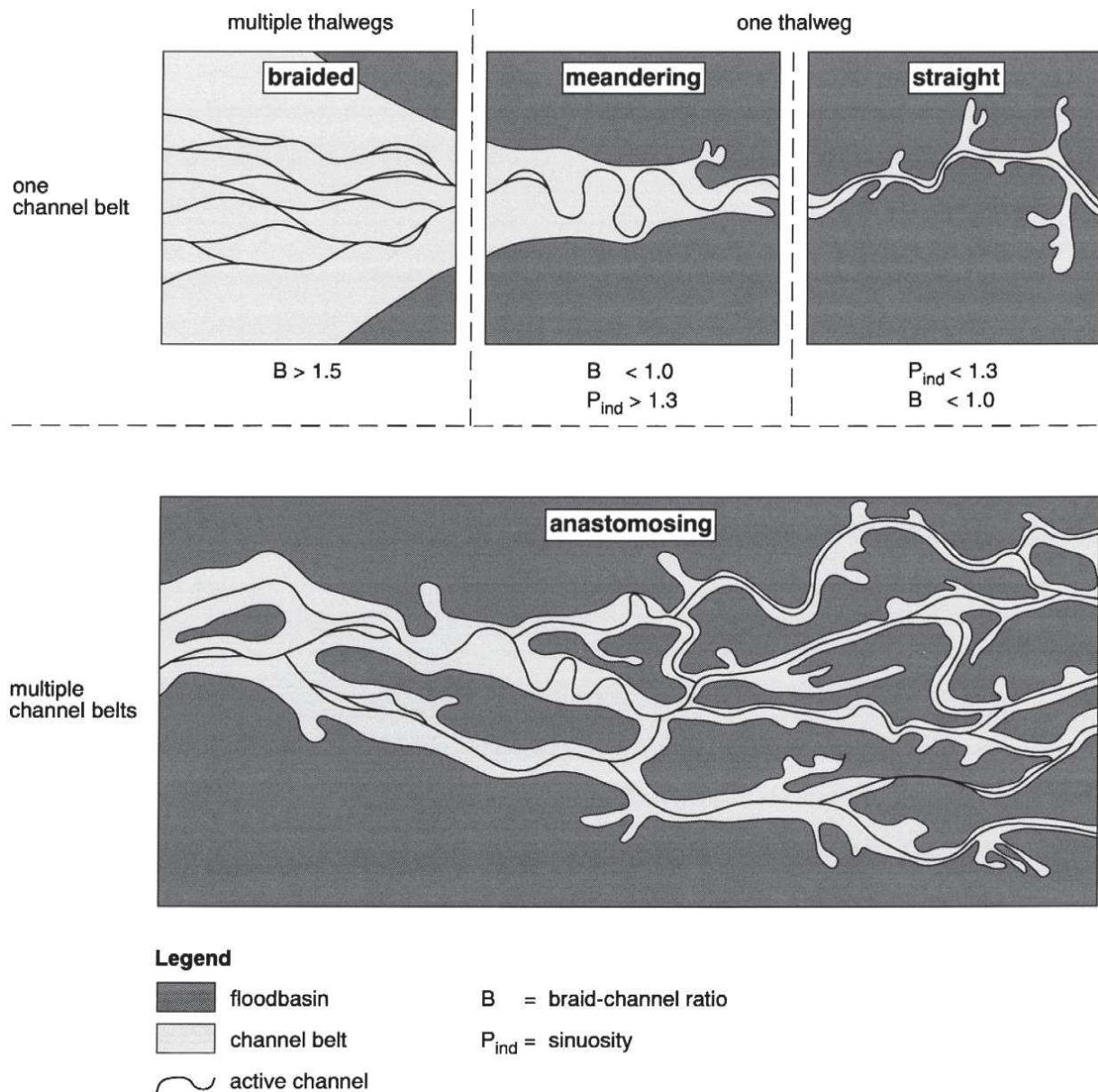


*Figure 1.12: Classification of channels (Makaske 2001).*

Understanding the transport and the deposition of the sediments in Alluvial systems is of a great importance. It was observed that the coarse grains are transported near the stream bed while the finer sediments are transported in suspension in the flow. Fluvial deposits have a great degree of variability; different deposits with a big variability in transmissivity are the result of a simple river. Usually, there is a sedimentation of coarse grains forming a transmissive sand bodies that are partially or totally connected and those sand bodies are referred as channels. The channel sands are surrounded by finer grains with low transmissivities referred as floodplain muds. Flow being governed by the most transmissive bodies, it is of an extreme importance in aquifer characterization to map the location of channel sands, hence the geological facies models. The construction of facies models using different source of data allows to predict the geometry of channel sands and distinguish them from floodplain

muds. It exists methods that help understanding the geometry of different sand bodies and the link that may exist between them (Bridge and Mackey 1993; Bridge 2006). The most valuable information that is mainly used in facies analysis is from well logs but remains limited. Bridge (2001) stated out that logs alone are not sufficient for the interpretation of specific fluvial depositional environments. Miall (1985) introduced the architectural element analysis: a method of facies analysis applied to fluvial systems. At a large scale, Miall (1985) noted that there are different architectural elements with different characteristics (see Figure 1.13)

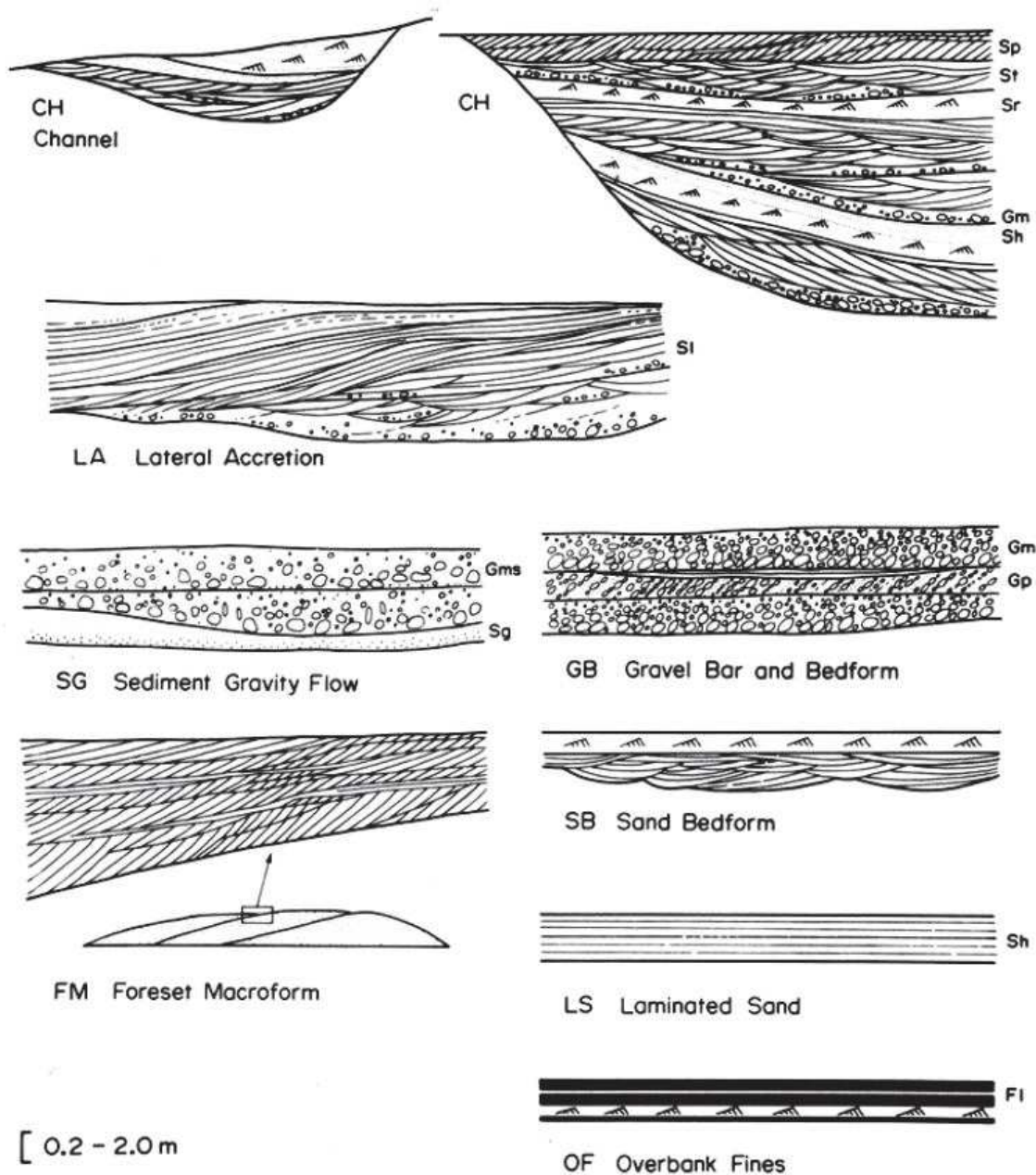
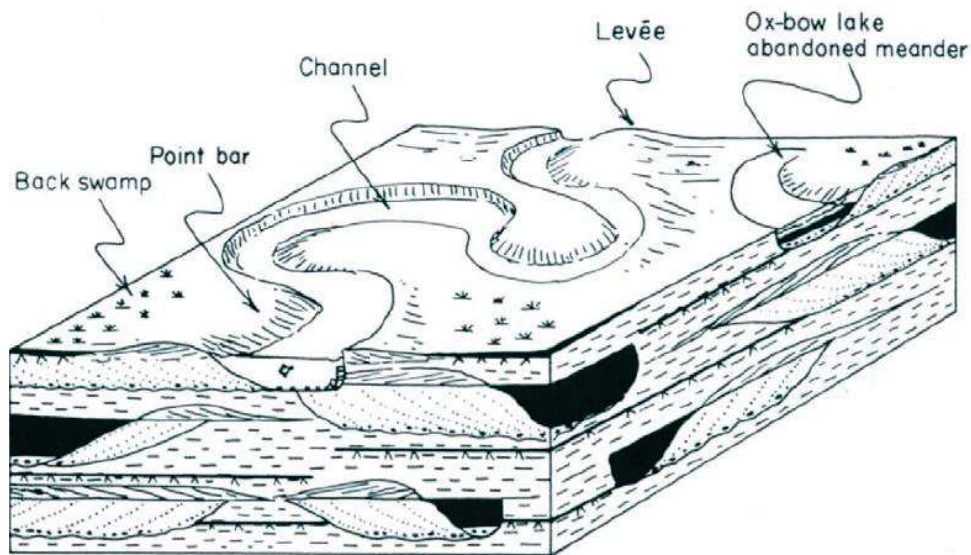


Figure 1.13: The major architectural elements (After Miall 1985).

### *Meandering river facies*

The meandering rivers are in a one channel belt and show a high sinuosity on their active channel. Meandering rivers are loops or bends in which erosion occurs at the outer (concave) side (cutbank), and deposition occurs at the inner (convex) side. Erosion in the outer side widens the channel and forces deposition at the opposite bank. The deposition in the inner side narrows the channel forcing erosion at the opposite bank (Parker et al. 2011). Such feedback loop increases the sinuosity of the channel and creates cut off bends. The inner side where deposition occurs is referred as a point bar. In meandering rivers, the channels are relatively deep especially in the eroding side of the channel. The main conditions that allow meandering rivers to occur are: low hydraulic gradient, high suspended load/bed load ratios, and cohesive bank materials.



*Figure 1.14: Meandering river facies (Selly, 2000).*

Deposition occurs within both channel and overbank environments. Lateral accretion occur in point bars laterally and in the direction of the stream and during seasonal flood events, fine sediments deposit on the adjacent floodplains and they may include plant debris and fossils.

### *Braided-stream facies*

Braided rivers have low sinuosity and several channels in the same belt. They carry coarser sediments than meandering rivers and their flood velocity is high. Braided rivers are relatively straight, wide, and shallow and they include several dunes and bars inside. The dunes and the bars separate the flow which makes different sub-channels to emerge in braided pattern. High seasonal floods can submerge the dunes and the bars under water (Miall 1977, Cant 1982, Cant and Walker 1978, Rust 1978). In braided streams, sand and gravel are transported as bed load and fine sediments are in suspension. Braided

streams are rather unstable and the position of the channels changes which makes the depositions of fine grains uncommon while sand and gravels are more often.

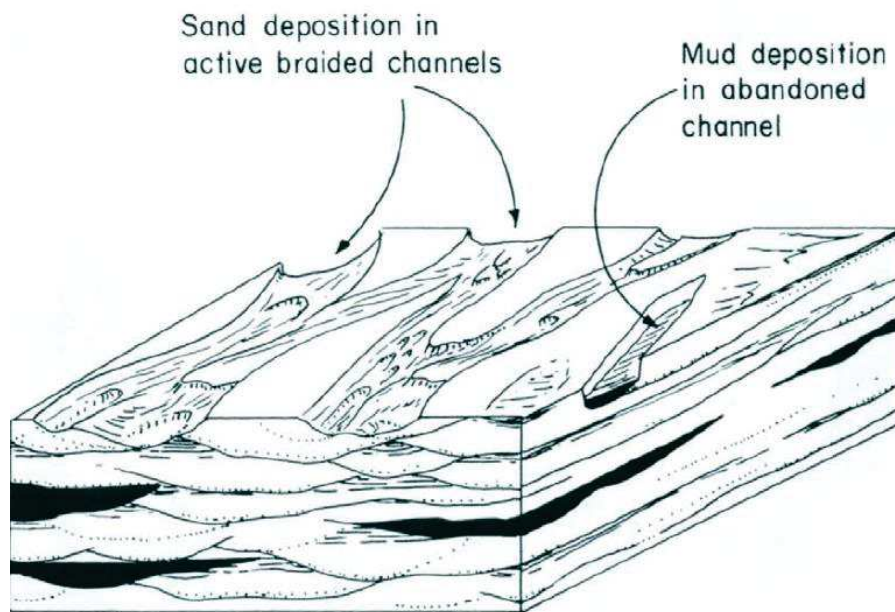


**Figure 1.15:** Braided stream facies (Selly, 2000)

Braided rivers have two or more channels that are divided by bars or small islands. Usually, one channel will be dominant but more than one can be found in some sections.

#### *Straight river*

Straight rivers are stable systems with relatively gentle slopes (Schumm, 1968). They are commonly mixed- or suspension-load streams with sinuosity being nearly equal to 1.0. Modern straight rivers are rare and little is known regarding their deposits. Ikeda (1981) simulated different runs of the time evolution of the cross section of a straight river. Kovacs and Parker (1994) constructed models to describe the time evolution of cross section of straight rivers and its erosional/depositional relation of an initially trapezoidal channel and stated that the simulation converge toward an equilibrium cross-sectional shape. This equilibrium is characterized by a constant width, vanishing sediment transport in the transverse direction, and a small but non-vanishing streamwise transport rate of bed sediment.

#### *Anastomosing rivers*

To not confuse with braided streams, an anastomosing river is composed of two or more interconnected channels that enclose flood basins. This definition explicitly excludes the phenomenon of channel splitting by convex-up bar-like forms that characterize braided channels (Makaske 2000). However, braided, meandering and straight rivers can all be part of an anastomosing river and use its

characteristics at the level of one channel belt. A rapid rise of base level is conducive to anastomosis, but is not a necessary condition.

### 1.3.2.2 Alluvial fans systems

Alluvial fans are formed where a river course passes from an area of high slope to one of low slope where sediments are able to spread out into wide. The feeding main channel is either divided into several very shallow channels, or, its water infiltrates the surface. Alluvial fans have triangular shapes and they are mostly composed of gravel and sand. Its apex is usually narrow connected to a canyon, confined valley or a gorge. Alluvial fans are common in desert mountains, however, Harvey et al. (2005) stated that they can occur in any climatic environment.

In alluvial fans, the sediment deposition is mainly caused by the abrupt change in slope. Having open wide fans with lower slope permit the sediment to expand horizontally. The deposited sediments are angular, poorly sorted, and coarse-grained. The size of the grain relatively decreases with the distance from the apex. Alluvial fan can be divided into three belts (see Figure 1.16): proximal with debris flows and conglomerate deposits, mid with sandy deposits and proximal with finer grains. Alluvial fans can be stream dominated, mixed or debris flow dominated.

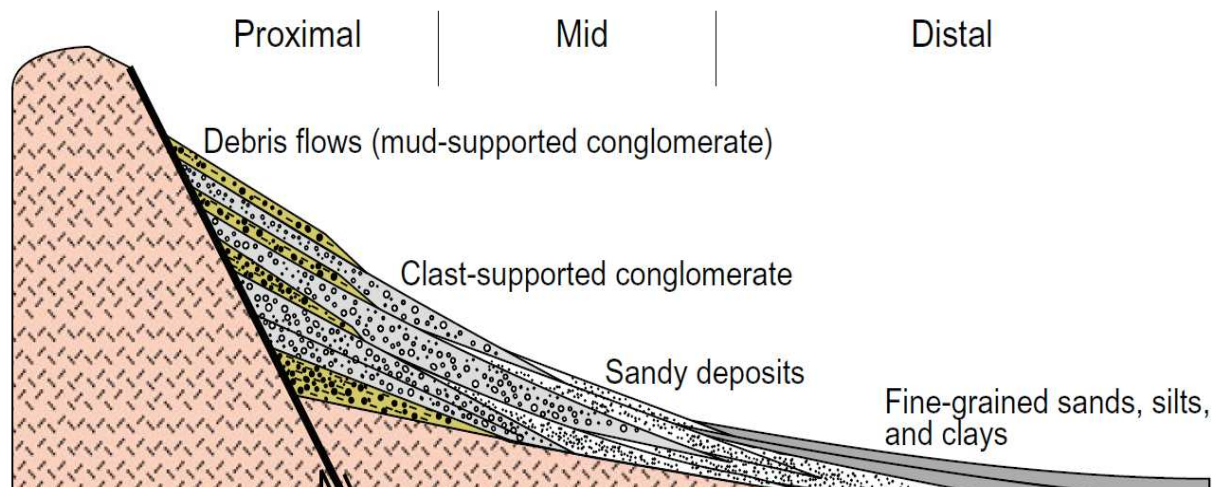


*Figure 1.16: Alluvial-fan cross section (After Rust and Koster 1984).*

### 1.3.2.3 Deltas

Deltas occur where a stream runs into an open water surface as a receiving basin. In deltas there may be a mix between fluvial and marine processes but one of them may be dominant. And the mix of different processes can help the geologist to distinguish a sedimentary rock issue from deltaic systems. When the stream is dominant and the sediments are mainly terrigenous, sand bodies can deposit and construct a clastic rock after diagenesis. The geometry of sand deposits varies depending upon the delta types and the transport processes upon the sediments. In river-dominated delta, sediments deposit as

elongated sand bodies perpendicular to the shore, whereas sand bodies in wave-dominated deltas are parallel to the shore. Deltas can also be tide dominated in some scenarios (see Figure 1.17):

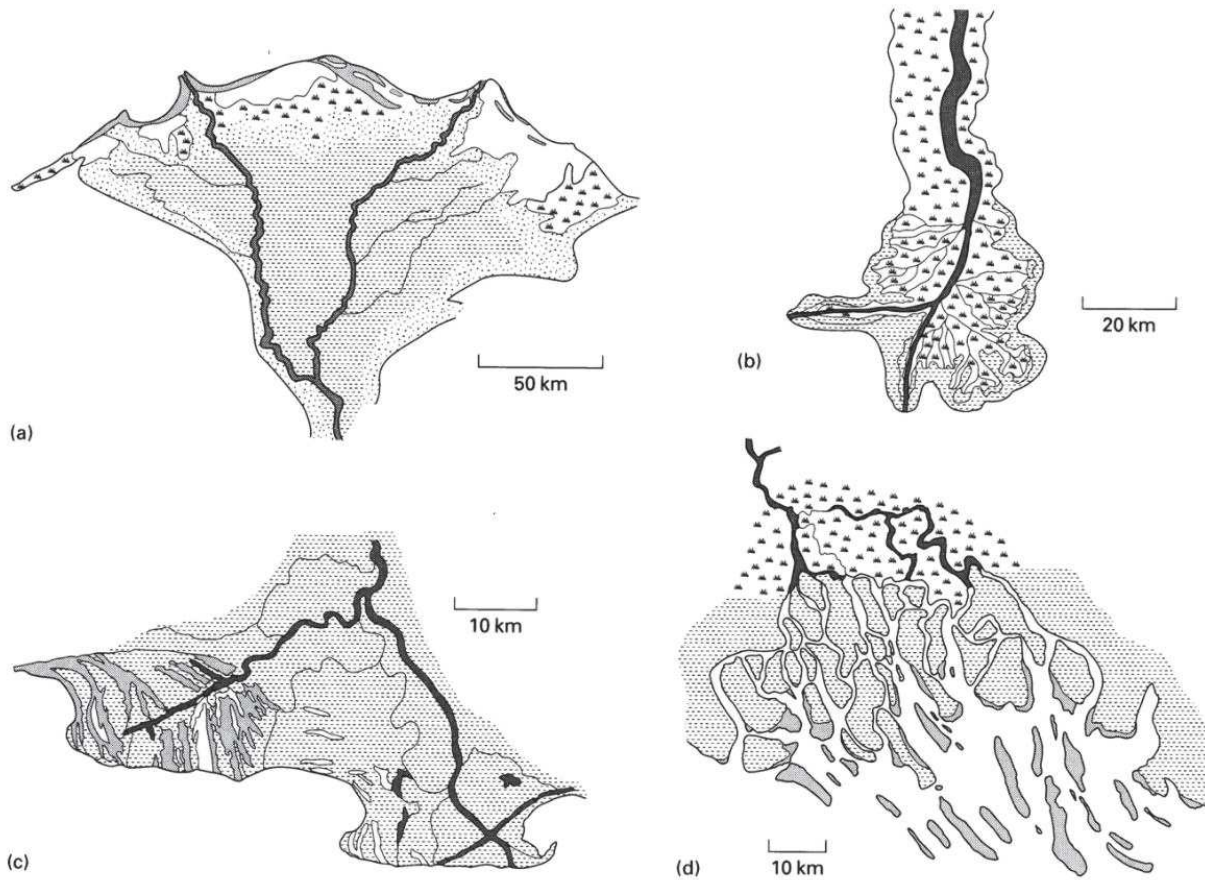


**Figure 1.17:** (a,c) wave dominated deltas, (b) river dominated delta, (d) tide dominated delta (Nichols, 2009).

The most common and documented type is the river dominated delta. It has three main geomorphic depositional environments:

- The bottomset called prodelta with fine sediments and mud
- The foreset called the delta front with sand bodies
- The topset called subaerial delta plain with a variety of sub-environments (levee, swamps, marshes, ...etc.)

The characteristic facies sequence of river-dominated deltas is the progradational coarsening-upwards sequence. Deltaic environments are very heterogeneous due to the different sub-environments with very different energy levels that may occur during the deposition.

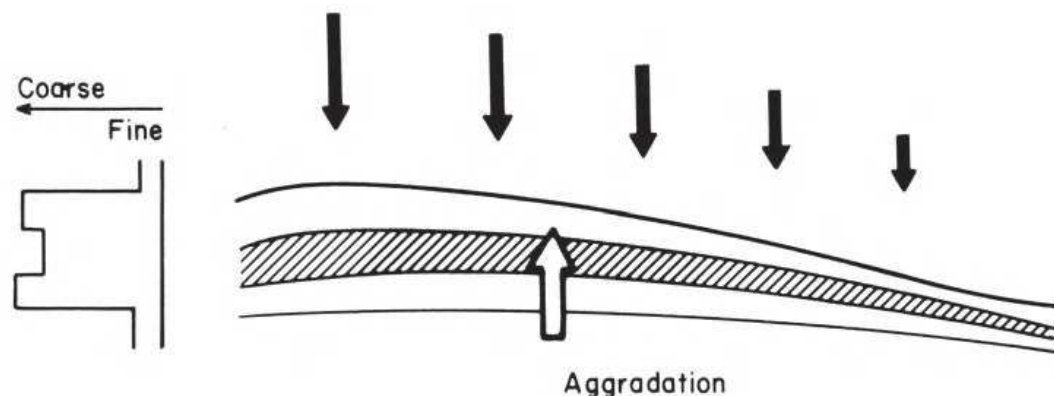
## 1.4 Sequence stratigraphy

Sequence stratigraphy attempts to reconstruct the history of sedimentation and basin filling of a given region. It integrates time and relative sea level changes to predict the migration and distribution of facies. It is relevant to distinguish the different bounds of different units and link the different sedimentary deposits. Sequence stratigraphy can be applied at different scales according to different needs. To decrease the uncertainty of the stratigraphy interpretation, it is also important to detect the main changes that could have happened during the deposition such as the variations in sediment supply and rate, relative base water level, tectonics ...etc. The sequence stratigraphy is based on defining time lines that correspond to the bounds of the different facies composing the sequence.

It exists three main depositional architectures of basin filling (see Figure 1.18):

- Aggradation, which consists on the vertical filling of the basin. It is characterized on the succession of several facies that present relatively constant sediment size.
- Progradation, where the sediments come from the margin and wash into the basin. It is characterized by a coarsening up of sediments in its facies.
- Lateral accretion, where the sediments are transported within the basin and accumulate against the margin. It is characterized by a coarsening down of sediments in its facies.

The three architectures may however be seen in the same environment. Understanding the basin filling and the description of the bedding type and the depositional architecture is fundamental to characterize the depositional environment which helps greatly on the characterization of the hydraulic properties of the sedimentary rocks.



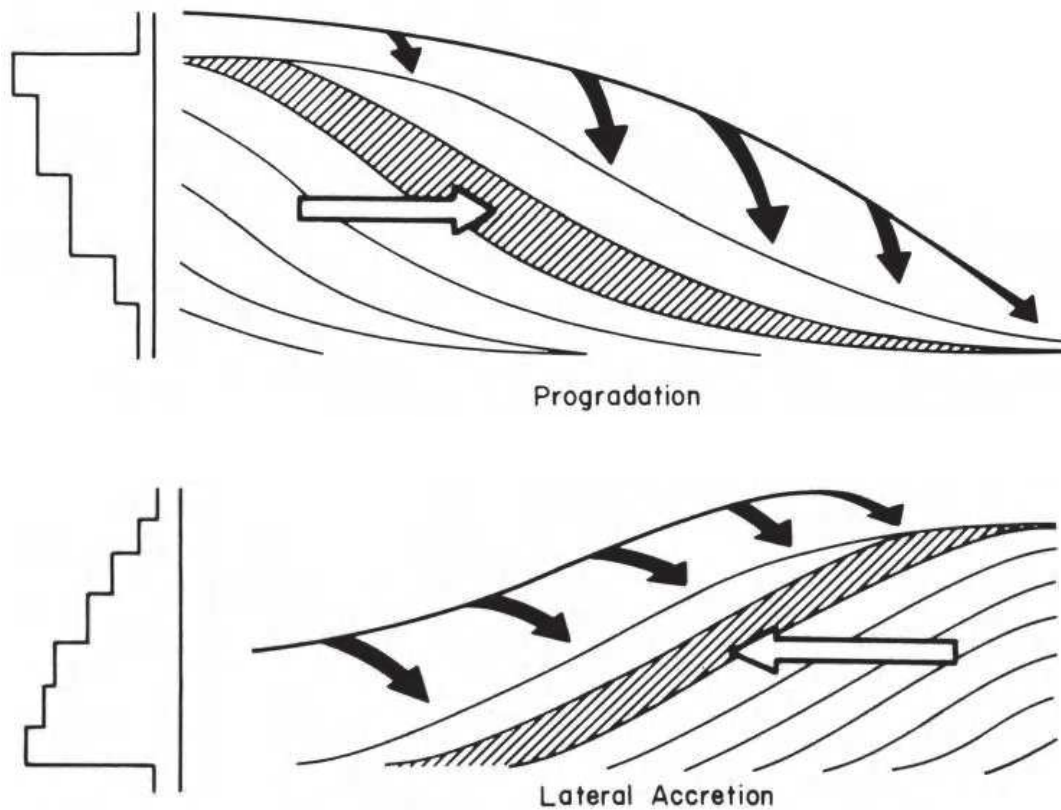


**Figure 1.18:** Three basic styles of basin-filling and their resultant bedding geometries and vertical textural sequences. (Galloway and Hobday, 1983).

The limits and boundaries that are marked by an important change in depositional processes, such as fall of base water level, are referred as sequence boundaries. With less importance and usually harder to detect, para-sequence boundaries are caused by smaller changes in the depositional conditions, an example can be a change of water salinity.

Multiple depositional events combine to produce a depositional episode. The depositional episode is a complex of facies sequences deposited in a period of relative base-level or tectonic stability (Frazier, 1974). Each depositional episode is ended by major transgressive events (see Figure 1.19).

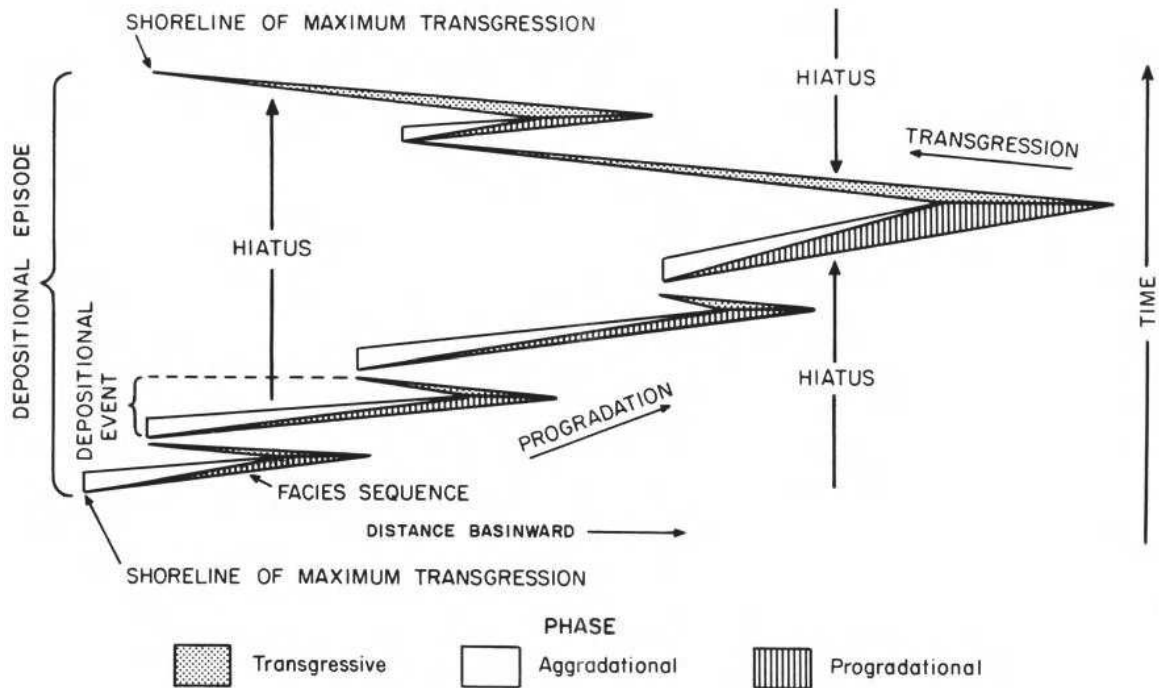


*Figure 1.19: Schematic time-distance diagram illustrating the temporal and spatial relationships of a depositional episode and the phases of its component depositional events (Frazier, 1974).*

The most important system tracts are (see Figure 1.20):

- A lowstand system tract (LST) occurs when the sediment supply rate outpaces the base level rise.
- A transgressive system tract (TST) occurs when the sediment supply rate is outpaced by the base level rise.
- A highstand system tract (HST) occurs when the rate of sea level rise drops below the sediment supply rate.
- Regressive systems tract forms occur at base water level fall.

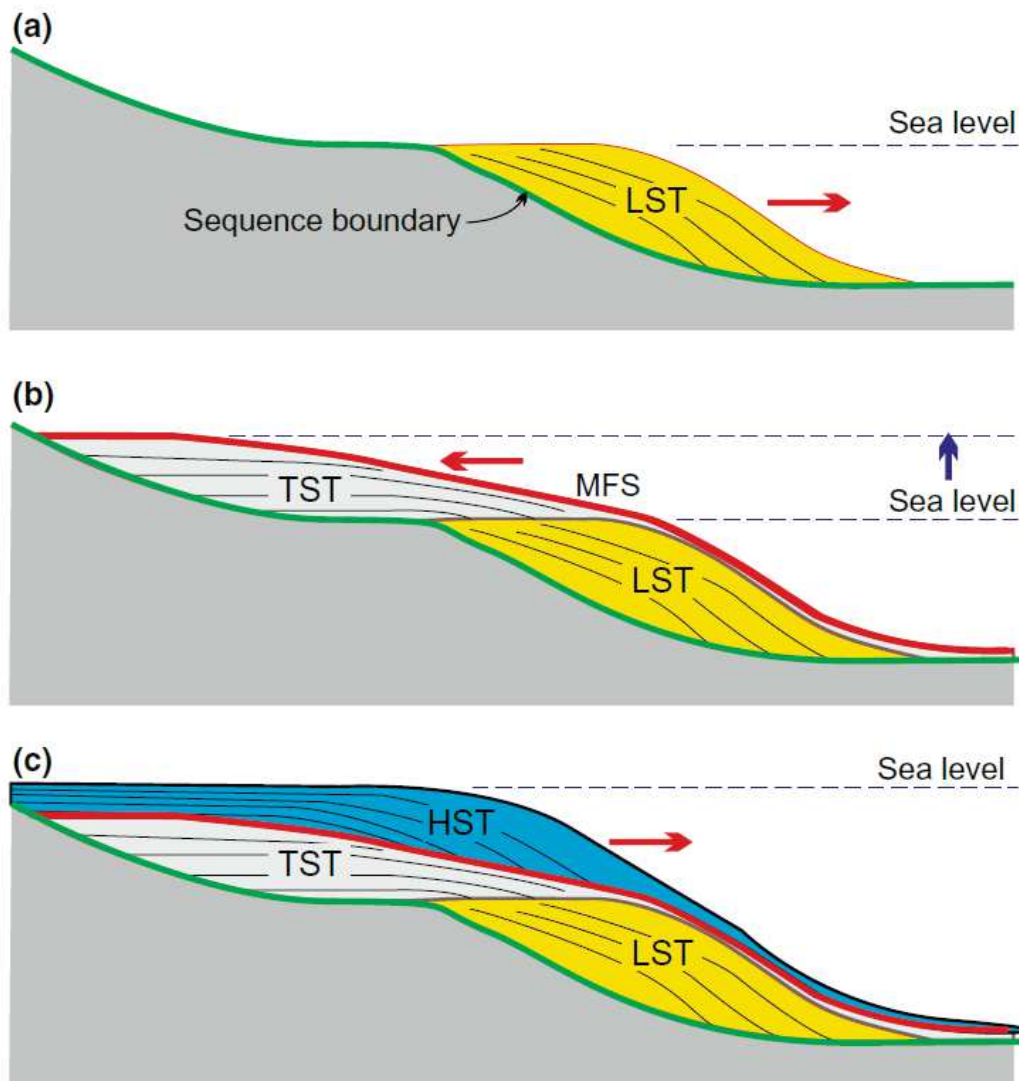


**Figure 1.20:** Basic sequence stratigraphy diagram. A) Lowstand system tract (LST) offlaps on the sequence boundary. B) Transgressive system tract (TST) onlaps the sequence boundary. Its upper boundary is the maximum flooding surface (MFS), which is the surface of deposition at its maximum landward position (i.e., time of maximum transgression). C) Highstand systems tract (HST) marks return of progradation with the offlap of strata on the MFS (Maliva 2016).

## 1.5 Influence of geological structure and processes

An aquifer is not only built from the deposit of sediments. Several processes occur during the burial and diagenesis of those sediments that can alter their properties. Earth crust has always been in a constant movement and tectonic events occurred so often, mountains got created, hills got eroded, the oceanic ridge and subduction process are still active...etc. such intense events can apply strong stresses on sedimentary rocks which causes several Physical deformations and changes. The sedimentary rocks can also face chemical processes that can change its structure and create secondary hydraulic properties. The main deformations of sedimentary rocks in aquifer characterization are:

- Fractures
- Faults
- Folds
- Dissolution and karst systems

Such alterations create even more complex and heterogeneous aquifer systems that make their characterization rather challenging.

### 1.5.1 Fractures

A fracture corresponds to a break, a joint or a crack issue from rock failure to mechanical stresses at yielding threshold. A sedimentary rock can deal with several fracturing episodes which can create distinct fracture sets. Fractures can be characterized by their density, orientation, length distribution, Aperture, fracture connectivity, number of sets, etc. the flow and the transmissivity of a fractured rock is governed by the fractures while fluid storage is mainly focused in the matrix.



*Figure 1.21: Example of a highly fractured rock showing two fractures sets (from shutterstock.com).*

Fractures can be classified in several ways: fractures can be open or closed, they can be linear, longitudinal, transverse or oblique. They can also be classified into different sets according to orientation or length. According to the condition of the bone, fractures can be complete or incomplete. Other classifications of fractures according to different parameters can also be found.

### 1.5.2 Faults

A fault is a discontinuity in the rock where the two sides shifted by a significant displacement in opposite directions. They are formed because of the stresses, tractions and forces generated by the

movement of tectonic plates, it can occur slowly or rapidly by dissipating energy through earthquakes. Faults dimensions can vary from small faults in bedding to regional faults impacting the whole studied sequence. The faults can be categorized according to the direction of their slip into (see Figure 1.22):

- Dip-slip fault: can be subdivided into normal or reverse fault where the offset is in the vertical direction
- Strike-slip fault: can be sinistral or dextral where the offset is in the horizontal direction parallel to the fault
- Oblique-slip fault: is the combination of the two types, dip and strike slip

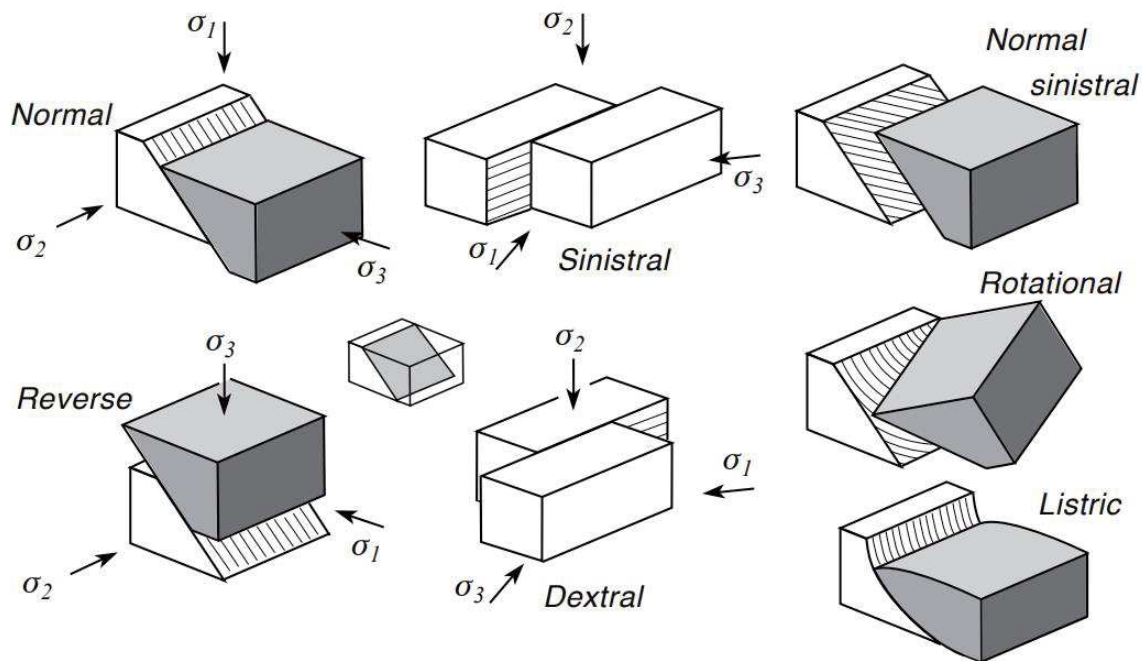


*Figure 1.22: Different types of faults.*

The fault zone is characterized by the core zone where the discontinuity that initiated the slip is and where the rock got smashed into reworked sediments. A fault zone can have one or more core zones. Around the core zone, it exists a damaged zone with a fractured rock. The fractures intensity in the damaged zoned is relatively high. (see Figure 1.23)

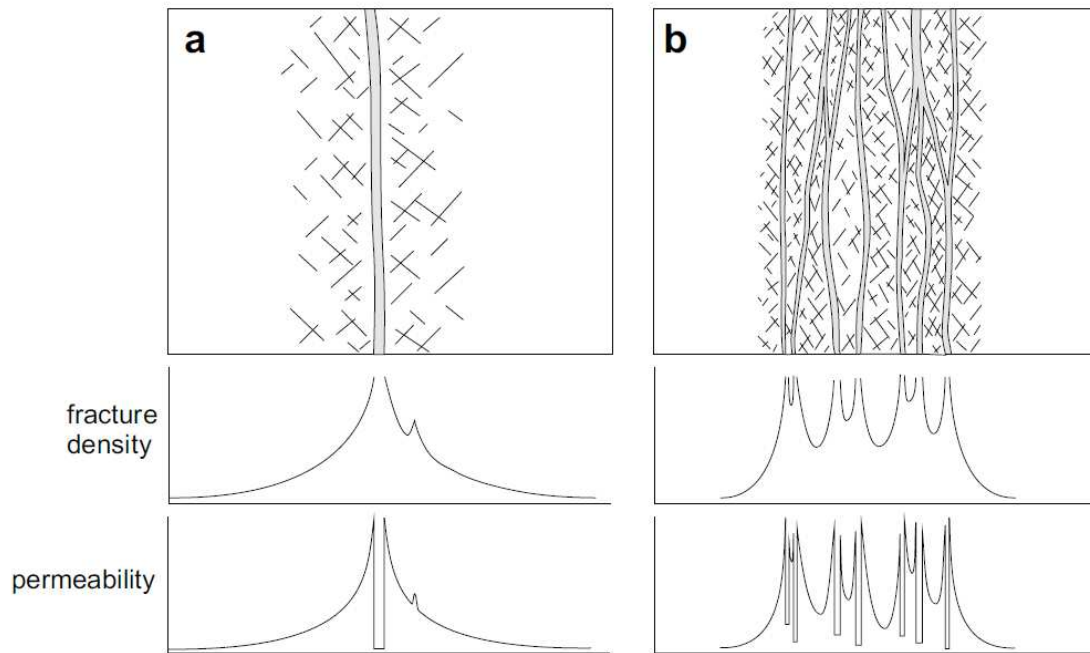


*Figure 1.23: Some physical properties of fault zones related to their structure (damage zone and fault core). (a) Single fault core and (b) multiple fault core, which illustrates the resulting complexity in characterizing the resultant properties (Faulkner 2010).*

### 1.5.3 Folds

Folds are geological structures formed from the bent and curving of sedimentary strata that were originally planar. Folds result from the slow deformation of rocks which usually happens deep underground where the rocks are under pressure and high temperature. If the medium is cold and the rock is brittle, that rock won't behave in a plastic manner but the stress and pore pressure conditions will make it susceptible to fracturing instead. Folds can be observed at different scales, from microscopic to mountain size scale. They can be caused by stress, pore pressure, temperature gradient or even formed during the sedimentation.

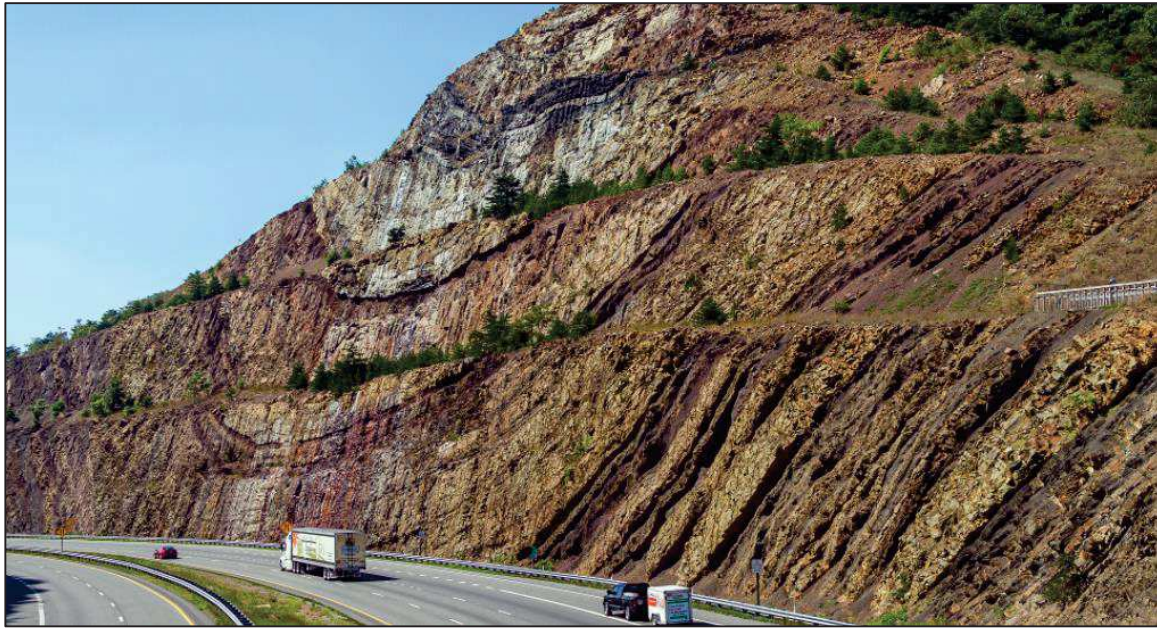


*Figure 1.24: Example of a fold forming a syncline in Interstate 68 road cut in Sideling Hill in western Maryland (Wikipedia commons).*

Folds are characterized by their size, shape, symmetry, tightness and deformation classes. They are the source of the observed synclines and anticlines. Folds are abundant and they change the hydraulic properties of its rock which makes their characterization important in the total aquifer/reservoir characterization. Hudleston and Treagus (2010) reviewed the most relevant analysis done on folds where they focused on: information on rheology, strain and deformation history, locally or regionally.

#### **1.5.4 Dissolution and karst systems**

At late times of the diagenesis, a sedimentary rock may face a dissolution phase which causes the development of karstified systems. The dissolution mainly initiates in fractures or bedding discontinuities and develop into larger connected karsts through a positive feedback loop. Karstified aquifers show extreme heterogeneities with the existence of secondary and tertiary hydraulic properties that govern the flow. Limestones are the rocks that reacts to the presence of water and carbon dioxide and thus dissolve its calcite. Dolomite and gypsum are also rocks that are subject to dissolution. Hartmann et al. (2014) showed the relevance of the characterization of karst systems for its potential in water resources supply. He reviewed the exploration methods and the data required for karst modelling.

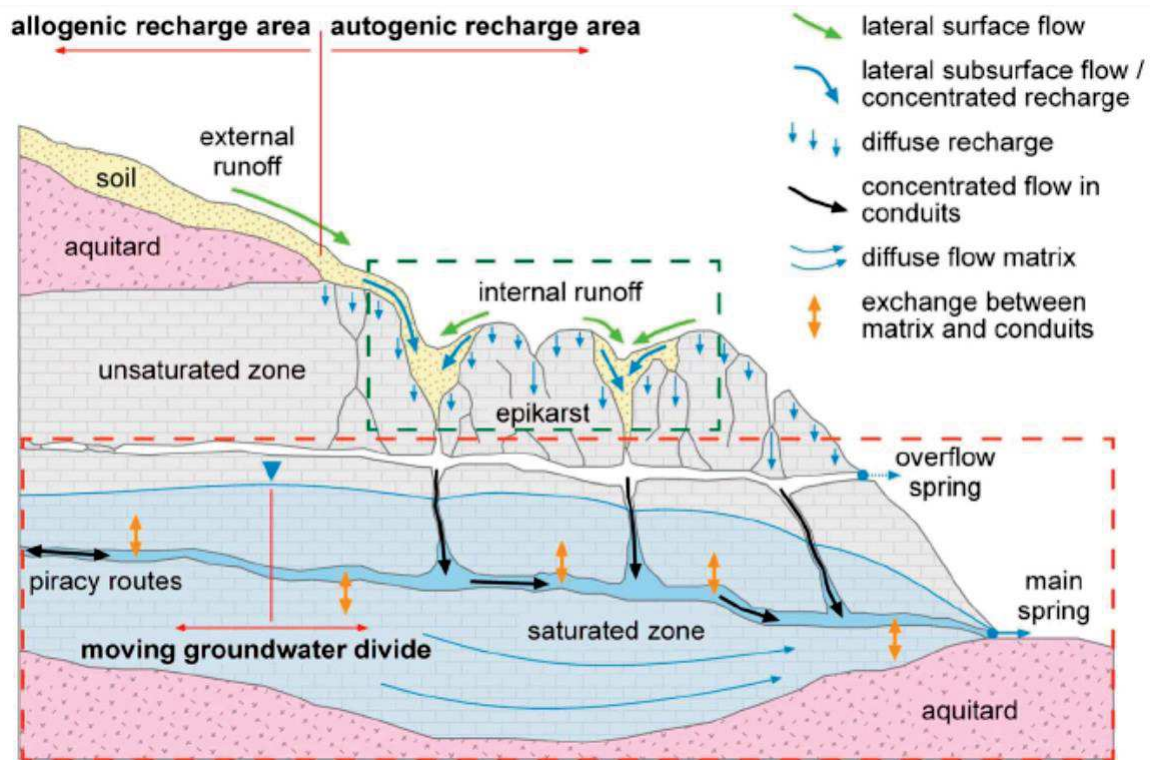


*Figure 1.25: Conceptual model of a karst system including all characteristic karst processes; dark green and red dashed lines represent the soil/epikarst and the groundwater subsystems (Hartmann et al. 2014).*

## 1.6 Geological heterogeneities and flow

Hydraulic properties are strongly correlated to the sedimentary rock at its microscopic scale (grain size, pore size and shape and cementation) and at its larger scales (bedding, clay layering, geological structures, depositional environment, etc.). Such a link pushes researchers to interpret the geological history about the formation of that rock through the whole processes: sedimentation, diagenesis and potential secondary processes after its uplift. The way the sediments and the grains are assembled and altered through time of deposition and diagenesis is the origin of the high observed heterogeneities and anisotropies. Characterizing different properties enhance the characterization of aquifers/reservoirs and lead into the construction of better three-dimensional geological and numerical model.

### 1.6.1 Importance of the scale

The hydraulic properties of aquifers/reservoirs can vary considerably with changing the scale of investigation. Groundwater flow and solute transport are very complex to reproduce. Hence, researchers often divide and simplify the characterization of these reservoirs through different scales to better understand their complex behaviors in an easier way.

The main scales in aquifer characterization can be summarized as follow

- Pore scale: investigation about grain size and shape, pore size and connectivity, cementation, etc. Such properties affect greatly the hydraulics and fluid saturation.
- Laboratory scale: studies on samples (cores, plugs, blocks, water samples...). They allow to obtain direct measurements of hydraulic properties of the rock at the scale of the sample size.
- Well scale: characterizes mainly the vertical profile of the different penetrated layers and allows quickly the construction of a litho-facies model. Well loggings investigate the near well are.
- Site scale: is related to the size of the zone covered by wells and experimental tests. It investigates the hydrodynamics between the wells and nearby area.
- Reservoir scale: is the total investigated unit which is isolated partially or totally by impermeable seals. It allows the investigation of the boundaries of the aquifer/reservoir.
- Regional scale: mainly about the geological model and sedimentology of the region surrounding the studied aquifer/reservoirs.

### 1.6.2 Heterogeneity

Heterogeneity is the spatial variation in hydraulic, transport, and geochemical properties through the medium (e.g. sedimentary rock of aquifers). All aquifers are heterogeneous with different degree of heterogeneity. The degree of heterogeneity is related to the scale of the study. In a porous media, it exists aquifers that could be considered with a very low degree of heterogeneity, however, that degree increases with the decrease of the scale. A fundamental challenge in aquifer characterization is the development of a data collection and modeling approach that captures the scale of heterogeneity. For example, several empirical equations were proposed to estimate the hydraulic conductivity of a rock knowing the size of the pore scale properties. Rosas et al. (2010) reviewed different empirical equation and compared their estimated values to the measured hydraulic conductivity through samples at different depositional environments and proposed modifications to decrease the uncertainty of their estimation. The scale of an aquifer heterogeneity can extend from microscopic to regional scale. Sampling in underground aquifers remains very challenging and only few sparse data are available.

The heterogeneity issue from pore and grain sizes is referred to as the primary hydraulic properties. Different empirical methods arisen to try to estimate the hydraulic properties from the microscopic heterogeneity (Rosas et al., 2014). The sedimentary rock is often subject to geological process that may create secondary and tertiary hydraulic properties which makes the system strongly heterogeneous.

### 1.6.3 Anisotropy

Anisotropy is characterized when hydraulic properties vary with direction. For instance, sedimentary rocks have bigger horizontal conductivity compared to the vertical direction. However, tectonics can

alter the sequence: dips can be changed, folds can be formed or even fractures and faults. Moreover, heterogeneous media creates anisotropy which can greatly vary with scale. The scale of investigation is very important when talking about anisotropy, advanced flow simulations use a three dimensional permeability tensors to represent both heterogeneity and anisotropy instead of using just one geometric mean in each cell. Within one sedimentary body, flow tends to be perpendicular to the direction of deposition; clay thin layers can be seen in between laminae which confront the flow. In the other hand, at larger scale with different sedimentary bodies, flow will prefer to pass through the sand bodies with greater permeability. Moreover, in a fractured aquifer, the direction of the main flow will follow the direction of the main fracture set. Heterogeneity and anisotropy are related and both control groundwater flow and solute transport in addition to hydraulic gradients.

#### **1.6.4 Connectivity**

Heterogeneity and anisotropy characterize the spatial variation of the hydraulic properties and identify the preferred flow direction. During deposition, different bodies with different grains size are gather next to each other. The main objective of characterizing the heterogeneity is to identify the sand bodies with the greatest hydraulic conductivities that will mainly control the flow. Another important parameter is the connectivity between those sand bodies. An aquifer can show a low effective transmissivity if the main sand bodies are not connected between them even though these sand bodies are highly permeable. Connectivity can be characterized and discussed in different ways according to different scenarios. For example, by defining the continuity of low permeability strata that may isolate the sand bodies, or by investigating the degree of connectivity between two locations (e.g. wells), or in a fractured/karstified aquifer by finding if the fractures/karsts are connected at a large scale.

## References

- B. Makaske, Anastomosing rivers: a review of their classification, origin and sedimentary products *Earth Sci. Rev.*, 53 (2001), pp. 149-196
- Bathurst, R. G. C., 1971, *carbonate Sediments and their Diagenesis*: Elsevier, New York, pp. 321-543.
- Bridge, J. S. (2001) Characterization of fluvial hydrocarbon reservoirs and aquifers: problems and solutions: *AAS [Asociación Argentina de Sedimentología]* 8(2): 87–114.
- Bridge, J. S. (2006) Fluvial facies models: Recent developments. In H. W. Posamentier & R. G. Walker (Eds.) *Facies models revisited*. Special Publication No. 84 (pp. 85–170). Tulsa: SEPM (Society for Sedimentary Geology).
- Bridge, J. S., & Mackey, S. D. (1993) A theoretical study of fluvial sandstone body dimensions. In S. S. Flint & I. D. Bryant (Eds.), *Geological modeling of hydrocarbon reservoirs*. Special Publication 15 (pp. 213–236). International Association of Sedimentologists.
- Budd DA 2002 The relative roles of compaction and early cementation in the destruction of permeability in carbonate grainstones: a case study of the Paleogene of west-central Florida, U.S.A. *J Sediment Research* 72, 1:116-128
- Cant, D. J., & Walker, R. J. (1978) Fluvial processes and facies sequences in the sandy braided South Saskatchewan River, Canada. *Sedimentology*, 25, 625–648.
- Cant, D. J. (1982) Alluvial facies models and their application. In P. A. Scolle, P.A. & D Spearing (Eds.), *Sandstone depositional environments*. Memoir 31 (pp. 115–138). Tulsa: American Association of Petroleum.
- Cook, P. G. (2003) *A guide to regional groundwater flow in fractured rock aquifers*. Adelaide: CSIRO.
- D.R. Faulkner, C. Jackson, R. Lunn, R. Schlische, Z. Shipton, C. Wibberley, M. Withjack. A review of recent developments concerning the structure, mechanics and fluid flow properties of fault zones. *J. Struct. Geol.*, 32 (2010), pp. 1557-1575
- De H.-E. Reineck, I.B. Singh, *Depositional Sedimentary Environments: With Reference to Terrigenous Clastics*
- Dott, R. H. (1964) Wacke, graywacke and matrix; what approach to immature sandstone classification? *Journal of Sedimentary Petrology*, 34, 625–632.
- Dunham, R.J., 1962. Classification of carbonate rocks according to depositional texture. *Mem. Am. Assoc. Pet. Geol.*, 1: 108-121.
- Faulkner, D.R., A.C.Lewis, and E.H.Rutter. 2003. On the internal structure and mechanics of large strike slip fault zones.: field observations from Carboneras fault in southeastern Spain. *Tectonophysics* 367 (3-4): 235-25
- Folk, R.L., 1959. Practical petrographic classification of limestones. *Bull. Am. Assoc. Pet. Geol.*, 43: 1-38
- Frazier, D.E. 1974. Depositional episodes: their relationship to the Quaternary stratigraphic framework in the northwestern portion of the Gulf Basin. *Bur. Econ. Geol. Univ. Texas, Austin, Geol. Circ.* 71-1.
- G. Shanmugam, in *Encyclopedia of Geology (Second Edition)*, 2021
- Galloway, W.E. and Hobday, D.K. 1983. *Terrigenous Clastic Depositional Systems; Applications to Petroleum, Coal, and Uranium Exploration*, 423. New York: Springer-Verlag.

- Gingras, M.K., MacEachern, J.A., Dashtgard, S.E., Zonneveld, J.-P., Schoengut, J., Ranger, M.J., Pemberton, S.G., 2012. *Estuaries. Dev. Sedimentol.* 64, 467–497. <https://doi.org/10.1016/B978-0-444-53813-0.00016-2>.
- Hardie, L. A. (1987). Dolomitization; a critical view of some current views. *Journal of Sedimentary Research*, 57(1), 166–183. <https://doi:10.1306/212F8AD5-2B24-11D7-8648000102C1865D>
- Hartmann, A., Goldscheider, N., Wagener, T., Lange, J., and Weiler, M. (2014), Karst water resources in a changing world: Review of hydrological modeling approaches, *Rev. Geophys.*, 52, 218– 242, <https://doi:10.1002/2013RG000443>.
- Harvey, A. M., Mather, A .E., & Stokes, M. (2005) Alluvial fans: geomorphology, sedimentology, dynamics – introduction. A review of alluvial fan research. In A. M. Harvey, A. E. Mather, & M. Stokes (Eds.) *Alluvial fans: Geomorphology, sedimentology, dynamics*. Special Publication 251 (pp. 1–7). London: Geological Society.
- IKEDA, S. 1981 Self-formed straight channels in sandy beds. *J. Hydraul. Div. ASCE* 107 (4), 389-406.
- James, N.P. 1984. Shallowing-upward sequences in carbonates, in Walker, R.G. ed. *Facies Models: Geological Association of Canada, Geoscience Canada, Reprint Series 1: 213–228*.
- Kovacs, Agnes; Parker, Gary (1994). A new vectorial bedload formulation and its application to the time evolution of straight river channels. *Journal of Fluid Mechanics*, 267(-1), 153–. [doi:10.1017/S002211209400114X](https://doi:10.1017/S002211209400114X)
- Lucia, J. F., Kerans, C., & Jennings, J. W., Jr. (2003) Carbonate reservoir characterization. *Journal of Petroleum Technology*, June 2003, 70–72.
- Matthew A. Perras & Mark S. Diederichs, 2011, The importance of classification for carbonates and mudrocks in engineering, CGS Geotechnical conference
- Miall, A. D. (1985) Architectural-element analysis: A new method of facies analysis applied to fluvial deposits. *Earth Science Reviews*, 22, 261–308.
- Moore, C. H. (2001) Carbonate reservoirs: porosity evolution and diagenesis in a sequence stratigraphic framework. *Developments in Sedimentology* 55. Amsterdam: Elsevier.
- Mousavi, Maryam A.; Prodanovic, Maša; Jacobi, David (2013). New Classification of Carbonate Rocks for Process-Based Pore-Scale Modeling. *SPE Journal*, 18(2), 243–263. <https://doi:10.2118/163073-PA>
- P.J. Hudleston, S.H. Treagus, 2010. Information from folds: a review *J. Struct. Geol.*, 32 (2010), pp. 2042-2071, <https://doi:10.1016/j.jsg.2010.08.011>
- Palmer, A. N. (1991) Origin and morphology of limestone caves. *Geological Society of America Bulletin*, 103, 1–21.
- Parker, G., Shimizu, Y., Wilkerson, G.V., Eke, E.C., Abad, J.D., Lauer, J.W., Paola, C., Dietrich, W.E. and Voller, V.R. (2011), A new framework for modeling the migration of meandering rivers. *Earth Surf. Process. Landforms*, 36: 70-86. <https://doi.org/10.1002/esp.2113>
- Pomar Luis. Types of carbonate platforms: a genetic approach in: *Géologie Méditerranéenne*. Tome 28, numéro 1-2, 2001. *Anatomy of Carbonate Bodies / Anatomie des corps carbonates*. International Meeting / Colloque international. Marseille, 9-12 mai 2001, France. pp. 139-143 ; doi : <https://doi.org/10.3406/geolm.2001.1706>
- Reading, H. G., 1978, *Sedimentary Environments and Facies*: Elsevier, 557 p.

- Renard, P. (2007), Stochastic Hydrogeology: What Professionals Really Need?. *Groundwater*, 45: 531-541. <https://doi.org/10.1111/j.1745-6584.2007.00340.x>
- Robert. G. Maliva, 2016, Aquifer Characterization Techniques Schlumberger Methods in Water Resources Evaluation Series No. 4 Fort Myers, FL USA. DOI 10.1007/978-3-319-32137-0
- Rosas, J., Lopez, O., Missimer, T.M., Coulibaly, K.M., Dehwah, A.H., Sesler, K., Lujan, L.R. and Mantilla, D. (2014), Determination of Hydraulic Conductivity from Grain-Size Distribution for Different Depositional Environments. *Groundwater*, 52: 399-413. <https://doi.org/10.1111/gwat.12078>
- Rust, B. R., & Koster, E. H. (1984) Coarse alluvial deposits. In R.G. Walker (Ed.), *Facies models* (pp. 53–69). Toronto: Geological Society of Canada.
- Schiebel, R., 2002. Planktic foraminiferal sedimentation and the marine calcite budget. *Global Biogeochem. Cy.* 16, 1065. <https://doi:10.1029/2001GB001459>.
- Scholle, P. A. and Ulmer-Scholle, D. S, 2003, *A Color Guide to the Petrography of Carbonate Rocks*: AAPG Memoir 77, 474 p
- Schumm, S. A. (1977) *The fluvial system*. New York: John Wiley & Sons.
- Seckler, David; Barker, Randolph; Amarasinghe, Upali (1999). "Water Scarcity in the Twenty-first Century". *International Journal of Water Resources Development*. 15 (1–2): 29–42. <https://doi:10.1080/07900629948916>
- Selley, Richard C. (2000). *Applied Sedimentology || Depositional Systems*. 181–305. doi:10.1016/B978-012636375-3/50007-0
- Selley, R C. *Ancient sedimentary environments and their subsurface diagnosis*, third edition. United States: N. p., 1985. Web.
- Sparks, Andrew G.; Rankey, Eugene C. (2013). Relations between geomorphic form and sedimentologic-stratigraphic variability: Holocene ooid sand shoal, Lily Bank, Bahamas. *AAPG Bulletin*, 97(1), 61–85. <https://doi:10.1306/05101211125>
- Tucker, M. E., & Bathurst, R. G. C. (Eds.) (1990) *Carbonate diagenesis: International Association Sedimentologists Reprint Series 1*. Oxford: Blackwell Scientific Publications.
- Tucker, ME and Wright, VP, 1990. *Carbonate Sedimentology*. Blackwell, 482p.
- Walton, William C. (November 1990). *Principles of Groundwater Engineering*
- Wilson, J. L., 1975, *Carbonate Facies in Geologic Time*: New York, Springer-Verlag, 471p.
- Wright, V.P., 1992. A revised classification of limestones. *Sediment. Geol.*, 76: 177-185

## CHAPTER 2

**Résumé :** Dans ce chapitre, l'histoire géologique régionale et le contexte sédimentaire côtier (calcaires coquillers) relatifs à la zone d'étude comprenant le site expérimental est tout d'abord présenté. Dans un second temps, les différentes mesures pétrophysiques, géologiques, géophysiques et hydrauliques acquises à différentes échelles (échelle régionale, échelle du site expérimental, échelle du forages) et utilisées dans la suite du travail, sont décrites de façon exhaustive.



## 2. EXPERIMENTAL SITE AND DATA (MOLLUSC SHELL LIMESTONE CONTEXT)

This chapter describes the experimental site that is used as a field application of the new developed approaches. It contains the main available data about the site. Firstly, we start by telling the geological history of the area based on previous investigations. Then, different data obtained from geophysical, petrophysical and hydrogeological surveys are presented. And finally we show the different conceptual and numerical models that are investigated to study the aquifer of the experimental site. this chapter can be delivered as a data paper accompanied with the corresponding data of the different surveys. A significant prospection work was carried out in order to select an experimental site meeting the following criteria:

- suitable type of land: heterogeneous detrital sedimentary rocks with absence of karstification,
- water table level close to the surface,
- richness of outcrops for in situ measurements,
- low pressure,
- site with areas without particular uses and little frequented,
- existing previous studies about the area,
- possibility of obtaining drilling authorization.

## 2.1 Experimental site in mollusc shell limestones context (Font d'Armand)

### 2.3.1 Localization and set up

The study area is located in Southern France, 20 km northeast of Montpellier (Figure 2.1c). The study area is located in the limestone of the Miocene era. The experimental site is built within the Castries incised valley (Rubino et al. 1990; Besson, 2005). The valley is composed of Burdigalian limestones.

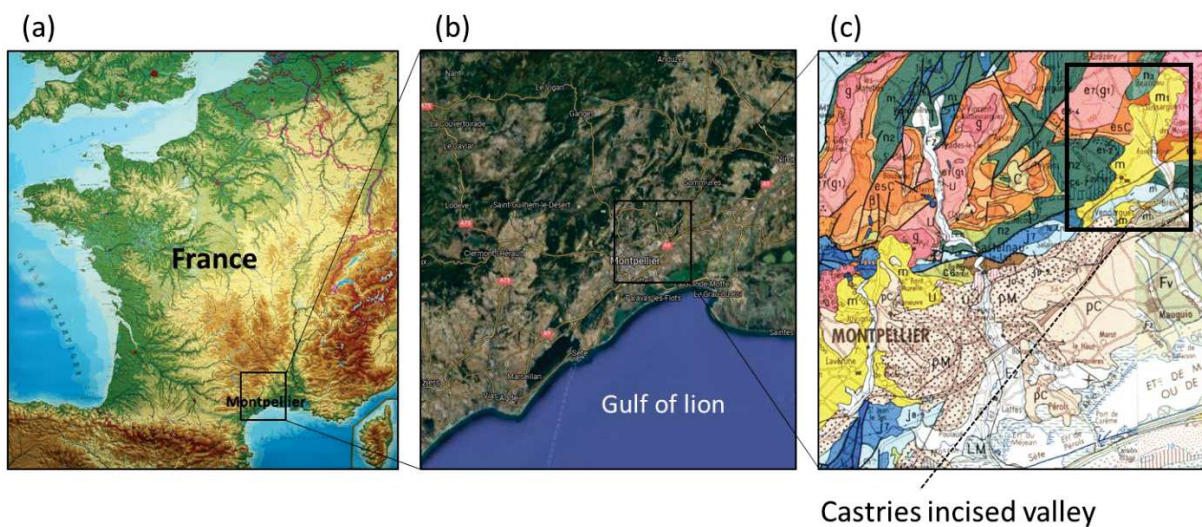


**Figure 2.1:** Geolocalization of the study area. A) Geo-relief map of France (from world maps online). B) zoom in of Montpellier region (from google maps). C) geological map showing the study area and its position compared to the city of Montpellier (from Infoterre; m: Miocene).

In 2015, a location where to set up the experimental site is picked near Sussargues for water research purposes. This choice is the result of a geological campaign that was done to find the optimal location. This location is mainly fixed because it is adjacent to an old Quarry which offers valuable outcrops.

Within the experimental site, 17 vertical wells were drilled; 13 boreholes during the first drilling phase and the remaining 4 were drilled during a second phase three years later. The new 4 wells were added to have a new larger scale of investigation. Contrary to the wells of the first phase which are within a square of 50 m by 50 m with a distance 7.5~10 m between them, the wells of the second phase are relatively farther (50~100 m distance from the wells of the first phase) (see Figure 2.2).

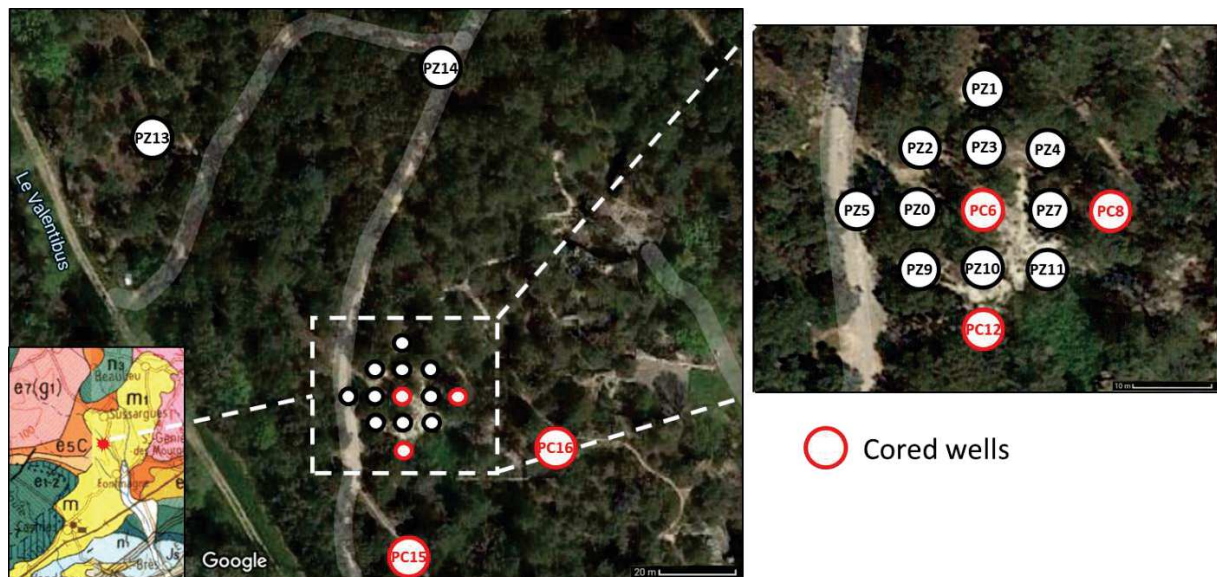


**Figure 2.2:** Localization of the experimental site in the Castries incised valley (geological map from *infoterre*; m:Miocene) and the distribution of the wells on top of a satellite view (google maps). The red circles refer to a fully cored wells. PZ0 to PC12 are drilled during the first phase. PZ13 to PC16 are drilled during the second phase.

All the wells have a depth of about 30 m and are fully-penetrating wells, since they crosscut the whole late Burdigalian strata, down to the roof of the mid Burdigalian which presents a very low permeability.

### 2.3.2 Geological history of study area

The experimental site is in an area which is located within the Miocene Rhodano-Provençal Basin (BMRP). The Miocene Rhodano-Provençal Basin is a foreland basin of the Western Alps. Numerous tectonic and erosional events had occurred during the Ante-Miocene period and considerably impacted its topography. The important result of the deformation is the division of the main basin into different sub-basins. The different sub-basins got further deformation caused by several episodes of fluvial incisions during the Miocene era. Later on, with the help of the tidal fluctuation and the sea level changes, these incisions might be filled with marine deposits. For instance, The Castries basin has been filled by cold water carbonates (Rubino et al., 1990; Lesueur et al., 1990; Besson et al., 2002; Besson, 2005). Moreover, it is located not far from alpine siliciclastic source. They have been accumulated and sorted by currents in the form of tidal dunes clearly identified in the quarry's outcrop. The valley of Castries is covered by Peilhou fault from North West and by Fontmagne fault from South East. This depression was then filled with up to 200 m of Burdigalian carbonate sediments. Figure 2.3 represents a paleo-geographic map of the Miocene Rhodano-Provençal Basin showing the upper Burdigalian sea and the different documented incised valleys of the area.

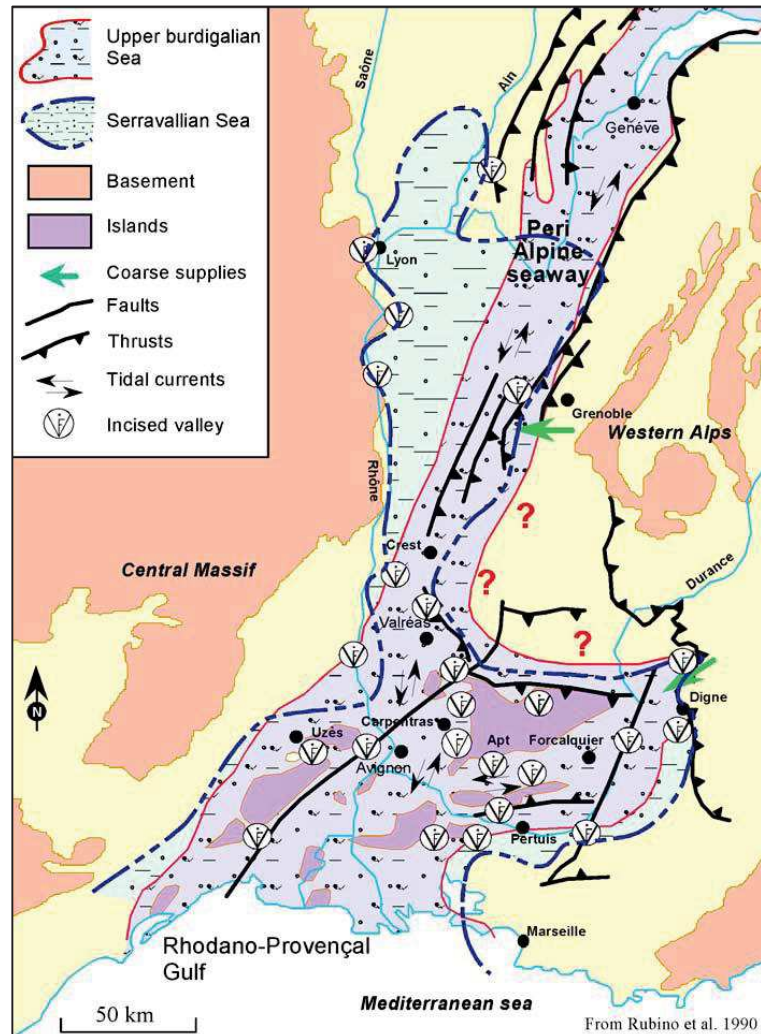


**Figure 2.3:** Paleo-geographic map of the Miocene Rhodano-Provençal Basin showing the upper Burdigalian sea and the different documented incised valley of the area (from Rubino et al. 1990).

The most singular character of the Miocene transgression is certainly the filling of numerous incised paleo-valleys (Rubino et al., 1990; Besson et al., 2002b; Reynaud et al. 2006; Besson, 2005) assured firstly by Early Miocene deposits. Figure 2.4 shows a paleo-geographic map of the gulf of lion during the early Burdigalian and highlights the incised valley of Castries.

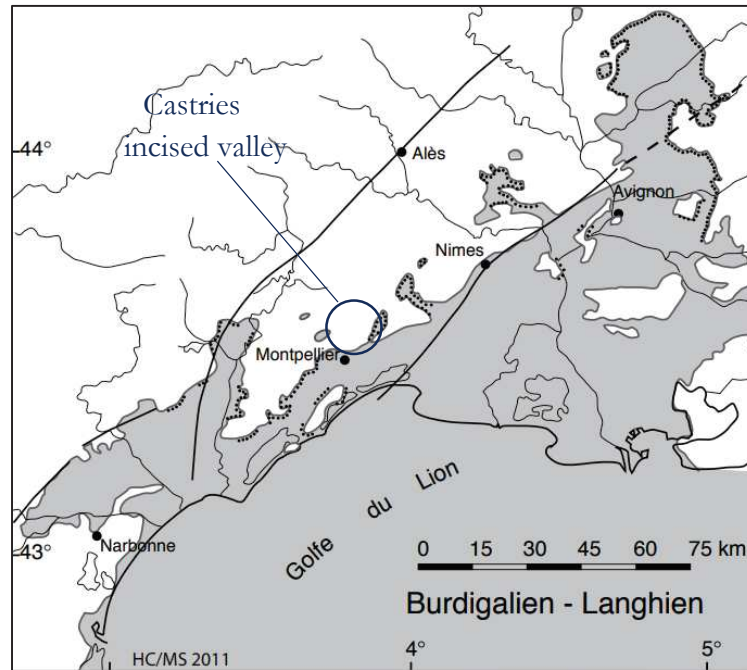


*Figure 2.4: paleo-geographic map of the gulf of lion at lower Burdigalian period (Seranne, 2012).*

The incision of these valleys is carried out in contrasted bedrocks. By the width, the fluvial erosion can be at least related to a fall of the base level and/or a tectonic uplift. It can also be related to the migration of the fore-bulge of the Western Alps (Rubino and Clauzon, 1996). This first set of incised valley fills is completed by two others (Besson et al., 2003): ones located at the base of Middle Miocene and the others at the base of Late Miocene, before the Messinian crisis record (Clauzon, 1979, 1982; Clauzon et al., 1996).

The different incised valleys of the Rhodano-Provençal basin which are located far from the alpine thrust belt and thus from siliciclastic sources, were filled, during the Miocene, by almost only cool water carbonates (Reynaud et al., 2006). Previous sedimentology investigation of the area concluded that the deposits are from tide dominated estuarine to offshore bars and dunes (see Figure 2.5) (Lesueur et al., 1990; Rubino et al., 1994; Dexcote, 2001; Parize et al., 2001). Indeed, they are mostly skeletal origins, sorted and accumulated by currents (Reynaud et al., 2006) including Castries incised valley. Figure 2.5 shows the type of deposits in a tidal dominated estuarine environment.

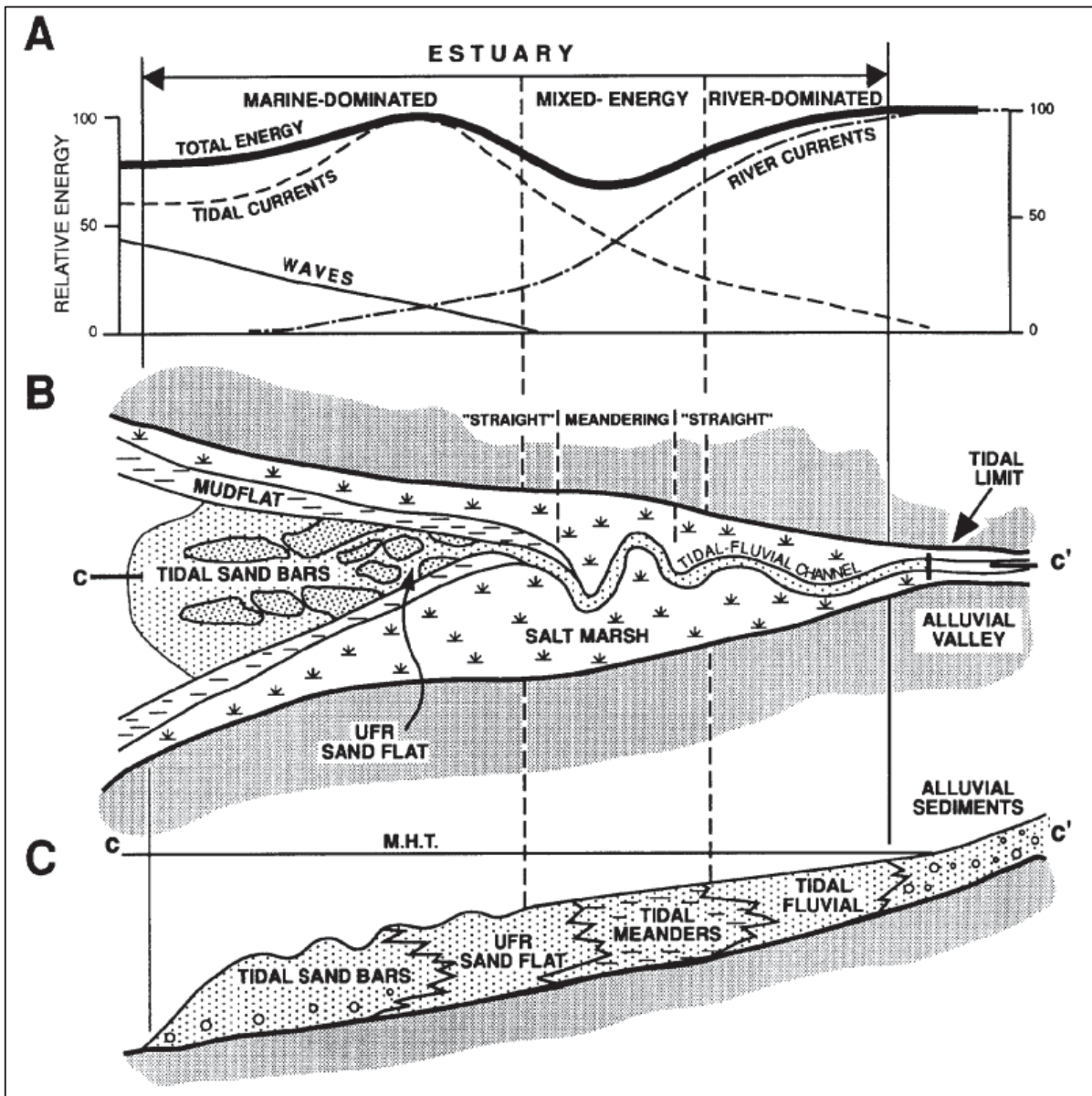


*Figure 2.5: Distribution of A) energy types, B) morphological elements in plan view, and C) sedimentary facies in longitudinal section within an idealized tide-dominated estuary. URF = upper flow regime; M.H.T. = mean high tide. The section in C is taken along the axis of the channel and does not show the marginal mudflat and salt marsh facies; it illustrates the onset of progradation following transgression, the full extent of which is not shown (from Dalrymple et al. 1992).*

The valley of Castries was filled during the Miocene by mollusc shells limestone which was part of the Aquitano-Burdigalian incised valley network. They came to rest discordantly on different layers including: The lower Cretaceous formations affected by the "fold of Montpellier," the Eocene formations pleated in a Syncline with a N120 axis, and finally the Oligocene formations of the Restinclières's rift basin.

After previous work and field trips to the near quarries of the area (Rubino et al., 1990; Lesueur et al., 1990; Besson, 2005), one can conclude that the valley of Castries is mainly tidal sand bars and dunes. And the rapid filling of the valley occurred under tide-dominated estuary conditions.

Dalrymple et al, 1992; Allen, 1991; stated that the shape of the valley system has a significant control on the nature of the facies developed in an estuary, particularly in the early stage of infilling. Estuaries which either initially have or subsequently develop a funnel-shaped geometry are more likely to be tide-dominated systems (Dalrymple and Rhodes., 1995; Dalrymple et al., 2012). The tide-dominated inner portion of the Gironde estuary is an example (Salomon and Allen 1983).

In tide-dominated estuaries, tidal currents redistribute the sediments which leads into a rapid filling of the deeper and wider parts (Dalrymple et al., 1992) and a funnel-shaped geometry is high probably to be observed. Once this situation exists, further sediment input should cause the facies zones to prograde seaward. The stages in the growth of the sand-bar facies have been discussed by Harris (1988), who shows that the bars become larger along the estuary filling. Figure 2.6 shows an approximate cross section of a tide-dominated estuary and its corresponding litho-facies models.

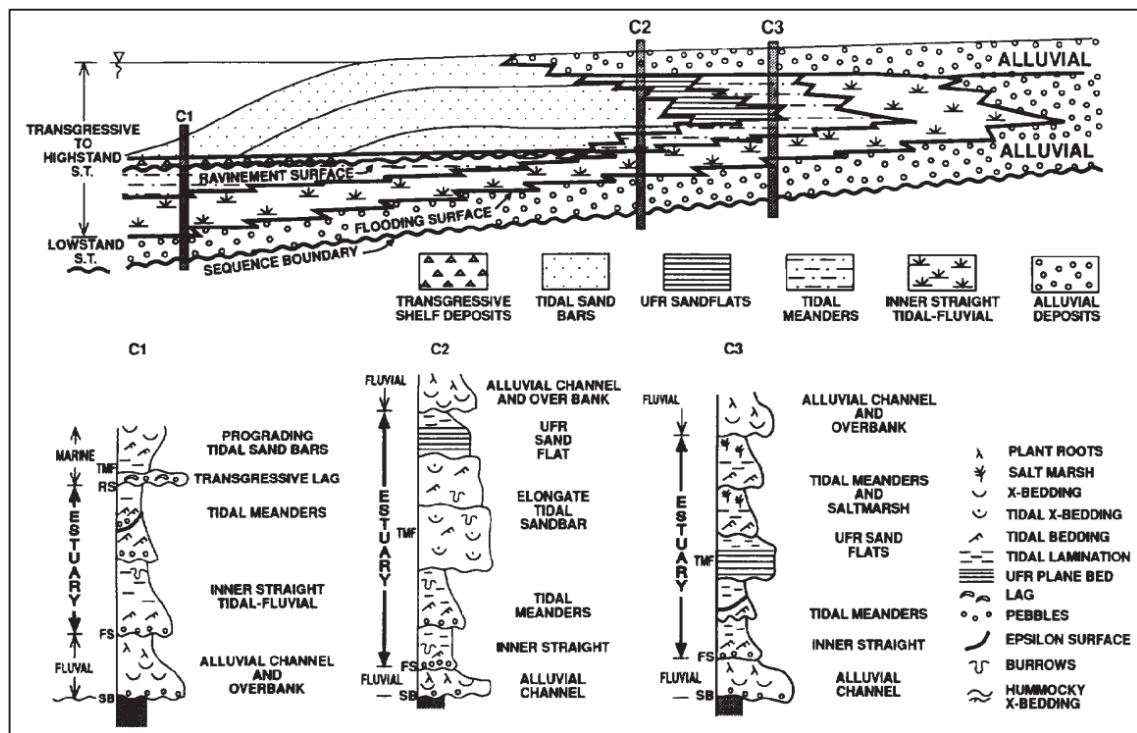


**Figure 2.6:** Schematic section along the axis of a tide-dominated estuary, showing the distribution of litho-facies resulting from transgression of the estuary, followed by estuary filling and progradation of sand bars or tidal flats. The amount of the transgressive succession preserved depends on the relative rates of sea-level rise and head-ward translation of the thalweg or the tidal channels (after Dalrymple, 1992).

Tidal bars are, first of all, classified according to their orientation with respect to the current as (Besson, 2005):

- Longitudinal bars (tidal banks): sandy accumulations of 15 to 50 meters high, up to 100 kilometers long, characterized by a zero or small angle between the direction of the peak of the dominant current and that of their crest (Reynaud, 1996). The largest dimension of the tidal banks is therefore parallel to the direction of the current.

- Transversal bars (tidal dunes): The terminology of transverse forms to the current are classified as dunes (Ashley, 1990; Berné, 1991). Thus the term submarine dunes or subaqueous dunes is used for all forms of transverse deposits to the current which are larger than that of small ripples. This type of body is found at all scales. There is a second group of dunes built by the superposition of large ripples; these shapes are both much more symmetrical and flattened than the previous ones. Hence, all sedimentary bodies smaller than 6 cm height are called ripples and all sedimentary bodies bigger than 6 cm height are classified as dunes.

The size (wavelength and height) of dunes is a complex function of many variables, the most important of these being water depth, current speed, and grain size. Currently all the forms of height greater than 6 centimeters are called dunes (Ashley, 1990): according to their amplitude  $H$  and their wavelength  $L$ , are differentiated from small, medium, large and very large dunes (Berné, 1991). Small and medium-sized dunes (less than 1.50 m in height and 20 m in wavelength) can also be found referred to as mega ripples (Gorsline & Swift, 1977; Stride, 1982).

Different forces can dominate the sediments dynamic on the tidal flats: tides, waves and even storms. Wind wave may be a major dynamical factor because a large amount of bed-load could be re-suspended. Also, tidal current processes greatly impact sedimentation, particularly in mouth-bar areas located at the alternation of tidal flats and outlets system where it can lead into uneven distribution of sediments. The sediment with poor sorting and positive skewness is often found in shallow coastal areas.

## 2.2 Available data of the experimental site

For simplicity, the different datasets are organized following their approximate scale of investigation. We consider all measurements that covers laterally over 100 m as large scale surveys, the near wellbore measurements are small scale and the rest of tests are considered as medium scale data.

We start by giving a summary of the main events and surveys that occurred in the experimental site in order to gather valuable data:

- In early 2015, permeability measurements (using TinyPermII tool) were performed at different locations and scales; from the scale of a plug, a rock blocks (octagons) to the scale of outcrops where measurements along lines in the outcrop were performed.

- A 3D topography campaign was conducted at the experimental site to collect elevation data for digital elevation modelling (DEM) of the experimental site.
- The first drilling (borehole PZ0, 43m depth) was carried out in July 2015 with the aim to obtain a geological log of the sediment units and an estimate of the hydrodynamic properties of the aquifer (consists of upper Burdigalian formations) chosen for the project.
- Between March 29 and April 26 2016, twelve additional wells were drilled; all of which reached the middle Burdigalian formation that form an impermeable lower limit of the aquifer. Among the boreholes, three were cored and the rest nine were destructively drilled.
- At the beginning of July 2016, a well logging campaign was performed, with the objective of systematically acquiring neutron porosity, natural gamma, trajectometry, sonic full-wave, electrical resistivity and borehole image logs in all thirteen drilled boreholes.
- A feasibility study of using Geo-Radar to detect sedimentary structure at the ground surface (17-18 May 2016) and in four wells (19-20 July 2016) was carried out by the Université de Pau et Pays de l'Adour.
- From July 29 to September 7 2016, a hydrodynamic properties acquisition campaign in the selected aquifer was carried out (pumping and slug tests) in each of the thirteen boreholes and acquisition of interference responses in all other twelve observational boreholes.
- At the end of November 2016, X-ray CT-Scan was performed only on the core extracted from PC12 to establish a 3D imagery of porosity. Measurements of rock density and natural gamma were also performed on that core.
- Throughout the year 2016, the original topography database was extended with new GPS measurements; total of 26,925 mesures performed on the quarry in the direct vicinity of the experimental site. In addition, the new measurements with TinyPermII permeameter were taken on quarry fronts, octagonal rock blocks extracted from the quarry, and on the cores extracted from PC6, PC8, and PC12 boreholes.
- During April 2017, petrography analysis was made on PC12 for the different facies observed in the site.
- The three cored wells were then subject to plug extraction. Around a 100 plugs were cut from each core after TinyPermII measurements. Then the plugs were used to measure their permeability and porosity using a PORO-PERM (laboratory permeameter). This campaign lasted for around two years, from 2017 to 2019.
- At November 2018, a flowmeter survey started at three wells then extended to the other wells on January, 2019.
- On March, 2019 the drilling of 4 new wells (PZ13, PZ14, PC15 and PC16) was performed. Two of the four new wells are cored wells.
- During August 2019, A new logging survey was performed in the new wells.

- On October 2019, a long pumping test were conducted on PC6 for a week to acquire the response of the new drilled wells.

## **2.2.1 Large scale**

### **2.2.1.1 Regional model of the valley**

Several information about the Castries incised valley (see Figure 2.7) have been gathered. We focused on the available logs of the drilled wells that penetrate partially or fully the Burdigalian strata. Data are mainly found in BRGM online database and Berga Sud reports. The different part of the Burdigalian have been identified in different wells, then, interpolated to construct a 3D facies model (see Figure 2.8).

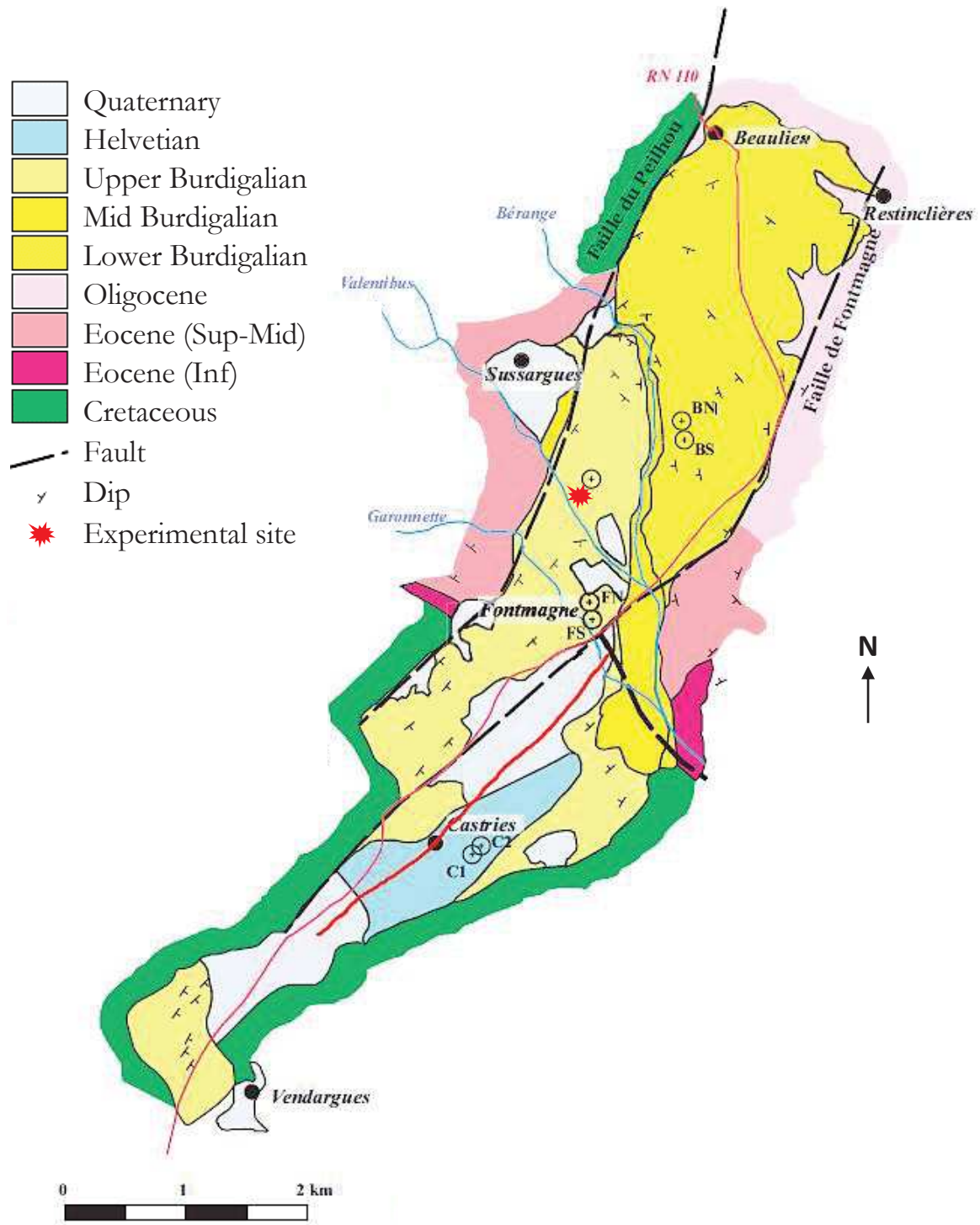


*Figure 2.7: Geological map of Castries incised valley (modified from BERGA Sud) with the localization of the experimental site.*

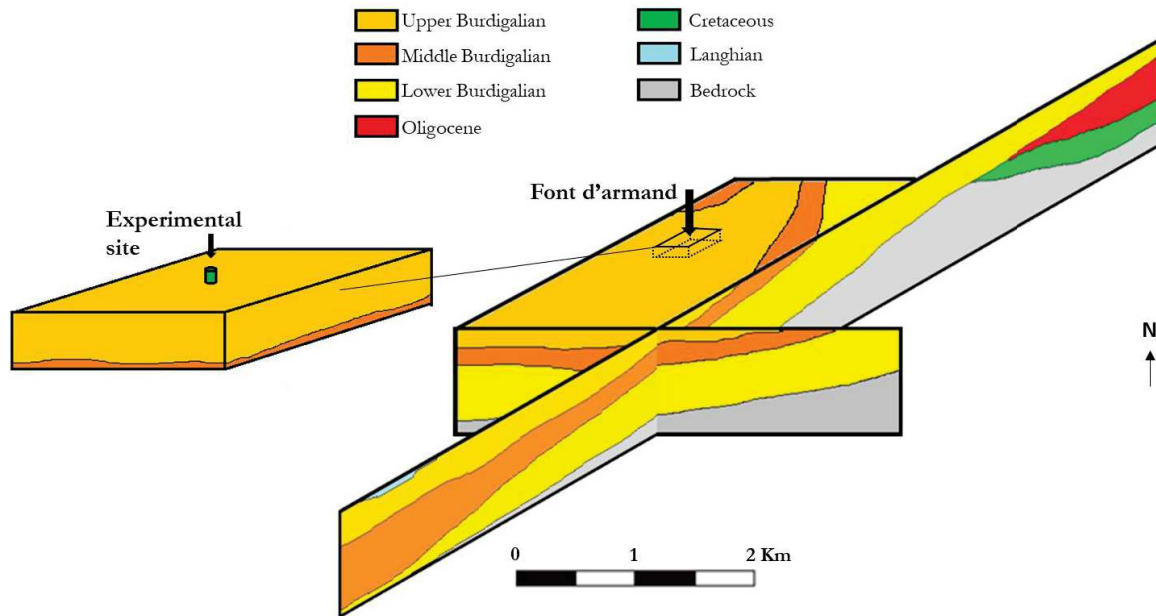


*Figure 2.8: Regional facies model of Castries incised valley; It is built based on the available well logs in the area provided by BRGM and Berga Sud.*

### 2.2.1.2 Electrical Resistivity profiles

At a much smaller scale than the regional model, 3 electrical resistivity surveys were carried out at the study site. These boreholes allowed in particular to locate the piezometric level before the installation of first boreholes. Figure 2.9 shows the position of these 3 profiles and one example of the results (profile 1). On each of the profiles, a dipole-dipole acquisition was carried out as well as a Wenner-Schlumberger acquisition.

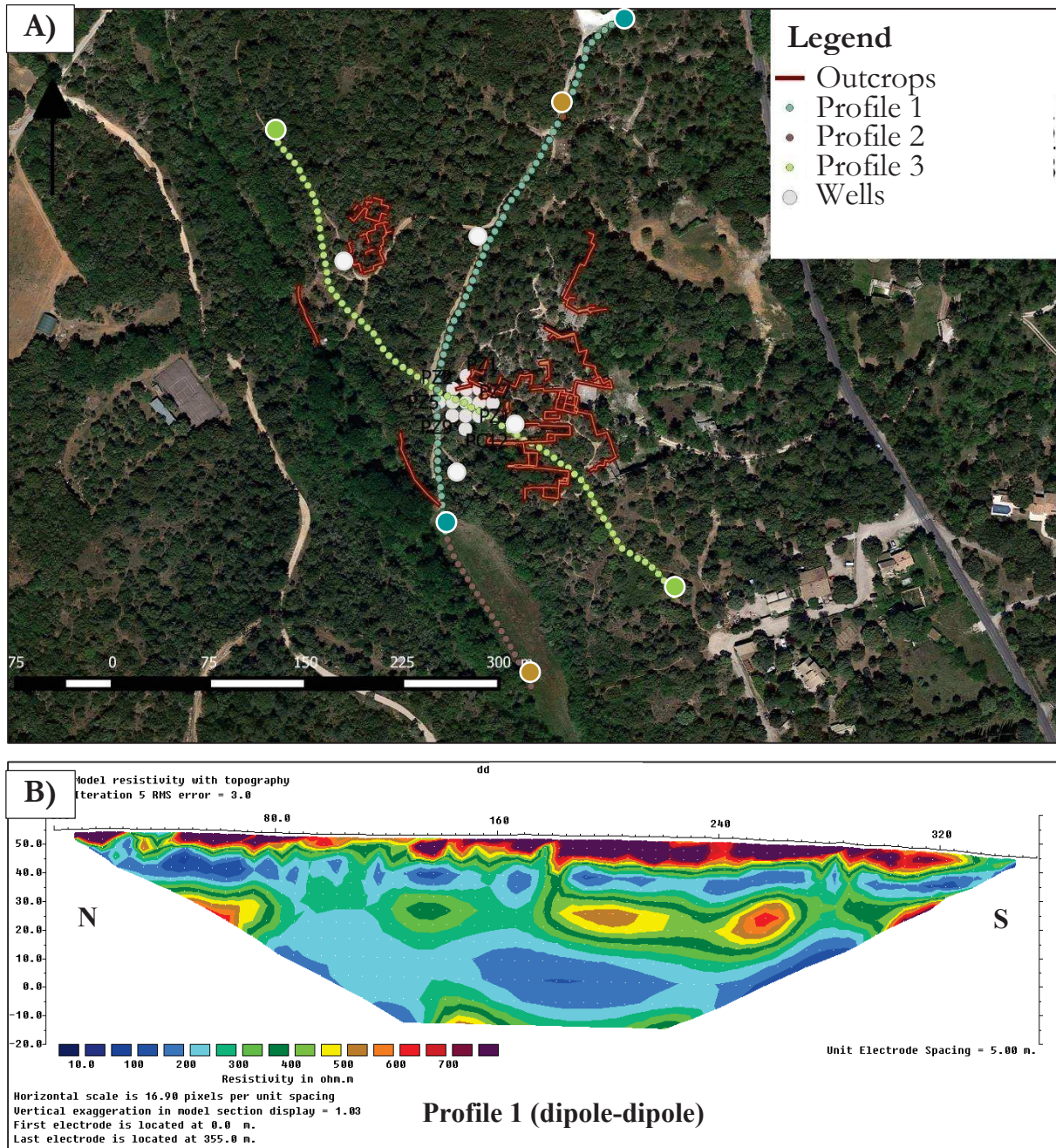
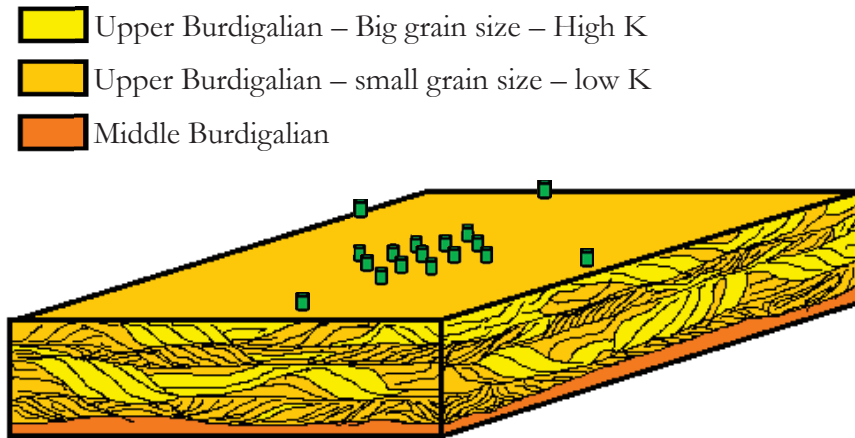


Figure 2.9: A) Localization of the electrical resistivity profiles, B) Example of electrical resistivity dipole-dipole result from profile 1 (P. BRUNET).

### 2.2.2 Medium scale

At this scale, we mainly focus on the data that investigate the region between the wells (site scale; see Figure 2.10).



*Figure 2.10: Conceptual facies model of the experimental site (conceptualized based on the observations on the cored wells of the site).*

### 2.2.2.1 Pumping tests

After the first phase of drilling (the drilling of the 13 boreholes that cover a roughly 50 m by 50 m area), a campaign of pumping tests was achieved. The objective was to perform in every borehole a pumping test with a constant pumping rate (pumping rates change from one well to another) for a duration of 5 to 6 hours and monitor the drawdown responses (example shown in Figure 2.11) on all the 13 wells using CTD sensors. Also, the buildup that followed up is also monitored for several hours. A year later, one long pumping test for a duration of one week was recorded. And more recently, after the construction of the new four wells (regional wells), a new long duration (1 week) pumping test is recorded.

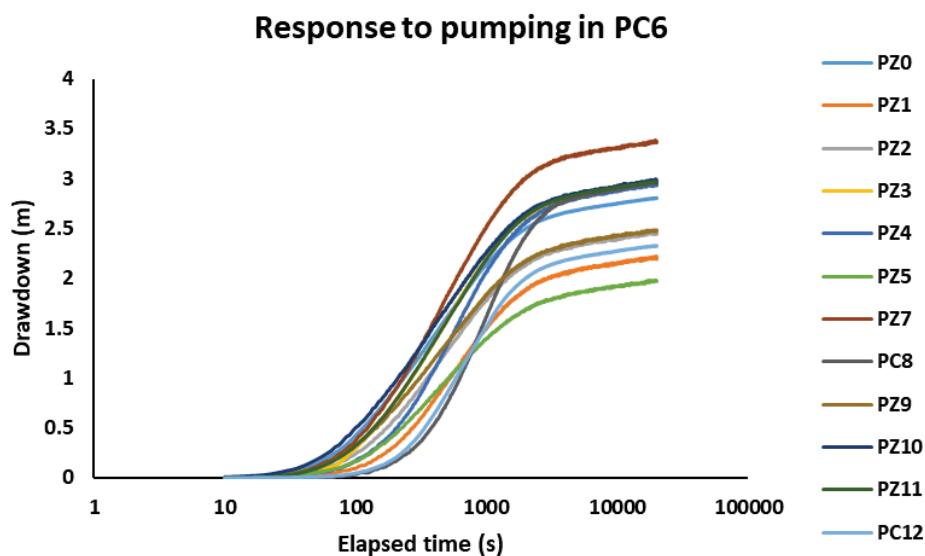


*Figure 2.11: Drawdown response of different observation wells to a constant-rate pumping test performed in PC6.*

Figure 2.12 shows the hydrodynamic behavior of the aquifer through: a) fitting the drawdown curve of pumping in PC6 to the theoretical Theis type curve and b) the corresponding drawdown derivative.

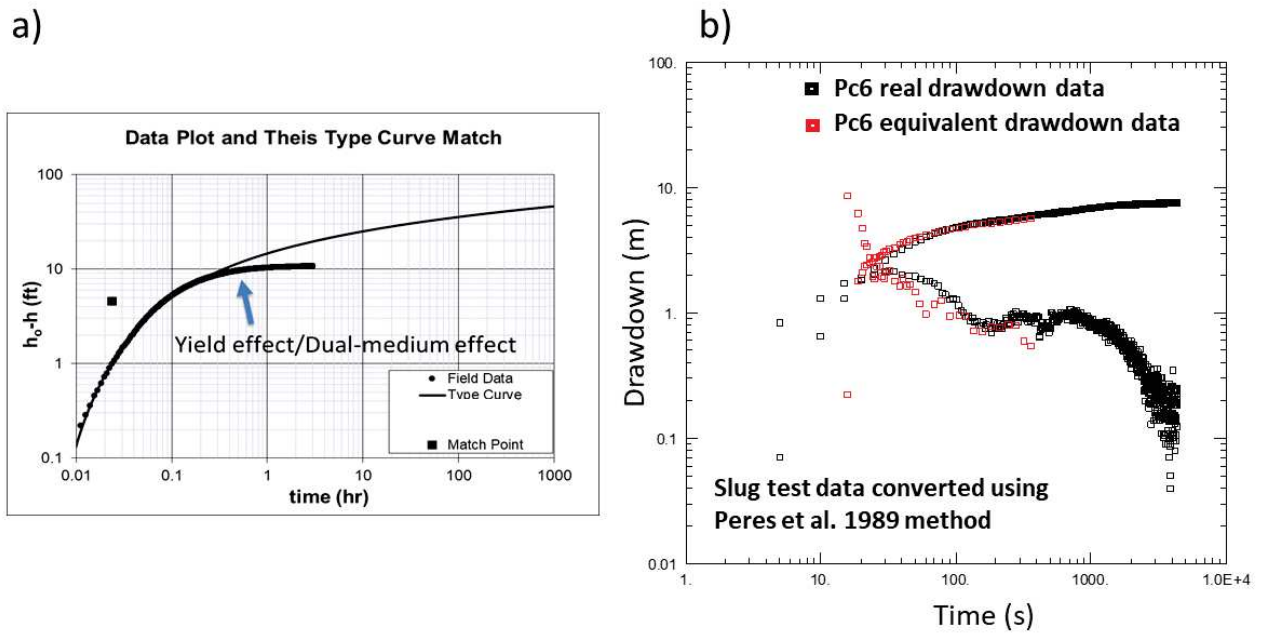


**Figure 2.12:** Hydrodynamic behavior of the aquifer in the experimental site. a) fitting the drawdown curve of pumping in PC6 to the theoretical Theis type curve. b) Plot of pressure transient derivative using drawdown response of PC6 to pumping in the same well (black) and equivalent drawdown response converted from PC6 slug test using Peres et al. method (red) (X. WANG).

### 2.2.2.2 Slug tests

From July 29 to September 7 2016, a hydrodynamic tests campaign in the selected aquifer was carried out. Slug tests were systematically performed in each of the thirteen boreholes (no slug tests are performed in the new wells yet) and interference responses in all other twelve observational boreholes (see Figure 2.13 for an example) were recorded. The used slug tool was made by the laboratory; it consists on a PVC tube that stores water which will be released into the well at the beginning of the test.

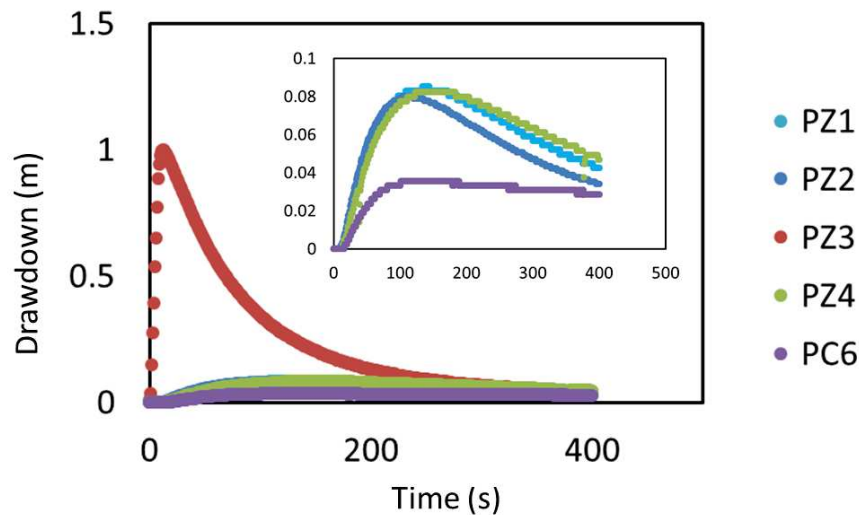


*Figure 2.13: Drawdown response of different wells to a slug test performed in PZ3.*

The preliminary analysis of hydrodynamic response to pumping test and slug tests (Wang et al., 2019) showed a pretty high lateral heterogeneity of the hydraulic conductivity field. Besides, both the well logs and laboratory measurements on cores, showed that the spatial distribution of the hydraulic conductivity field is constrained by a multilayered system.

### 2.2.2.3 Geo-Radar

From May 17 to 18, 2016, Geo-Radar measurements were carried out by the University of Pau and the Pays de l'Adour on the experimental site. 4 fixed antenna transects were studied at three different frequencies 100 MHz, 250 MHz and 500 MHz and 2 mobile antenna transects (see Figure 2.14). Acquisitions were also made to estimate the propagation speed of electromagnetic waves estimated at 9 cm / ns.

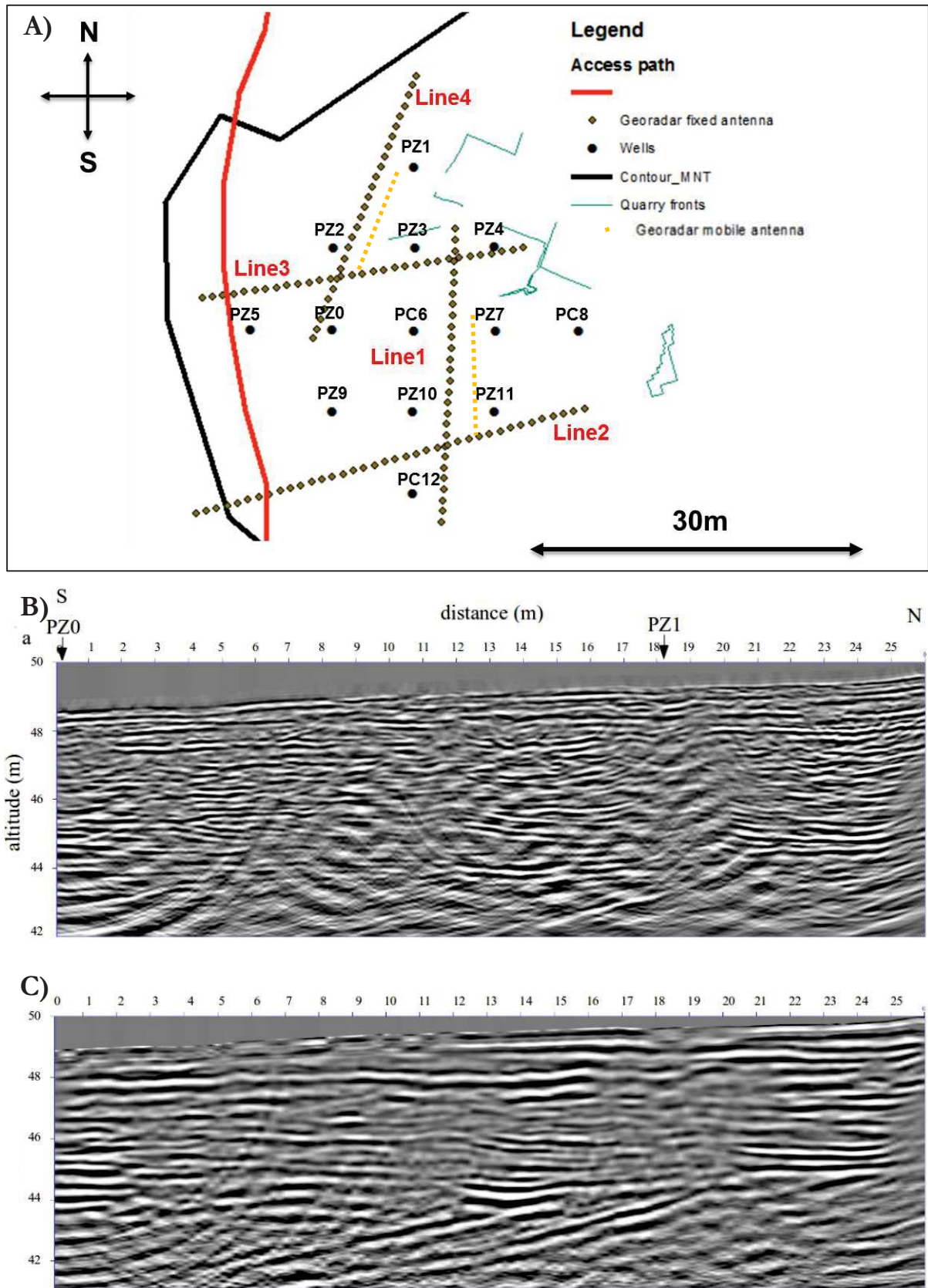


**Figure 2.14:** A) localization of the four transects of georadar. B) Example of results from transect n°4 at 250MHz. C) Example of results from transect n°4 at 100MHz (D. ROUSSET and G. SENECHAL).

## 2.2.3 Small scale

### 2.2.3.1 Cores and laboratory measurements

The hydraulic conductivity was measured on 330 one-inch diameter plugs sampled from the full-diameter cores. The measurements span four orders of magnitude ( $10^{-8}$  to  $10^{-4}$ ). Core and sample studies show a high connected porosity (20-40%). Thanks to this connectivity, porosity and permeability are strongly correlated. The saturated context and this high connectivity makes EM velocity useful for water content and consequently permeability.

The five cored wells were analyzed in order to construct litho-facies distributions and Tiny-Perm measurements were made (see Figure 2.15). The TinyPerm II is an instrument for measuring soil permeability. The push of the piston creates a vacuum at the tip of the device. A pressure sensor measures the return to equilibrium. Since the contact area and the volume are known, an infiltration rate is calculated. An instrumental calibration performed by the manufacturer makes it possible to establish the relationship between the values displayed by the device and the permeability expressed in Darcy. The volume investigated corresponds to a half-sphere of rock of approximately  $1 \text{ cm}^3$ .

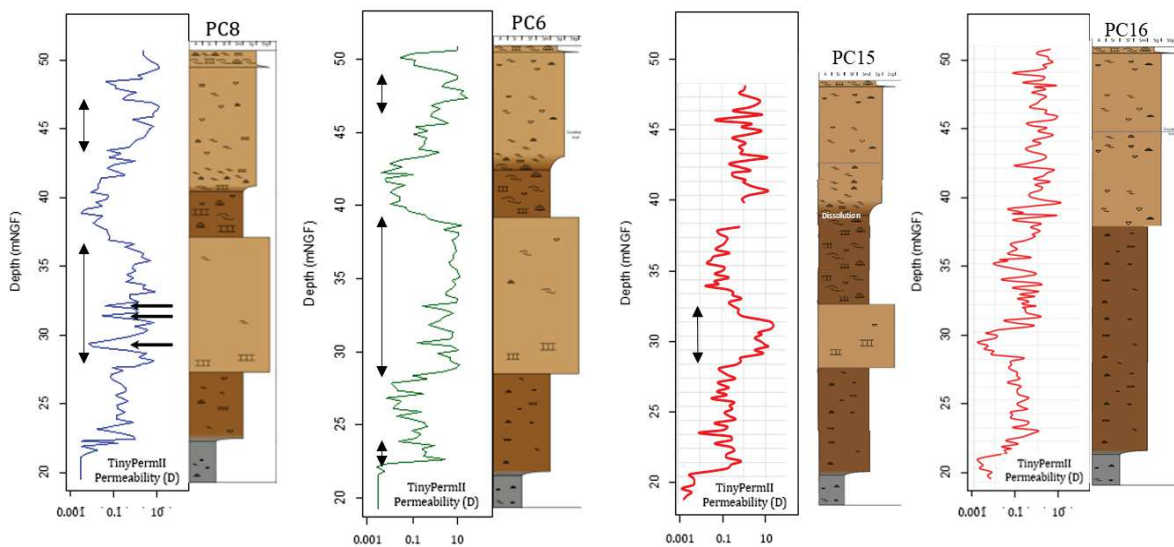


**Figure 2.15:** Tiny-Perm measurements log in wells PC8, PC6, PC15 and PC16, and the corresponding litho-facies models.

### 2.2.3.2 Well loggings

Table 2.1 summarizes an example (logs in PC12) of the various data acquired on the boreholes by logging on the well of the on the core:

- Acquisition of logs by the company *Semmlogging*: GN, OBI, BHTV, sonic full wave, HPHL, SPR, LNR SNR + trajectometry.

- Acquisition at *CSTJF* of CT-SCAN, density, GN, K, U TH, Vp, Vs, and  $K_{miniperm}$  imagery on the core of PC12.

**Table 2.1:** Summary of available logs in the experimental site.

<b>LOG</b>	<b>Available Data</b>
Natural Gamma (GN)	Available in all wells
Optical Borehole Imagery (OBI)	Available in all wells
Acoustic Borehole Imagery (BHTV)	Available in all wells except PC6, PC8 and PC12 where the imagery is highly biased because of the used polymer during the drilling
Sonic full wave	Available in all wells
Neutron porosity (NPHL)	Available in all wells
Single point resistivity (SPR)	Available in all wells
Short normal resistivity (SNR)	Available in all wells
Long normal resistivity (LNR)	Available in all wells
Caliper	Available in all wells
Acoustic (Vp/Vs)	PC12 only
CT Scan porosity	PC12 only
Density	PC12 only
Potassium	PC12 only
Uranium	PC12 only
Thorium	PC12 only
Continuous log of Permeability	PC12 only

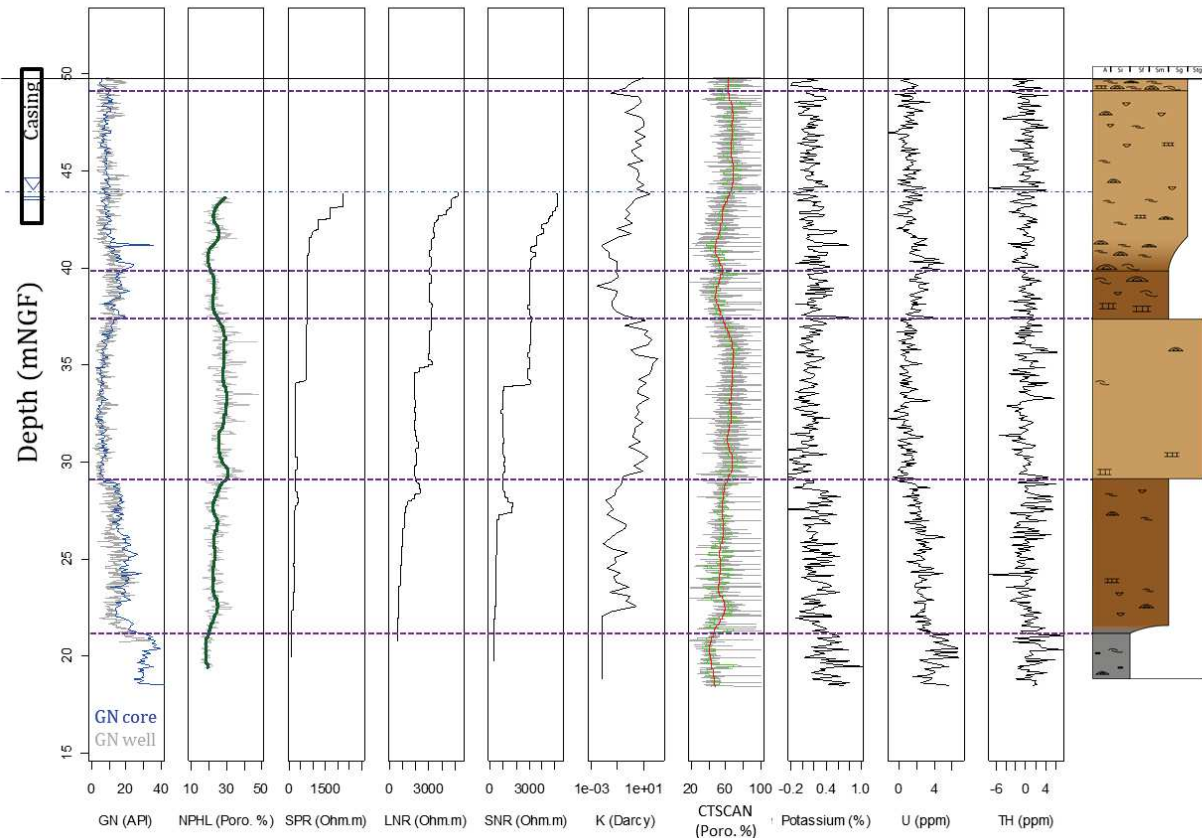


*Figure 2.16: List of the performed logs in each borehole. The measurements displayed in this figure as an example are obtained from well PC12.*

### 2.2.3.3 Flowmeter survey

On 2018, a spinner flowmeter tool was purchased for the laboratory and a flowmeter survey was carried out in the experimental site. Data of flowmeter tests have been collected in borehole P6, P8 and P12 during dry (June) and wet (November) seasons while flowmeter tests in other boreholes have only been collected in wet season (November and December). As a preliminary observation, ambient regional flow is very weak; no obvious signal was detected during flowmeter measurements under ambient condition.

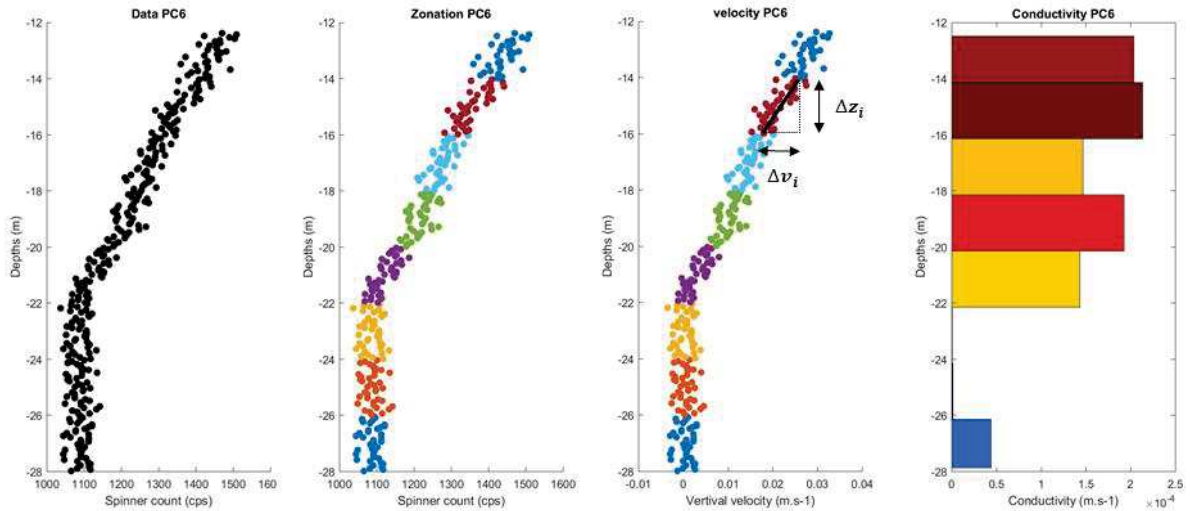


*Figure 2.17: Example of flowmeter data and its conversion into hydraulic conductivity gathered from the flowmeter survey of the experimental site (the method used for the interpretation of flowmeter tests is detailed in chapter 3 and Chapter 4 of the thesis).*

#### 2.2.3.4 Petrography

Thin slices from the core of the well PC12 are analyzed to show the mineral and textural content of the rock in details. Five thin slices are studied; each one studied a different type of rock according to Dunham's classification (wackstone, floatstone, rudstone, packstone and grainstone). Figure 2.18 shows an example obtained from petrography analysis.

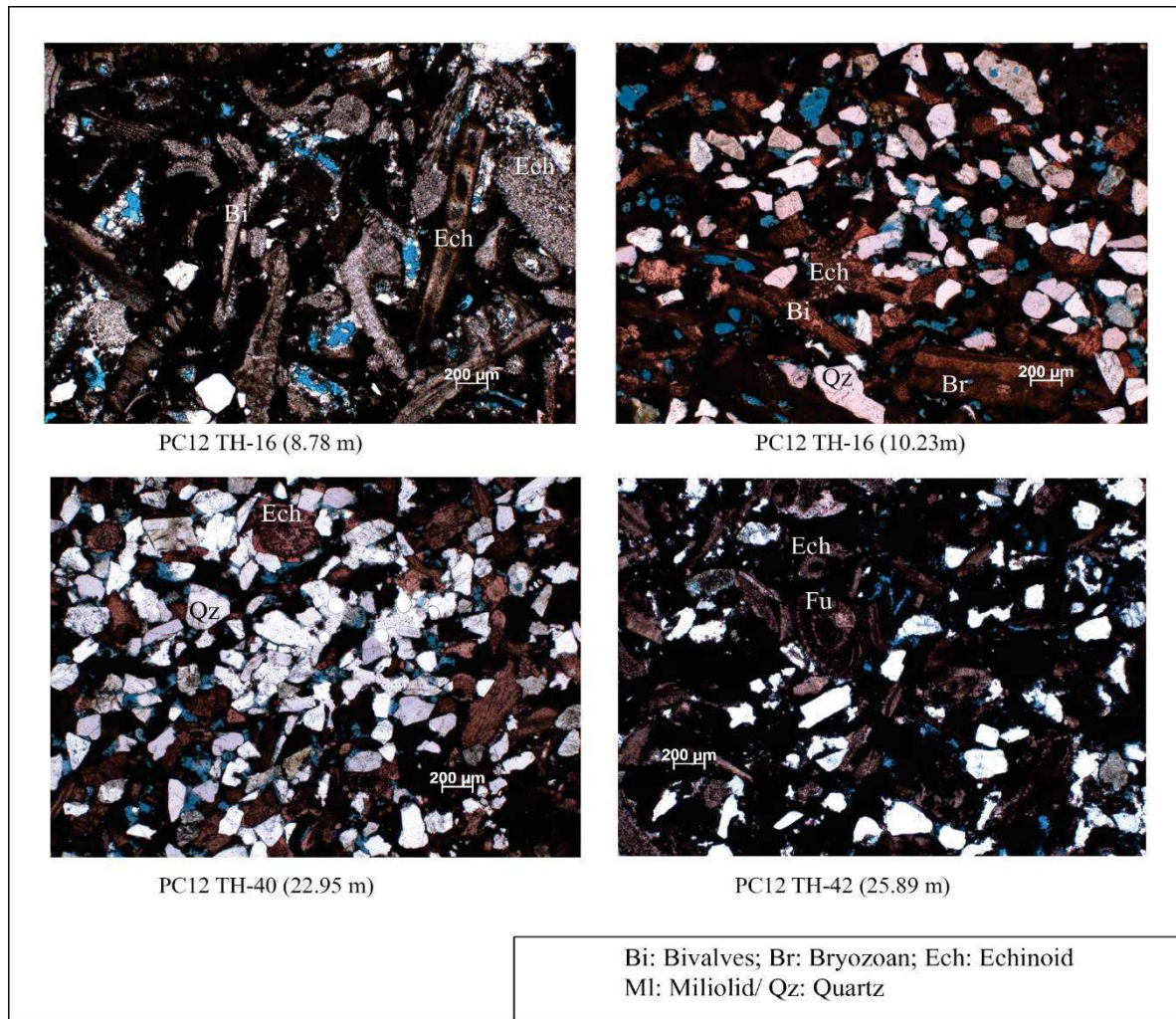


*Figure 2.18: Thin slices petrography from the core of PC12 at different depth.*

### 2.2.3.5 CT-Scan

An X-ray CT-scan has also been done on the core of PC12.

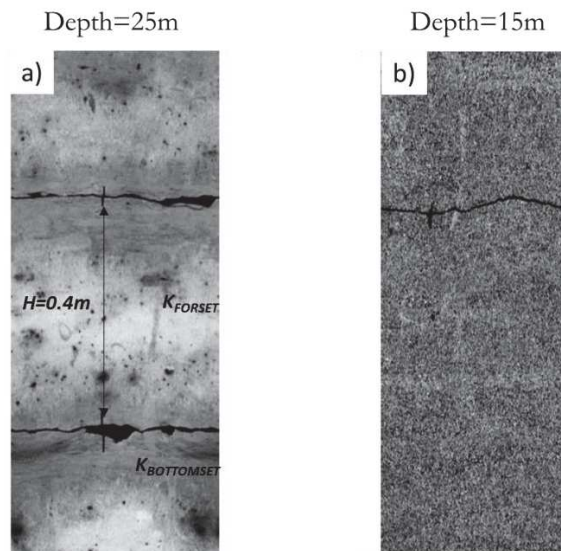


**Figure 2.19:** Extract of X-Ray imaging of PC12 at different depths. A) at depth=25m with fine sediments. B) at depth=15m which corresponds to the main permeable layer of the aquifer.

## 2.3 Numerical modelling

Different kind of numerical models have been investigated and used to attempt to mimic the hydraulic behavior of the aquifer. The models are either in 2D or 3D and are constructed based on the different observations that have been seen in the preliminary analysis of the datasets. It has been observed that the drawdown response to pumping tests is characterized by a flattened late time part which in an infinite homogeneous and idealized aquifer case, it cannot be obtained. In order to reproduce that behavior, different models are explored (see Figure 2.20):

- The 2D depth averaged model with a buffer zone which will impact the late time response. Changing the hydraulic properties values of the buffer region considerably impacts the late time response. This effect is seen if a contrast between the hydraulic properties of the domain between the wells and the hydraulic properties of the buffer region is created.
- A 2D vertical cross section; a leakage effect of the overlying and underlying aquitards can also create a flattened signature of late time drawdown responses.
- A 3D model for a fully characterization of the aquifer.

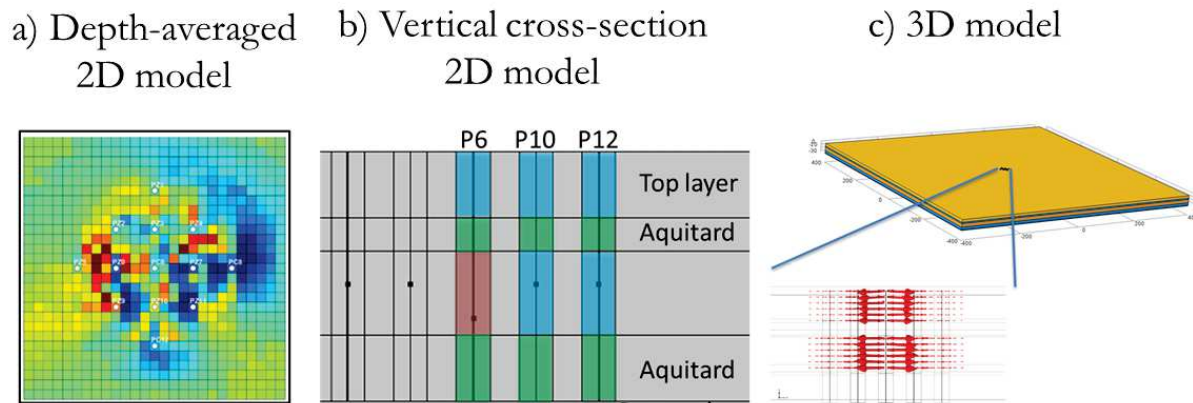


**Figure 2.20:** Different numerical modelling approaches to investigate the highly heterogeneous behavior of the studied aquifer. A) A 2D depth averaged model. B) A 2D vertical cross section. C) a 3D model.

## 2.4 Conclusion

We here summarized all information and data related to the experimental site used as a real-field application for the new developed approaches. This experimental site shows big advantages:

- A good amount of available data
- The data cover different scales of investigation which can be used to explore the change of scale effect
- The aquifer shows very high heterogeneity
- Complex hydrodynamic system for new studies and investigations
- Several drilled wells that cover a large scale
- The experimental set up allows the application of several existing methods

## References

- Allen, G.P., 1991, Sedimentary processes and facies in the Gironde estuary: a Recent model of macro-tidal estuarine systems, in Smith, G.D., Reinson, G.E., Zaitlin, B.A., and Rahmani, R.A., eds., *Clastic Tidal Sedimentology: Canadian Society of Petroleum Geologists Memoir 16*, p. 29-40.
- Allen G.P. & Posamentier H.W. (1991) - Facies and stratal patterns in incised valley complexes: examples from the recent Gironde Estuary (Fr) and the Cretaceous Viking Formation (Canada). *Am. Assoc. Pet. Geol., Annual Meeting, Dallas, Texas, April 7-10, 1991*.
- Ashley G.M. (1990) - Classification of large-scale subaqueous bed-forms: a new look at an old problem, *J. Sediment. Pet.*, 60, 1, p. 160-172.
- Berné S. (1991) - Architecture et dynamique des dunes tidales. Exemples de la marge atlantique Française. Thèse Doct. géol., Univ. Lille, 295 p.
- Besson, D., 2005. Architecture Du Bassin Rhodano-Provençal Miocène (Alpes, S.E. France): Relations Entre déformation, Physiographie et sédimentation Dans Un Bassin Molassique d'avant-Pays. Ecole Nationale Supérieure des Mines de Paris, Paris (250 pp.).
- Besson, D., Parize, O., 2001. Analyse géométrique quantitative d'un système de vallées incisées : les paléovallées miocènes de Saumane et de Fontaine-de-Vaucluse (bassin de Carpentras, SE France). *ASF Association des Sédimentologues Français* 36, 47–48.
- Besson, D., Parize, O., Rubino, J.-L., 2002. La paléovallée à remplissage burdigalien de Lourmarin-Buoux-Courennes; implications stratigraphique et paléogéographique (bassin d'Apt, SE de la France). *Documents des Laboratoires de Géologie, Université Claude Bernard, Département des Sciences de la Terre, Lyon* 156, 48–49.
- Besson D., Parize O., Dalrymple R.W., Reynaud J.Y. & Rubino J.L. (2003) - Evolution et dynamique des vallées incisées, à remplissage biodétritique, du Miocène inférieur périalpin. Une alternative au modèle siliciclastique. - 9<sup>e</sup> Congr. Français Sédimentologie, Livre des Résumés, Publ. A.S.F., Paris, 38, p. 52-53.
- Clauzon G., Suc J.P., Gautier F., Berger A. & Loutre M.F. (1996) - Alternate interpretation of the Messinian salinity crisis. Controversy resolved. *Geology*, 24, p. 363-366.
- Clauzon G. (1979) - Le canyon messinien de la Durance (Provence, France) : une preuve paléogéographique du bassin profond de dessiccation. *Palaeogeogr., Palaeoclimatol., Palaeoecol.*, 29, p. 15-40.
- Clauzon G. (1981) - Révision du stratotype du Pontien méditerranéen (Depéret, 1893) et relations de cet étage continental avec l'évolution géodynamique de la marge méditerranéenne Française au Miocène supérieur. *C. R. Acad. Sci. Paris, II*, 293, p. 309-314.
- Clauzon G. (1982) - Le canyon messinien du Rhône : une preuve décisive du « dessiccated deep-basin model » (Hsü, Cita et Ryan, 1973), *Bull. Soc. Géol. France, Paris (7), XXIV*, 3, p. 597-610.
- Dalrymple, R. W.; Zaitlin, B. A.; Boyd, R. (1992). Estuarine facies models; conceptual basis and stratigraphic implications. *Journal of Sedimentary Research*, 62(6), 1130–1146. doi:10.1306/D4267A69-2B26-11D7-8648000102C1865D
- Dalrymple, R.W., Mackay, D.A., Ichnas, A.A., Choi, K.S., 2012. Processes, morphodynamics and facies of tide-dominated estuaries. In: Davis, R.A., Dalrymple, R.W. (Eds.), *Principles of Tidal Sedimentology*. Springer, Berlin, pp. 79–107.

- Dalrymple, R.W., Rhodes, R.N., 1995. Estuarine dunes and bars. In: Perillo, G.M.E. (Ed.), *Geomorphology and Sedimentology of Estuaries*. Elsevier, Amsterdam.
- Dexcoté Y., Rubino J.L., Parize O. & Clauzon G. (2001) - Le Miocène de basse Provence : stratigraphie, architecture et faciès des séquences de dépôt autour des paléoreliefs pyrénéo-provençaux. - 8è Congr. Français Sédimentologie, Livre des Résumés, Publ. A.S.F., Paris, 36, Poster, p. 99.
- Dexcoté Y. (2001) - Architecture et évolutions des faciès des séquences de dépôts du Miocène de basse Provence, D.E.A. E.N.S. des Mines de Paris, UPMC, ENSPM, Rapp. TOTAL, 45 p.
- Gilles Brocard, Pieter van der Beek. Influence of incision rate, rock strength, and bedload supply on bedrock river gradients and valley-flat widths: Field-based evidence and calibrations from western Alpine rivers (southeast France).
- Gorsline D.S. & Swift D.J.P. (1977) - Continental shelf sediment dynamics. A national overview, p. 1-134.
- Harris P.T. (1988) - Large-scale bedforms as indicators of mutually evasive sand transport and the sequential infilling of wide-mouthed estuaries. *Sediment. Geol.*, 57, p. 273-298.
- Lesueur J. L., J. L. Rubino, M. Giraudmailet; Organisation et structures internes des dépôts tidaux du Miocene rhodanien. *Bulletin de la Société Géologique de France* 1990; VI (1): 49-65. doi: <https://doi.org/10.2113/gssgfbull.VI.1.49>
- Parize O., Rubino J.L., Besson D., Clauzon G., Colson J., Dalrymple B., Javaux C., Laporte-Galaa C., Villain J.M. & Soudet H. (2001) - Architecture and internal organization of bioclastic sandbodies infilling incised valley fill complexes in the Miocene Carpentras - Avignon basins, field-trip guide book international meeting « Anatomy of carbonate bodies, Marseille 2001 », Rapp. TOTAL - E.N.S. des Mines de Paris (en dépôt à la Soc. Géol. France), 40 p.
- Reynaud J.Y., Dalrymple R., Vennin E., Parize O., Besson D. & Rubino J.L. (2006) - A Miocene clastic carbonate flood-tidal delta, Uzès basin, SE France. *J. Sediment. Res.*, 76, 1, p. 117-130.
- Reynaud J.Y. (1996) - Architecture et évolution d'un banc sableux de mer celtique méridionale. Thèse Doct. Géol., Univ. Lille, 185 p.
- Rubino, J.-L., Lesueur, J.L., Guy, L., Clauzon, G., 1990. Le Miocène inférieur et Moyen Du Bassin Rhodanien. Stratigraphie séquentielle et sédimentologie. Livret Guide Excursion. ASF Association des Sedimentologues Français (67 pp.).
- Rubino J.L., Lesueur J.L., Guy L., Granier B. & Clauzon G. (1994) - Les Cortèges Transgressifs du Miocène Méditerranéen : des Plate-formes Carbonatées du Type Foramol Sous Contrôle Tidal. Séance Spéc. ASF/SGF, Géométrie et Productivité des Plate-formes Carbonatées, Paris, Publ. ASF, Paris, 21, p. 37-38.
- Rubino J.L. & Clauzon G. (1996) - Approche Stratigraphique et Géomorphologique de la surrection néogène de l'avant pays des alpes occidentales. Réunion. ASF-SGF, « Quantification de la tectonique et de l'eustatisme », Rennes, Publ. ASF, Paris, 25, p. 34-35.
- SALOMON, J.C. AND ALLEN, G.P., 1983, Rôle sédimentologique de la marée dans les estuaires a fort marnage : Compagnie Française des Pétroles, Notes et Mémoires 18, p. 35.-44.
- Seranne M., Camus H., Reynaud J.Y., Evolution post-rift du golfe du Lion en Languedoc : une marge pas si passive que ça!. GM: 11-160. Livret-guide. 2011, 50 p. <hal-00856255>

Stride A.H., Belderson R.H., Kenyon N.H. & Johnson M.A. (1982) - Offshore tidal deposits: sand sheet and sand bank facies. in "Offshore tidal sands, processes, and deposits", A.H. Stride ed., London, Chapman and Hall, p. 95-125.

Stride A.H. (1982) - Offshore tidal sands: processes and deposits. Chapman & Hall Publ., Londres, 222 p.

Wang, X., Jourde, H., Aliouache, M., Massonnat, G., Characterization of horizontal transmissivity anisotropy using cross-hole slug tests, J. Hydrol., 564 (2018), pp. 89-98, 10.1016/j.jhydrol.2018.06.068

Willett, S.D., Hovius, N., Brandon, M.T., and Fisher, D. Tectonics, Climate, and Landscape Evolution, Geological Society of America, pp.101-126, 2006, Geological Society of America Special Paper 398, ff10.1130/2006.2398(07). hal-00083659



## CHAPTER 3

**Résumé :** Dans ce chapitre, un état de l'art des différentes techniques hydrauliques permettant de caractériser l'hétérogénéité et l'anisotropie des réservoirs géologiques est proposé ; sur la base de modèles synthétiques, les performances de 5 différentes méthodes sont ensuite comparées et le potentiel de ces méthodes pour procéder au changement d'échelles (upscaling) des propriétés hydrauliques du milieu investigué est discuté. Ce chapitre aborde également la construction des modèles de facies sur la base des données géologiques et géophysiques acquises sur le site expérimental ainsi que les solutions numériques pouvant être mises en œuvre pour l'interprétation de tomographies hydrauliques. Il se conclue par une présentation exhaustive des différentes méthodes analytiques et numériques pour la caractérisation de l'anisotropie des propriétés hydrodynamiques.



### 3. STATE OF THE ART OF TECHNIQUES FOR THE HYDRAULIC CHARACTERIZATION AND MODELLING OF AQUIFERS AND RESERVOIRS

Aquifer characterization is fundamental and several approaches to delineate the heterogeneity of hydraulic parameters have been developed and tested over the last several decades [e.g., Sudicky, 1986; Boggs et al., 1992; Rehfeldt et al., 1992; Hess et al., 1992; Wu et al. 2005; Sudicky et al., 2010]. Conventionally, it is required to collect a large number of core samples from multiple boreholes and to conduct grain size or permeameter analyses. Other approaches include the slug testing of large numbers of piezometers and/or monitoring wells [e.g., Rehfeldt et al., 1992], flowmeter [e.g., Hufschmeid, 1986; Molz et al., 1989; Kabala, 1994; Boman et al., 1997], steady state dipole flow [ Zlotnik et al., 2001], or single-hole pumping or injection tests. More recently, geophysical methods [e.g., Hyndman and Gorelick, 1996; Hubbard and Rubin, 2000] and hydraulic tomography [e.g., Gottlieb and Dietrich, 1995; Yeh and Liu, 2000; Bohling et al., 2002; Zhu and Yeh, 2005, 2006] have been widely used to characterize subsurface heterogeneity. Aquifer characterization can also be categorized as a multi-step iterative process and its basic workflow includes four main elements. Firstly, develop a conceptual geological model of the studied area. Then, evaluate the type and scale of hydraulic parameters' heterogeneity. In the next step, comes data acquisition and hydraulic parameters evaluation. And finally, analyses and groundwater flow modelling.

The conceptual geologic model includes aspects of the study area such as aquifer boundaries. The conceptual geological model is then expanded to include an assessment of type and scale of aquifer heterogeneity. Petrophysical and hydraulic parameters evaluation consists on gathering field data by using appropriate techniques such as pumping tests, flowmeter surveys, geophysical surveys, laboratory measurements, etc. Different approaches to interpret and process the gathered data exist. For instance, hydraulic tomography showed a great potential in delineating the spatial distribution of aquifer hydraulic properties.

### **3.1 Groundwater hydraulic basics**

An aquifer is considered as an underground sedimentary rock that can store water and allows it to circulate thanks to its high permeability values. The sedimentary rock that construct an aquifer layer is constituted by different material types and shapes that create heterogeneity in hydraulic properties. Aquifers can also present other features that can impact considerably the flow such as fractures, faults, vugs, karst, etc. Groundwater resources are highly used and several extracting sites are constructed in order to exploit and distribute the resource. A site is composed of one to several production wells and its locations are chosen with care after preliminary studies that aim for the optimal outcome. The study of water flow in aquifers and the characterization of aquifers is categorized as hydrology.

#### **3.1.1 Simplified classification of hydraulic aquifers**

An aquifer is usually linked to other confining or semi confining layers (see Figure 3.1) that show much lower permeabilities. The semi confining strata are referred to as aquitards and the impermeable later that can exhibit a pressure are referred as aquiclude or aquifuge. Similar notation following the type of aquifer confinement leads into defining a confined or semi-confined aquifers.

We can classify aquifers following different terminologies. As described in the previous paragraph, aquifers can be categorized following its confining scheme into confined, semi confined or unconfined aquifers. They can also be classified following the degree of saturation of its pores with water into either saturated or unsaturated aquifers which forces the hydrogeologist to require different tools and flow simulation models. Underground is a succession of sedimentary layers that are constructed from different materials (sand, silt...). These materials create contrast in permeability that defines aquifers and aquitards; aquifers with the highest permeability and aquitards with the lowest. Aquifers can also be isotropic or anisotropic; isotropic aquifers show roughly similar hydraulic properties in different directions while anisotropic aquifers present a high difference of hydraulic properties at different location and different directions. Anisotropy is one of the major causes of the creation of preferential flow paths. Also, aquifers can exhibit specific features and thus classify them into porous, karstified, or

fractured aquifers. From an aquifer characterization perspective, the categorization or naming of strata is not especially relevant as long as the properties of the strata are adequately determined and modeled. However, aquifer types are relevant to identify in order to obtain a better and simpler characterization. For example, the difference in the confinement scheme of aquifers changes their relationship to the regional water table. Unconfined aquifers show similar water table level as the regional one so they can also be called water-table aquifers. The water table level is easily measurable from wells as the level at which water is met while descending the well. Sometimes, the water table level is defined as the upper boundary condition in saturated zone, but, cannot always be true because of capillary and pressure effects. The fact that these aquifers are not confined, their upper boundary is simply described being the water table (in a modelling perspective, a surface at atmospheric pressure can be used to simulate flow). Most unconfined aquifers are categorized as ‘semi-unconfined’ (Kruseman and de Ridder, 1970). Generally, the horizontal hydraulic conductivity of an aquifer is much higher than the vertical hydraulic conductivity and thus the  $K_h/K_v$  ratio is defined to describe the horizontal/vertical anisotropy. The sedimentation and diagenesis are the main reasons of such important anisotropy. For example, the presence of clay-rich strata, even a thin one, may substantially reduce the vertical hydraulic conductivity of an aquifer and creates a significant anisotropy ratio in hydraulic conductivity.

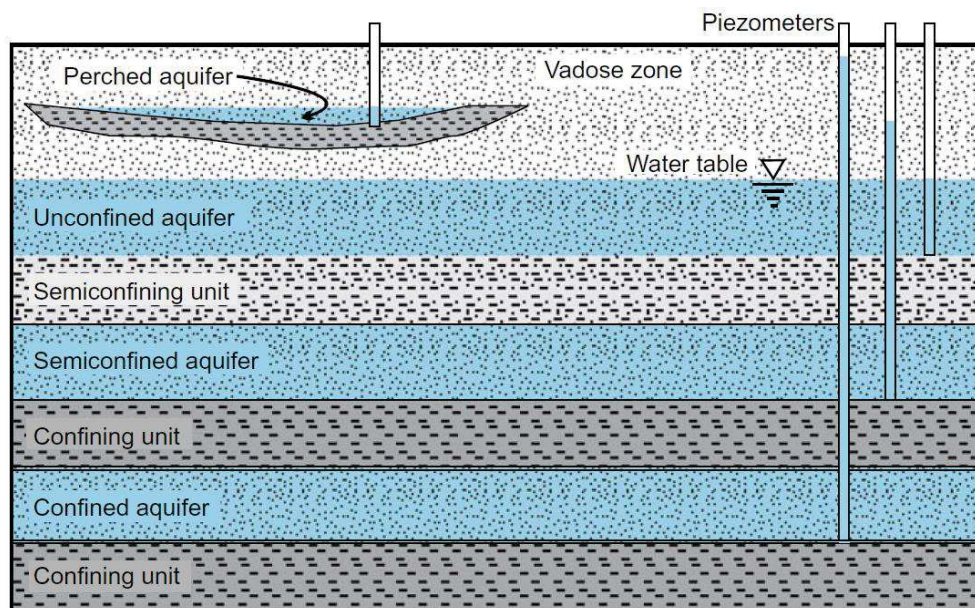


**Figure 3.1:** Conceptual diagram of the main aquifer types and the relationship of their piezometric surface level and the water table. The potentiometric surface of semiconfined and confined aquifers may be positioned alternatively below the water table, particularly where the aquifers are heavily exploited (from Maliva 2016).

A so-called perched aquifer (see Figure 3.1) can occur where the water table is deep and a low hydraulic conductivity stratum forming a synclinal is present. Perched aquifers can be permanent or temporary since its water could fade away because of a slow drainage or because of the hot season.

Perched groundwater aquifer is unconfined separated from an underlying body by an unsaturated zone and it also has a water level table referred as a perched water table (Lohman et al. 1979), whose elevation is higher than the regional water table.

Confined aquifers are bounded above and below by impermeable confining units. Such confinement leads into a water level seen in the piezometer being above the top of the aquifer. Confined aquifers are also called artesian aquifers and if the confining pressure is high enough to make the wells flow naturally at land surface, the aquifers become flowing artesian aquifers. It is noted that during a pumping test in a confined aquifer, the water level continues to decline and doesn't reach perfect steady state. The term confined aquifer is idealized and in real field, a perfect confinement cannot be seen because confining strata are not completely impermeable. In addition, some water may be drained from confining strata which makes the interpretation of pumping tests responses harder.

Most aquifers below the unconfined aquifer are referred as semiconfined or leaky aquifers. The term 'Leaky' is used because the semi confining strata have considerable leakage of water to the aquifer. In this type of aquifers, the degree of confinement is partial and the vertical hydraulic conductivity with the thickness of the bounding semi confining units allow considerable amount of water to flow into the actual aquifer. Leakance is added as an important hydraulic property for semiconfined aquifers in addition to transmissivity and storativity. Leakance is defined as the vertical hydraulic conductivity of the confining units divided by their thickness. When a semiconfined aquifer is pumped, the water table declines and thus induces leakage. Such income of water may lead into a stabilization of the water level if equilibrium is reached. Such equilibrium is related to the hydraulic properties, leakage rate and the pumping rate (Hantush and Jacob 1955; Hantush 1960; Walton 1960).

### 3.1.2 Aquifer hydraulic properties

#### 3.1.2.1 Porosity

The porosity is defined as the space of the rock that is able to store a fluid. It characterizes the degree of water containing per volume unit. It can be expressed quantitatively as the ratio of the volume of the interstices to the total volume of the bulk. Porosity is expressed as a decimal fraction or as a percentage. Thus

$$\theta = \frac{V_i}{V} = \frac{V - V_m}{V} = 1 - \frac{V_m}{V}$$

where  $\theta$  is the porosity, as a decimal fraction,  $V_i$  is the volume of interstices or void,  $V$  refers into the total bulk volume and  $V_m$  is the volume of solid and mineral particles.

Porosity can be expressed differently following different terminologies. For instance, we call an effective porosity the ratio between the pores volume that are connected between them and contribute

to flow and the total bulk volume of the sample. While the absolute porosity is calculated using the connected and non-connected pores volume. Every porous media has a porosity referred as a primary porosity. However, an aquifer can have features such as fractures which turn the aquifer into a dual porosity system.

Primary porosity is a result of the original interstices created during sedimentation and altered during diagenesis. While in intrusive and extrusive igneous rocks, the primary interstices result from cooling, crystallization and expansion of gas. These types of rocks show a large difference between the effective and absolute porosities because of non-connected openings. Metamorphism of igneous or sedimentary rocks generally reduces the primary porosity that may become even negligible in certain cases. The secondary porosity is commonly obtained from telogenesis stage where the sedimentary rock is subject to uplift and strong tectonic activity which lead into the nucleation of fractures, joints and faults. Openings along planes of bedding or schistosity in consolidated rocks can also develop and evolve into karst systems after dissolution processes. These structural alterations exhibit a large secondary porosity and permeability that may govern the flow within the aquifer. In some rocks, such secondary porosity becomes the only means for the storage and movement of ground water. Dissolution processes occur in carbonate rocks such as limestone or dolomite by the presence of water and dissolved carbon dioxide. It starts to take place mainly along joints and bedding planes and then enters a positive feedback loop that creates karstic systems that greatly increase the secondary porosity.

### 3.1.2.2 Permeability

The permeability of a rock characterizes its aptitude to transmit fluid, such as water, under a hydro-potential gradient. It has been mentioned that permeability is approximately proportional to the square of the grain diameter (Allen Hazen)

$$k \approx Cd^2$$

where  $k$  = intrinsic permeability,  $C$  is a dimensionless constant of proportionality which is dependent on porosity of the sample, range and distribution of particle size, shape of grains, etc. and  $d$  refers to the mean or effective grain diameter.

### 3.1.2.3 Hydraulic conductivity

The Water Resources Division, U.S. Geological Survey, adopted hydraulic conductivity and replaced permeability in hydrologic studies to use a different and simplified unit scheme. Hydraulic conductivity denoted by  $K$  may be defined as the ease of water to pass through pore space or fractures, its unit expresses the unit length per unit time. The hydraulic conductivity can be approximated empirically or measured experimentally by different methods and approaches (discussed furthermore during the chapter).

### 3.1.2.4 Transmissivity

The transmissivity denoted  $T$  is the measure of the rate at which water of the prevailing kinematic viscosity is transmitted through a unit width of the aquifer under a unit hydraulic gradient. Contrary to hydraulic conductivity which is used in three-dimensional measurements, transmissivity is measured per width unit which makes it useful in two dimensional measurements. Transmissivity and hydraulic conductivity are the most important parameter that is investigated in aquifer characterization procedures. The transmissivity is related to the hydraulic conductivity of an aquifer by its thickness  $b$  where  $T=Kb$ .

Higher transmissivities result in greater volumetric flow rates through an aquifer for the same hydraulic gradient. During a pumping test, low drawdown values are observed in aquifers that exhibit high transmissivities. The effective transmissivity is a bulk property of aquifers that is easily measured by aquifer pumping tests. It has been observed in unconfined aquifers that the reduction in the saturated thickness of the aquifer because of pumping can result in a decrease in transmissivity. Thus, as unconfined aquifers are depleted, their transmissivity decreases and drawdown increases, even if pumping rates remain unchanged.

### 3.1.2.5 Storage coefficients

The current version of 'Theis' definition (1938) of the storage coefficient is: "the volume of water an aquifer releases from or takes into storage per unit surface area of the aquifer per unit change in head". Note from the definition that the storage coefficient is dimensionless. Storativity denoted  $S$  is defined as the capacity of the aquifer to release water, it can also be reformulated as a volume of water that is released from a unit area of aquifer under a unit hydraulic gradient. It exists other terminologies for storage coefficient just like for permeability: specific storage and specific yield. Specific storage denoted  $S_s$  is defined as the volume of water that is released from a unit volume of aquifer under a unit of hydraulic gradient which makes the specific storage has the unit of the inverse of length. The storativity and the specific storage of a confined aquifer could be linked as follows: storativity is the vertically integrated specific storage value, which for a homogeneous aquifer, is the product of its specific storage and the thickness of the aquifer  $S=S_s b$ .

The storage coefficient of unconfined aquifers is virtually equal to the specific yield, as most of the water is released from storage by gravity drainage and only a very small part comes from compression of the aquifer and expansion of the water.

Diagenesis considerably impacts the primary hydraulic properties of sedimentary rocks. For instance, the porosity and permeability are normally reduced through the burial due to compaction and cementation; e. g. sediments composed of soft, clay-rich rock fragments may quickly lose nearly all of

their effective porosity while clean quartz sands, are much more resistant to mechanical compaction and usually lose porosity primarily through cementation.

### 3.1.3 Darcy's law

Hagen (1839) and Poiseuille (1846) found out that the rate of flow through capillary tubes is proportional to the hydraulic gradient. Furthermore, Darcy (1856) experimented the flow of water through sand, and he found that the rate of laminar (viscous) flow of water through sand is also proportional to the hydraulic gradient. This is known as Darcy's law and it is expressed as follows:

$$q = \frac{Q}{A} = -\frac{Kdh}{dl}$$

where  $K$  is the hydraulic conductivity, which has the units of length over time (m/s)  $Q$  discharge or flow rate with a unit (m<sup>3</sup>/s),  $h$  is the hydraulic head,  $l$  is the distance in flow direction,  $dh/dl$  is thus the hydraulic gradient,  $A$  is the cross-sectional area of the flow path.

Hydraulic conductivity as mentioned in the previous paragraphs depends upon the properties of the fluid. Permeability is an intrinsic property of a rock or sediment and is not dependent on other variables or conditions. The permeability  $k$  can be linked with hydraulic conductivity  $K$  as follows

$$K = \frac{k\rho g}{\mu}$$

where  $\rho$  is the water density,  $g$  is the gravitational acceleration and  $\mu$  is the dynamic viscosity. In the groundwater field, Because of the fact that aquifers are usually a single-phase system and the physical properties of water barely change within different study areas, hydraulic conductivity is used to quantify the ability of a material to conduct water instead of using permeability.

## 3.2 Heterogeneity of aquifers and scale of investigation

Heterogeneity of geological reservoirs corresponds to the spatial variation in its different properties such as hydraulic, transport, and geochemical properties which govern the physical processes that involve the aquifer. The term homogeneous aquifer is ideal and it is impossible to find homogeneous aquifers in real applications. However, there are some aquifers that can be idealized and have a homogenous like hydraulic behavior. Moreover, assumptions and simplifications related to the scale allow to characterize a highly heterogeneous rock. In addition to heterogeneity, anisotropy refers to the condition where those aquifer properties vary with direction. All real field aquifers are heterogeneous and the degree of heterogeneity varies with scale. At large scale for instance, a porous media could be considered as homogenous in some cases which allows us to use a simple Darcy's law and diffusivity equation to simulate the flow. Although, aquifer characterization remains very challenging in: data

acquisition, interpretation, modelling and scale assessment. It has been pointed out that the ultimate relevant scale for petroleum reservoir and groundwater investigations is the practical size of the model grid blocks (Haldorsen 1986). Aquifer heterogeneity can be caused by different parameters:

- variations in the sediment composition and texture, such as grain size, shape, and sorting
- sediment composition
- depositional environment or facies
- diagenesis
- structural geological process.

The heterogeneity starts from the depositional process. In fact, environmental deposits are characterized by different intensity of physical processes that govern the deposition at different locations which lead into different sorting of grains. The deposition of grains with different sizes permits the creation of permeable sand bodies with different geometries and different sizes. It exists a variety of depositional facies that are at different size, textures and bedding. The burial and diagenesis of the sediments will alter its structure and texture which will change the properties of the rock, the change of the properties during diagenesis can increase the degree of heterogeneity but also can decrease it depending on the rock constituents and the physical and chemical process that occur. The scale is very important because heterogeneity can be interpreted differently. For instance, if we look at a small scale of one stratum, the hydraulic properties could be classified as relatively isotropic but at bigger scale with adding more strata that have different properties, we will be at a multilayered system scale that present a high anisotropy ratio between  $K_h$  and  $K_v$ . Stratified aquifers typically have large vertical to horizontal anisotropy ratio because of the difference in hydraulic conductivity between beds and finer-scale anisotropy within beds. Layered heterogeneity occurs on multiple scales, and variations in properties may occur within a given layer. On a coarse scale for example, a stratigraphic succession may be divided into aquifer and (semi) confining strata, and if we decrease the scale to the strata, the aquifer may be divided into several hydro-stratigraphic zones with different transmissivities or maybe constructed with different sand bodies with different properties.

Dual-porosity or multiple-porosity conditions occur where the rock volume contains more than one pore system. Typically, the rock contains a matrix pore system consisting of primary porosity and a secondary pore system that includes fractures and conduits, which often have a high permeability relative to the matrix. Also, the scale of investigation may be very relevant to judge if we consider the medium as a single porosity system or as a dual or multiple porosity system.

**Table 3.1:** Classification of aquifer characterization scales.

Scale	Description	Investigation methods
-------	-------------	-----------------------

Microscopic	Scale of individual pores and sand grains	Thin section petrography
Mesoscopic	Scale of individual sub-facies and bedding	Core plugs, mini/tiny Permeameter
Macroscopic	Heterogeneity on a sedimentary facies scale including stratification	Borehole geophysical logs, drillings, slug tests
Megascopeic	Scale of a wellfield and model grid blocks, facies, units	Aquifer pumping tests
Gigascopeic	Total formational or regional scale	Interference tests, regional model

Aquifer heterogeneities occur at different scales and are superimposed between each other. Several classifications of heterogeneity scale have been proposed: e.g. the classification provided in Table 3.1 is based on the categories proposed by Dagan (1986), Haldorsen (1986), and Galloway and Sharp (1998).

The project objectives are necessary to fix the needed types and scales of aquifer heterogeneities to investigate. For example, bed-scale fracturing may not have to be explicitly considered in an investigation concerned only with groundwater flow and water levels, whereas it may have to be characterized and incorporated into models used to simulate local contaminant transport.

The most important step in aquifer characterization is data acquisition; a wide variety of tools that provide data at different scales are available. And following the project aim and the amount of available budget, professionals choose the tools that can most effectively provide the required quantity and quality of data. It is also necessary to understand what kind of information a tool can provide and know its limitations. In order to perform a given aquifer characterization method, it is relevant to check if it is available, gives the wanted information, can be performed in the current wells setup in the site, and of course affordable in terms of budget. This chapter will focus on describing the most relevant, simple and low-cost aquifer characterization methods and some of the data interpretation approaches that go along. Most efficient way to characterize an aquifer is to develop and use workflows that not only capture and interpret different available information but also integrate data at different scales into numerical groundwater models. The developed numerical models need then to be evaluated on their accuracy for predictions; if a groundwater model provides erroneous predictions, then the underlying conceptual model should be reevaluated. Groundwater models can be very different from one another, scale is relevant to choose which model is appropriate for different studies. Grid cell size, vertical extent, domain size and other parameters depend on the type of scale to emphasize in the constructed model. For example, if our objective is to construct a regional model, our model size will be in the kilometric

scale and the size of the cell will have several meters to several hundred meters (in some cases, the grid cell is not relevant at this scale and a simplified facies model is more preferred). The population of the model with hydraulic properties will then be done only if regional flow simulation is required in the study.

On the contrary, models to evaluate flow and interference tests between the wells will be at the site scale; a much smaller domain scale compared to the regional model. they require an even smaller grid cell size in order to simulate sensitive data such as solute transport at contamination sites. Models of solute transport, in general, require a smaller grid size in order to better capture flow-controlling aquifer heterogeneity.

Several studies have been achieved to characterize effective parameters under different scales (Neuman, 1994; Martinez-Landa and Carrera, 2005; Pina et al., 2019; Aziz Mohammadi and Matthäi, 2017). They showed that the obtained effective values are highly variable with the length of the scale. Some used techniques and approaches based on measurements of the hydraulic conductivity in boreholes, blocks and cores at a laboratory scale (Sudicky et al., 1986; Illman et al., 2010). At larger scales, Martinez-Landa and Carrera (2005) used different hydraulic tests and a numerical model at hundred meters' scale and then investigated the fracture and scale effect at later work (Martinez-Landa et al., 2016). They proposed a methodology that involves geophysics, hydro-geochemistry, hydraulic tests, and numerical models to better characterize groundwater systems, introducing identified individual fractures as dominant structures.

In aquifer characterization, the scale-effect is a lot discussed and many studies have already confirmed the variation of the hydraulic properties according to scale (De Marsily 1985; Neuman 1990; Rovey 1994; Schultze-Makuch and Cherkauer 1998; Zijl 1999; Nastev et al. 2004). Other authors investigated the scale effect in more complex aquifers; e.g. groundwater flow and scale effects occurring in fractured rocks (Hsieh 1998; Niemi et al. 2000; Yang et al. 2013). One of the biggest challenge is how to incorporate the measured properties obtained at different field scales into a single aquifer model. Intuitively, one may conclude that larger-scale tests yield more representative hydraulic conductivities for regional studies and that the small-scale test results can be neglected. However, integrating different data at different scales needs further investigation.

### **3.3 In-situ evaluation techniques of aquifer hydraulic properties**

Several evaluation techniques are available for aquifer characterization and hydraulic properties assessment. These techniques allow to answer relevant questions about solute transport, water quality, enhancement of water management and the properties of the rock of the aquifer. Nowadays, several hydrogeology textbooks are available and discuss aquifer characterization techniques in different

aspects and different degrees of extent. Figure 3.2 summarizes the common characterization techniques and tools with their approximate investigation scale as well as the main information that can be extracted from the acquired data. The scales of investigation are only approximately represented to allow the classification of the different techniques. In fine-scale techniques, we can find laboratory measurements that involve direct or indirect measurements of the porosity and permeability of sediments or sedimentary rock samples. We can also find the mini/tiny-permeameter measurements that approximate permeability from a rock surface of cores or outcrops. While, indirect measurements techniques include the estimation of permeability and hydraulic properties from sand grain-size analysis or from thin section petrography. Well loggings such as borehole-imaging can also be added into a fine scale category (e.i. borehole scale). They can provide more information about the lithology and sequence stratigraphy as well as confirms if there are signs of secondary porosity features (e.g., fractures, vugs).

We classify the aquifer characterization techniques that investigate the near wells area as small-scale aquifer characterization techniques. The main used ones are hydraulic tests that include pumping or injection tests. The pumping or injection rate can impact the investigation scale; bigger a pumping rate, larger can become the scale. Hence, small pumping rates are recommended in order to investigate small areas. The volumes of investigation are on the decimeter to 10 m scale.

Medium-scale aquifer characterization techniques include mainly pumping or injection test in a single well as well as packer tests with long durations and bigger rates. Such set ups usually have volumes of investigations on the order of 10 – 100 s of meters. We can also classify the tracer tests in medium-scale aquifer characterization techniques category, however, some tracer tests are performed in karstified areas which make the tracer travel much longer distances which can put the technique as large-scale method instead. Cross-well tomographic techniques also usually fall into the medium-scale aquifer characterization techniques where the scale being defined by the well spacing.

Large-scale aquifer characterization techniques have a distance of investigation in the 100 m–10 km range. The main large-scale aquifer characterization technique is multiple-well aquifer pumping tests if the different wells can interfere.

Very large-scale techniques have scales of investigation of 10 s of km or greater and include calibration of regional models and tidal fluctuation analyses.

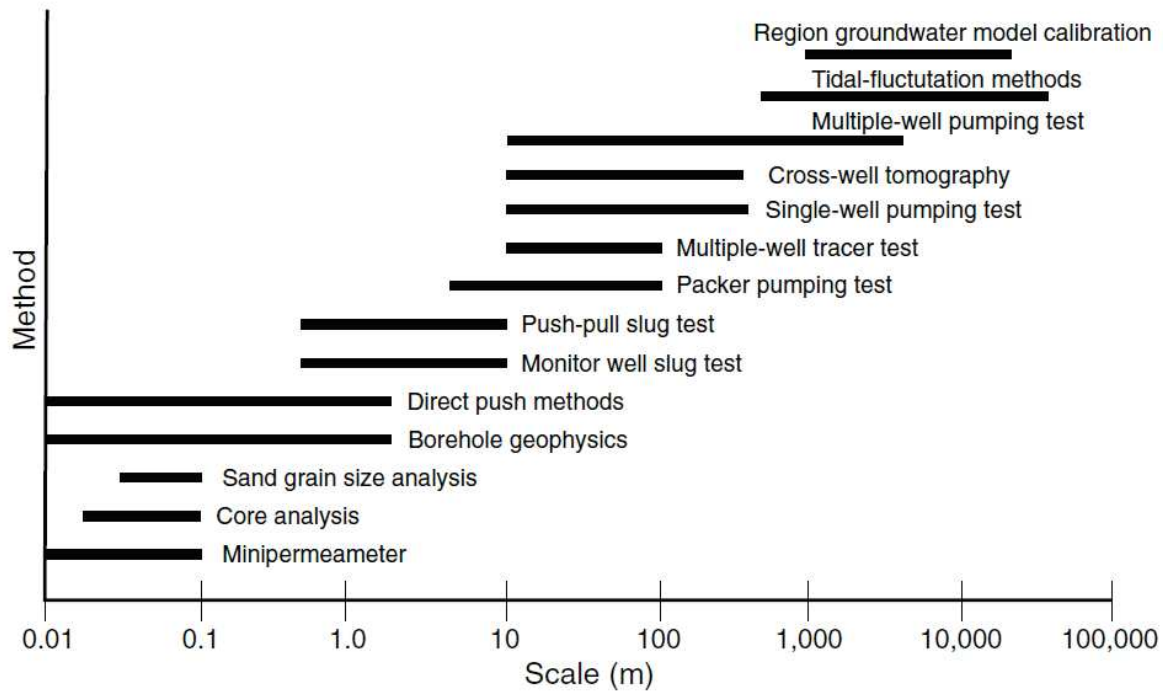


*Figure 3.2: Approximate scale (radius of investigated volume) of techniques used to measure hydraulic conductivity (from Maliva 2016)*

### 3.3.1 Indirect estimation of hydraulic conductivity

Indirect methods are mainly represented by empirical estimations of a given parameter. To develop an empirical equation, a large number of samples are required and studied to determine the coefficients used in the empirical equations. Most popular empirical equations to estimate the hydraulic properties of the rock use the grain size of the particles that construct that rock.

To estimate the hydraulic parameters of a given rock or soil, particle size distributions and percentile amount of that distribution are used and the two most used are the 60%, 40% percentiles denoted  $d_{60}$  and  $d_{40}$ . More details about these methods are reviewed in Bunte (2001).

It exists several empirical equations to estimate the hydraulic conductivity ( $K$ ). The empirical equations relate the hydraulic conductivity  $K$  to some size property of the sediment usually the effective grain diameter. Vukovic and Soro (1992) summarized several empirical methods from former studies and presented a general formula:

$$K = \frac{g}{\nu} \times C \times f(n) \times d_e^2$$

where  $K$  = hydraulic conductivity;  $g$  = acceleration due to gravity;  $\nu$  = kinematic viscosity;  $C$  = sorting coefficient;  $f(n)$  = porosity function, and  $d_e$  = effective grain diameter.

The most popular empirical equation to estimate permeability is Kozeny-Carman equation which was proposed by Kozeny in 1927 and modified by Carman in 1937 and 1956. It is considered as a semi-empirical, semi-theoretic formula (Carrier, 2003). The Kozeny-Carman equation is widely accepted and used for the indirect determination of permeability as a function of the characteristics of the grains constructing the rock or soil. As for many other approaches, it also has limitations; this estimation is not appropriate for either soil with effective size above 3mm or for clayed soils (Carrier 2003). The Kozeny-Carman equation is as follows

$$K = \frac{g}{\nu} \times 8.3 \times 10^{-3} \left[ \frac{n^3}{(1-n)^2} \right] d_{10}^2$$

where  $K$  is the hydraulic conductivity;  $g$  the gravitational acceleration;  $\nu$  the kinematic viscosity and  $d_{10}$  is the 10% percentile effective grain diameter.

The Kozeny-Carman equation assumes that the flow in porous rock is equivalent to the flow in channels that are not inter-connected (Carman, 1956). The pore space is assumed to be equivalent to several parallel capillaries with a common hydraulic radius. The shape factor is representative of the average shape of a pore cross-section and is based on the hydraulic radius.

### 3.3.2 Tiny/Mini permeameter measurements

The tiny/mini-permeameters (or probe permeameters) are a fast measurements tools that can estimate the permeability of the rock just by having access to a surface of that rock. These tools use air as the fluid that passes through the rock. Contrary to laboratory permeameter that allow the fluid to pass through the whole plug, mini-permeameters only investigate a small area near the contact surface/tool. And, the flow is different from the usual linear flow performed in laboratory measurements; it aspirates air from the rock which in turn will get air from the surroundings of tool contact (see Figure 3.3d). These measurements can then be directly compared to Hassler-cell-derived permeability measurements. Mini-permeameter measurements are governed by seal tightness which is strongly influenced by seal surface pressure, the angle of the probe tip with the sample surface and the roughness of the sample surface. The tool needs a very good sealing mechanism to obtain good results because potential leakage has a large influence on the measurements. The seal tightness of these devices is achieved by a tight contact between nozzle, sealing rubber, and sample surface, and can be further improved by a ring of putty.

With the simplicity of the tools, it is common to find Tiny-Permeameters that are easily portable and easily handled in order to make quick and efficient measurements directly from the outcrop. For example, the mini-permeameter “TinyPerm II” (Minipermeameter Tiny Perm = MTP) of “New England Research Inc.” was applied at the GeoZentrum Nordbayern, University of Erlangen-Nürnberg. It is a

portable handheld air permeameter that can be used in the laboratory or in the field directly on the surface of sampled plugs, well cores or cleaned outcrop walls. The tip of the tool consists of a 22 mm-sized rubber nozzle with an inlet diameter of 9 mm. To prevent leakage between probe tip and sample surface, the nozzle was additionally equipped with an impermeable expanded rubber ring of 9mm inner diameter (inlet) and 27mm outer diameter, providing a 9 mm-thick seal around the inlet. The use of additional seals is highly recommended to optimize MTP measurements.

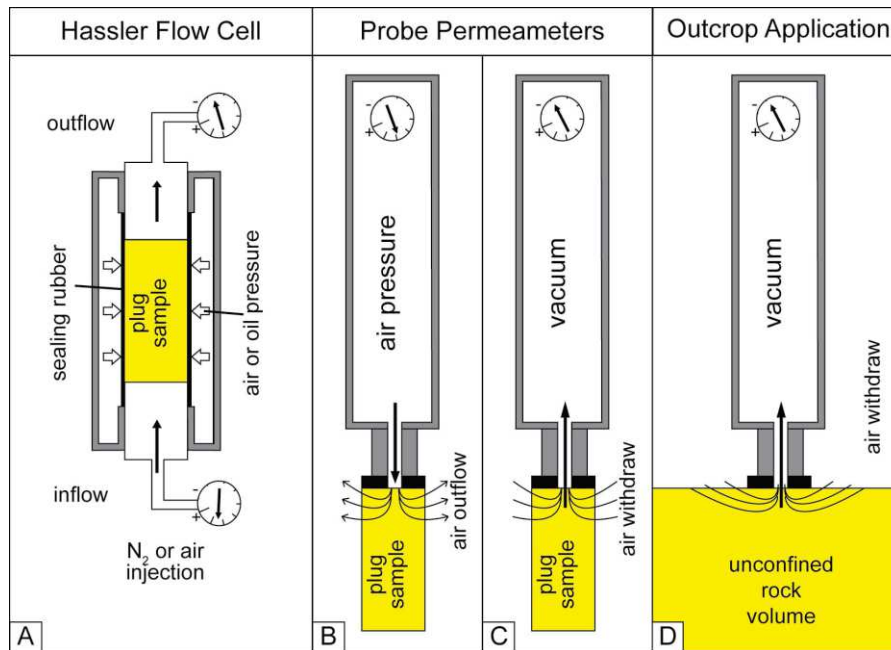


**Figure 3.3:** Principles of permeability measurements on plug samples: (A) Hassler cell, (B) mini-permeameter using air injection, and (C) mini-permeameter applying a vacuum. Note the difference in rock volume and flow trajectories in (A), (B), (C). Likewise, the difference in rock volume needs to be considered when conducting outcrop measurements = unconfined rock volume (D) (Filomena et al. 2014).

To enhance accuracy of different gas-driven permeability measurements, device-specific aberrations have been documented from Hassler cell and mini-permeameter measurements. It is also recommended to perform several measurements in the same surface then either take the mean or the smallest value of permeability as final. The choose of the smallest value is recommended because the tool tends to overestimate the measurement in case of the existence of a leakage during the handling (a small move can create a sudden gas transfer from the air to the tool. The air that is aspirated by the tool because of leakage will bias the measurement making the tool think that the air came from the rock which lead into an estimation of relatively very high permeability values. Permeability over- and underestimations either by mini-permeameters or Hassler cells may result from variable factors. Sealing quality and surface roughness play an important role in leak tightness of mini-permeameters. Due to shorter flow trajectories and a reduced rock volume, the TinyPerm II device largely overestimates plug sample permeabilities. Therefore, it is proposed correcting them for unconfined rock volumes.

Permeability underestimations, however, can be obtained if the measurement location is not well chosen. In fact, if the measurement location has silt or other material different from the global rock. It is also highly recommended to clean the surface before the measurement because the alteration that rock can be subject to from its contact to air. By covering only a very limited surface, mini-permeameter measurements are susceptible to even small-scale rock heterogeneities.

### 3.3.3 Well cuttings and coring

Well cuttings are small fragments of rock and sediment produced during the drilling and evacuated to the surface by the drilling fluid. For the non-cored wells, the well cuttings are valuable to access more information about lithology and the sediments are used for grains analysis, hence, the indirect estimation of the hydraulic properties of the soil using empirical equations as mentioned above. Even though cuttings are easily obtained from a drilling, their collection involves minimal additional effort and cost, and they are thus the least expensive source of lithological data. well cuttings are usually sampled at small depth steps (e.g. every 1 m) but can increase to several meters in case the well is deep and a fine sampling is not required.

limitations:

- The depth control of cuttings may be poor in deep wells.
- The small size of cuttings (often less than 1 cm) precludes observation of large-scale features in the formation, such as sedimentary structures, bedding, and large secondary pores.
- Drill cutting samples represent a mixture of the rock or sediment present in the sample interval. It is typically not possible to determine from the cuttings alone how the different rock types are distributed in the sampled interval.
- Drill cutting samples may be contaminated with material that fell into the borehole from above the sample interval.
- Cuttings may be biased towards harder lithology. Softer material and very fine-grained material (finer than the collection screen size) may be underrepresented.

For higher quality of data from the drilling, cores are highly wanted for further laboratory analyses. Coring is performed where high-quality, intact, formation samples are needed for petrophysical, mineralogical, and geochemical analyses. The choice of coring method depends on the characteristics of the formation to be sampled, the amount (length) and diameter of required cores, and the project budget. Typically, coring considerably slows the drilling and require different tools and is thus more expensive.

Well cuttings and well cores are essential for aquifer characterization procedures. They give valuable information at a well scale and usually give a reliable hydraulic conductivity profile.

### 3.3.4 Well logging

The wells penetrating the aquifer and adjacent strata expose the rock which makes them an aim to study. Well loggings are an aquifer characterization technique that investigate the walls of the wellbore. They give fundamental information about the lithofacies and near well area. they provide essentially continuous *insitu* measurements of the petrophysical properties and lithology. They became one of the most used tools in reservoir and aquifer characterization. Detailed reviews of geophysical logging principles and applications are provided by several authors(Asquith and Krygowski, 2004; Serra, 2008; Wempe, 2000; Kobr et al., 2005; Maliva, 2016).

Geophysical logging provides raw data that need to be interpreted into a useful parameter which is usually a petrophysical property, such as porosity, permeability, lithology, and mechanical rock properties. Ideally, authors always search for new ways of converting well logs into hydraulic conductivity in groundwater investigations. Hydraulic conductivity can be estimated indirectly from other parameters, such as porosity, grain size, and pore-size distribution. Flowmeter logs can also be used to estimate the relative hydraulic conductivity using transmissivity calculated by other means. Just like for flowmeter interpretation, geophysical wellbore loggings can be interpreted into relative hydraulic conductivity profiles using different methods: approaches that give qualitative interpretation of geophysical logs which is very simple, empirical equations that convert the raw data into hydraulic property values, or even more complex approaches such as machine learning and inversion. Maximum value from the logs through quantitative interpretation and not only qualitative interpretation is intended which push authors to put more efforts to develop new workflows and new approaches in order to get better estimates.

For better quantitative analyses of geophysical logs, accurate data and processing tools (e.g. algorithm precision) are required. Calibration and standardization are important parts of quantitative geophysical log interpretation, which are discussed by Keys (1989). We define the calibration as the process of converting the raw measured data rock characteristics. The most common logs are:

- Caliper logs measure the diameter of the logged borehole needed for the interpretation of other logs and for well construction.
- The natural gamma ray log is widely used for groundwater investigations. It gives a reliable correlation between wells and it provides a profile of shale or clay volumes.
- The electrical resistivity of the formation depends on its porosity and the resistivity of its water. In the oil and gas industry, resistivity-based logs are widely used to evaluate hydrocarbon saturation and in groundwater investigations, formation water resistivity depends on its salinity.

- The SP log records the natural potential between two electrodes: an electrode in the borehole and a fixed electrode at land surface. The main applications of SP logs for groundwater investigations are • location of permeable beds • location of shale or clay beds (confining units) • inter-well correlation • determination of formation water resistivity.
- Resistivity logs are very used in groundwater investigations for the detection of permeable zones and the evaluation of porosity and water salinity. It easily defines the lithology of the penetrated layers.
- Sonic or acoustic logs use the velocity, amplitude, and phase relationships of transmitted sound waves to obtain information on the physical properties of the tested formation.
- Density and neutron logs, are primarily used to determine the porosity of formations and they are more used in gas and oil industry compared to groundwater studies because they use radioactive sources which may contaminate water supply.

### 3.3.5 Flowmeter measurements

Flowmeter surveys characterize the vertical inflow profile of a given well (Paillet et al. 1998, Molz et al. 1994, Zlotnik and Zurbuchen 2003, Williams and Paillet. 2002, Day-Lewis et al. 2011). They are widely used to determine vertical profiles of hydraulic conductivities at well locations. Complex geological media are often layered systems and flowmeter analysis has shown its efficiency to detect the main layers contributing to the total pumped flux (Day-Lewis et al. 2011, Paillet and Reese 2000). Flowmeter profiling can also be used to detect the well crossing fractures (Day-Lewis et al. 2011, Roubinet et al. 2015). Flowmeter tests are easy and cheap but bulky and the investigated height is limited due to the space taken by the pump and the generated drawdown. Flowmeter tests may provide a new set of information and have been included in inverse modelling problems. For instance, Fienen et al. (2004) used a Bayesian inverse approach to interpret the vertical hydraulic conductivity in a heterogeneous fractured aquifer. Other applications used the interpreted hydraulic conductivity values from flowmeter tests in the transmissivity map to constrain the geostatistical inversions (e.g., Rehfeldt et al. 1992; Chen et al. 2001). In other studies, flux measurements have also been used as observation data additional to hydraulic heads in hydraulic tomography (Li et al. 2008, Zha et al. 2014, Tso et al. 2016).

#### 3.3.5.1. Spinner flowmeter

During a spinner flowmeter test, water is extracted from an open hole well and, once steady state is reached, a spinner flowmeter is swept along the well from the bottom of the well to the top and a vertical flow rate profile is measured. In most common cases, when the pump is located at the top, the flow rate log will have the trend of an increasing curve starting from a zero value at the bottom to a max value at the top, that will correspond to the total extracted flux from the well. The increase in flow

rate over a certain depth increment is correlated to the relative hydraulic conductivity profile; higher the hydraulic conductivity, stronger the rate increase. Flowmeter tests therefore provide relative values of hydraulic conductivity distribution along the borehole. In order to extract the absolute values, an effective value of hydraulic conductivity of the well (obtainable from the interpretation single hole of a pumping tests) will be used. Single-hole flowmeter data can be analyzed to estimate conductivity profiles along boreholes and characterize aquifer compartmentalization (Molz et al. 1989; Kabala 1994; Paillet et al. 1998).

If a well is subject to a pumping with a pump placed at the top of the well extracting with the rate  $Q_p$ , the underground layers connected to that well will contribute to the total extracted flux. Their contribution is proportional to their hydraulic conductivity. For the following equations,  $b$  (m) refers to the aquifer thickness,  $z_0$ (m) the reference level of the borehole bottom, and  $z$  (m) the height above the bottom (Figure 3.4). In an idealized layered aquifer, the flow into the well from a given layer is proportional to the transmissivity of that layer:

$$\Delta Q_i = \alpha \Delta z_i K_i$$

where  $\alpha$ (m) is a constant of proportionality,  $\Delta Q_i$ (m<sup>3</sup>/s) corresponds to the induced flow increments observed in the borehole along the  $i^{\text{th}}$  increment of height  $\Delta z_i$ (m) that has a hydraulic conductivity  $K_i$ (m/s). The average horizontal hydraulic conductivity  $K_{avg}$  can be expressed by:

$$K_{avg} = \frac{\sum K_i \Delta z_i}{b} .$$

The cumulative flow  $Q_{cum}(b)$  over the aquifer thickness can be expressed as follows:

$$Q_{cum}(b) = \int_{z_0}^b Q(z) dz = Q_p = \sum_i \Delta Q_i = \alpha \sum_i \Delta z_i K_i = \alpha K_{avg} b .$$

By substituting the sum,  $\alpha$  can be solved as:

$$\alpha = \frac{Q_p}{K_{avg} b}$$

Then, the hydraulic conductivity of each layer can be quantified by:

$$K_i = \frac{\Delta Q_i K_{avg} b}{Q_p \Delta z_i}$$

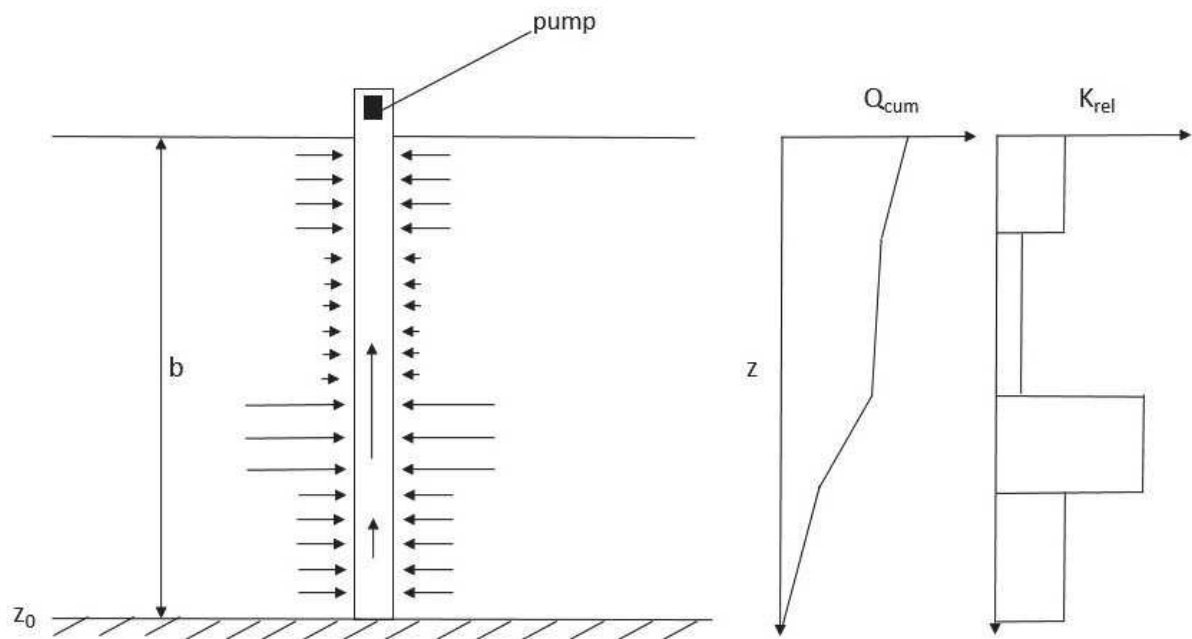


**Figure 3.4:** Flowmeter setup scheme with an interpretation example.  $Q_{cum}$  is the cumulative flow rate and  $K_{rel}$  is the interpreted relative permeability from flow log (Aliouache et al. 2021).

The pattern of flowmeter logs can provide insights into hydraulic conductivity distribution. Patterns of gradual increase in flow into a well are often indicative of a flow system dominated by primary porosity, although a system with evenly distributed secondary porosity might also give this response. On the contrary, sharp steps in logs may be indicative of a thin flow zone, such as a hydraulically active fracture or karst conduit.

### 3.3.6 Pumping tests

Pumping tests remain the most commonly used and low-cost method to obtain information about hydraulic properties of an aquifer for water-supply investigations. A pumping test consists of extracting water from a well (pumping well) and monitoring the water level change in all available wells (observation wells). In other terms, large volumes of water are pumped from a well for a period of time, and changes in head are monitored at the pumping well and/or nearby observation wells. Aquifer testing is a common tool that hydrogeologists use to characterize the heterogeneity of aquifers, to investigate the subjacent aquitards and to know about flow system boundaries. Aquifer tests are typically interpreted by using analytical solutions (discussed later in this chapter). The most common method is the Theis solution based on several assumptions to match the observed data for an idealized aquifer (see Figure 3.5). Furthermore, numerical models can be used to analyze the results of a pumping test. The drawdowns can be analyzed using various models of well-formation configuration (Kruseman and de Ridder, 1990; Batu, 1998). Several investigations (Butler and Liu, 1993; Sánchez-Vila et al., 1999) have shown that pumping tests investigate a relatively large volume of the aquifer.

Typically, monitoring and pumping wells are screened across the same aquifers.

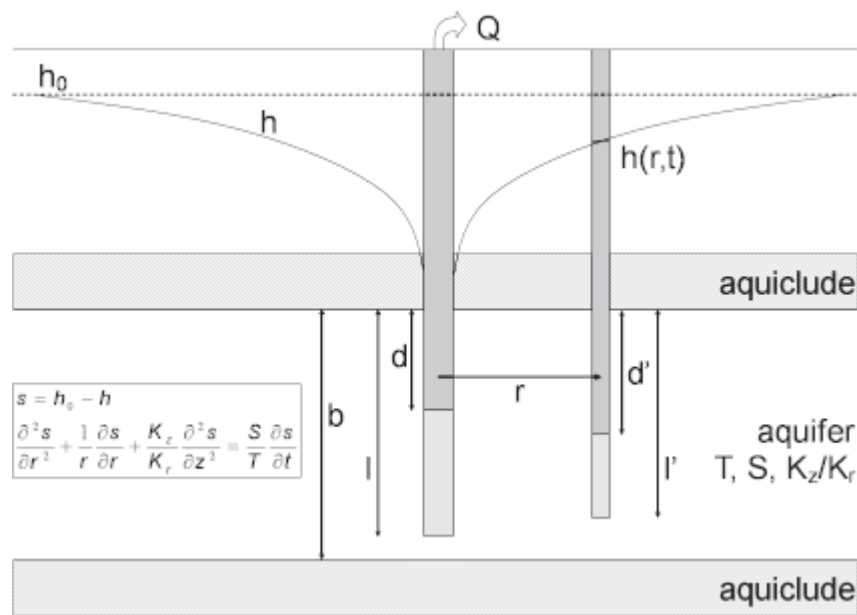


**Figure 3.5:** Typical well configuration for pumping test in non-leaky confined aquifer (from AQT SOLV).

The interpretation of the drawdowns provides estimation of the horizontal hydraulic conductivity and storage parameters of the pumped aquifer.

Single well pumping tests remain valuable; however, multiple-well tests are preferred because of:

- more accurate measurement of storativity values can be obtained
- less effect of skin in the observation wells
- possibility of use of different numerical methods that require observations at different locations, e.g. distance-drawdown methods
- it provides information about the heterogeneity between the wells
- aquifer anisotropy investigations.

### 3.3.7 Slug tests

Slug tests are a basic hydraulic test that consists on generating a sudden change (pulse, see Figure 3.6) of water level in one well and monitor in different wells. A slug test is a test where water is quickly added or removed from a groundwater well, and the change in hydraulic head is monitored through time. This approach is used to determine the near-well aquifer characteristics because its scale of investigation is smaller than the scale of a pumping test. Slug tests are used for studying the permeability of aquitards and is the most promising tool within the traditional aquifer characterization techniques. However, an important skin effect can bias the estimations. Although the slug test has the most

potential of the traditional approaches, most sites do not have the extensive well network required for effective applications.

A slug test can be simply achieved by adding a measured amount of water to the well or by dropping a heavy solid object into the well to create a sudden water level displacement. This makes it a very cheap approach for the valuable information that it gives.

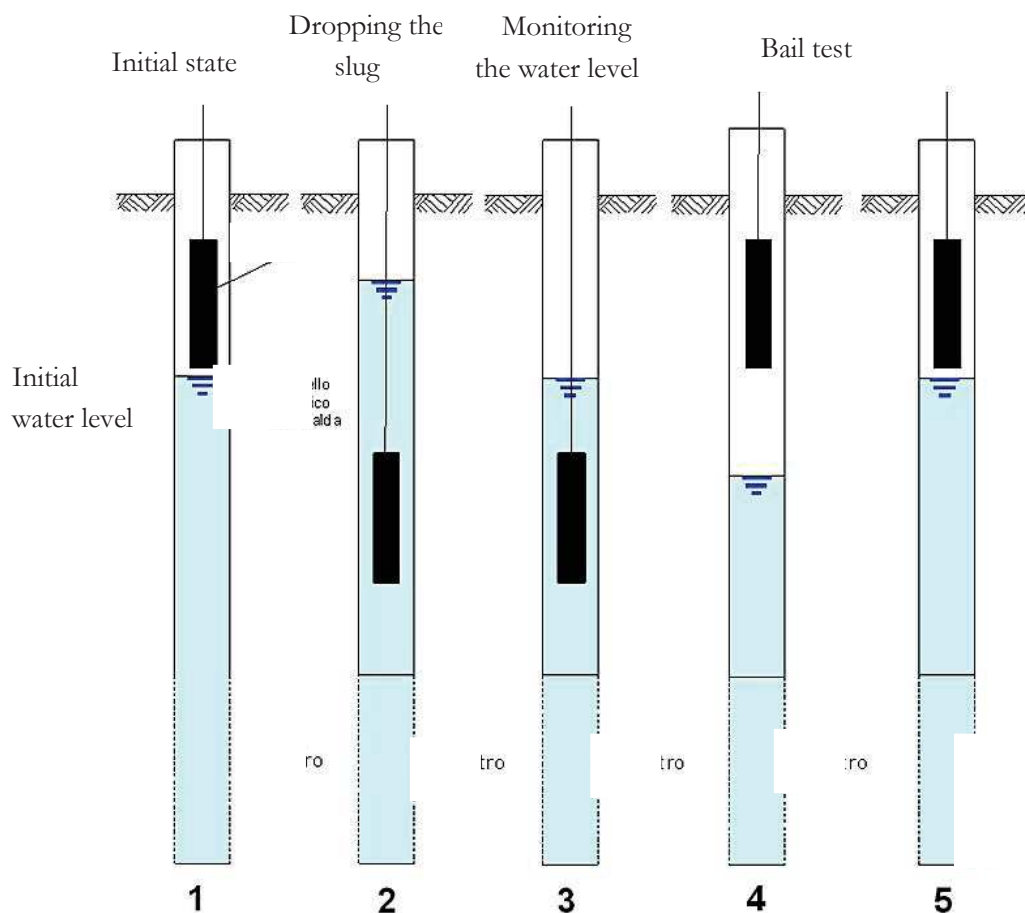


*Figure 3.6: Slug test set up (from Fileccia, 2015).*

### 3.3.8 Packer tests

Packer testing involves the use of inflatable packers (see Figure 3.7). They are used to isolate parts of the borehole. They can be used for hydraulic testing or for water sampling. Traditional pumping tests only provide horizontal information about heterogeneity while packer testing provides zonal isolation and thus greater vertical resolution of aquifer heterogeneity and can determine the hydraulic parameters of aquifer's confining units. The application of packer testing to hydrogeological investigation was reviewed by Brassington and Walthall (1985) and Quinn et al. 2012. To perform a packer test, the borehole needs to be stable and the tools are usually bulky and expensive. Also, the variable distribution

of skin effect can bias the estimations. Packer testing equipment is usually very heavy and, therefore, a crane is needed to install and support the equipment.

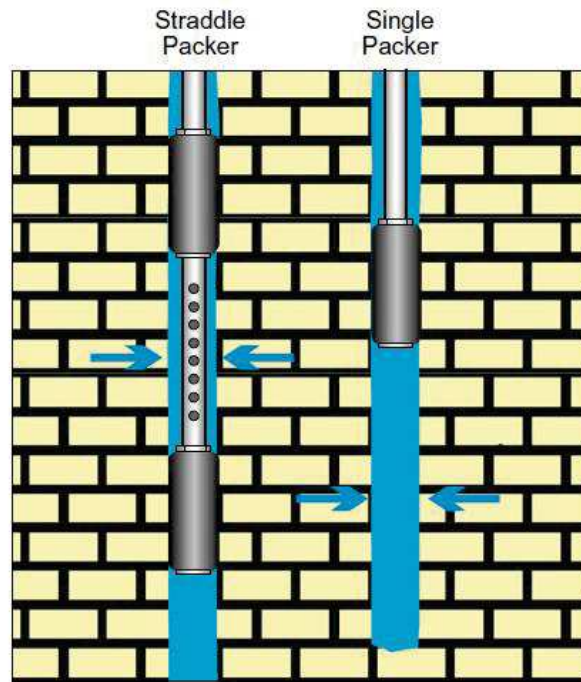


*Figure 3.7: Conceptual diagram of a straddle-packer and single-packer test.*

### 3.4 Tools and models for the interpretation of hydraulic data and estimation of hydraulic properties

#### 3.4.1 Estimation of effective hydraulic properties

every hydrogeological investigation requires an estimate of hydraulic conductivity ( $K$ ). The classical way of determining hydraulic properties of a studied aquifer is to sample cores and plugs from the aquifer rocks or from equivalent rock in the area (e.g. outcrops). Then, proceed to laboratory measurements of hydraulic conductivity and porosity. High heterogeneities in the values of measured hydraulic properties show how the investigation scale is important. The investigated volume of those cores is very small compared to the aquifer scale. Several hydraulic techniques that investigate larger volumes were used (e.g. pumping tests, slug tests, flowmeter tests, etc. Some of these techniques are discussed previously in this section). For water-supply investigations, a single estimate of  $K$  averaged over a relatively large volume of an aquifer can be sufficient. However, it cannot be the case for water-quality investigations. It has been shown at several times that spatial variations in hydraulic parameters play a major role on controlling the behavior of solute movement in saturated flow systems (e.g.,

Sudicky and Huyakorn, 1991; Zheng and Gorelick, 2003; Butler, 2005). The geometric mean K value determined from small-scale data and homogeneous interpretation of hydraulic tests remain non-sufficient and the spatial variability of hydraulic properties are thus needed. Illman et al. (2010) tested the reliability of these estimated effective parameter and revealed that the predictions of pumping tests using geometric mean and effective K estimates from various methods showed biased results in terms of predicting drawdowns from independent cross-hole tests.

Several researchers compared the validity of various characterization approaches in the field [e.g., Zlotnik and Zurbuchen, 2003; Butler, 2005; Illman et al., 2010]. For example, Butler [2005] compared the K results from permeameter analysis of core samples with different interpretations of hydraulic tests (e.i. traditional slug tests, dipole flow tests, multilevel slug tests, borehole flowmeter tests, direct-push slug tests, pumping tests). He found that different characterization approaches yield reliable estimates of K along the boreholes at the site. However, he found that most of the techniques lack on delineating the heterogeneity between wells and a simple kriging is usually uncertain. Illman et al. (2010) compared several techniques of hydraulic conductivity estimation and showed how hydraulic tomography is one of the most promising approaches.

Rubin and Hubbard, (2005) summarized different techniques that can provide the effective estimation of different hydrological parameters (see Table 3.2).

**Table 3.2:** Different methods and acquisition approaches that are used for estimating various hydrogeological parameters (from Rubin and Hubbard, 2005).

Hydrogeological parameter	Acquisition approach	Method
Water content	Airborne	Remote Sensing
		NMR
	Surface	Electrical Resistivity
		Electromagnetics
		GPR
	Cross-hole	Electrical Resistivity
		GPR
Water quality	Benchtop	TDR
	Airborne	Remote Sensing
		Electrical Resistivity
	Surface	Electromagnetics
		GPR

	Cross-hole	Electrical Resistivity GPR Well Logs
Hydraulic conductivity	Benchtop	X-ray attenuation
	Well Tests	Hydraulic Well tests
	Cross-hole	Tracer tests Hydraulic Tomography GPR Tomography Seismic Tomography
	Wellbore	Logs and Well Tests
Spatial correlation	Benchtop	Core measurements
	Surface	GPR
	Cross-hole	Seismic

---

### 3.4.2 Analytical methods for the interpretation of hydraulic tests

The simple way to interpret a hydraulic test is to rely on different assumptions and develop an analytical solution that can quickly provide an estimation of the effective hydraulic parameters of the aquifer. Several analytical methods are available to interpret aquifer hydraulic test data. However, different aquifers are subject to different conditions leading into different assumptions. This variety of conditions is the main cause of the existence of several analytical methods often limited to certain cases. In the following section, some of the widely used methods are mentioned. As stated before, the fact that all of the analytical methods have underlying assumptions, limitations of the methods quickly arise and the assumptions themselves can impact considerably the estimated values for aquifer hydraulic parameters. Even though, several limitations and disadvantages can be enumerated on these methods, they can still provide a quick estimation of the parameters with a satisfactory accuracy. Also, some applications only need a rough estimation of the effective hydraulic parameters and the estimates provided by the analytical solutions are often satisfactory for those applications. It is important to keep in mind that analytical methods do not necessarily provide unique result and the change of conditions and/or assumptions can change the estimates and those estimates are not necessarily accurate. This is why, it is relevant to start every aquifer characterization based on a solid conceptual model. Some of the widely used assumptions during analytical analysis are:

- Assume that the aquifer is homogeneous and/or isotropic; real field aquifers are often highly heterogeneous and anisotropic

- flow into the well is radial, horizontal, and laminar
- The wells are fully penetrating the aquifer
- no leakage of water into the aquifer from underlying and overlying strata
- Assumption that the aquifer has a uniform thickness
- the aquifer is confined and remains saturated throughout the entire test
- the aquifer is of infinite areal extent
- assume that the specific storage is constant

Several other assumptions and conditions can be met when dealing with analytical methods. And these different conditions are usually the ones that push a hydrologist to choose one method over another.

One of the biggest drawbacks of analytical methods is the fact that it is impossible to realistically represent a real field aquifer. Aquifers in nature are very complex and a single effective hydraulic value is way far from capturing and characterizing the complexity of the system. However, these methods are still widely used because of their simplicity, very low cost and help to build a basis for a conceptual model that will be used for a characterization with higher resolution. This explains why most hydrogeologists are still interpreting pumping tests by matching theoretical type-curves obtained from Theis (1935) and Theis-derived models (Cooper and Jacob, 1946). The advances in aquifer characterization research show how complex an aquifer in nature can be (Audouin et al., 2008; Ferroud et al., 2019; Odling et al., 2013).

#### 3.4.2.1 Thiem model

Thiem (1906) method applies to steady-state flow regime. True and perfect steady-state regime is basically unreachable in a real confined aquifer. The Thiem method is then used to pseudo-steady state cases in which the hydraulic gradient can be assumed constant over time. The Thiem method relates discharge to transmissivity and drawdown in two piezometers using

$$Q = 2\pi T \frac{s_1 - s_2}{\ln\left(\frac{r_2}{r_1}\right)}$$

where  $T$  is the effective transmissivity of the system,  $Q$  is the pumping rate,  $r_1$  and  $r_2$  are respectively the distances of piezometers '1' and '2' from the pumped well,  $s_1$  and  $s_2$  are respectively the steady-state drawdown in piezometers '1' and '2' response to the pumped well.

#### 3.4.2.2 Theis equation

Theis (1935) equation remains the most widely used equation in hydrology. The equation allows to relate between well hydraulics and aquifer parameters. The most common methods used for the

interpretation of aquifer hydraulic test data are based on the Theis (1935) non-equilibrium equation, where

$$s = \frac{Q}{4\pi T} \int_u^{\infty} \frac{e^{-y}}{y} dy = \frac{Q}{4\pi T} w(u),$$

where

$$u = \frac{r^2 S}{4Tt}$$

$$w(u) = -0.5772 - \ln(u) + u - \frac{u^2}{2.2!} + \frac{u^3}{3.3!} \dots$$

$s$  is the drawdown,  $Q$  is the pumping rate,  $T$  is the effective transmissivity of the aquifer,  $u$  and  $du$  are empirically derived functions,  $r$  is the distance from the observation well,  $t$  is the time since the pumping has started,  $S$  is the storage coefficient,  $W(u)$  is the integral well function.

The most common interpretation methods of aquifer hydraulic tests that are based on Theis equation are usually referred to as the 'log-log', 'curve-matching' or 'match point' methods. These two methods involve a graphical step which consists of plotting a set of time-drawdown data on a logarithmic grid (see Figure 3.8). For instance, the 'match point' method consist of plotting the time-drawdown data on a log-log scale of the same grid size as a plot of  $W(u)$  versus  $1/u$  (type curve). The type curve is usually plotted on a see through sheet which allows us to shift The graph until the time-drawdown data are superimposed on the Theis curve (Figure 3.8). A match point is then selected, at which a set of values of  $s$ ,  $t$ ,  $W(u)$ , and  $u$  are obtained. To simplify the calculations, a match point of  $W(u) = 1$ , and  $1/u = 1$  is commonly used and the  $s$  and  $t$  values are obtained for that match. with the help of Theis equation and knowing the other constant parameters of the hydraulic test, the transmissivity and storage coefficient of the aquifer can be estimated.

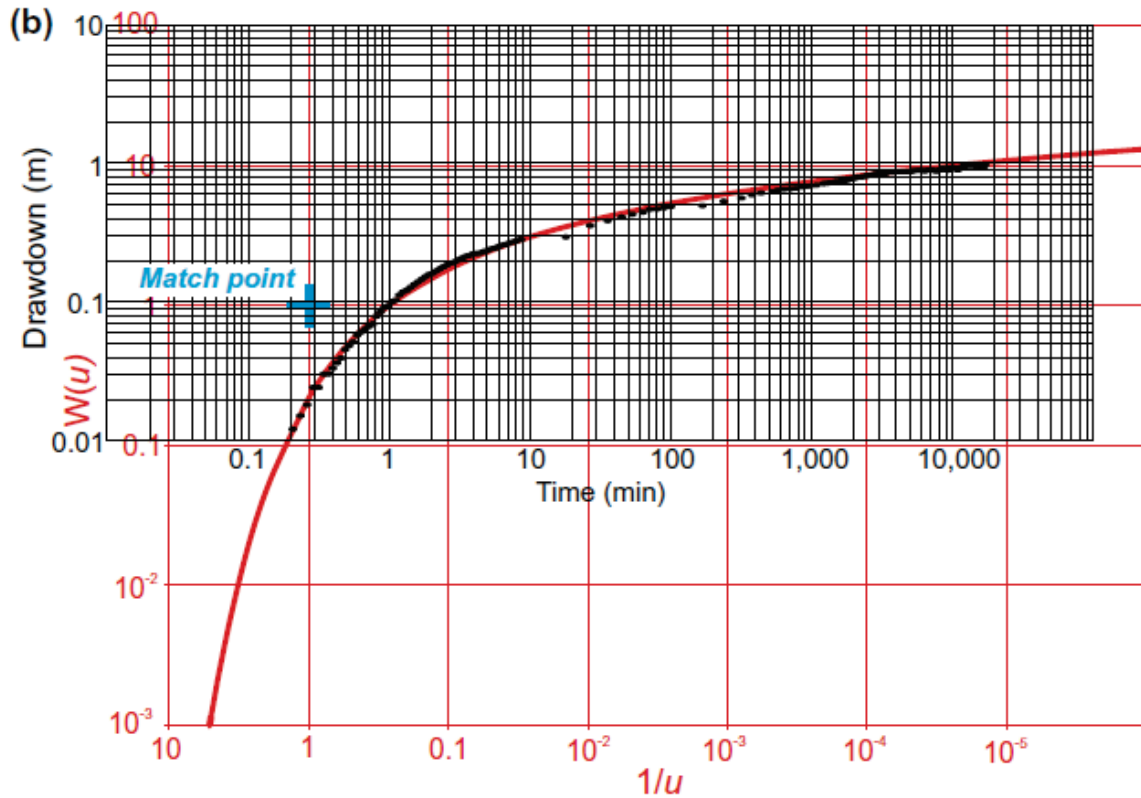


**Figure 3.8:** Example of match point method. Black dots on a black grid represent the time drawdown plot, the data are from a hydraulic pumping test. The red curve on a red grid is the Theis type curve (from Maliva 2016).

### 3.4.2.3 Cooper-Jacob solution

Another method that has been derived from Theis (1935) equation is the Cooper and Jacob (1946) solution. It is a late-time approximation (estimation of the hydraulic parameters using the pseudo-steady state part of the hydraulic tests). Compared to the previous method, Cooper and Jacob (1946) method uses a semi log plot instead of a log-log. Also, it only requires to match the straight line of the pseudo steady state part of the drawdown data curve. To adapt the Cooper and Jacob solution, the Theis solution is rewritten into:

$$s = \frac{Q}{4\pi T} \left( -0.5772 - \ln \left( \frac{r^2 S}{4 T t} \right) \right)$$

$$s = \frac{2,303 Q}{4\pi T} \log \left( \frac{2,25 T t}{r^2 S} \right)$$

where  $s$  is the drawdown,  $Q$  is the pumping rate,  $T$  is the effective transmissivity of the aquifer,  $r$  is the distance from the observation well,  $t$  is the time since the pumping has started,  $S$  is the storage coefficient. This equation allows us to find the mean values of  $T$  and  $S$  from only some late

observations. The Cooper and Jacob (1946) method is usually referred as the ‘straight-line’ method and is one of the widely used solution to analyze pumping test data because of its simplicity. Firstly, the time drawdown data are plotted in a semi-logarithmic grid (see Figure 3.9). In an assumed confined homogeneous aquifer, the plot will define a straight line at the pseudo-steady state regime. Then, the line parameters (e.i. slope and the intersection with time axis) are identified. To estimate the transmissivity and storativity of the tested aquifer, the following equations are used:

$$T = \frac{2.3Q}{4\pi\Delta s}$$

$$S = \frac{2.25Tt_0}{r^2}$$

where  $\Delta$  is the slope of the Cooper and Jacob straight line,  $Q$  is the pumping rate,  $T$  is the effective transmissivity of the aquifer,  $r$  is the distance from the observation well,  $t_0$  is the intersection of the Cooper and Jacob straight line with the time axis,  $S$  is the storage coefficient

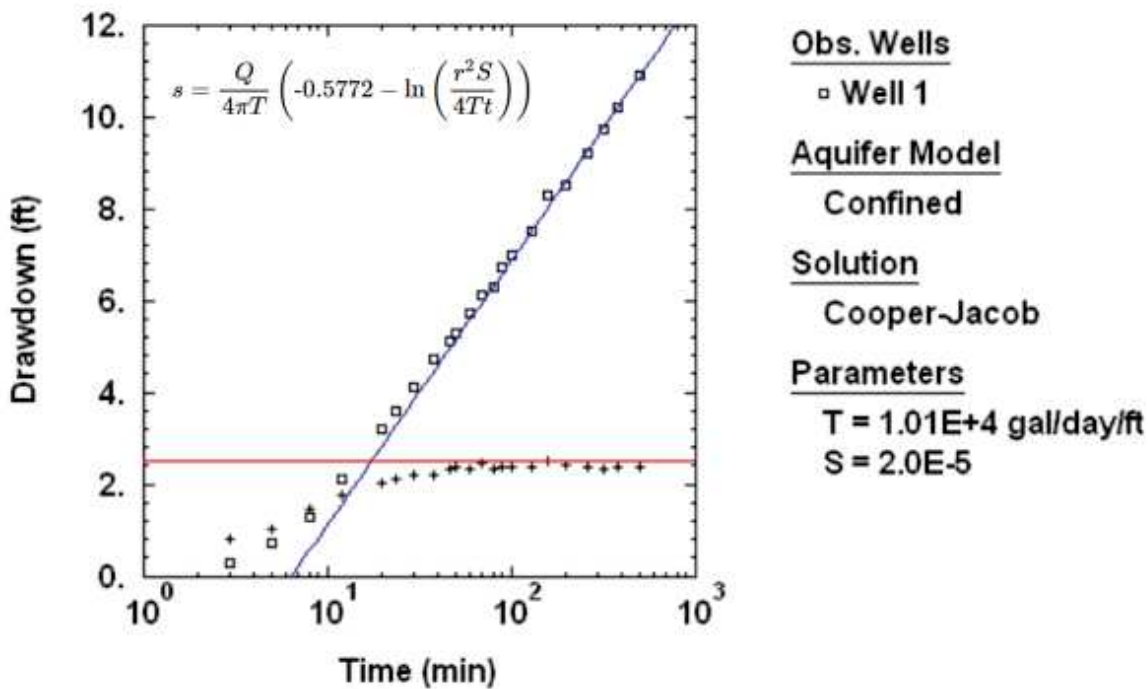


*Figure 3.9: Application example of the Cooper and Jacob (1946) solution, (from AQT SOLV). Blue line is the matched straight line; its slope and intersection with time axis are used to estimate the effective transmissivity  $T$  and the storage coefficient  $S$  of the tested aquifer.*

### 3.4.2.4 Partially penetrating wells

As mentioned at the beginning of the section, several analytical solutions assume that the wells subject to hydraulic tests are fully penetrating wells. However, in many sites, it is not always the case; either the aquifer is thicker in some areas or the initial drilling plan was already set to build wells that only penetrates the first couple meters from the roof of the aquifer (Figure 3.10). The existence of such wells arises the need of developing solutions that can interpret the response of partially penetrating wells. Indeed, the drawdown responses are affected by partial penetration and its effect is usually related to the distance from the pumped well, the saturated thickness of the aquifer, the degree of penetration, and the anisotropy ratio of the aquifer (Walton 1962). Some conditions can make partial penetration effects at a lesser extent than others. In such conditions, that effect can become negligible. For instance, if the well is penetrating the majority of the aquifer thickness (Kruseman and de Ridder 1991). Also, in the case of a heterogeneous aquifer in which the main flow part of the aquifer is identified, if the well is screened only in the main flow zone, partial penetration effects may become negligible. In general, Todd (2004) stated that any well that is screened (or completed with an open hole) through 85 % or more of the aquifer's thickness may be considered to be a fully penetrating well. In cases where the partial penetration effects are important, correction and calibration terms are usually added to take them into consideration. The main effect that comes from partial penetration is that groundwater flow has a vertical component, and the assumption of only horizontal flow to a well becomes invalid. There is strong anisotropy between vertical and horizontal hydraulic conductivities and vertical hydraulic conductivity is typically less than horizontal hydraulic conductivity.

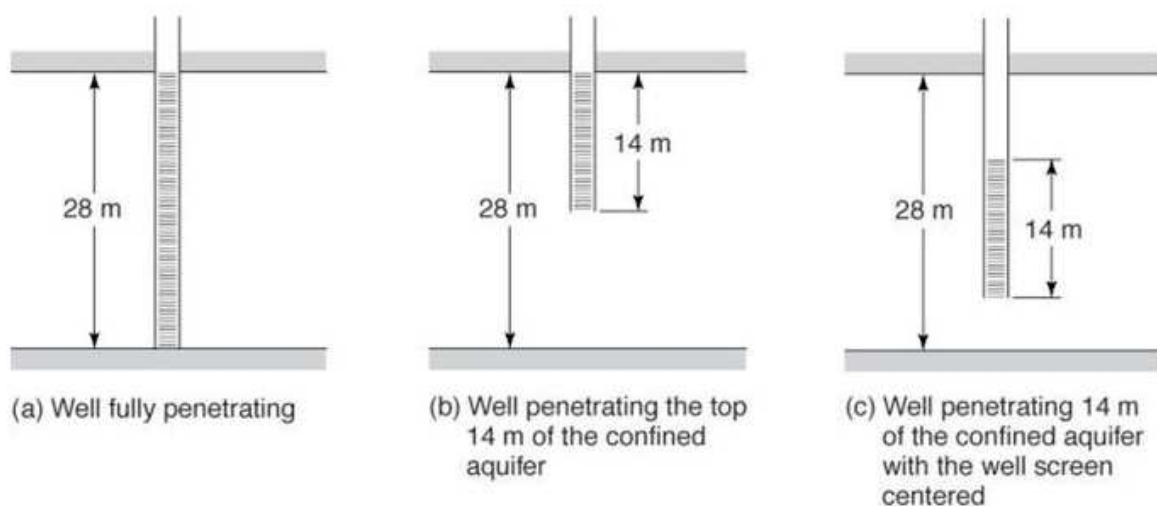


*Figure 3.10: fully vs Partially penetrating wells.*

### 3.4.2.5 Hantush-Walton method for leaky aquifers

Another assumption to use Theis solution is the non-leakage of underlying and overlying strata into the aquifer. Once again, this scenario remains ideal. Most of the aquifers have leakage when a pumping test is undergoing. This is the reason why solutions taking into consideration the leakage has been developed. The most widely used methods for leaky aquifers are Hantush–Jacob (1955) and Walton (1960, 1962). These methods modified the Theis non-equilibrium equation to provide a solution for leaky confined aquifers. The Hantush–Walton solution consists of type-curves that adjust the Theis curve at late times to take into consideration the leakage of underlying or overlying strata (see Figure 3.11). The Hantush–Walton method follows similar steps as the match point method, it only requires a curve-matching procedure and the use of the same equation as to estimate the hydraulic properties. For a leaky aquifer, the drawdown curve is more flattened at late times than the ideal Theis curve. For this kind of aquifers, a new parameter, the leakance  $L$ , is defined. The leakance of the confining units is calculated as follows:

$$L = \frac{\left(\frac{r}{B}\right)^2}{r^2} T$$

where  $B$  is the leakage factor,  $r$  the distance from the observation well and  $T$  effective transmissivity of the tested aquifer.

In order to calculate a leakance, the hydraulic test (e.i. pumping test) must last long enough depending on the hydrogeological system. some systems need longer test durations than the others in order to integrate the leakage effect. After matching the time-drawdown data into the Hantush-Walton type-curves, the  $(r/B)$  value can be determined. It is important to mention that the calculated leakance values are non-directional, but they characterize leakage from both the strata that overlie and underlie the pumped aquifer. Moreover, most of the leakage will be from the most conductive confining unit.

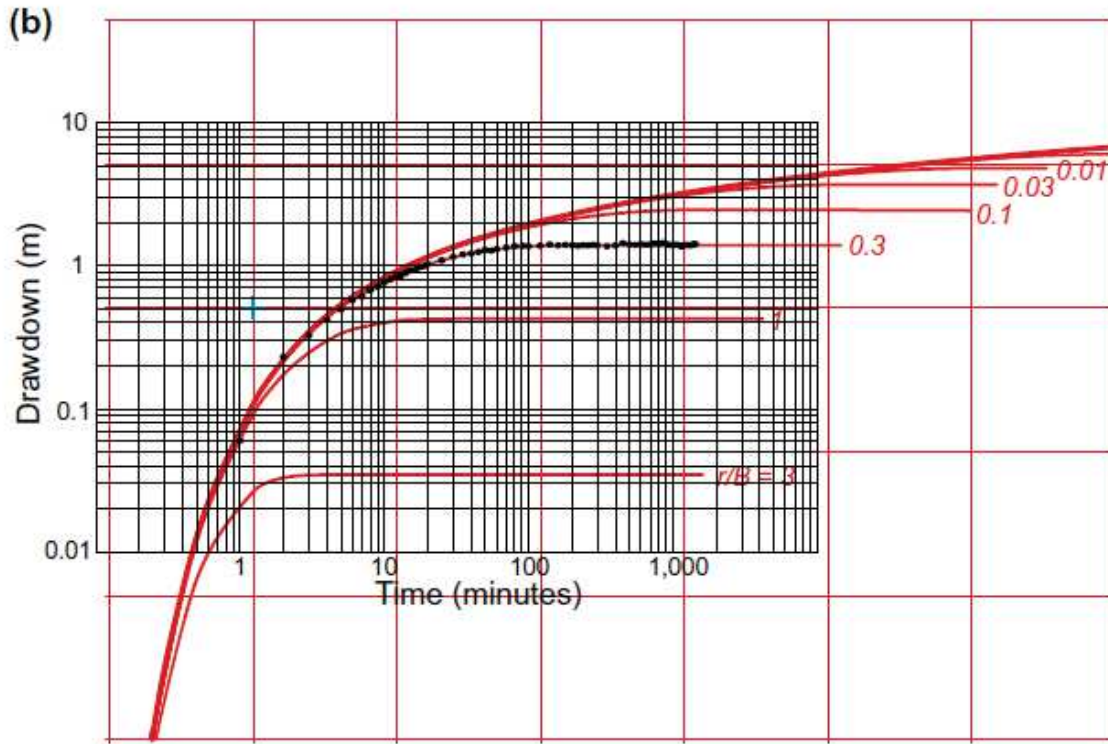


Figure 3.11: Application example using Hantush–Walton curve match for pumping test data.

### 3.4.2.6 Neuman method for unconfined aquifers

The simple Theis solution also assumes that the aquifer is confined. However, a solution for unconfined aquifers is needed. Indeed, many aquifers are unconfined and/or semi-confined. Neuman (1972) developed a method for unconfined aquifers where drawdown equations tend to provide reasonably accurate estimates for hydraulic conductivity and specific yield. Also, this method is also based on the equations used for confined aquifers. The Neuman method is also kind of a graphical method that involves the matching of the drawdown curve to a predefined type-curves (see Figure 3.12) for both the early and late time-drawdown data. Once the curve matching is achieved, different parameters can be identified and used to calculate the hydraulic properties of the tested aquifer. From the type curve, we obtain the values of  $u_A$ ,  $u_B$ ,  $W(u_A, \beta)$ , and  $W(u_B, \beta)$ . For the next step, the early-time data are interpreted using the following equations (Neuman 1975)

$$s = \frac{Q}{4\pi K_h} W(u_A, \beta)$$

$$u_A = \frac{r^2 S_A}{4K_h b t}$$

where  $K_h$  is the horizontal hydraulic conductivity,  $b$  is the original saturated aquifer thickness,  $\beta$  is the Neuman's parameter,  $Q$  is the well pumping rate,  $t$  is the time at match point,  $s$  is the drawdown at

match point,  $r$  distance to the pumped well,  $S_A$  is the storativity: volume of water released from storage per unit surface area per unit decline of the water table. And the late time data are interpreted using similar equations

$$s = \frac{Q}{4\pi K_h} W(u_B, \beta)$$

$$u_B = \frac{r^2 S_Y}{4K_h b t}$$

$$\beta = \frac{r^2 K_v}{b^2 K_h}$$

where  $Q$  is the well pumping rate,  $\beta$  is the Neuman's parameter,  $S_Y$  is the specific yield: volume of water release from storage per unit surface area per unit decline of the water table,  $K_v$  is the vertical hydraulic conductivity,  $K_h$  is the horizontal hydraulic conductivity and  $b$  is the aquifer thickness.

Kruseman and de Ridder 1991 summarized the methodology by the following steps:

1. Construct a family of type log-log curves of  $W(u_A, u_B, \beta)$  versus  $1/u_A$  and  $1/u_B$  for a series of values of  $\beta$ .
2. Construct a log-log plot of drawdown  $s$  versus time  $t$  for the test data on the same scale as the type curves.
3. Match the early test data with one of the type 'A' curves and record the  $\beta$  value. Note the values of  $s$ ,  $t$ ,  $1/u_A$  and  $W(u_A, \beta)$  for an arbitrary point (commonly  $1/u_A = 1$  and  $W(u_A, \beta) = 1$ ).
4. Calculate values of  $K_h b$  and  $S_A$ .
5. Match the late test data with a type 'B' curve with the same  $\beta$  value as the selected type 'A' curve.
6. Note the values of  $s$ ,  $t$ ,  $1/u_B$ , and  $W(u_B, \beta)$  for an arbitrary point (commonly  $1/u_B = 1$ , and  $W(u_B, \beta) = 1$ ).
7. Calculate values of  $K_h b$  and  $S_Y$ .
8. Calculate value of  $K_v$ .

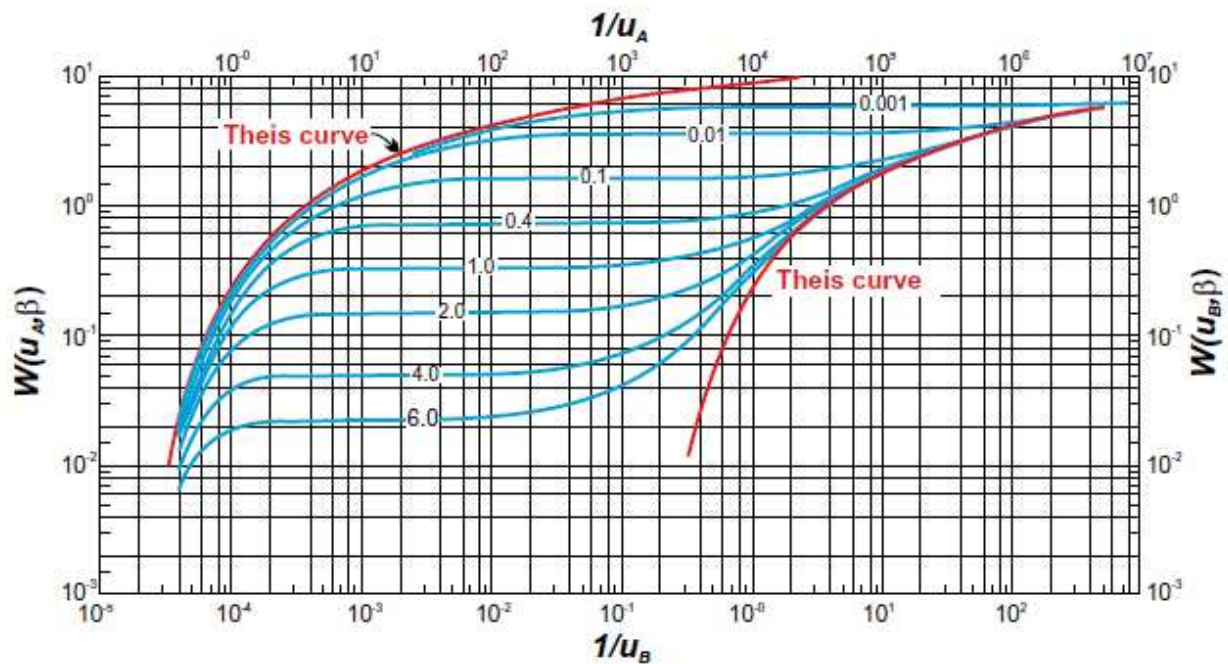


*Figure 3.12: Neuman (1975) delayed-yield type curves, which consists of early and late Theis curves (red) and a series of  $b$  curves (blue).*

### 3.4.3 Pressure transient and pressure derivative analysis

Another technique that evaluates the wellbore conditions and estimates the hydraulic properties of an aquifer or a reservoir is the pressure transient analysis. Well testing has been used in the oil and gas industry for the last century. Pressure transient testing can be categorized into different tests such as buildup, drawdown, fall-off or interference tests. Well testing usually uses type curves that define different conditions (Gringarten, 1979) or the pressure derivative that provides additional information to the normal pressure transient analysis. Several reviews and textbooks about the pressure transient and well testing can be found (Deruyck et al., 1992; Ahmed and McKinney, 2011; Kuchuk et al. 2010). In the oil and gas industry, pressure transient testing is very important and gives relevant information. The design and interpretation of pressure transient test is a specialized discipline and different software packages are developed and used (e.g. Saphir, Pie, AQT SOLV).

Renard, (2005) reviewed pressure transient testing in hydrology and described the main behaviors that can be seen in aquifer hydraulic responses. Figure 3.13 and Figure 3.14 represent some examples related to the pressure transient and pressure derivative analysis. Figure 3.13 shows the main aquifer behaviors (e.g. unconfined, leaky...) compared to the Theis solution. The shape of the pressure derivative plot is sometimes enough to describe a feature of the tested aquifer. Figure 3.14 summarizes the different interpretations of the pressure and pressure derivative of a well test.

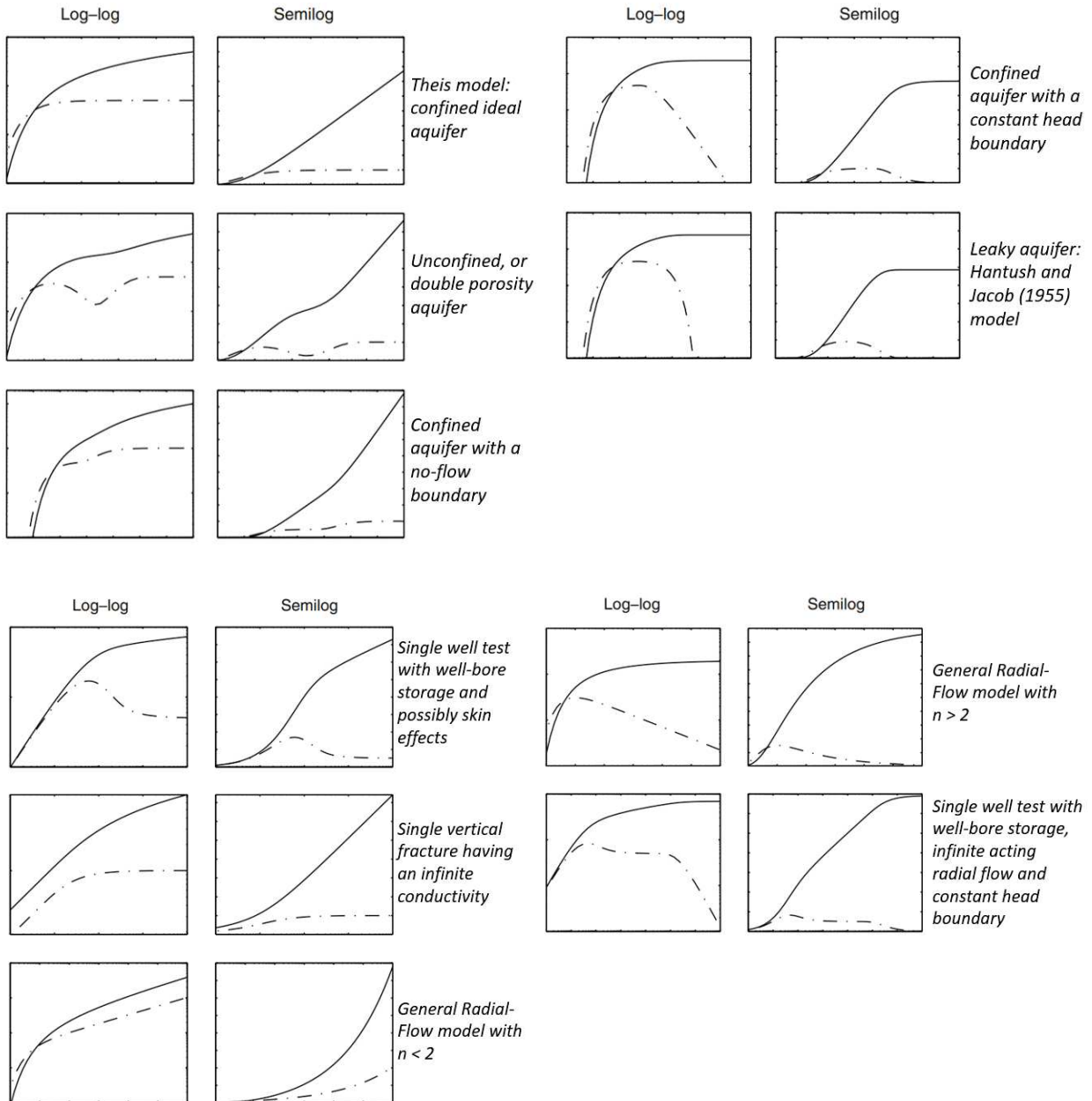
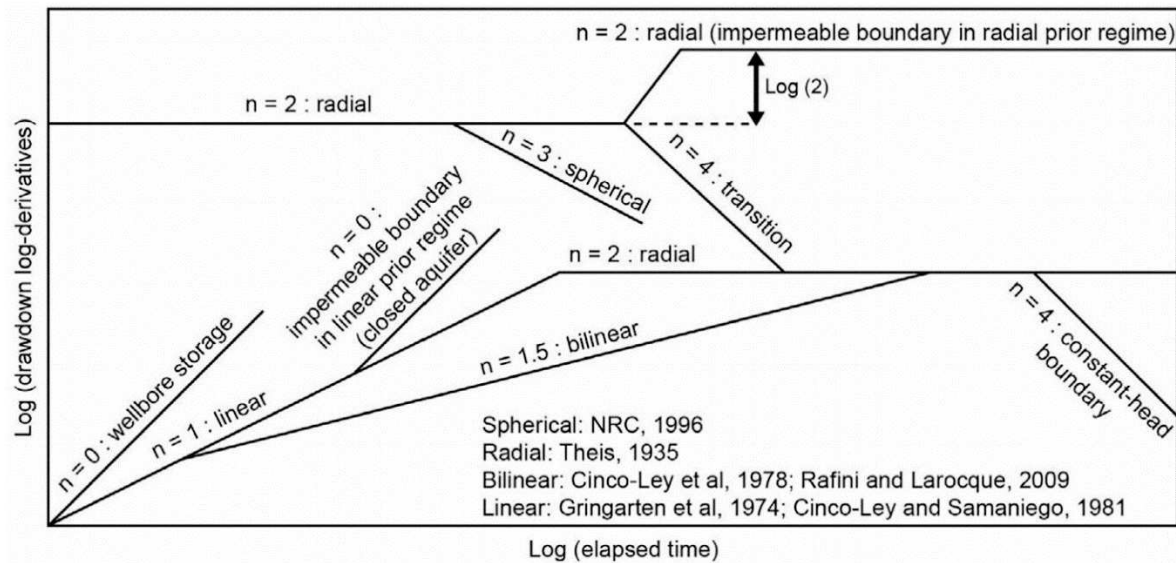


Figure 3.13: typical drawdown behaviors – pressure transient interpretations (Renard, 2005).



**Figure 3.14:** Summary of published theoretical flow regimes and their associated flow dimensions,  $n$  (from Ferroud et al. 2019 modified from Ehlig-Economides et al. 1994).

### 3.4.4 Inverse Modeling approach

An inverse problem is defined as the process of calculating from a set of observations the causal factors that produced them. It usually includes a prior model, forward model and an optimization tool. Inverse problems are some of the most important mathematical problems in science and mathematics because they tell us about parameters that we cannot directly observe. Inverse modelling is basically used in all branches of science; e.g. hydrology and geophysics. Inverse modelling is a key step in groundwater and several inversion techniques were developed during the last decades.

Analytical methods that have been traditionally used for the analysis of aquifer characterization quickly became non-sufficient because they are based on simplified conceptual models that are not representative of actual aquifers and they only provide an estimation of effective parameters. Analytical methods have underlying assumptions and typically involve ideal conditions which increase the bias in the estimation of the parameters. For instance, the basic analytical methods that are used for the interpretation of pumping test data assume that the medium is homogenous which is obviously far to be true. Such an assumption quickly cumulate bias in the estimates of hydraulic conductivity (Wu et al., 2005; Liu et al., 2007).

The most important advantage of inverse modelling is the fact that it provides solutions to nonlinear problems. And with the advances in computer sciences, the time-consuming burden starts to fade away which extends inversion applications. Inversion uses numerical modeling-based methods which have

the advantages of flexibility to simulate complex hydrogeological conditions. Another advantage of inverse modeling is that it allows data fusion in order to find the model representation which is most consistent with the observations. However, as seen in many studies, inverse modeling can suffer from the non-uniqueness of solutions. A basic scheme that summarizes the important steps for solving an inverse problem can be summarized in the following points:

- Collect data that are known to be dependent of the solved unknown
- Construct a forward model that simulate the same set of real data. Closer the forward model to real case, better the estimates of the unknown parameter (favor the increase of time simulation cost over the increase of number of assumptions)
- Build a prior model of the unknown parameter (use of the other available data and previous interpretation and estimations of the unknown: e.g. effective value). For example, analytical solutions may provide initial estimates of hydraulic parameters.
- Evaluate the sensitivity of the unknowns on the simulated observations
- Define an objective function between true and simulated observations
- Use an optimization tool that minimizes the defined objective function
- Note that inversions are iterative processes that converges to a solution and stops according to given criteria. However, it is possible that an inversion run totally diverge and won't be able to provide a consistent solution.

#### 3.4.5.1 Classification

Several methods have been proposed to solve inverse problems and every method can have its own advantages and disadvantages. Different reviews of inversion techniques have been carried out to summarize, compare and evaluate their performances (e.g. Zimmerman et al., 1998; Hendricks Franssen et al., 2009; Zhou et al., 2014). Zhou et al. (2014) showed the history of evolution of these methods. Numerous inverse methods have been applied to hydrology, such as the maximum likelihood method (MLM), the self-calibration method (SCM), the pilot point method (PiPM), Markov Chain Monte Carlo (MCMC), Quasi-Linear Geostatistical Approach (QLGA), et. Inversion techniques can be classified following several criteria; Figure 3.15 shows some of them. Indeed, the inversion approach can be:

- Deterministic or stochastic: the deterministic approaches often converge to a single and final solution conditioned by data while a stochastic method can lead into a different realization at every run.
- Direct or indirect: direct methods consist on solving directly the inverse equations of the forward model that links the parameters to the observation data. It can work with simple forward models but becomes impossible with very complex physics and for high resolution of parameter estimation, the observation data need to be sampled in the whole discretized

domain which not available in real field applications. That's the main reason why indirect methods quickly replaced the direct ones.

- Linear or nonlinear: Linearity in inverse methods is often referred to the forward model. For instance, the Quasi-Linear Geostatistical approach (Kitanidis, 1995) linearizes the relation between the parameter and the observation data.
- Minimization or sampling: some methods calculate the next best step by minimizing a given objective function while others sample from a random model (e.g. Training image, random field function...)
- Flexible or not: here we refer to the flexibility of the method in term of data integration ease. If a method allows to easily incorporate other data (e.g. geological facies model), then, it can be classified as flexible.
- Multi-Gaussian or not.

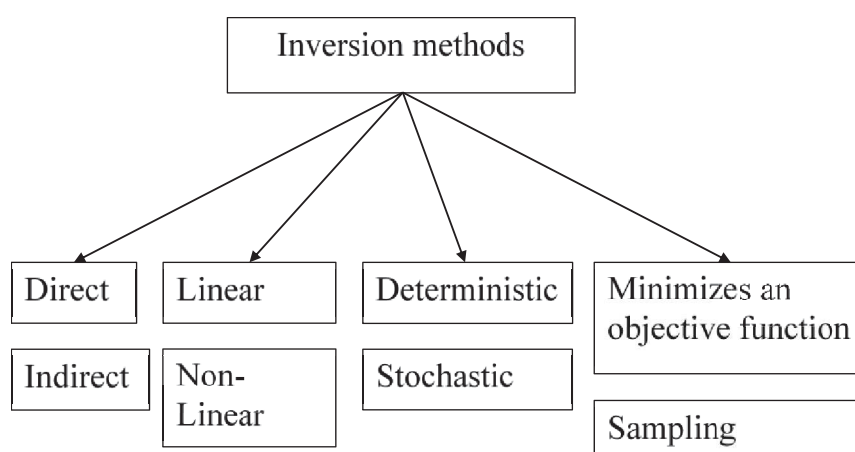


*Figure 3.15: Main criteria for the classification of inverse modelling methods. Other secondary criteria can be added to the chart (preserve the prior structure or not, real time integration or not, multi-Gaussian or not, integration of data...)*

### 3.4.5.2 Inverse modelling and hydrology

Inverse modelling approach has also been widely used in hydrology investigations in order to estimate the hydraulic properties of the studied aquifer and define its recharge and boundary conditions. Zhou et al. 2014, reviewed the evolution of the inverse modelling techniques that were famous in hydrology.

Firstly, hydrogeologists were using direct methods that were based on simply deriving algebraic equations that define the inverse problem. These equations are under several assumptions and calculate directly the parameters as a function of the observed data. Inversion methods fall into two groups: direct and indirect (Neuman, 1973; Yeh,W. 1989). However, only indirect methods are considered nowadays while the direct methods are very limited. The forward problem requires model parameters to be known over the entire domain. The theory of the direct methods is simple and straightforward,

but it is impossible to extract a satisfactory solution by solving the algebraic equations. Usually, in order to derive the inverse equations, many assumptions that simplifies the problem are set. The direct methods can still provide good estimations for simple inverse problems, however, the underground flow usually exhibits more complex behaviors. Authors quickly accepted the fact that aquifers are very complex systems and direct methods are not suitable to capture the behavior of such systems. Sun, (2013) pointed out different limitations related to direct methods (e.i. ill-posedness of the inverse equation and the singularity of the matrices involved in the numerical formulation). Authors proposed enhancements of the method and modifications to cope with these difficulties. For instance, Ponzini and Lozej, 1982 proposed to consider more equations than unknowns to build an over-determined system attempting to reduce the effect of measurement errors. Moreover, Authors start imposing a constraint on the objective function, which converts the inverse problem into a linear programming problem (Kleinecke, 1971; Neuman, 1973) or a minimization problem (Navarro, 1977).

The direct methods can be very instable because of the limited available data and the associated measurement errors. For example, in order to estimate the hydraulic properties of the aquifer, hydraulic heads need to be measured at all nodes of the discretized domain. Because of non-abundance of data in such a way, the indirect methods became more used because they still provide estimates even with a limited number of observations.

Kitanidis and Vomvoris (1983) proposed the geostatistical approach (GA) which had as a main objective to solve the ill-posedness problem. And their method succeeded on reducing the number of unknowns. The approach consists on identifying the parameters of the variogram that describes the spatial correlation of the parameters instead of identifying directly those parameters. Once the parameters of the variogram has been identified, the correlated parameters are simply interpolated by kriging. Zhou et al. (2014) stated that the advantages of the GA reside in two main aspects. First, it reduces the number of the effective parameters to be estimated by introducing the concept of random function into the inverse problem which removes the ill-posedness issue. Also, the estimated parameters are independent of grid discretization step. And as for the second strength of the GA, it is computationally efficient since it only uses first-order approximations and no optimization tool were involved. The method was first verified on a one-dimensional test and found to be stable with satisfying estimates(Kitanidis and Vomvoris, 1983). And later, Kitanidis (1995) further generalized it onto a quasi-linear approach (QLGA) which led into hydraulic tomography with its different approaches. The quasi-linear geostatistical approach is a linear inverse approach which is further described in this chapter.

Most of inverse approaches in hydrology are nonlinear. An inverse approach is considered linear if the observations are assumed linearly correlated to the parameters through a forward model. A typical example of nonlinear inverse approaches is the maximum likelihood method (MLM) developed by Carrera and Neuman (1986a). It allows to estimate simultaneously different hydraulic parameters by

incorporating head and concentration measurements as well as prior information (Medina and Carrera, 1996). However, fine discretization of the domain leads into a high number of unknowns which pushed to the use of a zonation to reduce the number of parameters where the parameter of a single zone is assumed constant. Also, some limitations of the MLM are apparent; since it uses a zonation in order to reduce the number of parameters, those zones need to be chosen carefully and in real field applications, defining the main facies of the aquifer is rather difficult. At the same time, the zonation scheme may introduce unacceptable discontinuities between zones. The maximum likelihood method was probably the first widely successful inverse method (several of other inverse approaches that are mentioned later are based on MLM). MLM is flexible in terms of using different data and it yielded a zoned map of hydraulic conductivities that reproduced very well the observed data. However, it produced a single map that too smooth to fully describe the heterogeneity observed in nature.

The heterogeneity of aquifers can vary considerably by changing the scale of investigation, this makes it very hard to capture hydraulic behavior just by a smooth map of hydraulic parameters at a big scale. Small scale variability is not captured by a method such as MLM, however, the small-scale heterogeneity had already been identified as one of the important scales controlling aquifer response. In order to introduce more variability, De Marsily et al. (1984) developed the pilot point method (PiPM). This procedure allows to discretize the aquifer at any scale and kriging was performed on the entire aquifer. Even though pilot point method provides estimates with more variability, the result still smooth to capture enough characteristics of the aquifer response. Also, PiPM still provides only a single representation of the aquifer.

Because of the limited representation of the system by a single estimation, approaches that seek different estimations were developed (e.i. stochastic approaches). For example, the self-calibrated method was proposed (SCM). The idea is not to obtain a single solution with the best fitting capabilities of the data but to generate multiple realizations than can show realistic patterns with a sufficient data fitting. The SCM is based on the PiPM but the two methods differ: PiPM starts from a kriging map and then adds local perturbations using fictitious pilot points, while, SCM starts from multiple realizations generated by a conditional simulation algorithm. The MLM, the PiPM and the SCM follow a very similar perturbation and updating scheme.

Hernandez et al. (2003, 2006) proposed the moment equation based inverse method. The method is also within the framework of maximum likelihood and is similar to the Monte Carlo approach. Optimum unbiased estimates are obtained by their first order moments and uncertainties by their second order moments. The method has been extended from steady state flow to transient flow (Riva et al., 2009) and from model state prediction to model parameter identification (Riva et al., 2011).

The Markov chain Monte Carlo method (MCMC) (Hastings, 1970; Metropolis et al., 1953; Oliver et al., 1997) is another stochastic inverse approach that has been widely used. the objective of the

approach is to generate multiple independent realizations by sampling from the posterior parameter distribution conditioned on the observations. However, the McMC can considerably suffer from heavy time calculations. It is computationally demanding since each proposed realization require a forward simulation run. Another drawback, the McMC should sample from the entire posterior distribution, but it takes quite a long chain until this happens (Fu and Gomez-Hernandez, 2009; Romary, 2010).

The EnKF method based on the Kalman filter (Kalman, 1960) is known to be computationally efficient because it avoids the calculation of the covariance evolution with time. The EnKF is also capable of incorporating the observations sequentially in time without the need to store all previous states nor the need to restart groundwater simulation from the very beginning. the EnKF is optimal when parameter and states are linearly related and follow a multiGaussian distribution (Evensen and Leeuwen, 2000).

Another feature of some inverse modelling approaches is the prior model. Some methods use the prior model just as a mathematical launcher of the algorithm. In opposite, there are methods that produce realizations consistent with the prior model structure, such as the McMC. There are two other methods that preserve the prior model during the inversion process: the gradual deformation method (GDM) and the probability perturbation method (PrPM). The GDM method, as initially proposed by Hu (2000), is based on successive linear combination of pairs of realizations. The main drawback of GDM method is related to the convergence rate. In the other hand, the probability perturbation method (PrPM) was proposed by (Hoffman and Caers, 2003) and is also based on the sequential simulation algorithm.

Freeze (1975) showed that hydraulic conductivity might be assumed to follow a univariate lognormal distribution according to experimental data. However, there are still many cases, such as aquifers in fluvial deposits, in which hydraulic conductivities don't necessarily follow this distribution. The nonGaussian models have also been explored (e.g., Rubin and Journel, 1991; Gomez Hernandez and Wen, 1998; Journel and Deutsch, 1993; Woodbury and Ulrych, 1993; Zinn and Harvey, 2003; Kerrou et al., 2008; Renard and Allard, 2011). Some of the methods discussed can handle non-multiGaussian patterns of variability, such as the McMC, the GDM or the PrPM. It is apparent that those methods can lead into techniques, such as multiple point geostatistical simulation, that can generate realizations of hydraulic conductivity with realistic patterns using training images (Mariethoz et al., 2009).

### **3.4.5.3 Hydraulic tomography**

#### *Background*

Traditional pumping test analysis methods are built upon assumptions. Most of them assume aquifer being homogeneous. These methods provide estimations that can only predict average drawdowns that cover some volume of the aquifer (Liu et al., 2007). On the other hand, inverse modelling techniques

that involve calibration of spatially distributed parameters lack of prior information and are ill-posed problems. Inversion techniques can also provide non-unique solutions or even totally diverge. Within inverse modelling techniques, Liu et al. (2007) stated that hydraulic tomography is one of the best ways to collect and analyze data and characterize an aquifer. However, hydraulic tomography requires several observation points at several locations to obtain a good spatial distribution of hydraulic properties.

Hydraulic tomography (HT) is an aquifer characterization approach that has already shown its efficiency (Gottlieb and Dietrich, 1995, Kitanidis 1995, Renshaw, 1996, Yeh and Liu 2000, Vasco et al. 2000, Yeh et al. 1996). It allows to spatially correlate hydraulic properties of geological media. Hydraulic conductivity and specific storage are two important and enough parameters to well predict flow and transport. Hydraulic tomography (HT) has been developed over the last two decades through several applications (e.g., Gottlieb and Dietrich, 1995, Butler et al., 1999, Bohling et al., 2002, Bohling and Butler, 2010, Yeh and Liu, 2000, Zhu and Yeh, 2005, Zhu and Yeh, 2006, Liu et al., 2002, Liu et al., 2007, Illman et al., 2010, Cardiff et al., 2009, Zha et al. 2014). Hydraulic tomography yields a detailed two- or three-dimensional map of hydraulic heterogeneity for regions in-between the testing boreholes. The efficiency of HT has been also shown at laboratory-scale studies(e.g., Liu et al., 2007, Illman et al., 2007, Illman et al., 2010, Zhao et al., 2016, Zhao and Illman 2017) and field-scale studies (e.g., Bohling et al., 2007, Brauchler et al., 2011, Brauchler et al., 2013, Berg and Illman, 2011, Cardiff et al., 2012, Fischer et al., 2020).

For a full 3D hydraulic tomography, using only one vertical observation from each testing well is not sufficient and packer tests are often required (Bholing et al. 2007, Berg and Illman 2011, Zha et al. 2016, Zha et al. 2017, Cardiff et al. 2012, Zhao and Illman 2017, Wen et al. 2020). However, packer tests, which are costly and complex to set up, are not always available in each site. Without packer tests, pumping tests data remain insufficient to capture the three-dimensional aquifer behavior and may lead to erroneous characterization and sometimes cannot provide an estimate.

In recent years, other information such as geological and geophysical data have been used to constrain the inverse process of HT (e.g., Zha et al. 2017, Tso et al. 2016, Soueid Ahmed et al. 2015). The most widely-used geostatistics-based inverse modelling approaches are the quasi-linear geostatistical approach (Kitanidis 1995) and the successive linear estimator (SLE) (Yeh et al. 1996). To improve efficiency when dealing with high-dimensional inverse problems, different approaches were developed, including principle component geostatistical approach (Kitanidis and Lee 2014), reduced-order SLE (Zha et al. 2018) and the use of geostatistical reduced order models (Liu et al. 2013). Previous works have highlighted the benefits of incorporating site-specific geologic structure information into groundwater models when HT data are limited (Zha et al. 2017, Tso et al. 2016). Zha et al. (2017) worked on quantitative incorporation of site-specific information into groundwater models and introduced a general method to derive conditional mean and conditional covariance, that can be used

in HT analysis as prior information. Tso et al. (2016) also concluded that only by incorporating a qualitative facies trend information into HT, results already yield a better hydraulic conductivity estimate. Such improvement can also be seen through laboratory/ field applications (Zhao et al. 2016, Zhao and Illman 2017). Moreover, De Clercq et al. (2020) used electrical resistivity maps to structure the distribution of the hydraulic properties in a 3D HT.

Several sandbox experiments were conducted in order to show the potential of HT (Yeh and Liu 2000, Illman et al. 2006). It started with simple applications using steady state observations where it has been shown that using steady state pumping tests data in hydraulic tomography is already effective to capture aquifer heterogeneities. Nevertheless, Zhu and Yeh (2005) extended steady state hydraulic tomography to transient HT and thus allows to invert both hydraulic conductivity and specific storage. Even though, computers and CPUs were enhanced, HT remains time consuming. To overpass such a burden, authors developed methods that considerably decrease inversion time by decreasing the number of forward model runs. Some methods used a different way of estimating the Jacobean matrix such as the adjoint state method that runs a proportional number of forward simulations to the number of observations. However, a small number of observations can considerably increase the number of available solutions that fits those data (Chavent 1979, Mao et al. 2012). Moreover, different methods use a low rank covariance matrix by the decomposition of the covariance matrix into eigenvalues and eigenvectors: e.g. Principle Component Geostatistical Approach derived from Geostatistical Approach (Kitanidis and Lee 2014) and the reduced order SLE derived from Successive Linear Estimators (Zha et al. 2018).

The investigated geological media are usually very complex systems and highly heterogeneous. Authors combined hydraulic tomography with additional data and additional analysis in order to improve the result quality and obtain geologically acceptable distributions of hydraulic properties. They showed that infusing different levels of geological information into HT considerably helps obtaining higher quality aquifer characterization (Zha et al. 2017, Illman 2016, 2017). Also, different alternative data other than cross-hole pumping tests data were used as conditional observations, e.g. solute transport data (Illman et al. 2009). Hydraulic tomography requires a forward model that is very essential and play a very important role on the inverted solution. Real field applications may exhibit inversion instabilities due to the lack of information about the boundary conditions or because of a wrong forward model setup. Most of HT work uses a simplified forward model to reduce the simulation time and this technique is mainly investigated using synthetic studies (Yeh and Liu 2000, Yeh and Zhang 1996, Zhu and Yeh 2005, Hao et al. 2007, Cardiff and Barrash 2011, Sun et al. 2013, Bohling et al. 2002, Bohling and Butler 2010) where the forward model and the system is fully controlled. Many authors also worked at laboratory scale using sandboxes to validate the efficiency of hydraulic tomography (Liu and Yeh 2002, Sharmeen et al. 2012, Illman et al. 2010, Liu and Kitanidis 2011, Xiang

et al. 2009, Yin and Illman 2009, Liu et al. 2007). Indeed, sandbox experiments allow to measure observations caused by true hydrodynamic systems instead of just simple simulations. However, lab scale experiments remain easier to control and easier to model compared to true aquifers that can be linked to highly heterogeneous systems and variable boundary conditions surrounding it.

Hydraulic tomography was also, at a lesser extent, applied to real field cases to characterize aquifer's hydraulic properties (Zhao and Illman 2016, Wen et al. 2020, Bohling et al. 2007, Zha et al. 2017, Cardiff et al. 2012, Zha et al. 2016, Berg and Illman 2011, Zha et al. 2018). Bohling et al. (2002) stated that boundary conditions will always be miss-specified to some extent and such misspecification have a significant effect on the estimated conductivities. The steady state analysis was introduced to avoid the deleterious effects of incorrectly specified boundary conditions. The impact of the boundary conditions decreases by increasing its distance from the pumping and the observation wells. Thus, authors handled the forward model differently: use of a simple domain with boundary conditions (Zha et al. 2018, Berg and Illman 2011, Wen et al. 2020), use of an additional buffer zone to make the boundary conditions far from the wells, use of a bigger domain (Zhao and Illman 2016) with adaptive mesh (Zha et al. 2016). Also, performing pumping tests with small flow rate decreases the effect of the regional area on the drawdown responses (Cardiff et al. 2012). Using a buffer area may indeed remove the effect of unknown boundary conditions but that buffer itself will impact the drawdown responses and needs also to be characterized instead of using just a mean hydraulic property observed from pumping tests analyses. Moreover, most HT inversions just avoid using the late time drawdown observations because they are the most impacted by boundary conditions.

Yeh et al. (2015) emphasized the discussion about the instabilities of inverse problems in relation with scale, resolution and non-uniqueness of solutions. They also showed the importance of the boundary conditions and the forward model. Only few work investigated the influence of boundary conditions on HT inversion. Sun et al. (2013) conducted some simulations where he showed that a wrong imposed boundary condition led into an overestimation or an underestimation of the hydraulic conductivity near boundaries. Jiao and Zhang (2014), and Zhang et al. (2014) used an approach where boundary conditions are included as unknowns in the inversion. Daranond et al. (2020) showed that HT can identify the impermeable boundaries by a low transmissivity zone. Liu et al. (2020) showed the potential of HT on identifying the boundary conditions: they confirmed that impermeable boundaries can be identified by low transmissivity zone and also showed that the constant head boundary condition can be identified by a high transmissivity zone. The following Figure 3.16 presents the main flowchart of inversion technique for hydraulic tomography applications.

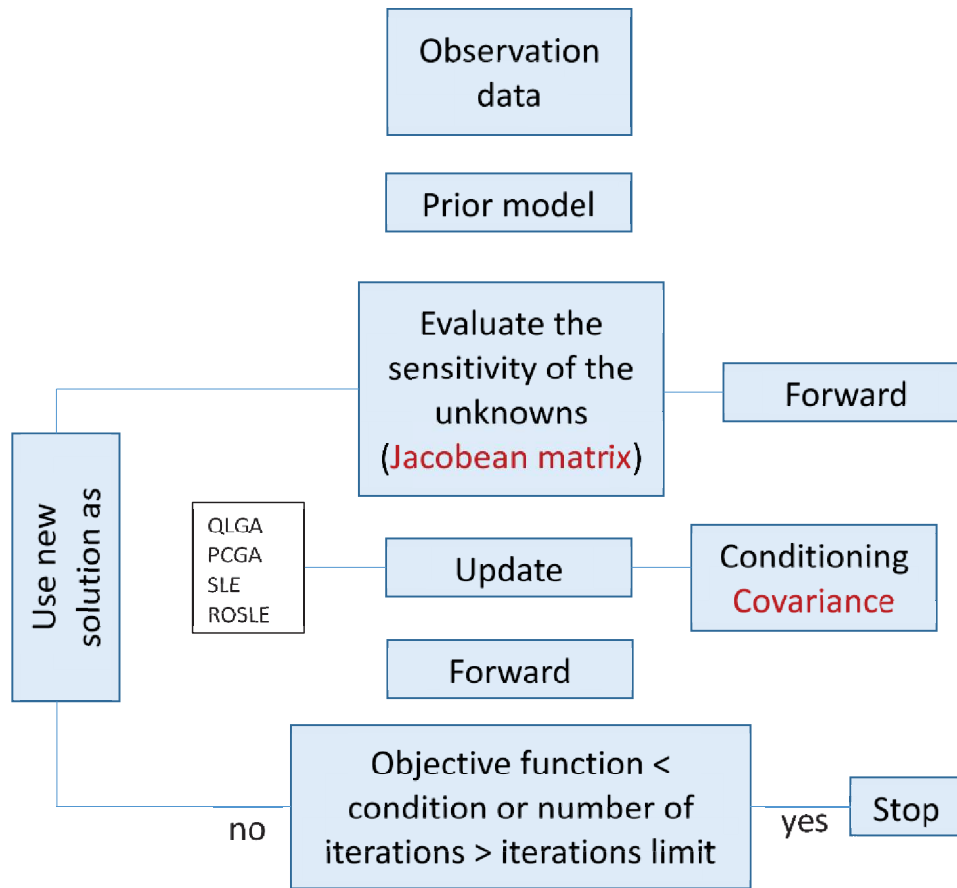


*Figure 3.16: Inversion flowchart for hydraulic tomography applications.*

### *Forward model*

Inverse modelling methods require a forward simulation model that allows at any step of the run to simulate a set of data structurally similar to the given observed data. The inverse algorithm is hence coupled to a forward model, especially when the forward model is complex. It is highly recommended to use a forward model that is best representative of the environment where the true observed data are collected.

### *Sensitivity (Jacobean) matrix*

The coefficients in the sensitivity matrix  $\mathbf{H}$  represent the change of an observation  $h$  caused by a change in the parameter  $s$  for each cell. The sensitivity matrix is defined as follow:

$$\mathbf{H} = \frac{\partial \mathbf{h}_{obs}}{\partial \mathbf{s}}$$

where  $\mathbf{s}$  is the parameter and  $\mathbf{h}$  is the conditioning observation.

The sensitivity matrix is one of the most important parameters that needs to be calculated in order to perform hydraulic tomography. The following example of a sensitivity matrix gives an idea of how it is structured in the hydraulic tomography application of this manuscript. The coefficients of the

sensitivity matrix can be positive or negative to define the effect direction of the parameter on the observation.

Sensitivity of the 2<sup>nd</sup> observation  
to the change on the 4<sup>th</sup> parameter

$$H = \begin{pmatrix} 0 & 0.1 & -0.1 & 0.3 & 0.1 & 0 \\ 0.3 & 0.05 & 0 & -0.3 & -0.1 & 0.3 \\ 0 & -0.4 & 0.01 & 0 & -0.2 & 0.02 \end{pmatrix}$$

← parameters →

↑ observations ↓

### Covariance matrix

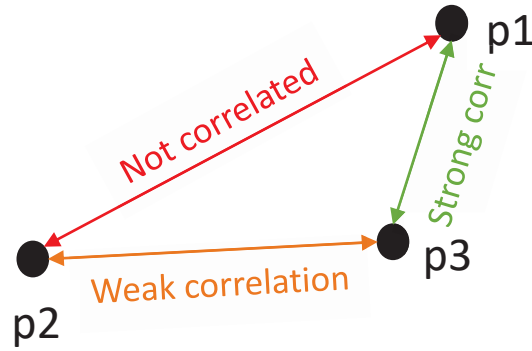
The covariance matrix is a square matrix that defines the correlation between several parameters of a given vector. The covariance matrix can be constructed using a covariance model or a variogram that represent the set of parameters. An example of a covariance model is an exponential correlation function defined as

$$Q = \sigma e^{-\frac{1}{2} \left( \frac{abs(x_2-x_1)}{L_x} + \frac{abs(y_2-y_1)}{L_y} + \frac{abs(z_2-z_1)}{L_z} \right)}$$

where  $\sigma$  is the standard deviation,  $L_x$ ,  $L_y$  and  $L_z$  are respectively the correlation lengths in  $x$ ,  $y$  and  $z$  direction,  $x$ ,  $y$  and  $z$  are the coordinates and '1' and '2' correspond to two given points in the space. The covariance model can follow different model and it is recommended to use a model that can represent well the spatial correlation of the parameter.

The following example shows how to construct a covariance matrix  $Q$  of the parameter  $p$ . In hydraulic tomography applications, the covariance matrix  $Q$  is structured as follows:

$$Q = \begin{pmatrix} 1 & 0 & 0.75 \\ 0 & 1 & 0.25 \\ 0.75 & 0.25 & 1 \end{pmatrix} \quad p = \begin{pmatrix} p1 \\ p2 \\ p3 \end{pmatrix}$$



### *Quasi Linear Geostatistical Approach*

The approach has been introduced by Kitanidis 1995, Let  $\mathbf{s}$  be the unknown which is spatially variable and its variability can be modelled through covariance functions and variogram. Sedimentary structures are very complex and the representation of its hydraulic properties is very hard. An efficient way is to describe those properties with a simple mean function and their structure with a variogram. Which pushed authors to characterize the random field by functions of a few parameters that describe its statistics. In geostatistics, the adopted approach is to represent the mean function simply as a linear function of  $\boldsymbol{\beta}$  and the covariance as a known function of  $\boldsymbol{\theta}$ , where  $\boldsymbol{\beta}$  and  $\boldsymbol{\theta}$  are the statistical or "structural" parameters of the process.

As a next step, the unknown parameter  $\mathbf{s}$  is spatially discretized into  $n \times 1$  vector, the expected value of the unknown  $\mathbf{s}$  can be described as (Kitanidis 1995)

$$E[\mathbf{s}] = \mathbf{X}\boldsymbol{\beta}$$

where  $\mathbf{X}$  is a known  $n \times p$  matrix,  $\boldsymbol{\beta}$  are  $p$  unknown drift coefficients and  $E[\ ]$  denotes the expected value. And the covariance matrix of the parameter  $\mathbf{s}$  can be expressed as follows

$$E[(\mathbf{s} - \mathbf{X}\boldsymbol{\beta})(\mathbf{s} - \mathbf{X}\boldsymbol{\beta})^T] = \mathbf{Q}(\boldsymbol{\theta})$$

The covariance matrix is assumed known and expressed with the parameters  $\boldsymbol{\theta}$ . The exponent  $T$  denotes transpose. For cases where two or more spatially variable parameters need be estimated,  $\mathbf{s}$  just need to be adopted as the aggregation of all spatially variable parameters and the covariance matrix accordingly.  $\mathbf{r}$  is defined as additional unknown parameters that are not necessary spatially distributed and most of the time can be expressed by single values (e.i. boundary condition). The  $\boldsymbol{\beta}$ ,  $\boldsymbol{\theta}$ , and  $\mathbf{r}$  parameters are considered unknown constants and are supposed to be much less than the observations. Then, the relation between the observations and the unknowns can be expressed as

$$\mathbf{y} = \mathbf{h}(\mathbf{s}, \mathbf{r}) + \mathbf{v}$$

where  $\mathbf{y}$  is the  $m \times 1$  vector of observations.  $\mathbf{h}(\ )$  is the forward model of the inverse problem and  $\mathbf{v}$  is the observation error which is random with normal distribution defined by a zero mean and a

covariance matrix  $\mathbf{R}$  that is fixed or a known function. The standard deviations of the measurement errors are expressed as the square root of the diagonal elements of the covariance matrix  $\mathbf{R}$ . Those standard deviations in a physical meaning define how closely the observations should be reproduced. If  $\mathbf{s}$  and  $\mathbf{r}$  are given, the response can be predicted through the forward model  $\mathbf{h}(\theta)$ .

The probability distribution of  $\mathbf{y}$  depends on the distribution of  $\mathbf{s}$  and  $\mathbf{v}$  and also on the function  $\mathbf{h}(\theta)$  and is generally hard to derive explicitly. Nevertheless, using the fact that  $\mathbf{y}$  is jointly distributed with  $\mathbf{s}$  the probability distribution can be expressed as (Kitanidis, 1995)

$$p(\mathbf{y}) = \int p(\mathbf{y}, \mathbf{s}) d\mathbf{s} = \int p(\mathbf{y}|\mathbf{s})p(\mathbf{s})d\mathbf{s}$$

where

$$p(\mathbf{y}|\mathbf{s}) \propto |\mathbf{R}|^{-\frac{1}{2}} \exp\left[-\frac{1}{2}(\mathbf{y} - \mathbf{h}(\mathbf{s}, \mathbf{r}))^T \mathbf{R}^{-1}(\mathbf{y} - \mathbf{h}(\mathbf{s}, \mathbf{r}))\right]$$

and

$$p(\mathbf{s}) \propto |\mathbf{Q}|^{-\frac{1}{2}} \exp\left[-\frac{1}{2}(\mathbf{s} - \mathbf{X}\boldsymbol{\beta})^T \mathbf{Q}^{-1}(\mathbf{s} - \mathbf{X}\boldsymbol{\beta})\right]$$

$|\mathbf{R}|$  denotes the matrix determinant of  $\mathbf{R}$ . And for consistency with the other work in geostatistics, the unknown drift coefficients are ignored (Kitanidis and Lane, 1985). The elimination of  $\boldsymbol{\beta}$  can be achieved by working with the restricted likelihood obtained by averaging over all values.

$$p(\mathbf{y}|\boldsymbol{\theta}, \mathbf{r}) = \int p(\mathbf{y}|\boldsymbol{\beta}, \boldsymbol{\theta}, \mathbf{r}) d\boldsymbol{\beta} \propto |\mathbf{R}|^{-\frac{1}{2}} |\mathbf{Q}|^{-\frac{1}{2}} |\mathbf{X}^T \mathbf{Q}^{-1} \mathbf{X}|^{-\frac{1}{2}} \int I(\mathbf{s}) d\mathbf{s}$$

where

$$I(\mathbf{s}) = \exp\left[-\frac{1}{2}\{(\mathbf{y} - \mathbf{h}(\mathbf{s}, \mathbf{r}))^T \mathbf{R}^{-1}(\mathbf{y} - \mathbf{h}(\mathbf{s}, \mathbf{r})) + \mathbf{s}^T \mathbf{G} \mathbf{s}\}\right]$$

$$\mathbf{G} = \mathbf{Q}^{-1} - \mathbf{Q}^{-1} \mathbf{X} (\mathbf{X}^T \mathbf{Q}^{-1} \mathbf{X})^{-1} \mathbf{X}^T \mathbf{Q}^{-1}$$

The next step is to use the restricted maximum likelihood estimation. Maximum likelihood estimation (MLE) is a method of estimating the parameters of an assumed probability distribution, given some observed data which is achieved by maximizing a likelihood function so that, under the assumed statistical model (Carrera and Neuman, 1986), the observed data is most probable. So, in this analysis, the integrand  $I(\mathbf{s})$  is maximized using an iterative procedure (e.i. Gauss-Newton method). It exists many ways of implementing the Gauss-Newton method and the recommended procedure is described in the following steps. Find the derivative of  $\mathbf{h}(\theta)$  about  $\mathbf{s}$ . this step is usually referred as the sensitivity matrix  $\mathbf{H}$  calculation (or Jacobean matrix)

$$\mathbf{H} = \left( \frac{\partial \mathbf{h}(\mathbf{s} + \partial \mathbf{s})}{\partial \mathbf{s}} \right)$$

Then solve the following system of equations

$$\begin{bmatrix} \Sigma & \cdot & \mathbf{HX} \\ (\mathbf{HX})^T & \cdot & \mathbf{0} \end{bmatrix} \begin{bmatrix} \bar{\xi} \\ \bar{\beta} \end{bmatrix} = \begin{bmatrix} \mathbf{y} - \mathbf{h}(\bar{\mathbf{s}}) + \mathbf{H}\bar{\mathbf{s}} \\ \mathbf{0} \end{bmatrix}$$

where

$$\Sigma = \mathbf{H}\mathbf{Q}\mathbf{H}^T + \mathbf{R}$$

Then the solution is updated using

$$\bar{\mathbf{s}} = \mathbf{X}\bar{\beta} + \mathbf{Q}\mathbf{H}^T\bar{\xi}$$

The maximum likelihood estimation is equivalent to minimizing the following objective function L

$$L = \frac{1}{2}(\mathbf{y} - \mathbf{h}(\mathbf{s}))^T \mathbf{R}^{-1}(\mathbf{y} - \mathbf{h}(\mathbf{s})) + \frac{1}{2}(\mathbf{s} - \mathbf{X}\beta)^T \mathbf{Q}^{-1}(\mathbf{s} - \mathbf{X}\beta)$$

#### *Successive linear estimator*

SLE and QLGA methods share similarities in term of the minimized objective function and the methods used to calculate the sensitivity matrix. However, some differences between them exist. One difference resides during the best estimate update, SLE approach calculate the new step based on the previous step while quasi-linear geostatistical approach always solves a new mean of the parameter to which some variation is also solved and added to it. Another difference is that the covariance of unknown parameters in SLE is updated to derive the residual covariance every iteration (Nowak & Cirpka, 2004; Zha et al., 2017). The initial provided covariance matrix specifies the spatial variability of the parameters. After the first iteration, the initial covariance becomes the conditional covariance or residual covariance. At the end of the iterative process, the diagonal of this conditional covariance describes the uncertainty associated with the parameters estimates. Because this residual covariance is a linear approximation, it must be updated every iteration to reflect a further reduction in uncertainty of the estimates due to additional information extracted from the nonlinear relationship between data and parameters.

The fact that SLE approach constructs new cross-covariance between parameter and data, and auto covariance of observation data, added to the continuous updating of residual covariance allow SLE to correctly address the uncertainty and enhance convergence of the inverse solution.

The following steps describe the SLE algorithm assuming that the sensitivity matrix for each iteration is already calculated. During SLE procedure, the domain is also discretized into  $\mathbf{n}$  elements which are initially given a prior unconditional mean and correlated by a covariance matrix  $\mathbf{Q}$ . The initial hydraulic

parameters are then updated conditioned by  $\mathbf{m}$  observed drawdown data in vector  $\mathbf{y}$ . SLE iteratively estimates the new solution for each element as follows:

$$\mathbf{s}_{i+1} = \mathbf{s}_i + \boldsymbol{\omega}_i^T (\mathbf{y} - \mathbf{h}(\mathbf{s}_i))$$

where  $i$  is the iteration index;  $\mathbf{s}$  is the hydraulic parameter vector of  $\mathbf{n} \times \mathbf{1}$  elements;  $\mathbf{h}(\ )$  refers to the forward model used to produce simulated drawdown data using the current hydraulic parameter (refer to forward model description subsection).  $\boldsymbol{\omega}$  which denotes the weights, has a size of  $\mathbf{m} \times \mathbf{n}$  and adjusts the added difference between the observed and simulated drawdown to the current solution. The coefficient matrix  $\boldsymbol{\omega}$  is estimated by solving the following equation:

$$[\mathbf{E}_i^{yy} + \boldsymbol{\theta} \mathit{diag}(\mathbf{E}_i^{yy})] \boldsymbol{\omega}_i = \mathbf{E}_i^{sy}$$

where  $\boldsymbol{\theta}$  is a dynamic stability multiplier.  $\mathbf{E}_i^{yy}$  and  $\mathbf{E}_i^{sy}$  are, respectively, the conditional covariance of observation data and the residual cross-covariance between parameter and data. Although, the SLE can exhibit an instability while solving the equation system that determines  $\boldsymbol{\omega}$ . Hence, a stabilizer term is usually added to ensure the equation system stability.  $\mathbf{E}_i^{yy}$  and  $\mathbf{E}_i^{sy}$  are obtained from the following first order approximation (Yeh and Liu, 2000):

$$\mathbf{E}_i^{yy} = \mathbf{H}_i \mathbf{Q}_i \mathbf{H}_i^T$$

$$\mathbf{E}_i^{sy} = \mathbf{H}_i \mathbf{Q}_i$$

where  $\mathbf{H}$  is the sensitivity matrix estimated using the current parameter. The Jacobean matrix calculation is the most time consuming in hydraulic tomography and methods using a reduced covariance rank, based on the SVD decomposition of the covariance matrix  $\mathbf{Q}$ , have been introduced (Kitanidis and Lee 2014, Zha et al. 2019) to considerably reduce the number of forward model runs.

At  $i=0$ ,  $\mathbf{Q}$  is the unconditional covariance matrix of parameter  $\mathbf{s}$  constructed from a prior variance, correlation lengths and covariance model (see inputs parameters subsection). the residual covariance at each step is defined as follows (Yeh and Liu, 2000):

$$\mathbf{Q}_{i+1} = \mathbf{Q}_i - \boldsymbol{\omega}_i^T \mathbf{E}_i^{sy}$$

### *Principal component geostatistical approach*

Recently, Kitanidis and Lee (2014) proposed an efficient technique, the Principal Component Geostatistical Approach (PCGA) used for large-dimensional inversion based on the Quasi-Linear Geostatistical Approach (QLGA). The main advantage of this method is the greatly reduced time calculation. Indeed, the calculation of the sensitivity matrix often requires several forward simulation runs that are themselves dependent on the complexity of the model (e.g. transient or steady state, 2D or 3D). Using a finite difference method to calculate the sensitivity matrix will need as many unknowns as forward model runs. And, fine discretization of the inverted domain is often used for resolution purposes and sometimes for inverse problem stability. The complexity of the forward model and the high resolution discretization of the unknowns quickly create calculation times limitations. The principal component geostatistical approach greatly decreases the number of the forward models by only estimating the Jacobean matrix instead of fully calculate it. Figure 3.17 shows a comparison of the group  $HQH^T$  calculated using a full Jacobean calculation and using the PCGA.

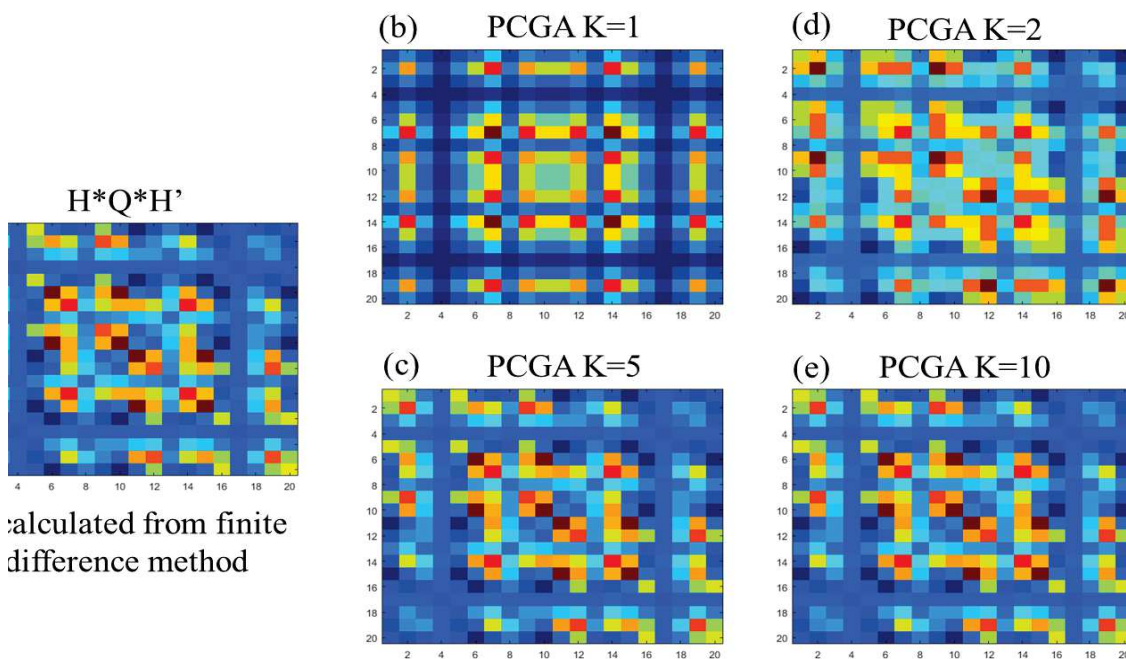


**Figure 3.17:** Comparison of  $HQH^T$  group calculated from finite difference method (a) and estimated using PCGA approach with different truncation numbers (b, c, d and e).

To give an order of magnitude of how faster the PCGA is, we compare the number of forward model runs of the full Jacobean calculation (Figure 3.17a) to the number of forward model runs using the PCGA with a truncation number  $K=10$  (Figure 3.17e). the domain in this example is discretized into  $n_x=20$  and  $n_y=20$  which in total correspond to 400 cells (400 unknowns if only transmissivity is

inverted, 800 unknowns if transmissivity and specific storage are inverted). The finite difference method that calculate the sensitivity matrix will perform 400 runs while the PCGA will only perform 12 forward runs with  $K=10$ . Which makes the PCGA in this example up to 30 times faster.

The observation equation that links the  $m$  unknown hydraulic conductivities, stored in a vector  $\mathbf{s}$ , to the observation data (hydraulic heads) stored in a matrix  $\mathbf{y}$  is (Kitanidis 1995):

$$\mathbf{y} = \mathbf{h}(\mathbf{s}) + \mathbf{v},$$

where  $\mathbf{h}(\mathbf{s})$  is the forward model,  $\mathbf{v}$  is the observation error with a random normal distribution with mean 0 and variance  $\mathbf{R}$ , which is usually the error measurement multiplied by the identity matrix. The prior probability of  $\mathbf{s}$  is a Gaussian distribution with mean  $\mathbf{X}\boldsymbol{\beta}$  generalized by a covariance matrix  $\mathbf{Q}$ .  $\mathbf{X}$  is a  $m$ -vector of ones and  $\boldsymbol{\beta}$  represents the mean hydraulic conductivity value. The posterior probability density function (objective function  $\mathbf{L}$ ) of  $\mathbf{s}$  and  $\boldsymbol{\beta}$  is given by:

$$\mathbf{L} = \frac{1}{2}(\mathbf{y} - \mathbf{h}(\mathbf{s}))^T \mathbf{R}^{-1}(\mathbf{y} - \mathbf{h}(\mathbf{s})) + \frac{1}{2}(\mathbf{s} - \mathbf{X}\boldsymbol{\beta})^T \mathbf{Q}^{-1}(\mathbf{s} - \mathbf{X}\boldsymbol{\beta})$$

The optimization of the hydraulic conductivity values is obtained by minimizing this objective function through an iterative method.

Inversion process requires the calculation of the sensitivity matrix (Jacobian matrix) which require as much forward model simulations as unknowns  $m$ . Despite the computer science advancement, the forward model itself can be time consuming when dealing with high dimensional problems (3D simulations, fine mesh, presence of complex structures). In order to bypass this difficulty, the principal component geostatistical approach which avoids the full Jacobian matrix calculation, was proposed. The reduced order successive linear estimator ROSLE (Zha et al. 2018) based on SLE (Yeh et al., 1996) can be one alternative to the PCGA. These methods use a singular value decomposition and then a truncation based on the eigenvalues and Eigen functions of the covariance matrix  $\mathbf{Q}$ . The covariance matrix can be rewritten with its decomposed form as:

$$\mathbf{Q} = \mathbf{V}\mathbf{S}\mathbf{V}^T,$$

where  $\mathbf{V}$ 's columns correspond to the eigenvectors of the covariance matrix and  $\mathbf{S}$  is a diagonal matrix of its eigenvalues  $\boldsymbol{\lambda}$  which are decreasingly organized. The eigenvectors and eigenvalues are then  $\mathbf{k}$ -rank truncated. The  $\mathbf{k}$  first eigenvalues and its corresponding eigenvectors are kept. The compressed covariance can be calculated as:

$$\mathbf{Q}_k = \mathbf{V}_k \mathbf{S}_k \mathbf{V}_k^T,$$

where

$$\mathbf{Q}_k \approx \mathbf{Q},$$

It can be also written as a sum:

$$\mathbf{Q}_k = \mathbf{V}_k \mathbf{S}_k \mathbf{V}_k^T = \sum_{i=1}^k \xi_i \xi_i^T,$$

where

$$\xi_i = \sqrt{\lambda_i} \mathbf{V}_i.$$

The accuracy of the low-rank covariance depends on the truncation number. However, it is already shown that a much smaller truncation number than the number of unknowns ( $k \ll m$ ) can be used (Kitanidis and Lee, 2014). The quasi-Linear geostatistical approach (Kitanidis, 1995) updates the actual best estimate  $\bar{\mathbf{s}}$  for the next iteration as:

$$\bar{\mathbf{s}} = \mathbf{X}\bar{\boldsymbol{\beta}} + \mathbf{Q}\mathbf{H}^T\bar{\boldsymbol{\xi}},$$

where  $\mathbf{H}$  is the Jacobian matrix and the accentuation-bar denotes the best estimate.  $\bar{\boldsymbol{\beta}}$  and  $\bar{\boldsymbol{\xi}}$  are solved from the following linear system:

$$\begin{bmatrix} \mathbf{H}\mathbf{Q}\mathbf{H}^T + \mathbf{R} & \mathbf{H}\mathbf{X} \\ (\mathbf{H}\mathbf{X})^T & \mathbf{0} \end{bmatrix} \begin{bmatrix} \bar{\boldsymbol{\xi}} \\ \bar{\boldsymbol{\beta}} \end{bmatrix} = \begin{bmatrix} \mathbf{y} - \mathbf{h}(\bar{\mathbf{s}}) + \mathbf{H}\bar{\mathbf{s}} \\ \mathbf{0} \end{bmatrix}.$$

The minimized objective function  $\mathbf{L}$  can also be written as:

$$\mathbf{L} = \frac{1}{2} \left( \mathbf{y} - \mathbf{h}(\mathbf{X}\boldsymbol{\beta} + \mathbf{Q}\mathbf{H}^T\boldsymbol{\xi}) \right)^T \mathbf{R}^{-1} \left( \mathbf{y} - \mathbf{h}(\mathbf{X}\boldsymbol{\beta} + \mathbf{Q}\mathbf{H}^T\boldsymbol{\xi}) \right) + \frac{1}{2} \boldsymbol{\xi}^T \mathbf{H}\mathbf{Q}\mathbf{H}^T \boldsymbol{\xi}.$$

In PCGA, the sensitivity matrix  $\mathbf{H}$  is not fully calculated and an alternative way to approximate it is proposed.

In order to estimate  $\mathbf{H}\mathbf{Q}$  and  $\mathbf{H}\mathbf{Q}\mathbf{H}^T$ ,  $k$  forward runs are needed to be solved in addition to the forward run of the actual best estimate, the forward models are used to calculate  $\boldsymbol{\eta}$  defined as follows:

$$\boldsymbol{\eta}_i = \mathbf{H}\xi_i \approx \frac{1}{\delta} [\mathbf{h}(\mathbf{s} + \delta\xi_i) - \mathbf{h}(\mathbf{s})],$$

$\delta$  is the finite difference interval from the Taylor series expansion (Kitanidis and Lee, 2014). Then  $\mathbf{H}\mathbf{Q}$  and  $\mathbf{H}\mathbf{Q}\mathbf{H}^T$  are defined as:

$$\mathbf{H}\mathbf{Q} \approx \mathbf{H}\mathbf{Q}_k = \mathbf{H} \sum_{i=1}^k \xi_i \xi_i^T = \sum_{i=1}^k (\mathbf{H}\xi_i) \xi_i^T = \sum_{i=1}^k \boldsymbol{\eta}_i \xi_i^T,$$



which allows iterations during inversion to be faster. As for PCGA which is based on QLGA, the ROSLE is based on SLE. The ROSLE approach uses the truncated Karhunen-Loeve Expansion (KLE) to approximate a reduced order covariance of the unknown parameters which avoids the full-rank covariance matrix to be explicitly computed and stored. Furthermore, only few directional sensitivities are calculated to form the covariance and cross-covariance matrix used in the cokriging-like inverse equation. The uncertainty of the estimates (conditional covariance) is then updated during each iteration via updating the leading eigenvalues and eigen-functions associated with the residual covariance. The KLE allows to generate random fields based using correlation functions (e.i. initial covariance matrix and conditional covariance through iterations) (Ghanem & Spanos, 2003). The following steps summarizes the main workflow of the ROSLE approach. The parameter random field  $s$  can be expanded as (Zhang & Lu, 2004):

$$\mathbf{s} = \mathbf{E}[\mathbf{s}] + \mathbf{g}\boldsymbol{\lambda}^{\frac{1}{2}}\boldsymbol{\xi}$$

where  $\mathbf{E}[\mathbf{s}]$  is the mean of the discretized random field  $\mathbf{s}$ ,  $\boldsymbol{\xi}$  ( $n \times 1$ ) are a set of uncorrelated random variables with zero mean and unity variance.,  $\mathbf{g}$  ( $n \times n$ ) are orthogonal eigen-functions, and  $\boldsymbol{\lambda}$  ( $n \times n$ ) is a diagonal matrix filling with corresponding nonnegative eigenvalues  $\lambda_i$ . The eigenvalues and eigenvectors are obtained by eigenvalue decomposition of the covariance function of  $\mathbf{s}$ :

$$\boldsymbol{\varepsilon}_{ss} = \mathbf{g}^T \boldsymbol{\lambda} \mathbf{g}$$

The covariance matrix is symmetrical and its eigen decomposition results in  $n$  real eigenvalues and mutually orthogonal eigen functions. In the PCGA approach, the randomized eigen decomposition method (Halko et al., 2011) is employed to approximate the prior covariance. The computational costs for the latter two approaches are closely related to the cost of random field generation. The choice of the truncation number is usually related to the decaying of the eigenvalues. It is recommended to take the  $K$  first eigenvalues and eigen-functions when the summation of those  $K$  eigenvalues dominates the summation of all eigenvalues.

At a given iteration, the covariance and cross-covariance defined in SLE are respectively expressed as (Zha et al. 2018):

$$\boldsymbol{\varepsilon}_{yy} = \mathbf{J}_y \mathbf{f} \mathbf{f}^T \mathbf{J}_y^T$$

$$\boldsymbol{\varepsilon}_{ys} = \mathbf{J}_y \mathbf{f} \mathbf{f}^T$$

with

$$\mathbf{f} = \mathbf{g}\boldsymbol{\lambda}^{\frac{1}{2}}$$

where  $\boldsymbol{\varepsilon}_{yy}$  is the conditional or residual auto-covariance of observation data,  $\boldsymbol{\varepsilon}_{ys}$  is the residual cross-covariance between parameter and data,  $\mathbf{J}$  the Jacobean matrix.

The coefficients matrix  $\boldsymbol{\omega}$  and the directional sensitivity or directional gradient (Elsheikh et al. 2013)  $\mathbf{H}$  are denoted respectively as

$$\boldsymbol{\omega} = \mathbf{v}\mathbf{f}^T = \mathbf{v}\lambda^{\frac{1}{2}}\mathbf{g}^T$$

$$\mathbf{H} = \mathbf{J}_y\mathbf{f}$$

where  $\mathbf{v}$  are the coefficients to form  $\boldsymbol{\omega}$ . The new system of equations to solve is written as

$$[\mathbf{H}\mathbf{H}^T + \boldsymbol{\theta}\mathit{diag}(\mathbf{H}\mathbf{H}^T)]\mathbf{v} = \mathbf{H}$$

Again, the stabilization term is necessary to ensure a solution of this equation. After  $\mathbf{v}$  is solved, the parameter is updated

$$\mathbf{s}^{i+1} = \mathbf{s}^i + \mathbf{f}\mathbf{v}^T(\mathbf{y} - \mathbf{h}(\mathbf{s}^i))$$

The main calculation part is to estimate the directional sensitivities  $\mathbf{H}$ . Elsheikh et al. (2013) and Kitanidis and Lee (2014) suggest using the first-order approximation to evaluate this matrix:

$$\mathbf{H} \approx \frac{\mathbf{1}}{\boldsymbol{\delta}}[\mathbf{h}(\mathbf{s} + \boldsymbol{\delta}\mathbf{f}) - \mathbf{h}(\mathbf{s})]$$

where  $\mathbf{h}(\cdot)$  is the forward model. As noted by Kitanidis and Lee (2014) and Lee and Kitanidis (2014), the difference step  $\boldsymbol{\delta}$  is crucial to the successful calculation of  $\mathbf{H}$ . Since the vector  $\mathbf{f}$  is scalable to  $\sqrt{\lambda}$ , it is favorable to set  $\boldsymbol{\delta}$  as a parameter inversely proportional to  $\sqrt{\lambda}$ , so that

$$\mathbf{H} \approx \frac{\sqrt{\lambda}}{\boldsymbol{\delta}}[\mathbf{h}(\mathbf{s} + \boldsymbol{\delta}\mathbf{g}) - \mathbf{h}(\mathbf{s})]$$

By using this approximation, only  $K+1$  forward simulations are needed to construct  $\mathbf{H}$ .  $\boldsymbol{\delta}$  is a user specified small number related to the machine round-off error (Kitanidis & Lee, 2014).

After the first iteration, the conditional covariance can be decomposed in the same form

$$\mathbf{Q} = \mathbf{f}\mathbf{f}^T = \mathbf{g}\lambda\mathbf{g}^T$$

The updating of the covariance matrix can be rewritten as

$$\mathbf{Q}^{i+1} = \mathbf{Q}^i - (\mathbf{v}\mathbf{f}^T)^T\boldsymbol{\varepsilon}_{ys}$$

When the conditional random field becomes nonstationary after the conditioning of data by hydraulic tomography, a direct decomposition becomes costly. Lu and Zhang (2004), extended by Zha et al. 2018, proposed an efficient method to obtain the eigenvalues and the eigen-vectors of the conditional covariance.

### *Synthetic example*

Here we apply the hydraulic tomography approach to a simple synthetic example. Firstly, a true synthetic transmissivity field is generated (binary transmissivity map; the objective is to show the potential of hydraulic tomography to capture zones of high and low transmissivity). Then we model several wells and simulate cross-hole pumping tests. The simulated drawdowns are used to perform a HT and thus invert the transmissivity field. The storativity is assumed constant and SLE method is used. The results are shown in Figure 3.19.

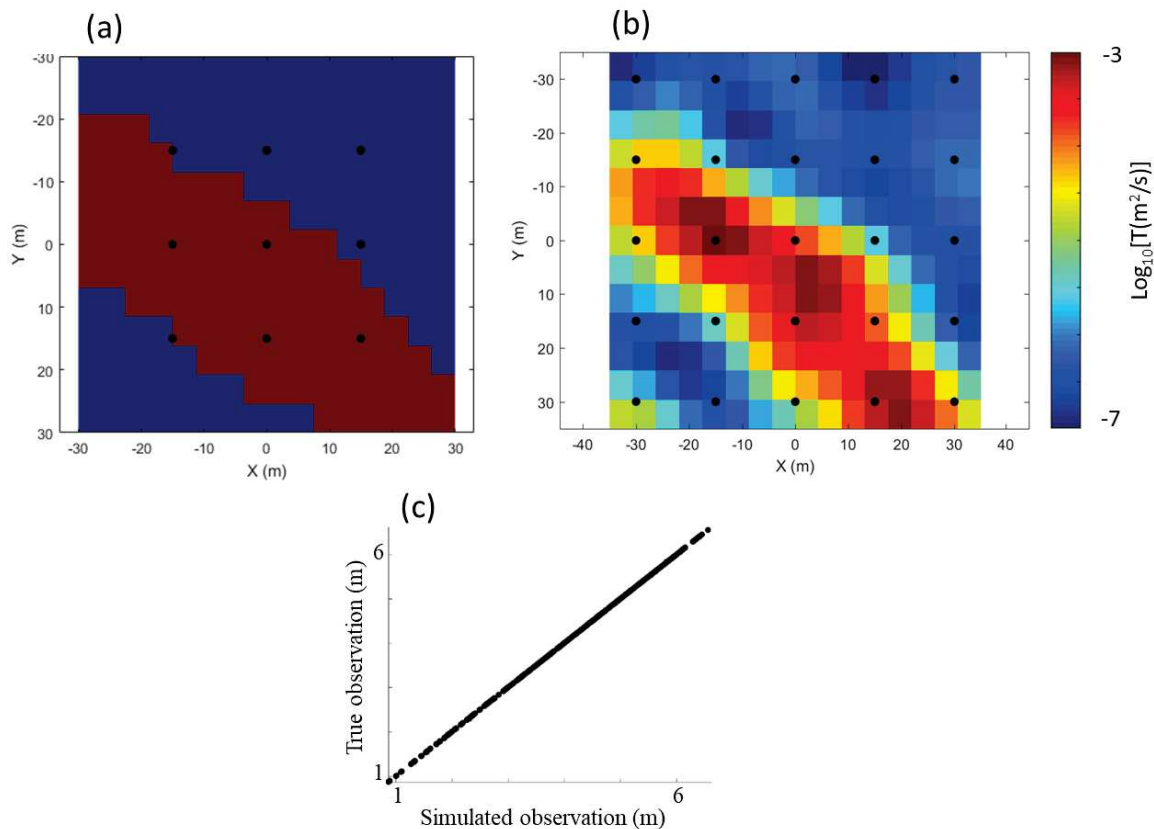


**Figure 3.19:** Results of HT synthetic example. A) true transmissivity field. B) inverted transmissivity field. C) data measurements fitting; true observations versus simulated observations.

### *Flexibility of HT to incorporate geological data*

Zha et al. (2017) showed how geological data can be easily incorporated into hydraulic tomography in order to improve the estimates and obtain realizations with better geological realism. The covariance matrix has the flexibility to store these geological or additional data as strong or soft constraints. Zha

et al. (2017) simply constructed the total covariance matrix as a sum of different covariance sub-matrices: a) a covariance matrix that defines the different facies (layers) will be of high importance and its construction is achieved only by using a strong correlation between the cells that belong to the same facies, b) another covariance matrix that defines the correlation between the cells of the same facies, referred as an intra-facies covariance, c) a third covariance matrix, referred as an inter-facies covariance, is used on the global inverted domain. By conditioning the prior covariance with facies information distinguished from geological data, more realistic estimations could be obtained. The following Figure 3.20 shows a simple synthetic application and highlights how the estimation is improved if prior facies is known.

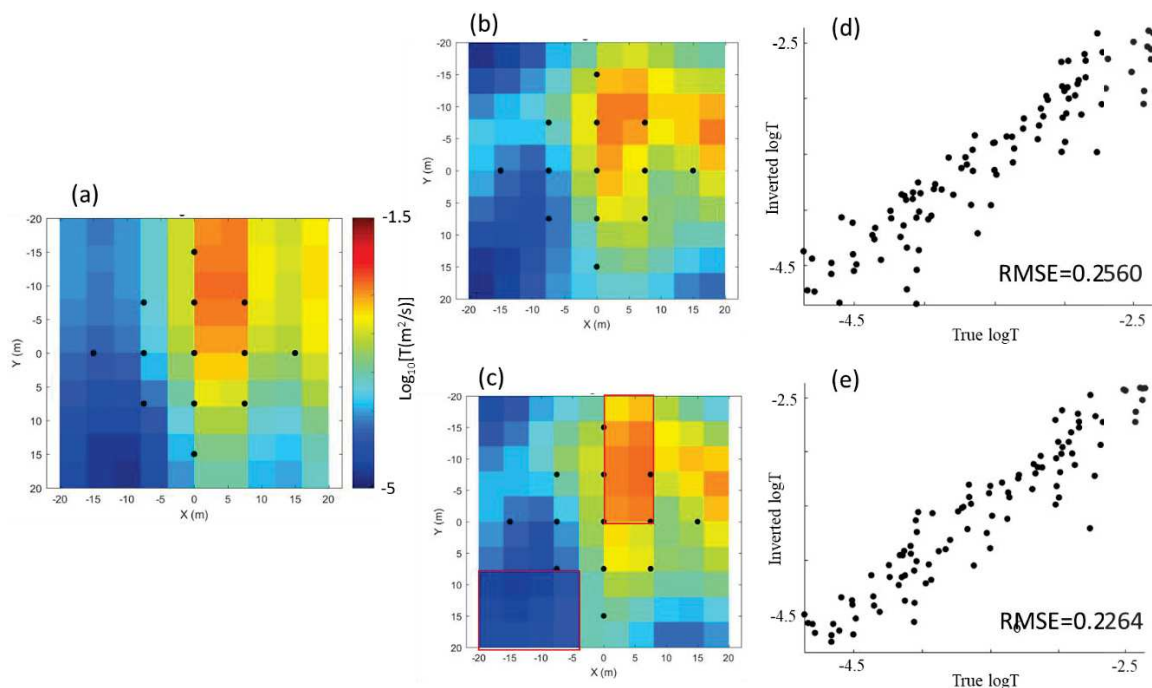


**Figure 3.20:** HT results comparing between a simple hydraulic tomography and a hydraulic tomography incorporating facies data. A) true transmissivity field. B) inverted transmissivity field using a simple hydraulic tomography. C) inverted transmissivity field using the two red rectangles as known prior facies. D) and e) are a scatter plot of inverted  $T$  versus true  $T$  for the two cases respectively.

Hydraulic tomography showed a great potential during the last decades on delineating the spatial distribution of hydraulic properties. Inversion can be time consuming because of the number of forward model runs. Fortunately, approaches using a singular values decomposition reduce considerably the time cost (e.i. PCGA and ROSLE). Hydraulic tomography is thus very flexible:

- Use of personalized prior model and custom forward models
- Data fusion
- Modification and calibration can be added at different steps of the algorithm

However, multiple wells and data are required for high resolution of property estimates. This approach is used as a main approach in this thesis applications because of its potential and also because of the availability of an experimental site that meets the approach requirements.

### **3.4.5 Review of analytical and numerical methods for anisotropy characterization of hydraulic properties**

## REVIEW OF ANALYTICAL AND NUMERICAL METHODS FOR HORIZONTAL ANISOTROPY CHARACTERIZATION OF HYDRAULIC PROPERTIES

Mohammed Aliouache<sup>a,\*</sup>, Xiaoguang Wang<sup>b</sup>, Gerard Massonnat<sup>c</sup>, Herve Jourde<sup>a</sup>

<sup>a</sup> *Laboratories Hydrosiences Montpellier, UMR 5151 CNRS-UM-IRD, Montpellier, France, 34000*

<sup>b</sup> *Chengdu University of Technology, Sichuan, China, 610059*

<sup>c</sup> *CSTJF-PAU Total Energies, Avenue Larribau, Pau, France, 64000*

\*Correspondence: [mohammed.aliouache@umontpellier.fr](mailto:mohammed.aliouache@umontpellier.fr)

### Highlights

1. Horizontal anisotropy characterization
2. Performance of different developed techniques and drawbacks
3. Scale of investigation and upscaling are discussed

### 3.4.5.1 Abstract

The characterization of heterogeneous porous rocks is an important task for many applications, including aquifer management, oil field development and environmental protection. When applying the traditional approaches based on single-well hydraulic tests to estimate the hydraulic parameters of porous formations, the estimation is often erroneous. The main reason of the failure is that all these single-well methods assume that the subsurface system can be represented by one or at most a few isotropic homogeneous hydraulic units. However, in reality preferential flow directions often occur in natural porous systems due to the presence of complex depositional geometries. Thus, significant permeability anisotropy exists. To achieve an enhanced characterization, hydraulic interpretation approaches based on information from multiple testing wells are required. In this work, we present a review and comparative study of five methods for detecting aquifer anisotropy. Depending on the formulation, either based on analytical calculations or graphical fittings, their utilizations are of different levels of complexity. To make quantitative comparison, the various methods are applied to analyze synthetically porous media with homogeneous anisotropic transmissivities. We discuss the effectiveness (i.e., the accuracy of result) and efficiency (i.e., the time and effort spent why applying the method), and offer a guidance for the selection of optimal method based on a variety of realistic constrains.

### 3.4.5.2 Introduction

The previously presented analytical methods that evaluate the effective hydraulic properties of the tested aquifer are all under the assumption of an isotropic aquifer. However, most of aquifers in nature show strong anisotropies especially when dealing with fractured-rock and karstic aquifers. Horizontal and vertical anisotropy exists in all naturally deposited formations, but horizontal anisotropy is negligible for most of them. In some sedimentary deposits, horizontal anisotropy may cause flow to be more dominant along the plane of deposition as compared with the direction perpendicular to the direction of deposition. Horizontal anisotropy depends on sediment deposition rate, depositional environment, and shape, size, and orientation of particles (Quinones-Aponte, 1989). Anisotropy (Marcus, 1962) is a common feature in water-laid sedimentary deposits (e.g. fluvial, clastic lake, deltaic and glacial outwash deposits). Aquifers that are composed of water-laid deposits may exhibit anisotropy on the horizontal plane (Kruseman and De Ridder, 1994). Like for the interpretation of tested aquifers assumed isotropic, methods to interpret tests in anisotropic aquifers were developed. Papadopulos (1965) is one of the first to work on anisotropy and developed a method for analysis of pumping test data based on non-steady-state continuous pumping from an infinite homogenous aquifer. The flow in anisotropic aquifers is altered and the velocity vector becomes non-parallel to the hydraulic gradient direction. The drawdown cone becomes elliptic, this is why transmissivity in anisotropic aquifers are characterized by an ellipse with a major and minor which follow the same direction as the drawdown cone. The short axis of the ellipse corresponds to the low transmissivity direction and the long axis of the ellipse corresponds to the major transmissivity direction. To define a transmissivity ellipse,  $T_{max}$ ,

$T_{min}$  and  $\theta$  parameters are required and a minimum of three observation wells at different directions and distances from the pumping well are necessary. The Papadopoulos (1965) method defines the necessary equations to calculate the values of the principal (major, minor and the angle between the major axis and the x-axis) transmissivity components. Papadopoulos (1965) developed a method of determining the principal directions of anisotropy and the corresponding minimum and maximum transmissivities. This method requires drawdown data from at least three wells, other than the pumped well, all three located on different rays from the pumped well. Liakopoulos (1965) conducted an experiment on anisotropic sandstone where he sampled core plugs in different directions and found out an ellipsoid 2D transmissivity tensor and he proposed a graphical method to obtain the velocity direction of hydraulic gradient direction given a transmissivity tensor. Walton (1979) and Bear (1979) inventoried available analytical groundwater models and describe their usefulness and limitations and also proposed needed additional progress in modeling to cover more aquifer systems. Between the analytical models that can be applied to anisotropic systems, we can find: Boulton and Streltsova, (1977a, b) that proposed analytical solution for anisotropic fractured rock aquifers for non-leaky confined systems, while, other works focused on water table aquifer systems for fully and partially penetrating well (Streltsova, 1974; Neuman, 1975; Boulton and Streltsova, 1976, 1978). Long et al. (1982) proposed a numerical approach to estimate an equivalent anisotropic porous media of a fracture network through a permeability tensor. Meier et al. (1998) used a parallel flow numerical model to estimate the directional transmissivities. Also, Heilweil and Hsieh, (2006) proposed a simplification of Papadopoulos (1965) for fractured media where the principal tensor directions were known prior to implementation.

Neuman et al. (1984) proposed an extension and showed that Papadopoulos method can be used with drawdown data from only three wells, provided that two pumping tests are conducted in sequence in two of those wells. When water is pumped from well 1 at a constant rate  $Q_1$ , two sets of drawdown data are available from wells 2 and 3. This is not sufficient to allow the use of Papadopoulos equations. However, if at least one other pumping test is conducted, e.g. in well 2, at a constant rate  $Q_2$ , and the resulting drawdown is observed at least in well 3, these drawdown data provide the third set of data needed to complete the analysis. Later on, Kern and Dobson, (1998) extended the least squared method developed by Neuman et al. (1984) to analyze uncertainty and build a confidence interval for the angles and principal transmissivity tensor components.

Hantush, (1966) proposed a modification to the Theis (1935) solution to take into consideration the anisotropy in the horizontal plane. Hantush and Thomas 1966, developed a simple method for estimating the degree and direction of anisotropy for two-dimensional flow. Hantush (1966) extended the anisotropy detection into leaky aquifers where the leakage factor is added as an unknown. The

method requires data from three groups of observation wells which are interpreted using standard leaky isotropic aquifer methods separately. While Weeks (1969) method deals with the vertical anisotropy.

Louis (1974) proposed a method that requires drilling one injection borehole and two monitoring boreholes parallel to any of the three (known) principal directions of the hydraulic conductivity tensor. This technique also requires packers to make it possible to compute all the three unknown principal hydraulic conductivities. Hsieh and Neuman, 1985, proposed a new field method to determine the three-dimensional hydraulic conductivity tensor of an anisotropic medium. They stated that their method differs from previous techniques in two ways: 1) it does not require that the principal directions be known prior to the tests and, 2) the boreholes may be drilled in any directions that are technically feasible. And the method is applicable to both porous and fractured media (Hsieh et al., 1985). Way and McKee (1982) proposed a three dimensional type curve solution of partially penetrating wells for horizontally and vertically anisotropic aquifers. However, Batu (2008) concluded that the method proposed by Way and McKee (1982) for partially penetrating wells for horizontally and vertically anisotropic aquifers is in error.

Maslia and Randolph (1987) developed A Fortran computer program, Tensor2D, that can be used to analyze pumping test data for an anisotropic confined non-leaky aquifer. Tensor2D is based on the equation of drawdown formulated by Papadopoulos (1965) for non-steady flow in an infinite anisotropic confined non-leaky aquifer. Data for more than three observation wells or piezometers can be analyzed with a weighted least-squares optimization procedure. Several other methods for analyzing pumping test data in anisotropic aquifers are described in the literature (Neuman et al., 1984; Hsieh et al., 1985). The approach has been applied for example to evaluate the anisotropic properties of a karst limestone system (Motz, 2009).

Aris (1956) introduced the spatial moments approach which was widely used in solute transport (e.g. Freyberg, 1986; Sudicky, 1986). The approach was later on applied to identify the components of hydraulic conductivity tensor (e.g. Yeh et al. 2005; Wu et al. 2005).

Sekhar et al. (1994) proposed A numerical inverse model for parameter estimation in an anisotropic leaky aquifer-water table aquitard system. The governing parameters are estimated using the sensitivity analysis technique where the sensitivity coefficients are evaluated based on a modified parameter perturbation technique using non-dimensional equations. Lebbe and Breuck (1997) also used an inverse numerical model to capture lateral anisotropy in a fractured media. Wu et al. (2008) used the Tabu search algorithm, along with the Adjoint State method, in a two-dimensional inverse model to optimize horizontal anisotropy delineation for short and long pumping tests in homogeneous and heterogeneous aquifers. Lin et al. (2010) used artificial neural network in order to estimate the hydraulic parameters of anisotropic aquifers.

Kucuk and Brigham (1979) studied transient flow in elliptical systems and concluded that an infinite anisotropic reservoir can be transformed into an isotropic one in which circular inner boundary becomes an ellipse. And, they presented a transient solution for flow to a finite diameter well (Papadopoulos and Cooper, 1967) in a horizontally anisotropic aquifer with negligible wellbore storage and found out that the effective well radius for elliptical flow is independent of whether the reservoir is producing at a constant flow rate or a constant pressure or whether the reservoir is isotropic or anisotropic. Moench (1997) proposed a solution to the problem of flow to a partially penetrating well of finite diameter in a water table aquifer. The solution is obtained in Laplace space and inverted numerically using the Stehfest (1970) algorithm. Fitts, (2006) proposed A new analytic solution is presented that meets the boundary condition at the well. Mathias and Butler, (2007) extended the solution of Kucuk and Brigham (1979) to take into account the wellbore storage as defined by Papadopoulos (1965). Cihan et al. (2011) developed a set of analytical solutions for transient flow through isotropic multilayered aquifers with alternating aquitards. Similar solutions for multilayered aquifer systems were developed using analytical element approaches, which also included heterogeneity by allowing presence of different subdomains with different hydraulic properties (Bakker, 2006). Later on, Cihan et al. (2014) extended the solutions given in Cihan et al. (2011) to account for horizontal anisotropy in multilayered aquifers.

Mutch (2005) and Wu et al. (2005) proposed the distance-drawdown analysis as an efficient approach to interpret hydraulic test data in horizontally anisotropic to evaluate the components of transmissivity tensor and storage coefficient. More recently, Huang et al., (2018) derived new analytical equations to estimate the properties of a horizontally anisotropic aquifers that are laterally bounded by a stream. The method consists on a straightforward inverse analytical method based on drawdown-time curves collected at minimum three non-collinear observation wells. Wang et al. (2018) proposed an approach using the inverse of the square root of the storage to estimate the radial transmissivities which can be converted into an ellipse using an elliptical regression, in a similar way as in the graphical method based on Hantush and Thomas (1966). Several investigations about horizontal anisotropy showed that its estimation can play an important role on improving the total aquifer or reservoir characterization (Stoner, 1981; Miller, 1985; Maslia, 1987; Ritzi and Andolsek, 1992; Chen, 2000; Bakker and Nieber, 2004; Wu et al., 2005; Lin et al., 2010; Wen et al., 2010; Dewandel et al., 2014; Chen et al., 2016; Paradis et al., 2016; Ren et al. 2021).

Different ways can be used to evaluate the anisotropy of the aquifer, such as graphical estimation method (Hantush and Thomas 1966), weighted least squares-based type-curve analysis (Maslia and Randolph 1987) or just numerically using Papadopoulos (1965) equations. In this study, five anisotropy detection techniques are implemented and tested on synthetic models to compare their performances and eventual drawbacks. The objective of the paper is to show the limited work on horizontal

anisotropy characterization, present the basic methods used to evaluate the horizontal transmissivity tensor. Further research on horizontal anisotropy can contribute greatly on groundwater flow models and may improve the upscaling field.

### 3.4.5.3 Methods

The performance of five existing methods that can detect tensor field from hydraulic pumping test will be reviewed. The five methods are: Distance drawdown, spatial moments, Papadopulos, Wang et al. 2018 method and a graphical method. The aim is to use different synthetic models with heterogeneous permeability field and simulate a pumping test in a given pumping well and get the transient Head response from surrounding observation wells. Figure 3.21 shows the well pattern used in all simulations.

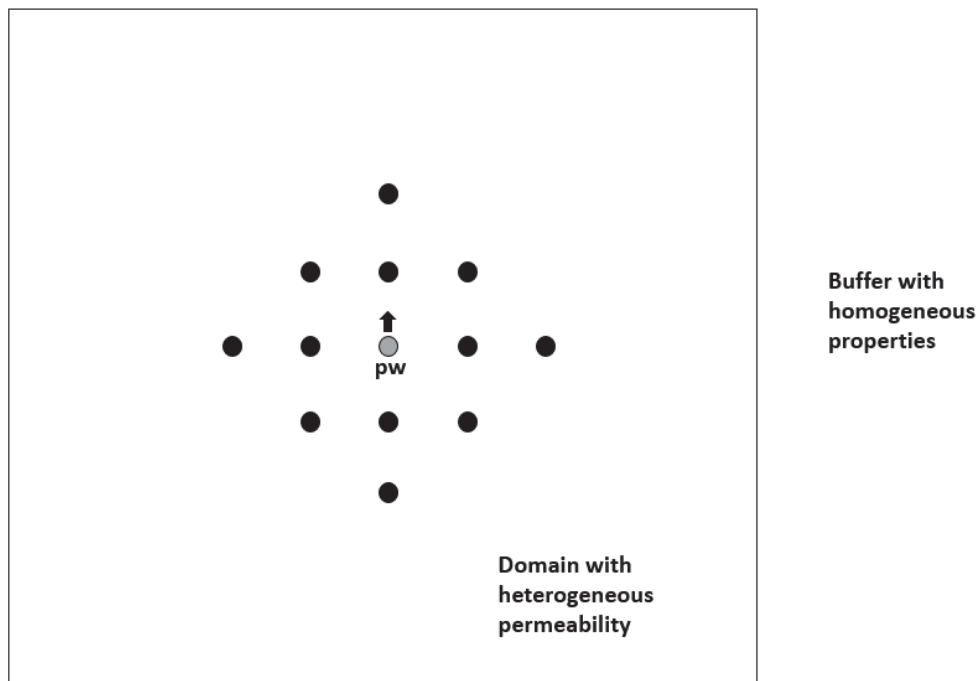


*Figure 3.21: Synthetic model used in simulation.*

The hydraulic pumping test is performed in the middle of the symmetrical pattern (**pw**). The heterogeneous map of permeability is mapped in the domain near the wells. The rest of the domain uses a constant mean property.

Once the simulation done, the observation response is used to extract a tensor issue from the heterogeneity with different methods cited above.

In traditional analysis of aquifer tests, the flow equation in a heterogeneous media is given by

$$T_{eff} \nabla^2 h(x, t) = S_{eff} \frac{\partial h(x, t)}{\partial t}$$

and to estimate the effective parameters of the aquifer we refer to Theis solution (Theis, 1935)

$$h(x, t) = \frac{Q}{4\pi T_{eff}} W(u), \quad W(u) = \int_u^\infty \frac{e^{-v}}{v} dv, \quad u = \frac{S_{eff} x^2}{4T_{eff} t}$$

where  $h(x, t)$  is the drawdown in at distance  $x$  from the pumping and at a time  $t$ ,  $Q$  is the pumping rate,  $T_{eff}$  is the effective permeability of the aquifer and  $S_{eff}$  is the effective storage.

The drawdown cone in anisotropic aquifers tends to be elliptical rather than circular. In other words, characterizing the depression cone caused by a pumping test will be equivalent to identifying the effective transmissivity tensor at the pumping well location. The major and minor axes of anisotropy of the drawdown ellipse  $\mathbf{a}$  and  $\mathbf{b}$ , respectively are related to the corresponding principal transmissivities of the aquifer  $T_x$  and  $T_y$ , by

$$\frac{\mathbf{a}}{\mathbf{b}} = \frac{T_e}{T_y} = \frac{T_x}{T_e}$$

The transmissivity in the direction of flow ' $r$ '  $T_r$  is calculated as

$$T_r = \left(\frac{r^2}{ab}\right) T_e$$

$$T_r = \frac{T_x}{[\cos^2 \theta + \left(\frac{T_x}{T_y}\right) \sin^2 \theta]}$$

where  $\theta$  is the angle between  $r$  and the x-axis,

*Papadopulos (1965):*

In order to get a homogeneous like estimation of the effective properties, the transient drawdown curve is matched to Theis solution, hence the minimization of the following objective function:

$$\sum_{i=1}^m [h(x, t_i) - h^*(x, t_i)]^2$$

where  $h^*(x, t_i)$  is the true observation and  $h(x, t_i)$  the theoretical solution,  $m$  is the number of time observations. This analysis could be also mentioned as a time drawdown analysis.

If we include the anisotropy in Theis solution, the equations become (Papadopulos 1965)

$$T_{xx} \frac{\partial^2 h(x, t)}{\partial x^2} + 2T_{xy} \frac{\partial^2 h(x, t)}{\partial xy} + T_{yy} \frac{\partial^2 h(x, t)}{\partial y^2} + Q = S \frac{\partial h(x, t)}{\partial t}$$

And the solution becomes

$$h(x, t) = \frac{Q}{4\pi\sqrt{D}} W(u_{xy}), \quad W(u) = \int_u^\infty \frac{e^{-v}}{v} dv$$

$$W(u) = \int_u^\infty \frac{e^{-v}}{v} dv$$

with,

$$u_{xy} = \frac{S [T_{xx} * y^2 + T_{yy} * x^2 - 2 * T_{xy} * xy]}{4tD}$$

and,

$$D = T_{xx} * T_{yy} - T_{xy}^2$$

$T_{xx}$ ,  $T_{yy}$  and  $T_{xy}$  are the tensor components,  $h(x, t)$  is the drawdown in the observation well positioned at a distance  $x$  from the pumping and at a given time  $t$ ,  $Q$  is the rate of the pumping,  $S$  is the Storage coefficient.

#### *Distance drawdown analysis*

This method tries to fit multiple observations at different locations for a given time. Then the objective function could be rewritten as (Wu et al. 2005)

$$\sum_{i=1}^n [h(x_i, t) - h^*(x_i, t)]^2$$

where  $h^*(x_i, t)$  is the true observation and  $h(x_i, t)$  the theoretical solution,  $n$  is the number of well observations. This method cannot well perform is the number of the observation wells is limited.

#### *Spatial moments analysis*

To derive the different components of the permeability tensor is a heterogeneous aquifer, the spatial moments could be used (Aris, 1956)

$$M_{ij}(t) = \int_{-\infty}^{+\infty} \int_{-\infty}^{+\infty} h(x, y, t) x^i y^j dx dy$$

where  $h(x, y, t)$  is the given drawdown at the time  $t$  and position  $(x, y)$ ,  $i$  and  $j$  varies with the condition  $i + j = 0, 1$  and  $2$ .  $M_{00}$  called the zeroth moment represent the change of the cone volume caused by the drawdown. The center of this cone is given by  $x_c$  and  $y_c$

$$x_c = \frac{M_{10}}{M_{00}} \quad y_c = \frac{M_{01}}{M_{00}}$$

The second spatial variance tensor is defined to describe the spreading of the cone

$$\sigma^2 = \begin{bmatrix} \sigma_{xx}^2 & \sigma_{xy}^2 \\ \sigma_{yx}^2 & \sigma_{yy}^2 \end{bmatrix} \quad \text{with} \quad \sigma_x^2 = \frac{M_{20}}{M_{00}} - x_c^2 \quad \sigma_y^2 = \frac{M_{02}}{M_{00}} - y_c^2$$

$$\sigma_{xy}^2 = \sigma_{yx}^2 = \frac{M_{11}}{M_{00}} - x_c y_c$$

The diffusivity tensor can be derived from the spatial variance tensor (Wu et al. 2005)

$$D_{eff}^{xx} = \frac{1}{2} \frac{\partial \sigma_{xx}^2}{\partial t}, \quad D_{eff}^y = \frac{1}{2} \frac{\partial \sigma_{yy}^2}{\partial t}, \quad D_{eff}^{xy} = D_{eff}^{yx} = \frac{1}{2} \frac{\partial \sigma_{xy}^2}{\partial t}$$

where  $D_{eff}^{xx}$ ,  $D_{eff}^{yy}$  are the diagonal components and  $D_{eff}^{xy}$ ,  $D_{eff}^{yx}$  are the off-diagonal components of the diffusivity tensor.

#### *Graphical and Wang et al. methods*

Both methods use an elliptical regression to fit a plotted parameter into a tensor. The graphical method plots the square root of directional transmissivity and Wang et al. plots the inverse of the square root of storativity.

Wang et al. 2018 proposed to use cross-hole slug test data to estimate horizontal anisotropy but remains applicable to pumping tests as well. Their method involves the following step-by-step procedures:

1. Interpret cross-hole slug test data for each observation well by fitting the data to a selected solution, and determine the transmissivity ( $T_g$ ) and storativity ( $S$ )
2. Calculate the inverse of the storage  $1/S'$  for each observation well and plot the value in the direction of the observation well on a polar-coordinate graph
3. Fit the data points to an ellipse and obtain the major and minor semi-axes and the tilted angle
4. Calculate the major and minor principle transmissivities,  $T_{max}$  and  $T_{min}$  using, the anisotropy ratio and the storativity  $S$ .

Here are summarized the needed equations to use the method. In radial coordinates, for an arbitrary  $r$  direction, the directional transmissivity is given by Bear (1972):

$$T_r = \frac{T_g}{\left[ \sqrt{\left(\frac{T_{min}}{T_{max}}\right) \cos^2 \theta} + \sqrt{\left(\frac{T_{max}}{T_{min}}\right) \sin^2 \theta} \right]}$$

with

$$T_g = \sqrt{T_{max} T_{min}}$$

where  $T_{max}$  and  $T_{min}$  are respectively the maximum and minimum transmissivities;  $\theta$  is the angle between the direction of the maximum transmissivity and  $r$  direction and  $T_g$  is the geometric mean of transmissivity.

The diffusion process of groundwater flow in response to an instantaneous change in water level obeys the basic law of mass conservation. This is reflected by the characteristic relationship between a scale measure, for instance the slug-observation well distance  $d_{ow}$ , and the aquifer storativity  $S$ , the only scaler term appears in the diffusivity equation, as given by

$$d_{ow}^2 S = cst$$

After scaling the distance and the storativity, the formal elliptical expression is:

$$1 = S \left[ \frac{r^2}{A^2} \cos^2 \theta + \frac{r^2}{B^2} \sin^2 \theta \right]$$

where

$$r = \sqrt{1/S'}$$

$$A^2 = \frac{1}{S \sqrt{T_{min}/T_{max}}}$$

$$B^2 = \frac{1}{S \sqrt{T_{max}/T_{min}}}$$

$$T_r = T_g S/S'$$

#### 3.4.5.4 Results and discussion

In the first model we use a homogeneous transmissivity tensor to simulate the hydraulic responses. The different methods are used to detect tensors from the hydraulic signals (see Figure 3.22).

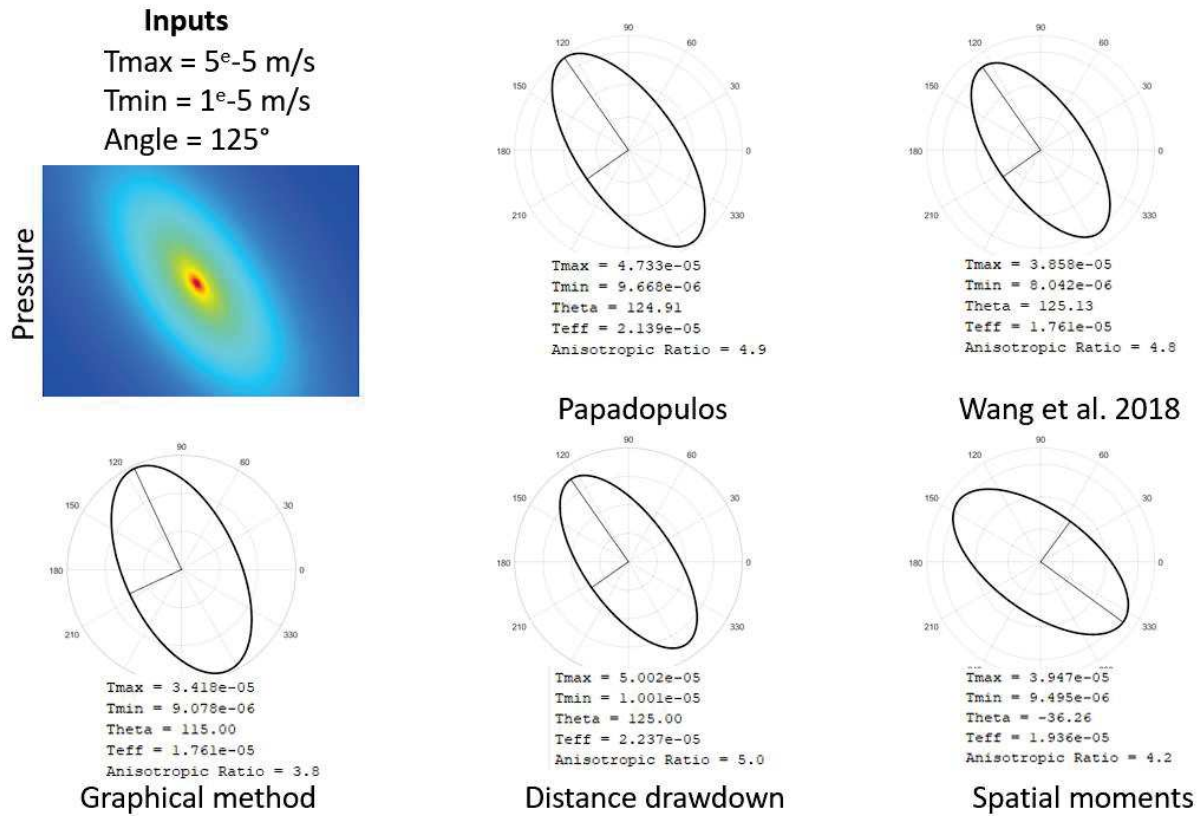


*Figure 3.22: Validation case for the different methods. For each method, a tensor and its values are presented.*

Different validation cases are simulated using different simulation times with different input tensors. It has been noticed that the spatial moments method presents instability (see Figure 3.23).

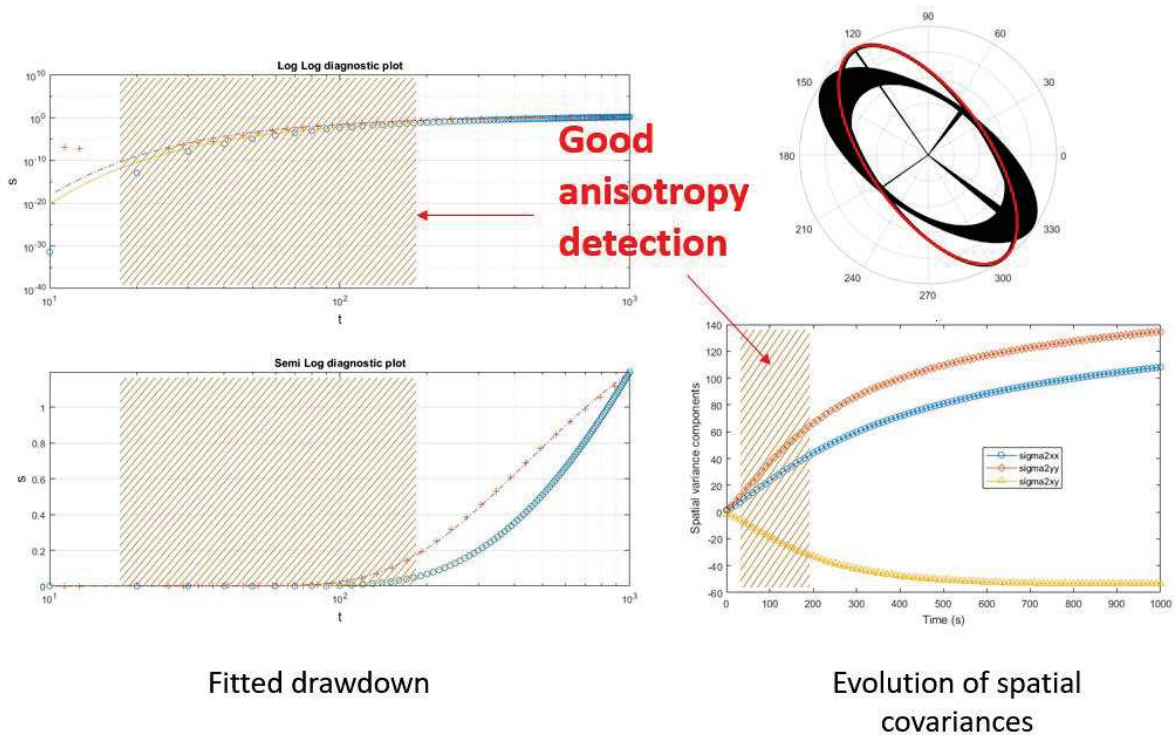
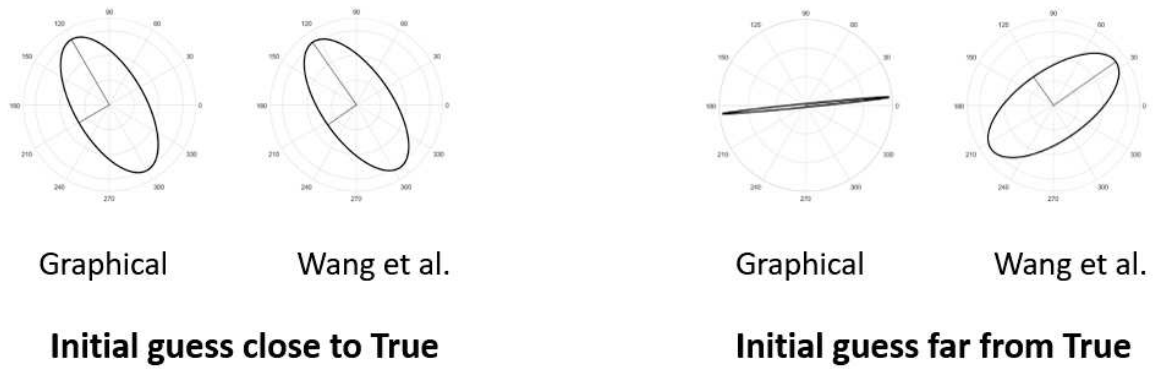


**Figure 3.23:** Plot of different tensors at different time steps (up right of the figure, the red tensor is the true). The plots (up left and down left) are the log-log and semi-log plots respectively of drawdown data and its derivative. The plot (down right) is the evolution of the spatial variance components calculated by the spatial moment method.

The given tensor by this method at middle or at longer transient time are of a bad quality. When the simulation arrives to pseudo steady-state, the tensor is totally erroneous. The Figure 3.23 shows the transient time interval where the spatial moments method’s performance is better.

It has been also found that the two methods using the elliptical regression may get the tensor wrong if the initial guess is far from the input tensor (see Figure 3.24). However, the tensor could be verified by scattering the directional parameter. When the initial guess (especially the direction angle) is close to the true one, the methods gets a much better fit. A manual check of the results and testing different initial guesses are highly recommended while using these two methods.



The regression is sensitive to the initial parameters – To choose carefully

*Figure 3.24: Case for showing the sensitivity of the elliptical regression to the initial guess.*

Next, the performance of the methods in catching the good main direction of the transmissivity tensor when heterogeneity is added to the anisotropy. The different methods perform quiet well. However, the obtained tensor is always the mean tensor of the covered area by the wells. This phenomenon is shown (Figure 3.25) when tests using different well coverage area. In model **A**, we put all our wells inside one homogeneous anisotropic domain ( $T_{max}=5^e-05$  m/s,  $T_{min}=1^e-05$  m/s,  $\Theta=90^\circ$ ) and in the buffer area, which represents the biggest part of the domain, we put a different tensor ( $T_{max}=5^e-05$  m/s,  $T_{min}=1^e-05$  m/s,  $\Theta=125^\circ$ ). The storage is constant in both domains. In this case at large scale, the direction should follow the tensor in the buffer. Then, the coverage is increased in model **B**. This test is made to see if at least a signature of the buffer zone can be caught by the tensor detection methods. Finally, we investigate the efficiency of the methods to find the good parameters:  $T_{max}$ ,  $T_{min}$  and  $\theta$ . We use the same workflow but using different parameters: inner domain ( $T_{max}=5^e-05$  m/s,

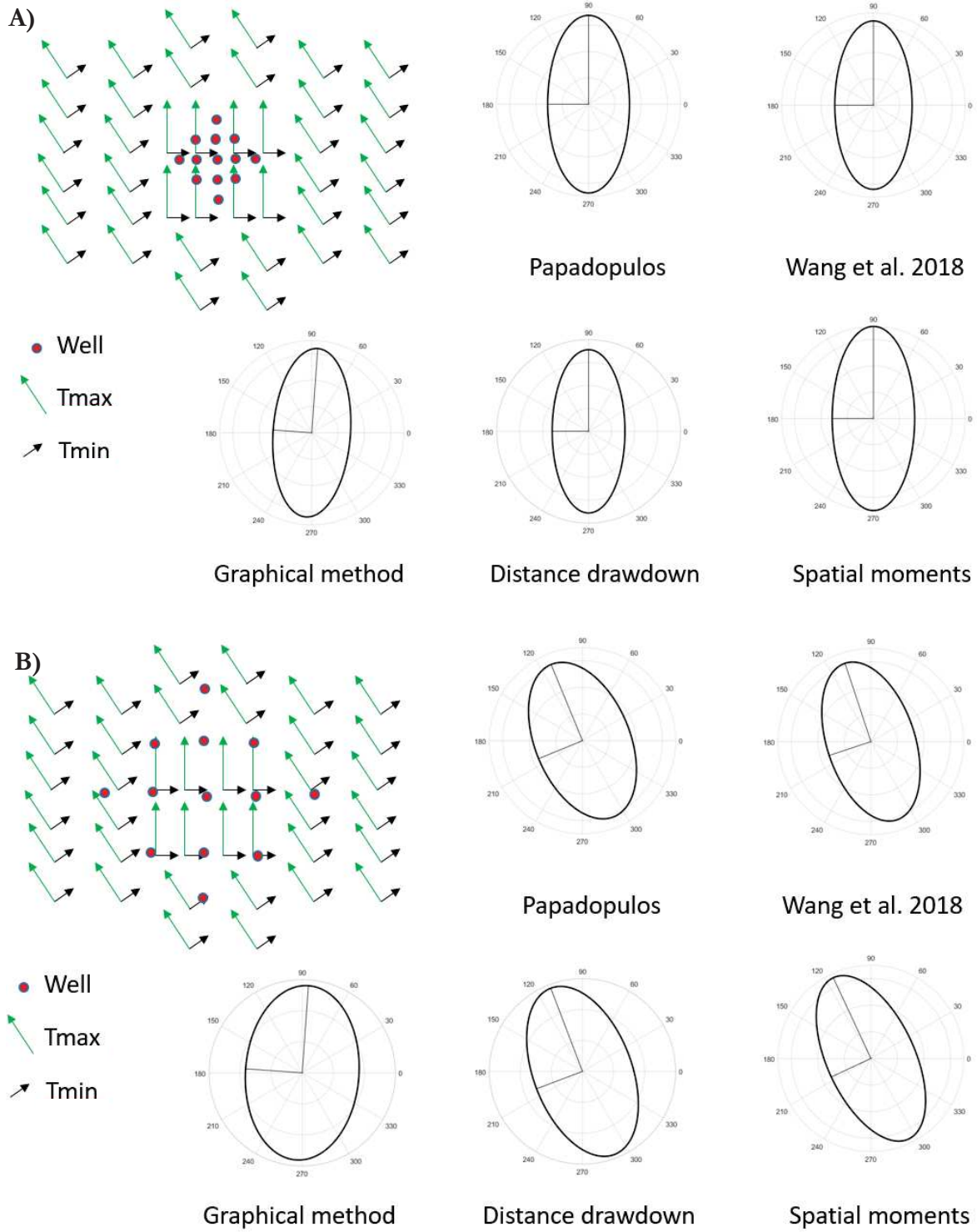


**Figure 3.25:** Results of efficiency of the methods to the direction of the tensor. (A) all the wells are inside a domain with same anisotropy. (B) the wells cover the heterogeneity.

$T_{min}=1 \times 10^{-5}$  m/s,  $\Theta=90^\circ$ ), buffer domain ( $T_{max}=2 \times 10^{-5}$  m/s,  $T_{min}=1 \times 10^{-5}$  m/s,  $\Theta=90^\circ$ ). The storage is constant in both domains. The results are shown in (Figure 3.26)

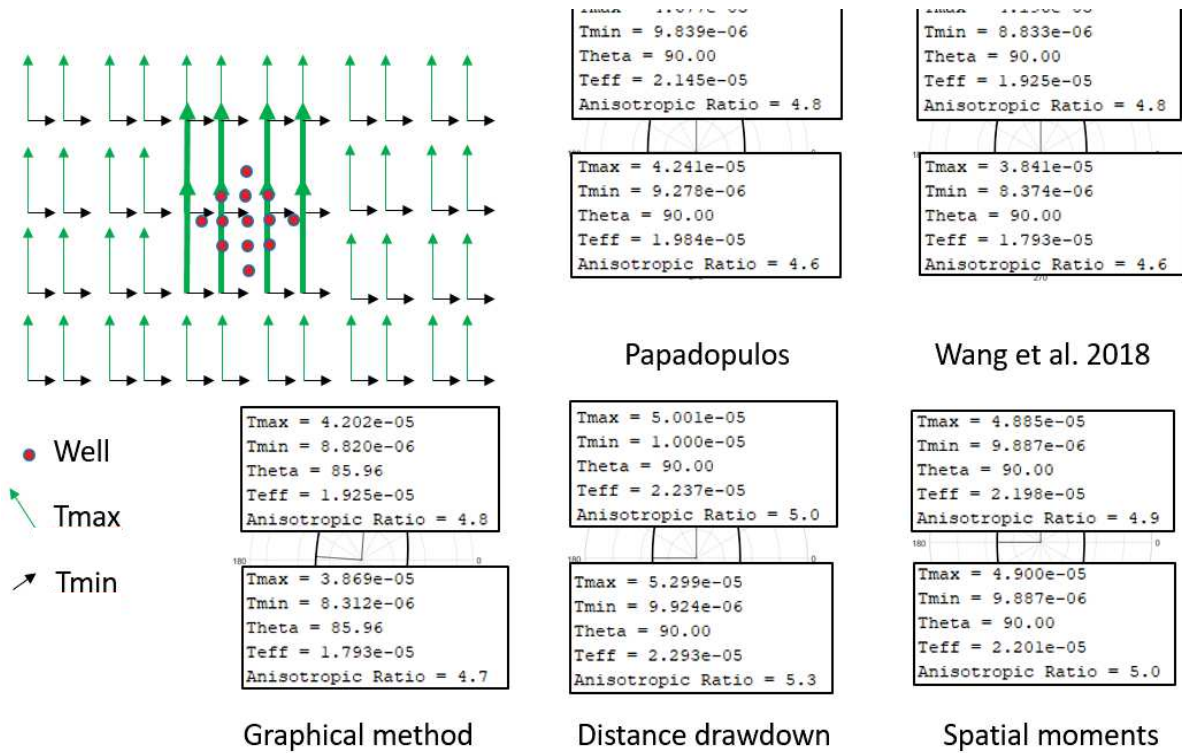


*Figure 3.26: Results of testing the efficiency of the methods to capture the tensor transmissivity values in case of heterogeneity presence.*

For the next synthetic test, we will design a domain which is divided into four subdomains that have different anisotropies. The aim of the test is to qualitatively evaluate the scale of investigation of the tensor detection methods. The test consists on simulating a pumping test in the middle well (see Figure 3.27b) and monitor the response in different observation wells. Those observations will then be used to estimate the transmissivity tensor using Papadopulos equations. We achieve different estimations using different combination of the wells as shown in Figure 3.27d. the results of the study are summarized in Figure 3.27.

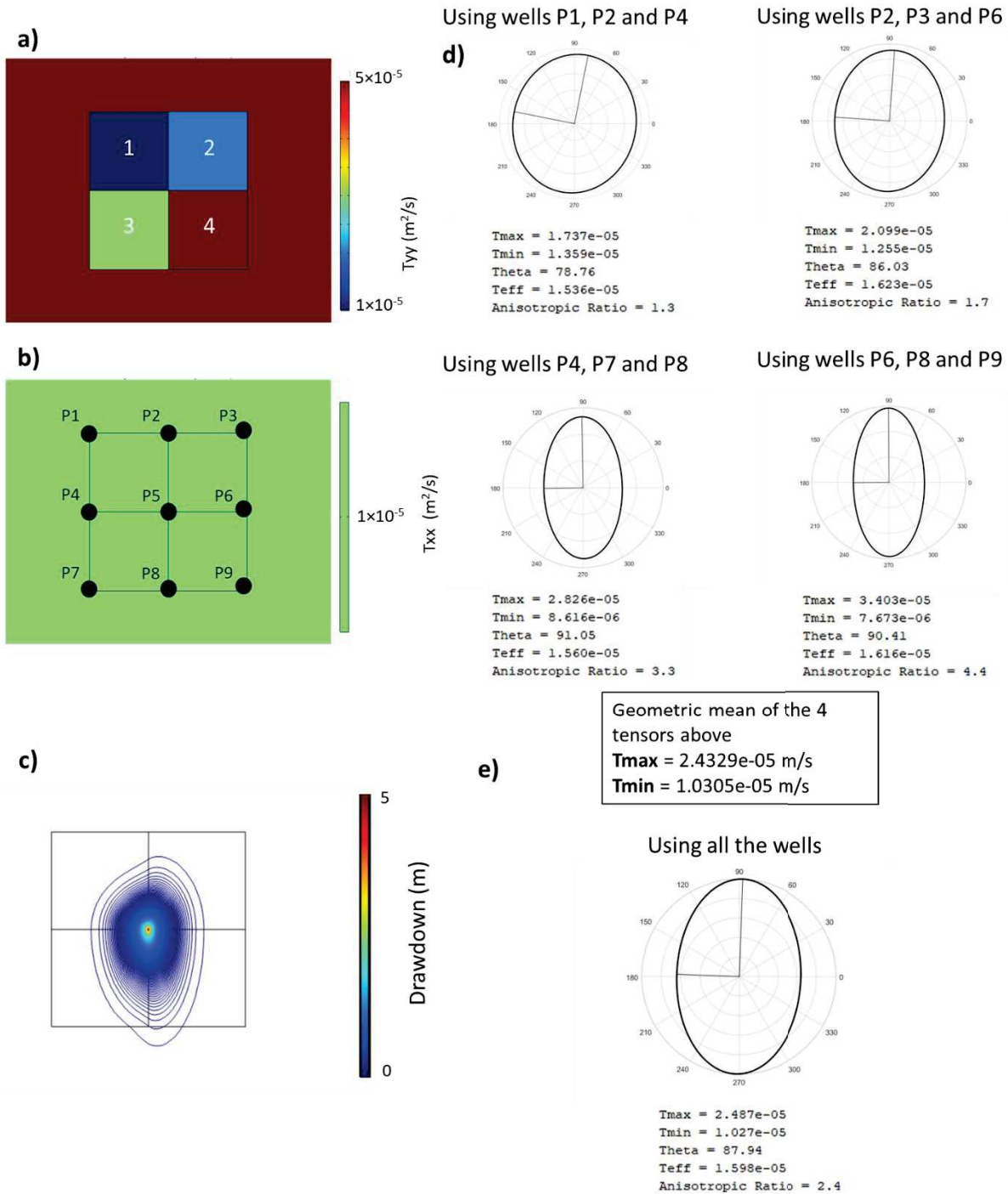


**Figure 3.27:** Results of the synthetic study to investigate the scale effect on the characterization of the horizontal anisotropy. A) map of the principal component of transmissivity tensor. B) map of the minor component of transmissivity tensor. C) contour plot of drawdown caused by a pumping in P5. D) estimated transmissivity tensors using different combination of wells. E) estimated transmissivity tensor using all observation wells compared the geometric mean of the tensors estimated in D).

### 3.4.5.5 Conclusion

We tested five existing tensor detection methods using synthetic models in order to compare their efficiency. The methods show the similar general behavior. The obtained tensor corresponds to anisotropy of the area covered by wells. Nevertheless, the spatial moment method shows stronger instability in the middle to late transient time. We also see that methods using an elliptical regression, which is sensitive to the initial guess, need to be used with great care. The Papadopoulos' and distance drawdown methods show stable performance in the characterization of permeability anisotropy from hydraulic tests. Another synthetic test results show that the horizontal tensor detection methods can characterize mainly the area between the used observation wells and it is recommended to use wells in different directions from the pumped well in order to have a better approximation of the total effective transmissivity tensor. It also shows that horizontal anisotropy investigations can play a great role on upscaling.

## References

- Ahmed, T., & McKinney, P. (2011). *Advanced reservoir engineering*. Elsevier.
- Aliouache, M., Wang, X., Fischer, P., Massonnat, G., & Jourde, H. (2021). An inverse approach integrating flowmeter and pumping test data for three-dimensional aquifer characterization. *Journal of Hydrology*, 126939.
- Aris, R. (1956), On the dispersion of a solute in a fluid flowing through a tube, *Proc. R. Soc. London, Ser. A*, 235, 67– 78.
- Asquith, G. B., Krygowski, D., & Gibson, C. R. (2004). *Basic well log analysis* (Vol. 16). Tulsa: American Association of Petroleum Geologists.
- Audouin, O., & Bodin, J. (2008). Cross-borehole slug test analysis in a fractured limestone aquifer. *Journal of hydrology*, 348(3-4), 510-523.
- Azizmohammadi, S. and Matthäi, S. K. (2017), Is the permeability of naturally fractured rocks scale dependent?, *Water Resour. Res.*, 53, 8041– 8063, doi:[10.1002/2016WR019764](https://doi.org/10.1002/2016WR019764).
- Batu, V (2008), An Assessment of the Way and McKee (1982) Type-Curve Method. *Groundwater*, 46: 522-523. <https://doi.org/10.1111/j.1745-6584.2008.00459.x>
- Batu, V. (1998). *Aquifer hydraulics: a comprehensive guide to hydrogeologic data analysis*. John Wiley & Sons.
- Bear, J. (1972). *Dynamics of fluids in porous media*. Courier Corporation.
- Bear, J. (1979). *Hydraulics of groundwater*. Courier Corporation.
- Berg, S. J., and W. A. Illman (2011), Three-dimensional transient hydraulic tomography in a highly heterogeneous glaciofluvial aquifer-aquitard system, *Water Resour. Res.*, 47, W10507, doi:[10.1029/2011WR010616](https://doi.org/10.1029/2011WR010616).
- Berg, S.J. and Illman, W.A. (2015), Comparison of Hydraulic Tomography with Traditional Methods at a Highly Heterogeneous Site. *Groundwater*, 53: 71-89. <https://doi.org/10.1111/gwat.12159>
- Boggs, J. M., Young, S. C., Beard, L. M., Gelhar, L. W., Rehfeldt, K. R., and Adams, E. E. (1992), Field study of dispersion in a heterogeneous aquifer: 1. Overview and site description, *Water Resour. Res.*, 28( 12), 3281– 3291, doi:[10.1029/92WR01756](https://doi.org/10.1029/92WR01756).
- Bohling, G. C., Butler Jr., J. J., Zhan, X., and Knoll, M. D. (2007), A field assessment of the value of steady shape hydraulic tomography for characterization of aquifer heterogeneities, *Water Resour. Res.*, 43, W05430, doi:[10.1029/2006WR004932](https://doi.org/10.1029/2006WR004932).
- Bohling, G. C., Zhan, X., Butler, J. J., and Zheng, L., Steady shape analysis of tomographic pumping tests for characterization of aquifer heterogeneities, *Water Resour. Res.*, 38( 12), 1324, doi:[10.1029/2001WR001176](https://doi.org/10.1029/2001WR001176), 2002.
- Bohling, G.C. and Butler, J.J., Jr. (2010), Inherent Limitations of Hydraulic Tomography. *Groundwater*, 48: 809-824. <https://doi.org/10.1111/j.1745-6584.2010.00757.x>
- Boman, G. K., Mole, F. J., & Boone, K. D. (1997) Borehole flowmeter application in fluvial sediments: methodology, results, and assessment. *Ground Water*, 53, 443–450.
- Boulton, N.S. and Streltsova, T.D., 1976. The drawdown near an abstraction well of large diameter under non-steady conditions in an unconfined aquifer. *J. Hydrol.*, 30:29-46.

- Boulton, N.S. and Streltsova, T.D., 1977b. Unsteady flow to a pumped well in a two-layered water-bearing formation. *J. Hydrol.*, 35 : 245-256.
- Boulton, N.S. and Streltsova, T.D., 1977a. Unsteady flow to a pumped well in a fissured water-bearing formation. *J. Hydrol.*, 35: 257-269.
- Boulton, N.S. and Streltsova, T.D., 1978. Unsteady flow to a pumped well in a fissured aquifer with a free surface level maintained constant. *Water Resour. Res.*, 14 (3):5 27-53 2
- Brassington, F. C., & Walthall, S. (1985). Field techniques using borehole packers in hydrogeological investigations. *Quarterly Journal of Engineering Geology and Hydrogeology*, 18(2), 181-193.
- Brauchler, R., R. Hu, L. Hu, S. Jimenez, P. Bayer, P. Dietrich, and T. Ptak (2013), Rapid field application of hydraulic tomography for resolving aquifer heterogeneity in unconsolidated sediments, *Water Resour. Res.*, 49, 2013–2024, doi:10.1002/wrcr.20181.
- Brauchler, R., R. Hu, P. Dietrich, and M. Sauter (2011), A field assessment of high-resolution aquifer characterization based on hydraulic travel time and hydraulic attenuation tomography, *Water Resour. Res.*, 47, W03503, doi:10.1029/2010WR009635.
- Bunte, K., & Abt, S. R. (2001). Sampling surface and subsurface particle-size distributions in wadable gravel-and cobble-bed streams for analyses in sediment transport, hydraulics, and streambed monitoring. US Department of Agriculture, Forest Service, Rocky Mountain Research Station.
- Butler, J. J. (2005). Hydrogeological methods for estimation of spatial variations in hydraulic conductivity. In *Hydrogeophysics* (pp. 23-58). Springer, Dordrecht.
- Butler, J. J., and Liu, W. (1993), Pumping tests in nonuniform aquifers: The radially asymmetric case, *Water Resour. Res.*, 29( 2), 259– 269, doi:[10.1029/92WR02128](https://doi.org/10.1029/92WR02128).
- Butler, J. J., McElwee, C. D., and Bohling, G. C. (1999), Pumping tests in networks of multilevel sampling wells: Motivation and methodology, *Water Resour. Res.*, 35( 11), 3553– 3560, doi:10.1029/1999WR900231.
- Cardiff, M., and Barrash, W. (2011), 3-D transient hydraulic tomography in unconfined aquifers with fast drainage response, *Water Resour. Res.*, 47, W12518, doi:[10.1029/2010WR010367](https://doi.org/10.1029/2010WR010367).
- Cardiff, M., Barrash, W., and Kitanidis, P. K. (2012), A field proof-of-concept of aquifer imaging using 3-D transient hydraulic tomography with modular, temporarily-emplaced equipment, *Water Resour. Res.*, 48, W05531, doi:10.1029/2011WR011704.
- Cardiff, M., W. Barrash, P. K. Kitanidis, B. Malama, A. Revil, S. Straface, and E. Rizzo (2009), A potential-based inversion of unconfined steady-state hydraulic tomography, *Ground Water*, 47(2), 259–270, doi:10.1111/j.1745-6584.2008.00541.x
- Carman, P. C. (1956). Flow of gases through porous media.
- Carrera, J., and Neuman, S. P. (1986), Estimation of Aquifer Parameters Under Transient and Steady State Conditions: 1. Maximum Likelihood Method Incorporating Prior Information, *Water Resour. Res.*, 22( 2), 199– 210, doi:[10.1029/WR022i002p00199](https://doi.org/10.1029/WR022i002p00199).
- Charles Vernon Theis; The significance and nature of the cone of depression in ground-water bodies. *Economic Geology* 1938; 33 (8): 889–902. doi: <https://doi.org/10.2113/gsecongeo.33.8.889>

- Chavent, G., About the stability of the optimal control solution of inverse problems, in *Inverse and Improperly Posed Problems in Differential Equations*, edited by G. Anger, pp. 45-58, Akademie-Verlag, Berlin, 1979a.
- Chen, J.S., S. Hubbard, and Y. Rubin. 2001. Estimating the hydraulic conductivity at the South Oyster Site from geo-physical tomographic data using Bayesian techniques based on the normal linear regression model. *Water Resources Research* 37, no. 6: 1603–1613
- Chen, T., Clauser, C., Marquart, G., Willbrand, K., & Büsing, H. (2016). Modeling anisotropic flow and heat transport by using mimetic finite differences. *Advances in water resources*, 94, 441-456.
- Chen, X. (2000). Measurement of streambed hydraulic conductivity and its anisotropy. *Environmental Geology*, 39(12), 1317-1324.
- Cihan, A., Q. Zhou, and J. Birkholzer (2011), Analytical solutions for pressure perturbation and fluid leakage through aquitards and wells in multilayered aquifer systems, *Water Resour. Res.*, 47, W10504, doi:10.1029/2011WR010721
- Cihan, A., Zhou, Q., Birkholzer, J. T., and Kraemer, S. R. (2014), Flow in horizontally anisotropic multilayered aquifer systems with leaky wells and aquitards, *Water Resour. Res.*, 50, 741– 747, doi:10.1002/2013WR013867.
- Clifton, P. M., and Neuman, S. P. (1982), Effects of kriging and inverse modeling on conditional simulation of the Avra Valley Aquifer in southern Arizona, *Water Resour. Res.*, 18( 4), 1215– 1234, doi:10.1029/WR018i004p01215.
- Cooper, H. H., and Jacob, C. E. (1946), A generalized graphical method for evaluating formation constants and summarizing well-field history, *Eos Trans. AGU*, 27( 4), 526– 534, doi:10.1029/TR027i004p00526
- Dagan, G. (1986). Statistical theory of groundwater flow and transport: Pore to laboratory, laboratory to formation, and formation to regional scale. *Water Resources Research*, 22(9S), 120S-134S.
- Dagan, G. Higher-order correction of effective permeability of heterogeneous isotropic formations of lognormal conductivity distribution. *Transp Porous Med* 12, 279–290 (1993). <https://doi.org/10.1007/BF00624462>
- Darcy, H. (1856). *Les fontaines publiques de la ville de Dijon: exposition et application...* Victor Dalmont.
- Day-Lewis, F.D., Johnson, C.D., Paillet, F.L. and Halford, K.J. (2011), A Computer Program for Flow-Log Analysis of Single Holes (FLASH). *Groundwater*, 49: 926-931. <https://doi.org/10.1111/j.1745-6584.2011.00798.x>
- De Clercq T., A. Jardani, P. Fischer, L. Thanberger, T.M. Vu, D. Pitaval, J.-M. Côme, P. Begassat. 2020. The use of electrical resistivity tomograms as a parameterization for the hydraulic characterization of a contaminated aquifer. *Journal of Hydrology* 587: 124986.
- De Marsily, G. (1984). Spatial variability of properties in porous media: a stochastic approach. In *Fundamentals of transport phenomena in porous media* (pp. 719-769). Springer, Dordrecht.
- De Marsily, G. (1985). Overview of coupled processes with emphasis in geohydrology (No. LBL--21850).
- Deruyck, B., Ehlig-Economides, C., & Joseph, J. (1992). Testing design and analysis. *Oilfield Review*, 4(2), 28-45.
- Dewandel, B., Aunay, B., Maréchal, J. C., Roques, C., Bour, O., Mougin, B., & Aquilina, L. (2014). Analytical solutions for analysing pumping tests in a sub-vertical and anisotropic fault zone draining shallow aquifers. *Journal of Hydrology*, 509, 115-131.

- Ehlig-Economides, C. A., Hegeman, P., & Vik, S. (1994). Guidelines simplify well test interpretation. *Oil and Gas Journal*; (United States), 92(29).
- Elsheikh, A. H., Wheeler, M. F., & Hoteit, I. (2013). Sparse calibration of subsurface flow models using nonlinear orthogonal matching pursuit and an iterative stochastic ensemble method. *Advances in Water Resources*, 56, 14-26.
- Evensen, G., & Van Leeuwen, P. J. (2000). An ensemble Kalman smoother for nonlinear dynamics. *Monthly Weather Review*, 128(6), 1852-1867.
- Ferroud, A., Rafini, S., & Chesnaux, R. (2019). Using flow dimension sequences to interpret non-uniform aquifers with constant-rate pumping-tests: a review. *Journal of Hydrology X*, 2, 100003.
- Fienen, M.N., P.K. Kitanidis, D. Watson, and P. Jardine. 2004. An application of Bayesian inverse methods to vertical de-convolution of hydraulic conductivity in a heterogeneous aquifer at Oak Ridge National Laboratory. *Mathematical Geology* 36, no. 1: 101–126.
- Filomena, C. M., Hornung, J., & Stollhofen, H. (2014). Assessing accuracy of gas-driven permeability measurements: a comparative study of diverse Hassler-cell and probe permeameter devices. *Solid Earth*, 5(1), 1-11.
- Fischer P., Jardani A., Jourde H., Hydraulic tomography in coupled discrete-continuum concept to image hydraulic properties of a fractured and karstified aquifer (Lez aquifer, France) *Adv. Water Resour.*, 137 (2020), p. 103523, [10.1016/j.advwatres.2020.103523](https://doi.org/10.1016/j.advwatres.2020.103523)
- Fitts, C.R. (2006), Exact Solution for Two-Dimensional Flow to a Well in an Anisotropic Domain. *Groundwater*, 44: 99-101. <https://doi.org/10.1111/j.1745-6584.2005.00082.x>
- Freeze, R. A. (1975), A stochastic-conceptual analysis of one-dimensional groundwater flow in nonuniform homogeneous media, *Water Resour. Res.*, 11( 5), 725– 741, doi:[10.1029/WR011i005p00725](https://doi.org/10.1029/WR011i005p00725).
- Freyberg, D. L. (1986), A natural gradient experiment on solute transport in a sand aquifer: 2. Spatial moments and the advection and dispersion of nonreactive tracers, *Water Resour. Res.*, 22(13), 2031– 2046, doi:[10.1029/WR022i013p02031](https://doi.org/10.1029/WR022i013p02031)
- Fu, J., & Gómez-Hernández, J. J. (2009). Uncertainty assessment and data worth in groundwater flow and mass transport modeling using a blocking Markov chain Monte Carlo method. *Journal of Hydrology*, 364(3-4), 328-341.
- Galloway, W. E., & Sharp Jr, J. M. (1998). Characterizing aquifer heterogeneity within terrigenous clastic depositional systems. *SEPM Concepts in Hydrogeology and Environmental Geology No. 1: Hydrogeologic Models of Sedimentary Aquifers*.
- Ghanem, R. G., & Spanos, P. D. (2003). *Stochastic finite elements: a spectral approach*. Courier Corporation.
- Glover, F., & Laguna, M. (1998). Tabu search. In *Handbook of combinatorial optimization* (pp. 2093-2229). Springer, Boston, MA.
- Gómez-Hernández, J. J., & Wen, X. H. (1998). To be or not to be multi-Gaussian? A reflection on stochastic hydrogeology. *Advances in Water Resources*, 21(1), 47-61.
- Gottlieb, J., and P. Dietrich (1995), Identification of the permeability distribution in soil by hydraulic tomography, *Inverse Probl.*, 11(2), 353– 360, doi:[10.1088/0266-5611/11/2/005](https://doi.org/10.1088/0266-5611/11/2/005)

- Gringarten, A. C., Bourdet, D. P., Landel, P. A., & Kniazeff, V. J. (1979, September). A comparison between different skin and wellbore storage type-curves for early-time transient analysis. In Spe annual technical conference and exhibition. OnePetro.
- Hagen, G. (1839), Ueber die Bewegung des Wassers in engen cylindrischen Röhren. *Ann. Phys.*, 122: 423-442. <https://doi.org/10.1002/andp.18391220304>
- Haldorsen, H. H. (1986) Simulator parameter assignment and the problem of scale in reservoir engineering. In L. W. Leake, & H. B. Carroll, Jr., (Eds.), *Reservoir characterization* (pp. 293–340). Orlando: Academic Press.
- Hantush, M. S. (1966), Analysis of data from pumping tests in anisotropic aquifers, *J. Geophys. Res.*, 71( 2), 421–426, doi:10.1029/JZ071i002p00421.
- Hantush, M. S. (1960), Modification of the theory of leaky aquifers, *J. Geophys. Res.*, 65( 11), 3713– 3725, doi:10.1029/JZ065i011p03713.
- Hantush, M. S. (1966), Analysis of data from pumping tests in anisotropic aquifers, *J. Geophys. Res.*, 71( 2), 421– 426, doi:10.1029/JZ071i002p00421.
- Hantush, M. S., and Thomas, R. G. (1966), A method for analyzing a drawdown test in anisotropic aquifers, *Water Resour. Res.*, 2(2), 281– 285, doi:10.1029/WR002i002p00281.
- Hantush, M. S., and Jacob, C. E. (1955), Non-steady radial flow in an infinite leaky aquifer, *Eos Trans. AGU*, 36( 1), 95– 100, doi:10.1029/TR036i001p00095.
- Hantush, M. S., and Thomas, R. G. (1966), A method for analyzing a drawdown test in anisotropic aquifers, *Water Resour. Res.*, 2( 2), 281– 285, doi:10.1029/WR002i002p00281.
- Hao, Y., Yeh, T.-C.J., Xiang, J., Illman, W.A., Ando, K., Hsu, K.-C. and Lee, C.-H. (2008), Hydraulic Tomography for Detecting Fracture Zone Connectivity. *Groundwater*, 46: 183-192. <https://doi.org/10.1111/j.1745-6584.2007.00388.x>
- Hastings, W. K. (1970). Monte Carlo sampling methods using Markov chains and their applications.
- Heilweil VM, Hsieh PA. Determining anisotropic transmissivity using a simplified Papadopulos method. *Ground Water*. 2006 Sep-Oct;44(5):749-53. doi: 10.1111/j.1745-6584.2006.00210.x. PMID: 16961497.
- Hendricks Franssen, H. J., Alcolea, A., Riva, M., Bakr, M., Van der Wiel, N., Stauffer, F., & Guadagnini, A. (2009). A comparison of seven methods for the inverse modelling of groundwater flow. Application to the characterisation of well catchments. *Advances in Water Resources*, 32(6), 851-872.
- Hernandez, A. F., Neuman, S. P., Guadagnini, A., & Carrera, J. (2003). Conditioning mean steady state flow on hydraulic head and conductivity through geostatistical inversion. *Stochastic Environmental Research and Risk Assessment*, 17(5), 329-338.
- Hernandez, A. F., Neuman, S. P., Guadagnini, A., and Carrera, J. (2006), Inverse stochastic moment analysis of steady state flow in randomly heterogeneous media, *Water Resour. Res.*, 42, W05425, doi:10.1029/2005WR004449.
- Hess, K. M., Wolf, S. H., & Celia, M. A. (1992) Large-scale natural gradient tracer test in sand and gravel, Cape Cod, Massachusetts, 3. Hydraulic conductivity variability and calculated macrodispersivities. *Water Resources Research*, 28, 2011–2027.

- Hoffman, B. T., & Caers, J. (2003, October). Geostatistical history matching using a regional probability perturbation method. In SPE Annual Technical Conference and Exhibition. OnePetro.
- Hsieh, P. A. (1998). Scale effects in fluid flow through fractured geologic media.
- Hsieh, P. A., and Neuman, S. P. (1985), Field Determination of the Three-Dimensional Hydraulic Conductivity Tensor of Anisotropic Media: 1. Theory, *Water Resour. Res.*, 21( 11), 1655– 1665, doi:10.1029/WR021i011p01655.
- Hsieh, P. A., Neuman, S. P., Stiles, G. K., and Simpson, E. S. (1985), Field Determination of the Three-Dimensional Hydraulic Conductivity Tensor of Anisotropic Media: 2. Methodology and Application to Fractured Rocks, *Water Resour. Res.*, 21( 11), 1667– 1676, doi:10.1029/WR021i011p01667.
- Hu, L. Y. (2000). Gradual deformation and iterative calibration of Gaussian-related stochastic models. *Mathematical Geology*, 32(1), 87-108.
- Huang, Y., Zhan, H., & Knappett, P. S. (2018). A novel analytical solution for estimating aquifer properties within a horizontally anisotropic aquifer bounded by a stream. *Journal of Hydrology*, 559, 920-931.
- Hubbard S.S., Rubin Y. (2005) Introduction to Hydrogeophysics. In: Rubin Y., Hubbard S.S. (eds) *Hydrogeophysics*. Water Science and Technology Library, vol 50. Springer, Dordrecht. [https://doi.org/10.1007/1-4020-3102-5\\_1](https://doi.org/10.1007/1-4020-3102-5_1)
- Hubbard, S. S., and Y. Rubin (2000), Hydrogeological parameter estimation using geophysical data: A review of selected techniques, *J. Contam. Hydrol.*, 45, 3– 34, doi:10.1016/S0169-7722(00)00117-0.
- Hufschmied, P, Estimation of three-dimensional statistically anisotropic hydraulic conductivity field, 1986, BRGM Database PASCAL INIST identifier 7923227
- Hyndman, D. W., and Gorelick, S. M. (1996), Estimating Lithologic and Transport Properties in Three Dimensions Using Seismic and Tracer Data: The Kesterson aquifer, *Water Resour. Res.*, 32( 9), 2659– 2670, doi:10.1029/96WR01269.
- Illman, W. A., Zhu, J., Craig, A. J., and Yin, D. (2010), Comparison of aquifer characterization approaches through steady state groundwater model validation: A controlled laboratory sandbox study, *Water Resour. Res.*, 46, W04502, doi:10.1029/2009WR007745.
- Illman, W.A., X. Liu, and A. Craig. 2007. Steady-state hydraulic tomography in a laboratory aquifer with deterministic heterogeneity: Multi-method and multiscale validation of hydraulic conductivity tomograms, *Journal of Hydrology* 341, no. 3–4: 222–234
- Javandel, I., and P.A. Witherspoon. 1969. A method of analyzing transient fluid flow in multilayered aquifer. *Water Resources Research* 5, no. 4: 856–869.
- Journel, A. G., & Deutsch, C. V. (1993). Entropy and spatial disorder. *Mathematical Geology*, 25(3), 329-355.
- Kabala, Z. J. (1994), Measuring distributions of hydraulic conductivity and specific storativity by the double flowmeter test, *Water Resour. Res.*, 30( 3), 685– 690, doi:10.1029/93WR03104
- Kalman, R. E. (1960). A new approach to linear filtering and prediction problems.
- Kern, J.W., & Dobson, C. (1998). Determination of Variances for Maximum and Minimum Transmissivities of Anisotropic Aquifers from Multiple Well Pumping Test Data. *Ground Water*, 36, 457-464.
- Kerrou, J., Renard, P., Franssen, H. J. H., & Lunati, I. (2008). Issues in characterizing heterogeneity and connectivity in non-multiGaussian media. *Advances in water resources*, 31(1), 147-159.

- Keys, W. S. (1989). Borehole geophysics applied to ground-water investigations (Vol. 6375). Dublin, OH: National Water Well Association.
- Kitanidis, P. K. (1995), Quasi-Linear Geostatistical Theory for Inversing, *Water Resour. Res.*, 31( 10), 2411– 2419, doi:[10.1029/95WR01945](https://doi.org/10.1029/95WR01945).
- Kitanidis, P. K., & Lane, R. W. (1985). Maximum likelihood parameter estimation of hydrologic spatial processes by the Gauss-Newton method. *Journal of Hydrology*, 79(1-2), 53-71.
- Kitanidis, P. K., and Lee, J. (2014), Principal Component Geostatistical Approach for large dimensional inverse problems, *Water Resour. Res.*, 50, 5428– 5443, doi:[10.1002/2013WR014630](https://doi.org/10.1002/2013WR014630).
- Kitanidis, P. K., and Vomvoris, E. G. (1983), A geostatistical approach to the inverse problem in groundwater modeling (steady state) and one-dimensional simulations, *Water Resour. Res.*, 19( 3), 677– 690, doi:[10.1029/WR019i003p00677](https://doi.org/10.1029/WR019i003p00677).
- Kitanidis, P.K. 1995. Quasi-linear geostatistical theory for inversing. *Water Resources Research* 31, no. 10: 2411– 2419.
- Kleinecke, D. (1971), Use of Linear Programing for Estimating Geohydrologic Parameters of Groundwater Basins, *Water Resour. Res.*, 7( 2), 367– 374, doi:[10.1029/WR007i002p00367](https://doi.org/10.1029/WR007i002p00367).
- Klepikova, M. V., Le Borgne, T., Bour, O., and de Dreuzy, J.-R. (2013), Inverse modeling of flow tomography experiments in fractured media, *Water Resour. Res.*, 49, 7255– 7265, doi:[10.1002/2013WR013722](https://doi.org/10.1002/2013WR013722).
- Kobr, M., Mareš, S., & Paillet, F. (2005). Geophysical well logging. In *Hydrogeophysics* (pp. 291-331). Springer, Dordrecht.
- Kozeny, J. (1927). Uber kapillare leitung der wasser in boden. *Royal Academy of Science, Vienna, Proc. Class I*, 136, 271-306.
- Kruseman, G. P., & de Ridder, N. A. (1970) Analysis and evaluation of pumping test data. International Institute for Land Reclamation and Improvement, Bulletin 11, Wageningen, The Netherlands.
- Kruseman, G. P., & De Ridder, N. A. (1990). Analysis and evaluation of pumping test data, ILRI publication 47. International Institute for Land Reclamation and Improvement, The Netherlands.
- Kruseman, G.P. and N.A. de Ridder, 1994. Analysis and Evaluation of Pumping Test Data (2nd ed.), Publication 47, Intern. Inst. for Land Reclamation and Improvement, Wageningen, The Netherlands, 370p.
- Kuchuk, F. J., Onur, M., & Hollaender, F. (2010). Pressure transient formation and well testing: convolution, deconvolution and nonlinear estimation. Elsevier.
- Kucuk, Fikri, and William E. Brigham. "Transient Flow in Elliptical Systems." *SPE J.* 19 (1979): 401–410. doi:<https://doi.org/10.2118/7488-PA>
- Lebbe, L., De Breuck, W. Analysis of a Pumping Test in an Anisotropic Aquifer by Use of an Inverse Numerical Model. *HYJO* 5, 44–59 (1997). <https://doi.org/10.1007/s100400050112>
- Li, W., Englert, A., Cirpka, O.A. and Vereecken, H. (2008), Three-Dimensional Geostatistical Inversion of Flowmeter and Pumping Test Data. *Groundwater*, 46: 193-201. <https://doi.org/10.1111/j.1745-6584.2007.00419.x>
- Liakopoulos, A. C. (1965), Variation of the permeability tensor ellipsoid in homogeneous anisotropic soils, *Water Resour. Res.*, 1( 1), 135– 141, doi:[10.1029/WR001i001p00135](https://doi.org/10.1029/WR001i001p00135).

- Lin, H. T., Tan, Y. C., Chen, C. H., Yu, H. L., Wu, S. C., & Ke, K. Y. (2010). Estimation of effective hydrogeological parameters in heterogeneous and anisotropic aquifers. *Journal of Hydrology*, 389(1-2), 57-68.
- Lin, H.-T., Ke, K.-Y., Chen, C.-H., Wu, S.-C. and Tan, Y.-C. (2010), Estimating anisotropic aquifer parameters by artificial neural networks. *Hydrol. Process.*, 24: 3237-3250. <https://doi.org/10.1002/hyp.7750>
- Liu, S., T.-C. J. Yeh, and R. Gardiner (2002), Effectiveness of hydraulic tomography: Sandbox experiments, *Water Resour. Res.*, 38(4), 1034, doi:10.1029/2001WR000338
- Liu, X., Illman, W. A., Craig, A. J., Zhu, J., and Yeh, T.-C. J. (2007), Laboratory sandbox validation of transient hydraulic tomography, *Water Resour. Res.*, 43, W05404, doi:10.1029/2006WR005144.
- Lohman, S. W. (1979) Ground-water hydraulics. U.S. Geological Survey Professional Paper 708.
- Long, J. C. S., Remer, J. S., Wilson, C. R., and Witherspoon, P. A. (1982), Porous media equivalents for networks of discontinuous fractures, *Water Resour. Res.*, 18( 3), 645– 658, doi:10.1029/WR018i003p00645
- Louis C. (1972) Rock Hydraulics. In: Müller L. (eds) *Rock Mechanics. International Centre for Mechanical Sciences (Courses and Lectures)*, vol 165. Springer, Vienna. [https://doi.org/10.1007/978-3-7091-4109-0\\_16](https://doi.org/10.1007/978-3-7091-4109-0_16)
- M. Sekhar, M.S.Mohan Kumar, K. Sridharan, Parameter estimation in an anisotropic leaky aquifer system, *Journal of Hydrology*, Volume 163, Issues 3–4, 1994, Pages 373-391, ISSN 0022-1694, [https://doi.org/10.1016/0022-1694\(94\)90149-X](https://doi.org/10.1016/0022-1694(94)90149-X).
- Mao, D., T.-C. J. Yeh, L. Wan, C.-H. Lee, K.-C. Hsu, J.-C. Wen, and W. Lu (2013a), Cross-correlation analysis and information content of observed heads during pumping in unconfined aquifers, *Water Resour. Res.*, 49, 713–731, doi:10.1002/wrcr.20066.
- Mao, D., T.-C. J. Yeh, L. Wan, K.-C. Hsu, C.-H. Lee, and J.-C. Wen (2013b), Necessary conditions for inverse modeling of flow through variably saturated porous media, *Adv. Water Resour.*, 52, 50–61, doi:10.1016/j.advwatres.2012.08.001.
- Marcus, H. (1962), The permeability of a sample of an anisotropic porous medium, *J. Geophys. Res.*, 67( 13), 5215– 5225, doi:10.1029/JZ067i013p05215.
- Mariéthoz, G. (2009). Geological stochastic imaging for aquifer characterization (Doctoral dissertation, Université de Neuchâtel).
- Mariéthoz, G., Renard, P., Cornaton, F. and Jaquet, O. (2009), Truncated Plurigaussian Simulations to Characterize Aquifer Heterogeneity. *Groundwater*, 47: 13-24. <https://doi.org/10.1111/j.1745-6584.2008.00489.x>
- Martinez-Landa, L., and Carrera, J. (2005), An analysis of hydraulic conductivity scale effects in granite (Full-scale Engineered Barrier Experiment (FEBEX), Grimsel, Switzerland), *Water Resour. Res.*, 41, W03006, doi:10.1029/2004WR003458.
- Martinez-Landa, L., Carrera, J., Pérez-Estaún, A., Gómez, P., & Bajos, C. (2016). Structural geology and geophysics as a support to build a hydrogeologic model of granite rock. *Solid Earth*, 7(3), 881-895.
- Maslia, M. L., & Randolph, R. B. (1986). Methods and computer program documentation for determining anisotropic transmissivity tensor components of two-dimensional ground-water flow (No. 86-227). US Geological Survey.

- Maslia, M. L., & Randolph, R. B. (1986). Methods and computer program documentation for determining anisotropic transmissivity tensor components of two-dimensional ground-water flow (No. 86-227). US Geological Survey.
- Maslia, Morris L. "Regional And Local Tensor Components Of A Fractured Carbonate Aquifer." Paper presented at the The 28th U.S. Symposium on Rock Mechanics (USRMS), Tucson, Arizona, June 1987.
- Mathias, S. A., and A. P. Butler (2007), Flow to a finite diameter well in a horizontally anisotropic aquifer with wellbore storage, *Water Resour. Res.*, 43, W07501, doi:10.1029/2006WR005839
- Medina, A., and Carrera, J. (1996), Coupled estimation of flow and solute transport parameters, *Water Resour. Res.*, 32( 10), 3063– 3076, doi:10.1029/96WR00754.
- Meier, P. M., Carrera, J., and Sánchez-Vila, X. (1998), An evaluation of Jacob's Method for the interpretation of pumping tests in heterogeneous formations, *Water Resour. Res.*, 34( 5), 1011– 1025, doi:10.1029/98WR00008
- Metropolis, N., Rosenbluth, A. W., Rosenbluth, M. N., Teller, A. H., & Teller, E. (1953). Equation of state calculations by fast computing machines. *The journal of chemical physics*, 21(6), 1087-1092.
- Miller, R.T. (1984), Anisotropy in the Ironton and Galesville Sandstones Near a Thermal-Energy-Storage Well, St. Paul, Minnesota. *Groundwater*, 22: 532-537. <https://doi.org/10.1111/j.1745-6584.1984.tb01421.x>
- Moench, A. F. (1997), Flow to a well of finite diameter in a homogeneous, anisotropic water table aquifer, *Water Resour. Res.*, 33( 6), 1397– 1407, doi:10.1029/97WR00651.
- Molz, F. J., Morin, R. H., Hess, A. E., Melville, J. G., and Güven, O. (1989), The Impeller Meter for measuring aquifer permeability variations: Evaluation and comparison with other tests, *Water Resour. Res.*, 25( 7), 1677– 1683, doi:10.1029/WR025i007p01677.
- Molz, F.J., G.K. Boman, S.C. Young, and W.R. Waldrop. 1994. Borehole flowmeters: Field application and data analysis. *Journal of Hydrology* 163, no. 4: 347–371.
- Motz, L.H. Multiple-pumped-well aquifer test to determine the anisotropic properties of a karst limestone aquifer in Pasco County, Florida, USA. *Hydrogeol J* 17, 855–869 (2009). <https://doi.org/10.1007/s10040-008-0408-9>
- Mutch, R.D., Jr (2005), A Distance-Drawdown Aquifer Test Method for Aquifers with Areal Anisotropy. *Groundwater*, 43: 935-938. <https://doi.org/10.1111/j.1745-6584.2005.00105.x>
- Nastev, M., Savard, M. M., Lapcevic, P., Lefebvre, R., & Martel, R. (2004). Hydraulic properties and scale effects investigation in regional rock aquifers, south-western Quebec, Canada. *Hydrogeology Journal*, 12(3), 257-269.
- Navarro, A. (1977), A modified optimization method of estimating aquifer parameters, *Water Resour. Res.*, 13( 6), 935– 939, doi:10.1029/WR013i006p00935.
- Neuman, S. P. (1975), Analysis of pumping test data from anisotropic unconfined aquifers considering delayed gravity response, *Water Resour. Res.*, 11(2), 329– 342, doi:10.1029/WR011i002p00329.
- Neuman, S. P. (1994). Generalized scaling of permeabilities: Validation and effect of support scale. *Geophysical research letters*, 21(5), 349-352.
- Neuman, S. P. (1972), Theory of flow in unconfined aquifers considering delayed response of the water table, *Water Resour. Res.*, 8( 4), 1031– 1045, doi:10.1029/WR008i004p01031.

- Neuman, S. P. (1973), Calibration of distributed parameter groundwater flow models viewed as a multiple-objective decision process under uncertainty, *Water Resour. Res.*, 9( 4), 1006– 1021, doi:[10.1029/WR009i004p01006](https://doi.org/10.1029/WR009i004p01006).
- Neuman, S. P. (1975), Analysis of pumping test data from anisotropic unconfined aquifers considering delayed gravity response, *Water Resour. Res.*, 11( 2), 329– 342, doi:[10.1029/WR011i002p00329](https://doi.org/10.1029/WR011i002p00329).
- Neuman, S. P. (1990), Universal scaling of hydraulic conductivities and dispersivities in geologic media, *Water Resour. Res.*, 26( 8), 1749– 1758, doi:[10.1029/WR026i008p01749](https://doi.org/10.1029/WR026i008p01749).
- Neuman, S.P., Walter, G.R., Bentley, H.W., Ward, J.J. and Gonzalez, D.D. (1984), Determination of Horizontal Aquifer Anisotropy with Three Wells. *Groundwater*, 22: 66-72. <https://doi.org/10.1111/j.1745-6584.1984.tb01477.x>
- Niemi, A., Kontio, K., Kuusela-Lahtinen, A., and Poteri, A. (2000), Hydraulic characterization and upscaling of fracture networks based on multiple-scale well test data, *Water Resour. Res.*, 36( 12), 3481– 3497, doi:[10.1029/2000WR900205](https://doi.org/10.1029/2000WR900205).
- Nowak, W., & Cirpka, O. A. (2004). A modified Levenberg–Marquardt algorithm for quasi-linear geostatistical inversing. *Advances in water resources*, 27(7), 737-750.
- Odling, N. E., West, L. J., Hartmann, S., & Kilpatrick, A. (2013). Fractional flow in fractured chalk; a flow and tracer test revisited. *Journal of contaminant hydrology*, 147, 96-111.
- Oliver, D. S., Cunha, L. B., & Reynolds, A. C. (1997). Markov chain Monte Carlo methods for conditioning a permeability field to pressure data. *Mathematical geology*, 29(1), 61-91.
- Paillet, F. L. (1998), Flow modeling and permeability estimation using borehole flow logs in heterogeneous fractured formations, *Water Resour. Res.*, 34( 5), 997– 1010, doi:[10.1029/98WR00268](https://doi.org/10.1029/98WR00268).
- Paillet, F.L. and Reese, R.S. (2000), Integrating Borehole Logs and Aquifer Tests in Aquifer Characterization. *Groundwater*, 38: 713-725. <https://doi.org/10.1111/j.1745-6584.2000.tb02707.x>
- Papadopoulos, I. S. (1965, September). Nonsteady flow to a well in an infinite anisotropic aquifer. In *Proceedings of Symposium International Association of Scientific Hydrology, Dubrovnik* (pp. 21-31).
- Papadopoulos, I. S. (1965, September). Nonsteady flow to a well in an infinite anisotropic aquifer. In *Proceedings of Symposium International Association of Scientific Hydrology, Dubrovnik* (pp. 21-31).
- Papadopoulos, I. S., and Cooper, H. H. (1967), Drawdown in a well of large diameter, *Water Resour. Res.*, 3( 1), 241– 244, doi:[10.1029/WR003i001p00241](https://doi.org/10.1029/WR003i001p00241).
- Paradis, D., Gloaguen, E., Lefebvre, R., & Giroux, B. (2016). A field proof-of-concept of tomographic slug tests in an anisotropic littoral aquifer. *Journal of Hydrology*, 536, 61-73.
- Piña, A., Donado, L. D., & Blessent, D. (2019). Analysis of the scale-dependence of the hydraulic conductivity in complex fractured media. *Journal of Hydrology*, 569, 556-572.
- Poiseuille, J. L. (1846). Experimental research on the movement of liquids in tubes of very small diameters. *Mémoires présentés par divers savants a l'Académie Royale des Sciences de l'Institut de France*, IX, 433-544.
- Ponzini, G., and Lozej, A. (1982), Identification of aquifer transmissivities: The comparison model method, *Water Resour. Res.*, 18( 3), 597– 622, doi:[10.1029/WR018i003p00597](https://doi.org/10.1029/WR018i003p00597).

- Quinn, P. M., Parker, B. L., & Cherry, J. A. (2013). Validation of non-Darcian flow effects in slug tests conducted in fractured rock boreholes. *Journal of hydrology*, 486, 505-518.
- Quinn, P., Cherry, J. A., & Parker, B. L. (2012). Hydraulic testing using a versatile straddle packer system for improved transmissivity estimation in fractured-rock boreholes. *Hydrogeology journal*, 20(8), 1529-1547.
- Quiñones-Aponte, V. (1989), Horizontal Anisotropy of the Principal Ground-Water Flow Zone in the Salinas Alluvial Fan, Puerto Rico. *Groundwater*, 27: 491-500. <https://doi.org/10.1111/j.1745-6584.1989.tb01969.x>
- Rehfeldt, K. R., Boggs, J. M., and Gelhar, L. W. (1992), Field study of dispersion in a heterogeneous aquifer: 3. Geostatistical analysis of hydraulic conductivity, *Water Resour. Res.*, 28( 12), 3309– 3324, doi:[10.1029/92WR01758](https://doi.org/10.1029/92WR01758).
- Ren, S., Zhang, Y., Jim Yeh, T.-C., Wang, Y., & Carr, B. J. (2021). Multiscale hydraulic conductivity characterization in a fractured granitic aquifer: The evaluation of scale effect. *Water Resources Research*, 57, e2020WR028482. <https://doi.org/10.1029/2020WR028482>
- Renard, P., & Allard, D. (2013). Connectivity metrics for subsurface flow and transport. *Advances in Water Resources*, 51, 168-196.
- Renard, Philippe (2005). 151 Hydraulics of wells and well testing. *Encyclopedia of hydrological sciences*. Wiley, Chichester, UK.
- Renshaw, C. E. (1996). Estimation of fracture zone geometry from steady-state hydraulic head data using iterative sequential cokriging. *Geophysical research letters*, 23(19), 2685-2688.
- Ritzi, R.W., Jr. and Andolsek, R.H. (1992), Relation Between Anisotropic Transmissivity and Azimuthal Resistivity Surveys in Shallow, Fractured, Carbonate Flow Systems. *Groundwater*, 30: 774-780. <https://doi.org/10.1111/j.1745-6584.1992.tb01563.x>
- Riva, M., Guadagnini, A., Neuman, S. P., Janetti, E. B., & Malama, B. (2009). Inverse analysis of stochastic moment equations for transient flow in randomly heterogeneous media. *Advances in water resources*, 32(10), 1495-1507.
- Riva, M., Panzeri, M., Guadagnini, A., and Neuman, S. P. (2011), Role of model selection criteria in geostatistical inverse estimation of statistical data- and model-parameters, *Water Resour. Res.*, 47, W07502, doi:[10.1029/2011WR010480](https://doi.org/10.1029/2011WR010480).
- Robert. G. Maliva, 2016, *Aquifer Characterization Techniques Schlumberger Methods in Water Resources Evaluation Series No. 4 Fort Myers, FL USA*. DOI 10.1007/978-3-319-32137-0
- Ronayne, M. J., Gorelick, S. M., and Caers, J. (2008), Identifying discrete geologic structures that produce anomalous hydraulic response: An inverse modeling approach, *Water Resour. Res.*, 44, W08426, doi:[10.1029/2007WR006635](https://doi.org/10.1029/2007WR006635).
- Roubinet D., Irving J., Day-Lewis F.D., Development of a new semi-analytical model for cross-borehole flow experiments in fractured media *Adv. Water Res.*, 76 (2015), pp. 97-108, [10.1016/j.advwatres.2014.12.002](https://doi.org/10.1016/j.advwatres.2014.12.002)
- Rovey, C. W. (1994). Assessing flow systems in carbonate aquifers using scale effects in hydraulic conductivity. *Environmental geology*, 24(4), 244-253.

- Rubin, Y., and Journel, A. G. (1991), Simulation of non-Gaussian space random functions for modeling transport in groundwater, *Water Resour. Res.*, 27( 7), 1711– 1721, doi:[10.1029/91WR00838](https://doi.org/10.1029/91WR00838).
- Sánchez-Vila, X., Meier, P. M., & Carrera, J. (1999). Pumping tests in heterogeneous aquifers: An analytical study of what can be obtained from their interpretation using Jacob's method. *Water Resources Research*, 35(4), 943-952.
- Schulze-Makuch, D., & Cherkauer, D. S. (1998). Variations in hydraulic conductivity with scale of measurement during aquifer tests in heterogeneous, porous carbonate rocks. *Hydrogeology Journal*, 6(2), 204-215.
- Serra, O. (2008). *Well logging handbook*. Editions Ophrys.
- Soueid Ahmed, A., Zhou, J. Jardani, A., Revil, A., Dupont, J.P., Image-guided inversion in steady-state hydraulic tomography *Adv. Water Resour.*, 82 (2015), pp. 83-97, [10.1016/j.advwatres.2015.04.001](https://doi.org/10.1016/j.advwatres.2015.04.001).
- Stehfest, H. (1970). Algorithm 368: Numerical inversion of Laplace transforms [D5]. *Communications of the ACM*, 13(1), 47-49.
- Stoner, J.D. (1981), Horizontal Anisotropy Determined by Pumping in Two Powder River Basin Coal Aquifers, Montana. *Groundwater*, 19: 34-40. <https://doi.org/10.1111/j.1745-6584.1981.tb03435.x>
- Streltsova, T. D. (1974). Drawdown in compressible unconfined aquifer. *Journal of the Hydraulics Division*, 100(11), 1601-1616.
- Sudicky, E. A. (1986) A natural gradient experiment on solute transport in a sand aquifer: Spatial variability of hydraulic conductivity and its role in dispersion processes. *Water Resources Research*, 22, 2069–2082.
- Sudicky, E. A. (1986), A natural gradient experiment on solute transport in a sand aquifer: Spatial variability of hydraulic conductivity and its role in the dispersion process, *Water Resour. Res.*, 22( 13), 2069– 2082, doi:[10.1029/WR022i013p02069](https://doi.org/10.1029/WR022i013p02069).
- Sudicky, E. A., Illman, W. A., Goltz, I. K., Adams, J. J., and McLaren, R. G. (2010), Heterogeneity in hydraulic conductivity and its role on the macroscale transport of a solute plume: From measurements to a practical application of stochastic flow and transport theory, *Water Resour. Res.*, 46, W01508, doi:[10.1029/2008WR007558](https://doi.org/10.1029/2008WR007558).
- SUDICKY, E.A. and HUYAKORN, P.S. (1991), Contaminant Migration in Imperfectly Known Heterogeneous Groundwater Systems. *Reviews of Geophysics*, 29: 240-253. <https://doi.org/10.1002/rog.1991.29.s1.240>
- Sun, N. Z. (2013). *Inverse problems in groundwater modeling (Vol. 6)*. Springer Science & Business Media.
- Tamayo-Mas, M. Bianchi, M. Mansour Impact of model complexity and multi-scale data integration on the estimation of hydrogeological parameters in a dual-porosity aquifer *Hydrogeol. J.*, 26 (6) (2018), pp. 1917-1933, [10.1007/s10040-018-1745-y](https://doi.org/10.1007/s10040-018-1745-y)
- Theis, C. V. (1935), The relation between the lowering of the Piezometric surface and the rate and duration of discharge of a well using ground-water storage, *Eos Trans. AGU*, 16( 2), 519– 524, doi:[10.1029/TR016i002p00519](https://doi.org/10.1029/TR016i002p00519).
- Theis, C. V. (1935), The relation between the lowering of the Piezometric surface and the rate and duration of discharge of a well using ground-water storage, *Eos Trans. AGU*, 16( 2), 519– 524, doi:[10.1029/TR016i002p00519](https://doi.org/10.1029/TR016i002p00519).
- Thiem, G. (1906). *Hydrologic methods*. Gebhardt, Leipzig, Germany.

- Thomas Romary (2010) Bayesian inversion by parallel interacting Markov chains, *Inverse Problems in Science and Engineering*, 18:1, 111-130, DOI: 10.1080/17415970903234620
- Todd, D. K., & Mays, L. W. (2004). *Groundwater hydrology*. John Wiley & Sons.
- Tso, M., C.-H., Zha, Y., J. Yeh, T.-C., and Wen, J.-C. (2016), The relative importance of head, flux, and prior information in hydraulic tomography analysis, *Water Resour. Res.*, 52, 3– 20, doi:10.1002/2015WR017191.
- Vasco, D. W., Keers, H., and Karasaki, K. (2000), Estimation of reservoir properties using transient pressure data: An asymptotic approach, *Water Resour. Res.*, 36( 12), 3447– 3465, doi:10.1029/2000WR900179.
- Vuković, M., & Soro, A. (1992). *Hydraulics of water wells: theory and application*. Water Resources Publications.
- Walton, W. C. (1960). Leaky artesian aquifer conditions in Illinois. Illinois State Water Survey Report of Investigation 39, Urbana. <http://hdl.handle.net/2142/101979>
- Walton, W. C. (1962). Selected analytical methods for well and aquifer evaluation. *Bulletin (Illinois State Water Survey)* no. 49.
- Walton, W. C. (1979). Progress in analytical groundwater modeling. In *Developments in Water Science (Vol. 12, pp. 149-159)*. Elsevier.
- Wang, X., Jourde, H., Aliouache, M., Massonnat, G., Characterization of horizontal transmissivity anisotropy using cross-hole slug tests, *J. Hydrol.*, 564 (2018), pp. 89-98, 10.1016/j.jhydrol.2018.06.068
- Way, S.-C. and McKee, C.R. (1982), In-Situ Determination of Three-Dimensional Aquifer Permeabilities. *Groundwater*, 20: 594-603. <https://doi.org/10.1111/j.1745-6584.1982.tb01375.x>
- Weeks, E. P. (1969), Determining the Ratio of Horizontal to Vertical Permeability by Aquifer-Test Analysis, *Water Resour. Res.*, 5(1), 196– 214, doi:10.1029/WR005i001p00196.
- Wempe, W. L. (2000). *Predicting flow properties using geophysical data: Improving aquifer characterization*. Stanford University.
- Wen, J. C., Wu, C. M., Yeh, T. C. J., & Tseng, C. M. (2010). Estimation of effective aquifer hydraulic properties from an aquifer test with multi-well observations (Taiwan). *Hydrogeology Journal*, 18(5), 1143-1155.
- Wen, J.-C., Chen, J.-L., Yeh, T.-C.J., Wang, Y.-L., Huang, S.-Y., Tian, Z. and Yu, C.-Y. (2020), Redundant and Nonredundant Information for Model Calibration or Hydraulic Tomography. *Groundwater*, 58: 79-92. <https://doi.org/10.1111/gwat.12879>
- Williams, J., and F. Paillet (2002), Using flowmeter pulse tests to define hydraulic connections in the subsurface: A fractured shale example, *J. Hydrol.*, 265, 100–117.
- Woodbury, A. D., and Ulrych, T. J. (1993), Minimum relative entropy: Forward probabilistic modeling, *Water Resour. Res.*, 29( 8), 2847– 2860, doi:10.1029/93WR00923.
- Wu, C.-M., T.-C. J. Yeh, J. Zhu, T. H. Lee, N.-S. Hsu, C.-H. Chen, and A. F. Sancho (2005), Traditional analysis of aquifer tests: Comparing apples to oranges?, *Water Resour. Res.*, 41, W09402, doi:10.1029/2004WR003717
- Wu, C.-M., Yeh, T.-C. J., Zhu, J., Lee, T. H., Hsu, N.-S., Chen, C.-H., and Sancho, A. F. (2005), Traditional analysis of aquifer tests: Comparing apples to oranges? *Water Resour. Res.*, 41, W09402, doi:10.1029/2004WR003717.

- Wu, S.-C., Tan, Y.-C., Chen, C.-H., Lin, S.-T. and Ke, K.-Y. (2008), A two-dimensional inverse model to identify transmissivity in an anisotropic aquifer. *Hydrol. Process.*, 22: 5086-5096. <https://doi.org/10.1002/hyp.7134>
- Xiang, J., Yeh, T.-C. J., Lee, C.-H., Hsu, K.-C., and Wen, J.-C. (2009), A simultaneous successive linear estimator and a guide for hydraulic tomography analysis, *Water Resour. Res.*, 45, W02432, doi:10.1029/2008WR007180.
- Xiaoguang Wang, Hervé Jourde, Mohammed Aliouache, Gérard Massonnat, Characterization of horizontal transmissivity anisotropy using cross-hole slug tests, *Journal of Hydrology*, Volume 564, 2018, Pages 89-98, ISSN 0022-1694, <https://doi.org/10.1016/j.jhydrol.2018.06.068>.
- Yang, Z., Niemi, A., Fagerlund, F., and Illangasekare, T. (2013), Two-phase flow in rough-walled fractures: Comparison of continuum and invasion-percolation models, *Water Resour. Res.*, 49, doi:10.1002/wrcr.20111.
- Yeh, T.-C., M. Jin, and S. Hanna, An iterative stochastic inverse method: Conditional effective transmissivity and hydraulic head fields, *Water Resour. Res.*, 32(1), 85-92, 1996
- Yeh, T.-C. J., and Liu, S. (2000), Hydraulic tomography: Development of a new aquifer test method, *Water Resour. Res.*, 36(8), 2095– 2105, doi:10.1029/2000WR900114.
- Yeh, T.-C. J., D. Mao, L. Wan, C.-H. Lee, J.-C. Wen, and K.-C. Hsu (2011), Well Definedness, Scale Consistency, and Resolution Issues in Groundwater Model Parameter Identification, *Dep. of Hydrol. and Water Resour.*, Univ. of Ariz., Tucson.
- Yeh, T.-C. J., D. Mao, L. Wan, C.-H. Lee, J.-C. Wen, and K.-C. Hsu (2015b), Well definedness, scale consistency, and resolution issues in groundwater model parameter identification, *Water Sci. Eng.*, 8(3), 175–194, doi:10.1016/j.wse.2015.08.002.
- Yeh, T.-C. J., Gelhar, L. W., and Gutjahr, A. L. (1985), Stochastic Analysis of Unsaturated Flow in Heterogeneous Soils: 2. Statistically Anisotropic Media With Variable  $\alpha$ , *Water Resour. Res.*, 21(4), 457– 464, doi:10.1029/WR021i004p00457.
- Yeh, T.-C. J., M. Jin, and S. Hanna (1996), An iterative stochastic inverse method: Conditional effective transmissivity and hydraulic head fields, *Water Resour. Res.*, 32(1), 85– 92, doi:10.1029/95WR02869.
- Yeh, T.-C. J., M. Ye, and R. Khaleel (2005), Estimation of effective unsaturated hydraulic conductivity tensor using spatial moments of observed moisture plume, *Water Resour. Res.*, 41, W03014, doi:10.1029/2004WR003736.
- Yeh, T.-C. J., R. Khaleel, and K. C. Carroll (2015a), *Flow Through Heterogeneous Geologic Media*, Cambridge Univ. Press, Cambridge, U. K.
- Yeh, T.-C., Mas-Pla, J., Williams, T. M., and McCarthy, J. F. (1995), Observation and Three-Dimensional Simulation of Chloride Plumes in a Sandy Aquifer Under Forced-Gradient Conditions, *Water Resour. Res.*, 31( 9), 2141– 2157, doi:10.1029/95WR01947.
- Yeh, W. W.-G. (1986), Review of Parameter Identification Procedures in Groundwater Hydrology: The Inverse Problem, *Water Resour. Res.*, 22( 2), 95– 108, doi:10.1029/WR022i002p00095.
- Yin, D., and Illman, W. A. (2009), Hydraulic tomography using temporal moments of drawdown recovery data: A laboratory sandbox study, *Water Resour. Res.*, 45, W01502, doi:10.1029/2007WR006623.

- Zha, Y., T.-C. J. Yeh, D. Mao, J. Yang, and W. Lu (2014), Usefulness of flux measurements during hydraulic tomographic survey for mapping hydraulic conductivity distribution in a fractured medium, *Adv. Water Resour.*, 71, 162–176, doi:10.1016/j.advwatres.2014.06.008.
- Zha, Y., Yeh, T.-C. J., Illman, W. A., Zeng, W., Zhang, Y., Sun, F., et al. (2018). A reduced-order successive linear estimator for geostatistical inversion and its application in hydraulic tomography. *Water Resources Research*, 54, 1616– 1632. <https://doi.org/10.1002/2017WR021884>
- Zha, Y., Yeh, T.-C.J., Illman, W.A., Tanaka, T., Bruines, P., Onoe, H., Saegusa, H., Mao, D., Takeuchi, S. and Wen, J.-C. (2016), An Application of Hydraulic Tomography to a Large-Scale Fractured Granite Site, Mizunami, Japan. *Groundwater*, 54: 793-804. <https://doi.org/10.1111/gwat.12421>
- Zha, Y., Yeh, T.-C. J., Illman, W. A., Onoe, H., Mok, C. M. W., Wen, J.-C., Huang, S.-Y., and Wang, W. (2017), Incorporating geologic information into hydraulic tomography: A general framework based on geostatistical approach, *Water Resour. Res.*, 53, 2850– 2876, doi:10.1002/2016WR019185.
- Zhang, D., & Lu, Z. (2004). An efficient, high-order perturbation approach for flow in random porous media via Karhunen–Loeve and polynomial expansions. *Journal of Computational Physics*, 194(2), 773-794.
- Zhao, Z., and W. A. Illman (2017), On the Importance of Geological Data for Three-dimensional Steady-State Hydraulic Tomography Analysis at a Highly Heterogeneous Aquifer-Aquitard System. *J. Hydrol.*, 544, 640– 657
- Zhao, Z., Illman, W.A., Berg,S.J., 2016. On the importance of geological data for hydraulic tomography analysis: laboratory sandbox study. *J.Hydrol.* <https://doi.org/10.1016/j.jhydrol.2016.08.061>
- Zheng, C. and Gorelick, S.M. (2003), Analysis of Solute Transport in Flow Fields Influenced by Preferential Flowpaths at the Decimeter Scale. *Groundwater*, 41: 142-155. <https://doi.org/10.1111/j.1745-6584.2003.tb02578.x>
- Zhou, H., Gómez-Hernández, J. J., & Li, L. (2014). Inverse methods in hydrogeology: Evolution and recent trends. *Advances in Water Resources*, 63, 22-37.
- Zhu, J., and T.-C. J. Yeh (2006), Analysis of hydraulic tomography using temporal moments of drawdown recovery data, *Water Resour. Res.*, 42, W02403, doi:10.1029/2005WR004309
- Zhu, J., and Yeh, T.-C. J. (2005), Characterization of aquifer heterogeneity using transient hydraulic tomography, *Water Resour. Res.*, 41, W07028, doi:10.1029/2004WR003790.
- Zhu, J., and Yeh, T.-C. J. (2006), Analysis of hydraulic tomography using temporal moments of drawdown recovery data, *Water Resour. Res.*, 42, W02403, doi:10.1029/2005WR004309.
- Zijl, W. (1999). Scale aspects of groundwater flow and transport systems. *Hydrogeology Journal*, 7(1), 139-150.
- Zimmerman, D. A., et al. (1998), A comparison of seven geostatistically based inverse approaches to estimate transmissivities for modeling advective transport by groundwater flow, *Water Resour. Res.*, 34( 6), 1373– 1413, doi:10.1029/98WR00003.
- Zinn, B., and Harvey, C. F. (2003), When good statistical models of aquifer heterogeneity go bad: A comparison of flow, dispersion, and mass transfer in connected and multivariate Gaussian hydraulic conductivity fields, *Water Resour. Res.*, 39, 1051, doi:10.1029/2001WR001146, 3.
- Zlotnik, V.A., and B.R. Zurbuchen. 2003. Estimation of hydraulic conductivity from borehole flowmeter tests considering head losses. *Journal of Hydrology* 281, no. 1–2: 115–128.

Zlotnik, V.A., Zurbuchen, B.R. and Ptak, T. (2001), The Steady-State Dipole-Flow Test for Characterization of Hydraulic Conductivity Statistics in a Highly Permeable Aquifer: Horkheimer Insel Site, Germany. *Groundwater*, 39: 504-516. <https://doi.org/10.1111/j.1745-6584.2001.tb02339.x>



## CHAPTER 4

**Résumé :** Ce chapitre traite de la prise en compte de données complémentaire dans l'interprétation des tomographies hydrauliques afin d'estimer les propriétés 3D du champ de perméabilité du milieu investigué. Les données de pompages, qui permettent de renseigner la distribution horizontale des propriétés hydrauliques du milieu sont ainsi complétées par des données de débitmétrie en forage qui permettent de préciser la distribution verticale de perméabilité sur chacun des forages investigués. Cette méthodologie est mise en œuvre sur des modèles synthétiques afin d'apprécier les performances et les limites de l'approche, puis appliquée au site expérimental. Les résultats obtenus sont comparés à la distribution spatiale des propriétés pétrophysiques (perméabilité et porosité) acquises sur les différents puits carottés du site expérimental. La bonne adéquation entre ces différentes données permet de conclure que l'approche proposée est un moyen efficace et économique pour une caractérisation rapide du champ de perméabilités en 3D.



## 4. AN INVERSE APPROACH INTEGRATING FLOWMETER AND PUMPING TEST DATA FOR THREE DIMENSIONAL AQUIFER CHARACTERIZATION

Journal of Hydrology 603 (2021) 126939



Contents lists available at [ScienceDirect](#)

Journal of Hydrology

journal homepage: [www.elsevier.com/locate/jhydrol](http://www.elsevier.com/locate/jhydrol)



Research papers

An inverse approach integrating flowmeter and pumping test data for  
three-dimensional aquifer characterization



Mohammed Aliouache<sup>a</sup>, Xiaoguang Wang<sup>a,b,\*</sup>, Pierre Fischer<sup>a</sup>, Gerard Massonnat<sup>c</sup>,  
Herve Jourde<sup>a</sup>

<sup>a</sup> Laboratories Hydrosociences Montpellier, UMR 5151 CNRS-UM-IRD, Montpellier 34000, France

<sup>b</sup> Chengdu University of Technology, Sichuan 610059, China

<sup>c</sup> CSTJF-PAU Total Energies, Avenue Larribau, Pau 64000, France

<https://doi.org/10.1016/j.jhydrol.2021.126939>



## AN INVERSE APPROACH INTEGRATING FLOWMETER AND PUMPING TEST DATA FOR THREE-DIMENSIONAL AQUIFER CHARACTERIZATION

Mohammed Aliouache<sup>a</sup>, Xiaoguang Wang<sup>a,b,\*</sup>, Pierre Fischer<sup>a</sup>, Gerard Massonnat<sup>c</sup>, Herve Jourde<sup>a</sup>

<sup>a</sup> *Laboratories Hydrosiences Montpellier, UMR 5151 CNRS-UM-IRD, Montpellier, France, 34000*

<sup>b</sup> *Chengdu University of Technology, Sichuan, China, 610059*

<sup>c</sup> *CSTJF-PAU Total Energies, Avenue Larribau, Pau, France, 64000*

### Highlights

1. Coupling flowmeter and pumping test data for low-cost 3D aquifer characterizations
2. 3D hydraulic conductivity distribution is assessed from an inverse approach
3. The effectiveness of integrating the two datasets is studied with 3D synthetic models

## 4.1 Abstract

The accurate characterization of the underground depositional structure and hydraulic property distribution is essential to understand flow and solute transport in heterogeneous rocks or soils. Hydraulic tomography was shown to be an efficient technique to infer the spatial distribution of hydraulic properties. Due to the fact that information about the sedimentary structures' distribution is not always available to allow a three-dimensional characterization, many of existing field applications of hydraulic tomography have been limited to two-dimensional imaging along horizontal layer or vertical profiles where hydraulic data were collected.

In this work, we explore the potential of combining tomographic pumping and flowmeter tests responses in an inverse approach for three-dimensional aquifer characterization. The tomographic pumping data provide information about the lateral hydraulic connections between boreholes, while the flowmeter data constrain the vertical heterogeneity structure. The inverse approach is first validated using two synthetic models composed of multi-layered depositional structures and heterogeneous hydraulic properties within each layer. It is shown that adding the information provided by the flowmeter profiles, the inverted model exhibits more realistic depositional features. We then apply the proposed approach to characterize the 3D hydraulic conductivity field controlled by sedimentary structure of an experimental site in layered porous rocks. The inverted hydraulic conductivity field is in a good agreement with permeability measurement on drilled cores. The proposed method offers an efficient and low-cost approach for rapid assessment of the hydraulic properties in 3D and could be extrapolated to other field applications.

## 4.2 Introduction

The characterization of hydraulic properties, such as hydraulic conductivity and specific storage, is very important in groundwater modeling and water resources management (Hubbard and Rubin, 2005). Contaminant transport has always been strongly dependent on the accuracy of the hydraulic properties' characterization. A minor change in hydraulic properties may alter transport behaviors significantly (Zheng and Gorelick, 2003). Because direct measurements of hydraulic properties are limited in real-world applications, early analytical analysis of aquifer hydraulic response to pumping/injection often adopts a homogeneous assumption (e.g., Theis 1935, Cooper and Jacob 1946). It may be enough to infer the bulk aquifer property; however, it cannot capture most of the transient behavior of the tested aquifer. In addition to pumping tests, several other hydraulic testing methods, such as slug tests (Yeh et al., 1995) and flowmeter tests (Rehfeldt et al., 1992, Klepikova et al., 2013, Tamayo-Mas et al., 2018), are being used to provide non-redundant information (with respect to pumping tests) about the aquifer.

Hydraulic tomography (HT) has been developed over the last two decades (e.g., Gottlieb and Dietrich, 1995, Butler et al., 1999, Bohling et al., 2002, Bohling and Butler, 2010, Yeh and Liu, 2000, Zhu and Yeh, 2005, Zhu and Yeh, 2006, Liu et al., 2002, Liu et al., 2007, Illman et al., 2010, Cardiff et al., 2009, Zha et al. 2014). This approach has shown a great potential for reconstructing detailed spatial distributions of hydraulic parameters comparing to the traditional analytical solutions. Hydraulic tomography yields a detailed two- or three-dimensional map of hydraulic heterogeneity for regions within between the testing boreholes where constraining hydraulic head responses to cross-hole pumping are collected. The efficiency of HT has been demonstrated in many laboratory-scale (e.g., Liu et al., 2007, Illman et al., 2007, Illman et al., 2010, Zhao et al., 2016, Zhao and Illman 2017) and field-scale studies (e.g., Bohling et al., 2007, Brauchler et al., 2011, Brauchler et al., 2013, Berg and Illman, 2011, Cardiff et al., 2012, Fischer et al., 2020).

For a full 3D hydraulic tomography, using only one observation from each testing well is not sufficient and packer tests are often required (Bohling et al. 2007, Berg and Illman 2011, Zha et al. 2016, Zha et al. 2017, Cardiff et al. 2012, Zhao and Illman 2017, Wen et al. 2020). However, packer tests, which are costly and complex to set up, are not always available in each experiment site. Without packer tests, pumping tests data remain insufficient to capture the three-dimensional aquifer behavior and may lead to erroneous characterization and sometimes model instability in layered aquifers.

In recent years, other information such as geological and geophysical data have been used to constrain the inverse process of HT (e.g., Zha et al. 2017, Tso et al. 2016, Soueid Ahmed et al. 2015). The most widely-used geostatistics-based inverse modelling approaches are the quasi-linear geostatistical approach (Kitanidis 1995) and the successive linear estimator (SLE) (Yeh et al. 1996). To improve efficiency when dealing with highly parameterized inverse problems, different approaches were developed, including principle component geostatistical approach (Kitanidis and Lee 2014), reduced-order SLE (Zha et al. 2018) and the use of geostatistical reduced order models (Liu et al. 2013). Previous works have highlighted the benefits of incorporating site-specific geologic structure information into groundwater models when HT data are limited (Zha et al. 2017, Tso et al. 2016). Zha et al. (2017) worked on quantitative incorporation of site-specific information into groundwater models and introduced a general method to derive conditional mean and conditional covariance, that can be used in HT analysis as prior information. Tso et al. (2016) also concluded that only incorporating a qualitative facies trend information already yields a better conductivity estimate. Such improvement can also be seen in hydraulic conductivity estimates through laboratory/ field applications (Zhao et al. 2016, Zhao and Illman 2017). De Clercq et al. (2020) used electrical resistivity maps to structure the distribution of the hydraulic properties in a 3D HT.

Flowmeter surveys characterize the vertical inflow profile of a given well (Paillet et al. 1998, Molz et al. 1994, Zlotnik and Zurbuchen 2003, Williams and Paillet. 2002, Day-Lewis et al. 2011). They are a

widely used approach to determine vertical profiles of hydraulic conductivities at well locations. Complex geological media are often layered systems and flowmeter analysis has shown its efficiency to detect the main layers contributing to the total pumped flux (Day-Lewis et al. 2011, Paillet and Reese 2000). Flowmeter profiling can also be used to detect the well crossing fractures that contribute to flow (Day-Lewis et al. 2011, Roubinet et al. 2015). Flowmeter tests are easy and cheap but bulky and the investigated height is limited due to the space taken by the pump and the generated drawdown. Flowmeter tests may provide a new set of information and have been included in inverse modelling problems. For instance, Fienen et al. (2004) used a Bayesian inverse approach to interpret the vertical hydraulic conductivity in a heterogeneous fractured aquifer. Other applications used the interpreted hydraulic conductivity values from flowmeter tests in the transmissivity map to constrain the geostatistical inversions (e.g., Rehfeldt et al. 1992; Chen et al. 2001). In other studies, flux measurements have also been used as observation data additional to hydraulic heads in hydraulic tomography (Li et al. 2008, Zha et al. 2014, Tso et al. 2016).

Combining different hydraulic tests that characterize different parts of the aquifer may lead into a good characterization; for example, combining flowmeter tests data that give vertical information with pumping tests data that give lateral information might be a good alternative to obtain a three-dimensional characterization of the aquifer without packer tests. In this paper, we integrate vertical hydrogeological information obtained from flowmeter surveys and horizontal information from cross-hole pumping tests to achieve a 3D transient hydraulic tomographic (THT) characterization of sedimentary layered rocks. The flowmeter data are incorporated to HT through the construction of conditional initial mean and covariance of model parameter. We first validate the proposed inversion framework using synthetic data from a two-dimensional cross-section model and a three-dimensional model. We then apply the inverse approach to a real-world study in an experimental site composed of layered porous rocks. In the end, we analyze the data fitting effectiveness and geological coherence of the inverted hydraulic conductivity fields.

### 4.3 Methodology

The objective of the study is to integrate two sets of data to obtain spatialized hydraulic conductivity estimates through hydraulic tomography. The first dataset corresponds to drawdown responses to pumping tests that give information about lateral variation of hydraulic properties. The second dataset consists in flowmeter logs measured in every well of the site that give vertical information (see Figure 4.1 for datasets scheme). Flowmeter logs are first interpreted and converted into hydraulic conductivity profiles. Then, the interpreted hydraulic conductivity profiles are interpolated using a triangular-base bilinear or trilinear interpolation in order to obtain a continuous two- or three-dimensional hydraulic conductivity map between the wells and we use ‘nearest neighbors’ interpolation for the rest of the

inversion domain where the linear interpolation cannot be evaluated. After that, an inverse modelling approach is used to reconstruct the hydraulic conductivity distribution using interpolated map as a prior information. We use the principal component geostatistical approach, a deterministic iterative procedure that updates the conditional mean and the conditional covariance by matching model responses to the pumping tests observations.

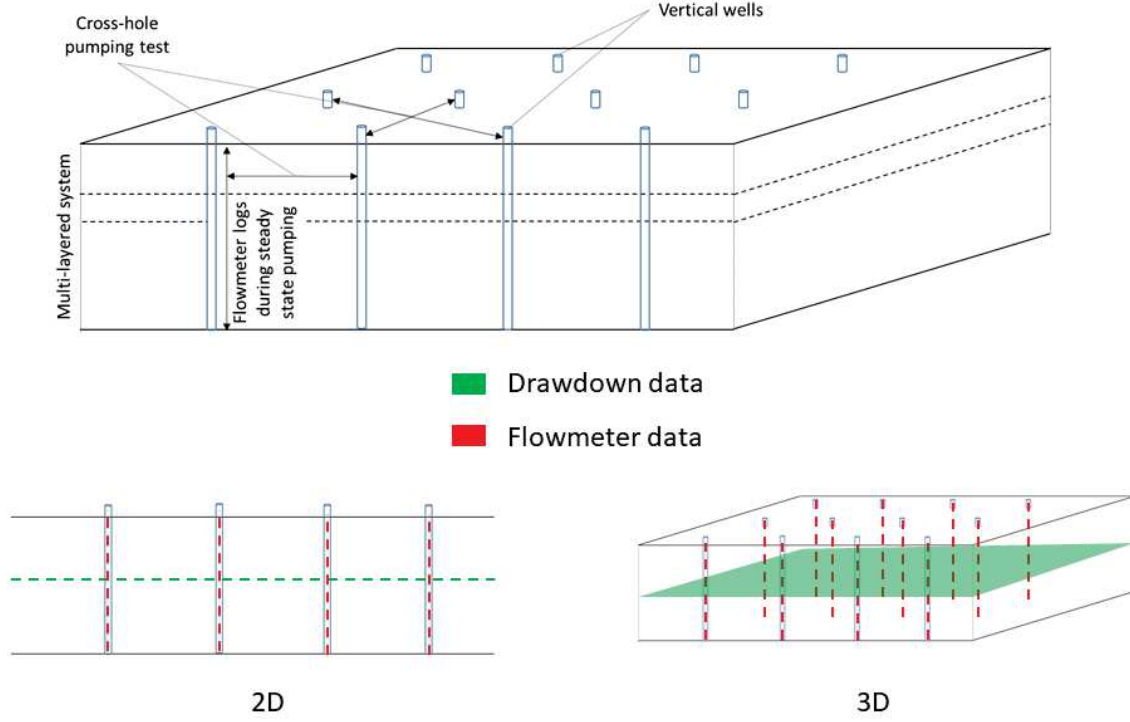


*Figure 4.1: Data usage scheme. Red dashes correspond to flowmeter log data and green surface corresponds to cross-hole pumping tests data. The wells are open hole and the drawdowns are sampled at the green z-level*

### 4.3.1 Groundwater flow model

We solve the problem of three-dimensional transient fluid flow through a confined, saturated and heterogeneous porous media. The system is solved in transient regime and is described by the following equations:

$$S_s \frac{\partial h}{\partial t} + \nabla(-K\nabla h) = Q, \quad (4.1)$$

with

$$h|_{t=0} = h_0, h|_{\varphi} = h_0, \quad (4.2)$$

where  $\nabla$  is the gradient operator,  $S_s$  is the specific storage which assumed constant in this study,  $h$  is the hydraulic head,  $K$  the hydraulic conductivity,  $Q$  the source term and  $h_0$  is the initial hydraulic head which remains constant at the boundary conditions  $\phi$ . The forward flow model is solved using a finite element method using unstructured mesh (See Figure S8 in the Appendix).

### 4.3.2 Flowmeter analysis

The applied approach of flowmeter data analyses is described in Molz et al. (1989), which is based on the study of flow in a layered, stratified aquifer by Javandel and Witherspoon (1969). Assuming that the idealized aquifer is layered and the flow quickly becomes horizontal even with high contrast of hydraulic conductivity between the layers. The flow of a given layer is proportional to the hydraulic conductivity of that layer and the sum of the different flow rates into the well is equal to the pump flow rate during the pumping test.

During our flowmeter test, water is extracted from an open hole well and, once steady state is reached, a spinner flowmeter is swept along the well from the bottom of the well to the top and a vertical flow rate profile is measured. In most common cases, when the pump is located at the top, the flow rate log will have the trend of an increasing curve starting from a zero value at the bottom to a max value at the top, that will correspond to the total extracted flux from the well. The increase in flow rate over a certain depth increment is correlated to the relative hydraulic conductivity profile; higher the hydraulic conductivity, stronger the rate increase. Flowmeter tests therefore provide relative values of hydraulic conductivity distribution along the borehole. In order to extract the absolute values, an effective value of hydraulic conductivity of the well (obtainable from the interpretation single hole of a pumping tests) will be used. Single-hole flowmeter data can be analyzed to estimate conductivity profiles along boreholes and characterize aquifer compartmentalization (Molz et al. 1989; Kabala 1994; Paillet et al. 1998).

If a well is subject to a pumping with a pump placed at the top of the well working at the rate  $Q_p$ , the underground layers connected to that well will contribute to the total extracted flux. Their contribution is proportional to their hydraulic conductivity. For the following equations,  $b$  (m) refers to the aquifer thickness,  $z_0$  (m) the reference level of the borehole bottom, and  $z$  (m) the height above the bottom (Figure 4.2). In an idealized layered aquifer, the flow into the well from a given layer is proportional to the transmissivity of that layer:

$$\Delta Q_i = \alpha \Delta z_i K_i, \quad (4.3)$$

where  $\alpha$  (m) is a constant of proportionality,  $\Delta Q_i$  ( $m^3/s$ ) corresponds to the induced flow increments observed in the borehole along the  $i^{th}$  increment of height  $\Delta z_i$  (m) that has a hydraulic conductivity  $K_i$  (m/s). The average horizontal hydraulic conductivity  $K_{avg}$  can be expressed by:

$$K_{avg} = \frac{\sum K_i \Delta z_i}{b} . \quad (4.4)$$

The cumulative flow  $Q_{cum}(b)$  over the aquifer thickness can be expressed as follows:

$$Q_{cum}(b) = \int_{z_0}^b Q(z) dz = Q_p = \sum_i \Delta Q_i = \alpha \sum_i \Delta z_i K_i = \alpha K_{avg} b . \quad (4.5)$$

By substituting the sum,  $\alpha$  can be solved as:

$$\alpha = \frac{Q_p}{K_{avg} b} . \quad (4.6)$$

Then, the hydraulic conductivity of each layer can be quantified by:

$$K_i = \frac{\Delta Q_i K_{avg} b}{Q_p \Delta z_i} . \quad (4.7)$$

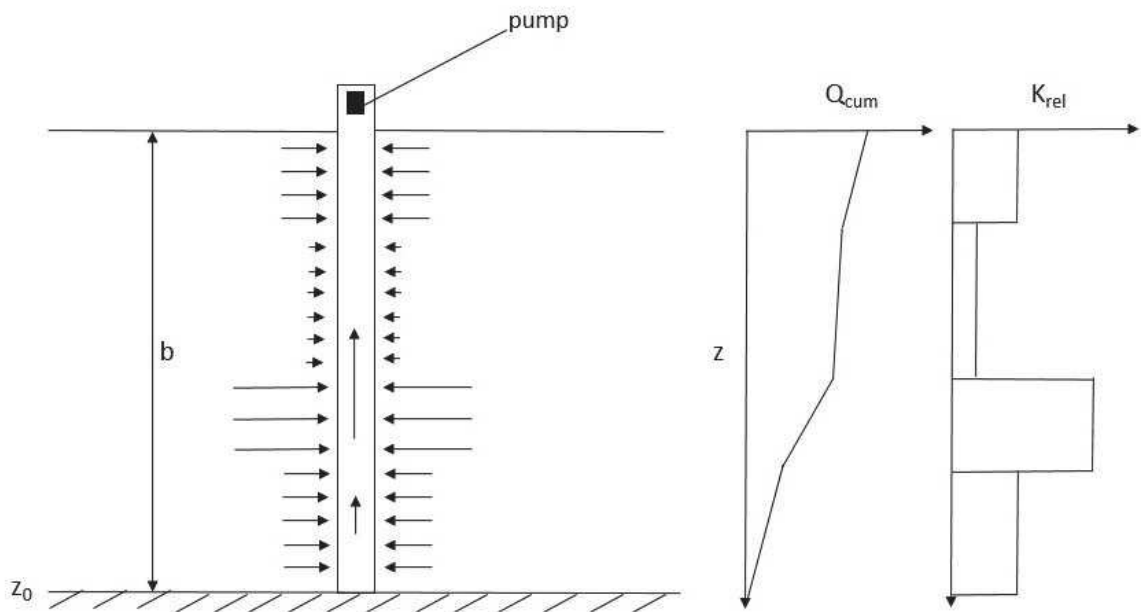


**Figure 4.2:** Flowmeter setup scheme with an interpretation example.  $Q_{cum}$  is the cumulative flow rate and  $K_{rel}$  is the interpreted relative permeability from flow log.

### 4.3.3 Principal component geostatistical approach

In order to optimize the hydraulic conductivity field in the model we use the principal component geostatistical approach (PCGA) (Kitanidis and Lee 2014). The observation equation that links the  $m$  unknown hydraulic conductivities, stored in a vector  $\mathbf{s}$ , to the observation data (hydraulic heads) stored in a matrix  $\mathbf{y}$  is (Kitanidis 1995):

$$\mathbf{y} = \mathbf{h}(\mathbf{s}) + \mathbf{v}, \quad (4.8)$$

where  $\mathbf{h}(\mathbf{s})$  is the forward model,  $\mathbf{v}$  is the observation error with a random normal distribution with mean 0 and variance  $\mathbf{R}$ , which is usually the error measurement multiplied by the identity matrix. The prior probability of  $\mathbf{s}$  is a Gaussian distribution with mean  $\mathbf{X}\boldsymbol{\beta}$  generalized by a covariance matrix  $\mathbf{Q}$ .  $\mathbf{X}$  is a  $m$ -vector of ones and  $\boldsymbol{\beta}$  represents the mean hydraulic conductivity value. The posterior probability density function (objective function  $\mathbf{L}$ ) of  $\mathbf{s}$  and  $\boldsymbol{\beta}$  is given by:

$$\mathbf{L} = \frac{1}{2}(\mathbf{y} - \mathbf{h}(\mathbf{s}))^T \mathbf{R}^{-1}(\mathbf{y} - \mathbf{h}(\mathbf{s})) + \frac{1}{2}(\mathbf{s} - \mathbf{X}\boldsymbol{\beta})^T \mathbf{Q}^{-1}(\mathbf{s} - \mathbf{X}\boldsymbol{\beta}). \quad (4.9)$$

The optimization of the hydraulic conductivity values is obtained by minimizing this objective function through an iterative method.

Inversion process requires the calculation of the sensitivity matrix (Jacobian matrix) which require as much forward model simulations as unknowns  $m$ . Despite the computer science advancement, the forward model itself can be time consuming when dealing with high dimensional problems (3D simulations, fine mesh, presence of complex structures). In order to bypass this difficulty, the principal component geostatistical approach which avoids the full Jacobian matrix calculation, was proposed. The reduced order successive linear estimator ROSLE (Zha et al. 2018) based on SLE (Yeh, 1996) can be one alternative to the PCGA. These methods use a singular value decomposition and then a truncation based on the eigenvalues and Eigen functions of the covariance matrix  $\mathbf{Q}$ . The covariance matrix can be rewritten with its decomposed form as:

$$\mathbf{Q} = \mathbf{V}\mathbf{S}\mathbf{V}^T, \quad (4.10)$$

where  $\mathbf{V}$ 's columns correspond to the eigenvectors of the covariance matrix and  $\mathbf{S}$  is a diagonal matrix of its eigenvalues  $\boldsymbol{\lambda}$  which are decreasingly organized. The eigenvectors and eigenvalues are then  $\mathbf{k}$ -rank truncated. The  $\mathbf{k}$  first eigenvalues and its corresponding eigenvectors are kept. The compressed covariance can be calculated as:

$$\mathbf{Q}_k = \mathbf{V}_k \mathbf{S}_k \mathbf{V}_k^T, \quad (4.11)$$

where

$$\mathbf{Q}_k \approx \mathbf{Q}, \quad (4.12)$$

It can be also written as a sum:

$$\mathbf{Q}_k = \mathbf{V}_k \mathbf{S}_k \mathbf{V}_k^T = \sum_{i=1}^k \xi_i \xi_i^T, \quad (4.13)$$

where

$$\xi_i = \sqrt{\lambda_i} \mathbf{V}_i. \quad (4.14)$$

The accuracy of the low-rank covariance depends on the truncation number. However, it is already shown that a much smaller truncation number than the number of unknowns ( $\mathbf{k} \ll m$ ) can be used (Kitanidis and Lee, 2014). The quasi-Linear geostatistical approach (Kitanidis, 1995) updates the actual best estimate  $\bar{\mathbf{s}}$  for the next iteration as:

$$\bar{\mathbf{s}} = \mathbf{X}\bar{\boldsymbol{\beta}} + \mathbf{Q}\mathbf{H}^T\bar{\boldsymbol{\xi}}, \quad (4.15)$$

where  $\mathbf{H}$  is the Jacobian matrix and the accentuation-bar denotes the best estimate.  $\bar{\boldsymbol{\beta}}$  and  $\bar{\boldsymbol{\xi}}$  are solved from the following linear system:

$$\begin{bmatrix} \mathbf{H}\mathbf{Q}\mathbf{H}^T + \mathbf{R} & \mathbf{H}\mathbf{X} \\ (\mathbf{H}\mathbf{X})^T & \mathbf{0} \end{bmatrix} \begin{bmatrix} \bar{\boldsymbol{\xi}} \\ \bar{\boldsymbol{\beta}} \end{bmatrix} = \begin{bmatrix} \mathbf{y} - \mathbf{h}(\bar{\mathbf{s}}) + \mathbf{H}\bar{\mathbf{s}} \\ \mathbf{0} \end{bmatrix}. \quad (4.16)$$

The minimized objective function  $\mathbf{L}$  can also be written as:

$$\mathbf{L} = \frac{1}{2} \left( \mathbf{y} - \mathbf{h}(\mathbf{X}\boldsymbol{\beta} + \mathbf{Q}\mathbf{H}^T\boldsymbol{\xi}) \right)^T \mathbf{R}^{-1} \left( \mathbf{y} - \mathbf{h}(\mathbf{X}\boldsymbol{\beta} + \mathbf{Q}\mathbf{H}^T\boldsymbol{\xi}) \right) + \frac{1}{2} \boldsymbol{\xi}^T \mathbf{H}\mathbf{Q}\mathbf{H}^T \boldsymbol{\xi}. \quad (4.17)$$

In PCGA, the sensitivity matrix  $\mathbf{H}$  is not fully calculated and an alternative way to approximate it is proposed.

In order to estimate  $\mathbf{H}\mathbf{Q}$  and  $\mathbf{H}\mathbf{Q}\mathbf{H}^T$ ,  $\mathbf{k}$  forward runs are needed to be solved in addition to the forward run of the actual best estimate, the forward models are used to calculate  $\boldsymbol{\eta}$  defined as follows:

$$\boldsymbol{\eta}_i = \mathbf{H}\xi_i \approx \frac{1}{\delta} [\mathbf{h}(\mathbf{s} + \delta\xi_i) - \mathbf{h}(\mathbf{s})], \quad (4.18)$$

$\delta$  is the finite difference interval from the Taylor series expansion (Kitanidis and Lee, 2014). Then  $\mathbf{HQ}$  and  $\mathbf{HQH}^T$  are defined as:

$$\mathbf{HQ} \approx \mathbf{HQ}_k = \mathbf{H} \sum_{i=1}^k \xi_i \xi_i^T = \sum_{i=1}^k (\mathbf{H}\xi_i) \xi_i^T = \sum_{i=1}^k \eta_i \xi_i^T, \quad (4.19)$$

$$\mathbf{HQH}^T \approx \mathbf{HQ}_k \mathbf{H}^T = \mathbf{H} [\sum_{i=1}^k \xi_i \xi_i^T] \mathbf{H}^T = \sum_{i=1}^k (\mathbf{H}\xi_i)(\mathbf{H}\xi_i)^T = \sum_{i=1}^k \eta_i \eta_i^T. \quad (4.20)$$

In order to estimate  $\mathbf{HX}$ , one (columns of  $\mathbf{X}$ ) forward run is needed, following:

$$\mathbf{HX}_i \approx \frac{1}{\delta} [\mathbf{h}(\bar{\mathbf{s}} + \delta \mathbf{X}_i) - \mathbf{h}(\bar{\mathbf{s}})]. \quad (4.21)$$

In order to estimate  $\mathbf{H}\bar{\mathbf{s}}$ , one forward run is needed in addition to the forward model of the actual best estimate, following:

$$\mathbf{H}\bar{\mathbf{s}} = \frac{1}{\delta} [\mathbf{h}(\bar{\mathbf{s}} + \delta \bar{\mathbf{s}}) - \mathbf{h}(\bar{\mathbf{s}})] + \mathbf{O}(\delta) \approx \frac{1}{\delta} [\mathbf{h}(\bar{\mathbf{s}} + \delta \bar{\mathbf{s}}) - \mathbf{h}(\bar{\mathbf{s}})]. \quad (4.22)$$

In total, each iteration requires  $\mathbf{k}+3$  forward runs; 1 forward run of the actual best estimate, 1 forward run to estimate  $\mathbf{H}\bar{\mathbf{s}}$ , 1 forward run to estimate  $\mathbf{HX}$  and  $\mathbf{k}$  forward models to estimate  $\mathbf{HQ}$  and  $\mathbf{HQH}^T$ . The above steps are repeated iteratively until convergence of the objective function value is reached.

#### 4.3.4 Prior information

The approach of conditional mean and conditional covariance using geological information as presented in Zha et al. (2017) work is used in this study. The two main prior information are the initial guess and the initial covariance matrix. The prior input of the inversion is constructed using interpreted flowmeter data. The 3D interpolated conductivity is mapped into inversion grid, stored in  $\mathbf{s}$ , and used as an initial guess for the first iteration instead of using an initial mean.; an interpolation or/and an extrapolation might be often used. It also allows identifying the main facies and constructing the prior covariance accordingly (Zha et al. 2017). However, the covariance matrix  $\mathbf{Q}$  is constructed as a sum of different covariance sub-matrixes (Zha et al., 2017): a) a covariance matrix that defines the different facies (layers) will be of high importance and its construction is achieved only by using a strong correlation between the cells that belong to the same facies, b) another covariance matrix that defines the correlation between the cells of the same facies, defined as an intra-facies covariance, c) a third covariance matrix, defined as an inter-facies covariance, can be used on the global inverted domain. By conditioning the prior covariance with facies information distinguished from flowmeter data, we try to incorporate the vertical information into the inversion process and constrain its convergence path.

## 4.4 Validation of concept

The main objective of the paper is the use of two different datasets which are easily available to better characterize the hydraulic conductivity of a multi-layered sedimentary structure constitutive of the aquifer. The first dataset corresponds to flowmeter data along the profile of each well. Flowmeter logs are obtained by pumping in the top of each well and the flowmeter tool is swept under the pump to get the flow contribution along the borehole. The second dataset corresponds to measured hydraulic response (drawdowns) to pumping tests. Here we try to perform a 3D inversion of the hydraulic conductivity field to characterize the aquifer on the basis of pumping tests data and incorporating flowmeter information. In order to validate this concept, the proposed inverse approach is first applied on two synthetic cases. The first case is performed in 2D and the second one in 3D.

### 4.4.1 2D synthetic case

By using a two-dimensional random field generator tool (Paul Constantine 2021), a random hydraulic conductivity field is generated following an exponential correlation function using the parameters of standard deviation  $\sigma=1.5$ , the correlation length in x direction  $L_x=100$  m, the correlation length in y direction  $L_y=5$  m. With such set of parameters, the obtained hydraulic conductivity field displays multi-layered hydraulic properties (see Figure 4.3a). We consider the obtained 2D map as a vertical cross-section of an aquifer centered on the inverted domain which is extended using a buffer area until the boundary conditions. The dimensions of the inverted domain are 70 m by 50 m; the dimensions of the buffer area are 700 m by 50 m. The lateral boundaries are set to constant zero hydraulic head while the upper and lower boundaries are set to no flow condition. The initial condition is set to zero hydraulic head in the whole domain. For forward flow simulations, we use the Darcy's law module of Comsol Multiphysics<sup>[1]</sup>. We assume the aquifer to be confined. The specific storage is assumed constant and a value of  $S_s = 10^{-4} \text{ m}^{-1}$  was used.

The wells are modeled explicitly with a radius of  $r_w=0.1$  m. We attribute to wells a high hydraulic conductivity ( $K=1 \text{ m.s}^{-1}$ ) and a low specific storage ( $10^{-10} \text{ m}^{-1}$ ) (see Figure S1 in the Appendix). The spacing of wells in the x direction is 15m (Figure 4.3a). We simulate five cross-hole pumping tests, which are considered as the 'data' for inversion. The location of selected wells is indicated in Figure S4 in the Appendix. We simulate flowmeter data for each well by using a point source at the top of the well and applying a steady-state pumping flow rate. Once the steady-state flow regime is reached, we evaluate the vertical velocity along a line in the middle of the well. In our flow simulations, extra fine meshes are adopted to discretize the well domain (Figure S8 in Appendix). Examples of simulated flowmeter measurements for the 2D case can be found in Appendix (Figure S7). For cross-hole pumping tests dataset to be used in HT, we simulate the transient hydraulic heads using a point source

in the middle of explicitly modelled wells. The black dots shown in Figure 4.3 are the position of the points to be used as point source for the pumping tests and the monitoring points. For hydraulic head data, we sample at five different time steps covering the early to middle times for all pumping tests. The total number of drawdown data used for inversions are  $5$  (number of time steps)  $\times$   $5$  (number of pumping tests)  $\times$   $4$  (number of observation wells) =  $100$ .

The simulated vertical velocity curves are converted into hydraulic conductivity distributions following the procedure described as follows (An example of the manipulation is provided in the supplementary information file).

- Step1: Discretize the vertical velocity profile into depth intervals  $\Delta z$
- Step2: In each interval, evaluate the change in velocity  $\Delta v_i$  corresponding to the change in depth  $\Delta z_i$
- Step3: Use Equation 7 to estimate  $K_i$  for each  $\Delta z_i$
- Step4: Hydraulic conductivity profile is obtained in each well.

The hydraulic conductivity profiles are then interpolated using a triangular-base bilinear interpolation to obtain a hydraulic conductivity map for areas within between the wells. For the rest of the inversion domain where the linear interpolation cannot be evaluated, we use a nearest neighbors' extrapolation.

In the next step, we construct a nested covariance using the interpolated hydraulic conductivity map. The nested covariance is constructed by the combination of multiscale correlated heterogeneities (Zha et al. 2017). For example, a geological facies from another survey can be used a soft constraint added into the initial covariance matrix for HT. The interface between different facies or zones may exhibit an abrupt change of hydraulic properties. On the other hand, the variability inside a particular facies or zone (compared to its large-scale mean) can be described by a zero mean and a small-scale covariance function.

The covariance matrix used in HT of the 2D study is either calculated using a covariance model similar to the one used to generate the true random field (Figures 4.3b and 4.3c), or built from a nested covariance which is a sum of different covariance matrices: a covariance matrix built using a covariance model similar to the one used to generate the true random field plus a covariance matrix defining the important facies of flowmeter interpreted map (Figure 4.3e and 4.3f). The first covariance matrix is simply calculated using an exponential covariance model with standard deviation=1.5, correlation length in x direction  $L_x=100$  m and correlation length in y direction  $L_y=5$  m. For the second covariance matrix that defines the facies, we simply identify the facies from flowmeter map (Figure 4.3g) and we build a binary covariance that correlates the cells that belong to the same facies.

In the inverse problem, a structured grid is used to discretize the model domain. For the two-dimensional cases, the number of grid blocks in x and y directions are  $n_x = 30$  and  $n_y = 15$  respectively (See Figure S8 in the Appendix). As a result, the total number of unknown K parameters is 450. For PCGA setup, we use a truncation number of  $k=20$  for a number of unknowns  $n=30*15$ ,  $R=0.001*Id$  where Id is the identity matrix, and  $\delta=0.0001$  for the finite difference interval. The specific storage was kept constant in the inversion and the value is the same as in the forward simulation, i.e.,  $S_s = 10^{-4} m^{-1}$ . Figure 4.3 shows the results of the two-dimensional validation case. Figure 4.3a corresponds to the generated, considered true, hydraulic conductivity field. Figure 4.3b is the inverted hydraulic conductivity field using a classical hydraulic tomography that used similar covariance information as in the generation of the random field. Figure 4.3d shows the interpreted hydraulic conductivity from flowmeter analysis. Figures 4.3c, 4.3e and 4.3f show the inverted hydraulic conductivity by integrating flowmeter interpretations into prior information of the inversion; Figure 4.3c used the interpreted hydraulic conductivity in Figure 4.3d to initialize only the parameter; Figure 4.3e used the interpreted hydraulic conductivity in Figure 4.3d to initialize both the parameter and the covariance matrix which remained constant during inversion iterations; Figure 4.3f used the interpreted hydraulic conductivity in Figure 4.3d to initialize both the parameter and the covariance matrix which was updated during inversion iterations.

The flowmeter interpretation allows the detection of the main layers in the system (Figure 4.3d) while the attempt of an inversion using only pumping tests data couldn't assess the vertical profiles of hydraulic conductivity (Figure 4.3b). Figure 4.3c, 4.3e and 4.3f show better K estimates. Flowmeter data clearly carry non-redundant information on the vertical hydraulic conductivity profiles along the wells. By only using the obtained hydraulic conductivity map from flowmeter interpretation as an initial guess, the inverted conductivity already contains vertical profile information and show different layers (Figure 4.3c). The inverted hydraulic conductivity shown in (Figure 4.3e) is also representative of a layered system but clearly not better than the inverted hydraulic conductivity shown in (Figure 4.3c). On the contrary, when the nested covariance has the freedom to update through inversion iterations, the best parameter estimate was obtained compared to all other configurations (Figure 4.3f).

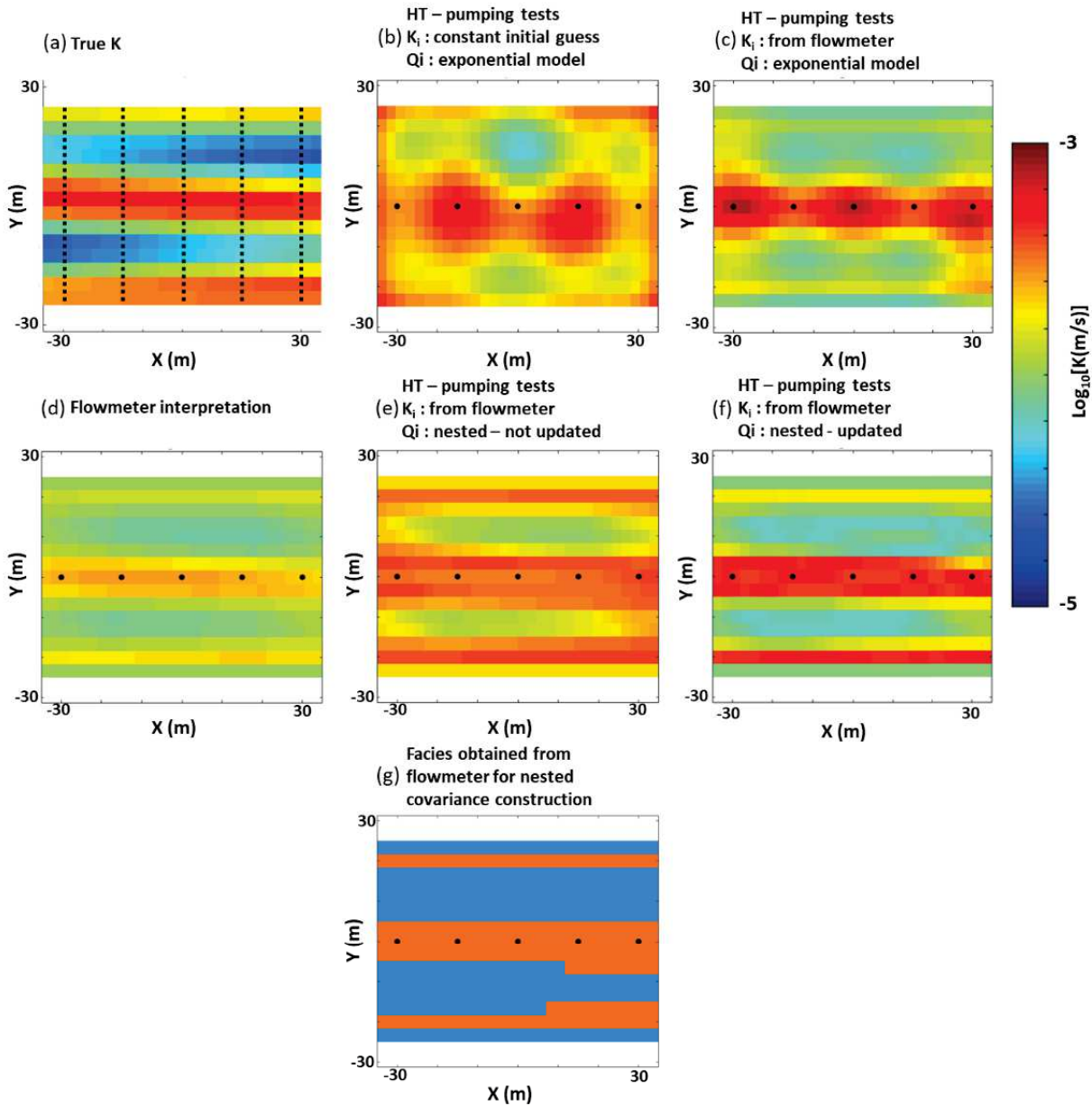


**Figure 4.3:** Two-dimensional validation case – results of HT using different prior information. a) true hydraulic conductivity, d) interpreted hydraulic conductivity from flowmeter tests, b, c, e and f are inverted hydraulic conductivities using different prior models.  $K_i$  and  $Q_i$  correspond to the initial hydraulic conductivity and initial covariance matrix respectively, g) is the constructed facies from flowmeter analyses to use in order to construct the nested covariance.

Figure 4.4 shows a scatter plot of true hydraulic conductivity and estimated hydraulic conductivity shown in Figure 4.3. In each scatter plot we plot a linear model of data fitting (red dashed line) and calculated the coefficient of determination, i.e.,  $R^2$  shown in Figure 4.4. The solid line is the first bisector line of  $y=x$ . Figures 4.4a and 4.4b present results of using pumping tests and an exponential covariance model for inversion. The difference is that in Figure 4.4a the initial guess of hydraulic conductivity was assumed constant while in Figure 4.4b the hydraulic conductivity distribution constructed by interpolating measured flowmeter profiles was used as the initial model. When the flowmeter data are

integrated, the inverted hydraulic conductivities represent the true model better ( $R^2$  of Figure 4.4b is lower than that of Figure 4.4a). On the other hand, Figure 4.4c confirms that the flowmeter data can capture the true K distribution to some extent indicated by the strong linear trend and high value of  $R^2$ . However, the variance of the hydraulic conductivity estimates seems underestimated. The improved hydraulic conductivity estimation is obtained when flowmeter data are used to construct both the initial model and the covariance model (Figure 4.4d). Comparing results shown in Figures 4.4d and 4.4e indicates that allowing the update of the nested covariance improves the estimation considerably.

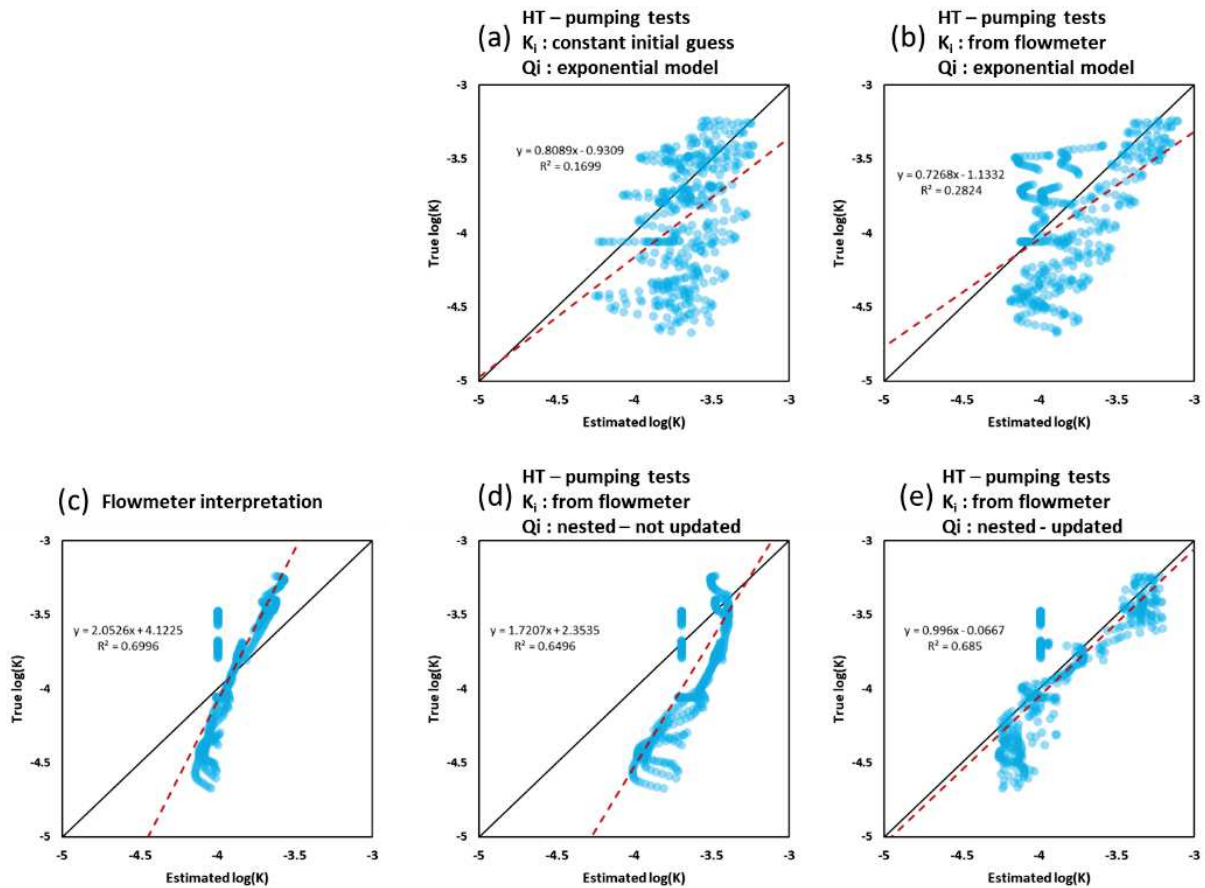


**Figure 4.4:** Scatterplots of true hydraulic conductivity versus estimated hydraulic conductivity for the different cases of the two-dimensional synthetic case. c) scatter plot of true K versus interpreted K from flowmeter. a, b, d and e are scatter plots of true K versus inverted K using different prior models.

#### 4.4.2 3D synthetic case

We extend the approach to a three-dimensional synthetic case and try to show if flowmeter data can provide the vertical information for a 3D aquifer characterization instead of packer tests. Similar to the simplified two-dimensional case, we use a three-dimensional random field generator (Rass et al. 2019) to generate a three-dimensional synthetic hydraulic conductivity map using the following parameters (Correlation function: exponential, standard deviation = 1.5,  $L_x=100$  m,  $L_y=100$  m and  $L_z= 5$  m). Such

parameters provide a hydraulic conductivity map that is representative of a multilayered system. The dimensions of the inverted domain are length=70 m, width=70 m and height=30 m; the lateral dimensions of the buffer area are length=700 m and width=700 m; the buffer was not extended in the vertical direction. The outer boundaries are set to constant zero hydraulic head while the upper and lower boundaries (top and bottom) are set to no flow condition. The initial condition is set to zero hydraulic head in the whole domain. The specific storage is assumed constant and a value of  $S_s = 10^{-4}$  m<sup>-1</sup> was used.

As for the two-dimensional case, we simulate flowmeter and cross-hole datasets by modelling explicit wells and point source pump (the point source in the top for the flowmeter simulation and in the middle for cross-hole tests simulations). Extra fine meshes are adopted to discretize the well domain (Figure S8 in Appendix). See Figure S7 in Appendix for an example of simulated flowmeter measurements for the 3D case. Five cross-hole pumping tests data are simulated and considered as the ‘data’ for the inversions. The location of selected wells is indicated in Figure S4 of the Appendix. As for the 2D cases, the total number of observations for the 3D cases is 100. The flowmeter data are interpreted and the hydraulic conductivity profiles are then interpolated using a triangular-base trilinear interpolation to fill the area between the wells. The rest of the inversion domain where the linear interpolation cannot be evaluated, we use a nearest neighbors’ extrapolation.

We construct a nested covariance using the interpreted flowmeter map as described for the two-dimensional case. In the inverse problem, a structured grid is used to discretize the model domain. For the three-dimensional cases, the number of grid blocks in x, y and z directions are  $n_x = 20$ ,  $n_y = 20$ ,  $n_z = 8$  respectively (See Figure S8 in Appendix). For PCGA setup, we use a truncation number of  $k=30$  for a number of unknowns  $n=20*20*8$ ,  $R=0.001*Id$  where  $Id$  is the identity matrix and  $\delta=0.0001$  for the finite difference interval. The specific storage was kept constant ( $S_s = 10^{-4}$  m<sup>-1</sup>) in the inversion and we focus on the characterization of K fields.

Figure 4.5 shows the results of the three-dimensional validation case. Figure 4.5c corresponds to the generated, considered true, hydraulic conductivity field. Figure 4.5a is the inverted hydraulic conductivity field using a classical hydraulic tomography that used same covariance information as in the random field generation. Figure 4.5b shows the interpreted hydraulic conductivity from flowmeter analysis. Figures 4.5d and 4.5e show the inverted hydraulic conductivity by integrating flowmeter interpretations into prior information of the inversion; Figure 4.5d used the interpreted hydraulic conductivity in Figure 4.5b to initialize only the parameter; Figure 4.5e used the interpreted hydraulic conductivity in Figure 4.5b to initialize both the parameter and the covariance matrix which was updated during inversion iterations.

The results of the 3D validation case agree with the observed results of the 2D validation case. The flowmeter interpretation allows vaguely the detection of the main layers in the system (Figure 4.5b)

while the attempt of an inversion using only pumping tests data couldn't assess the vertical profiles of hydraulic conductivity (Figure 4.5a). Figures 4.5d and 4.5e show better characterization in the vertical profiles due to non-redundant added information brought by flowmeter data. Using the flowmeter's interpreted hydraulic conductivity as an initial guess in the inversion already improves considerably the results (Figure 4.5d). Also, as seen in the 2D validation case, the best K estimate was obtained when flowmeter interpretation was used to initialize both the parameter and the covariance matrix (Figure 4.5e).

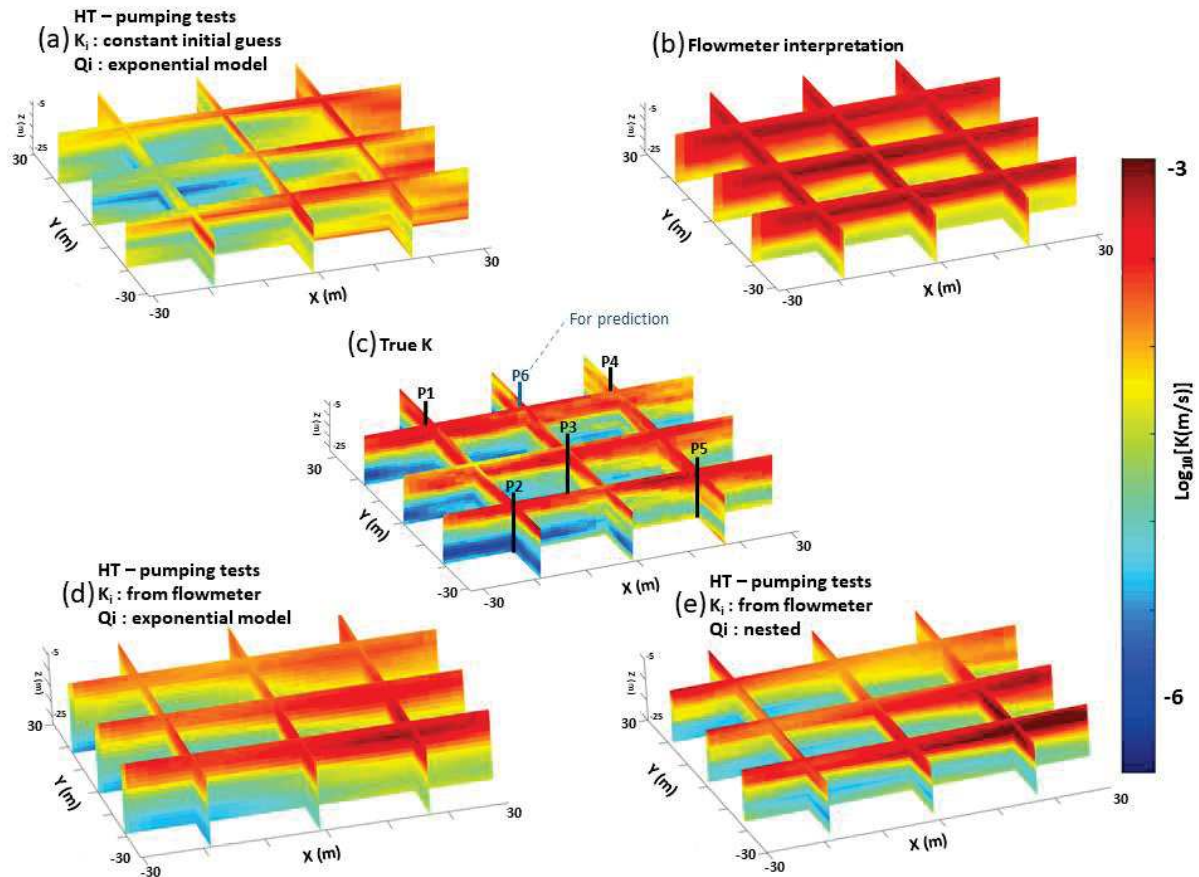


**Figure 4.5:** Three-dimensional validation case - results of HT using different prior information; b) interpreted hydraulic conductivity from flowmeter tests, c) true hydraulic conductivity, a, d and e are inverted hydraulic conductivities using different prior models.  $K_i$  and  $Q_i$  correspond to the initial hydraulic conductivity and initial covariance matrix respectively.

These results obtained with the 3D synthetic case are similar to the ones obtained with the 2D synthetic case, and thus confirm that adding flowmeter information allows improving the hydraulic permeability field. This conclusion is consistent with the fact that flux, in addition to hydraulic head measurements, enhance K values estimate (Yeh et al. (2011, 2015a, 2015b), Mao et al. (2013a, 2013b), Tso et al. 2016).

To better evaluate the quality of the estimated hydraulic conductivity field, we simulate a transient pumping test in well P6 (see Figure 4.5c) using this inverted hydraulic conductivity map and compare the simulated drawdowns to the simulated drawdowns obtained with the true hydraulic conductivity field (see Figure 4.6).

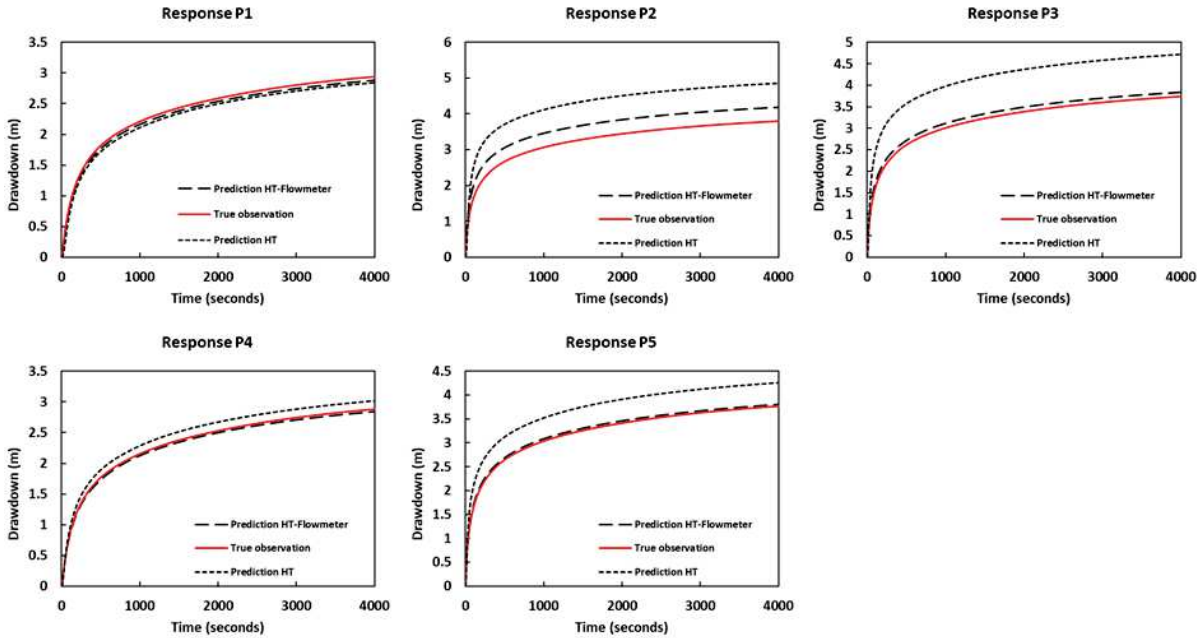


*Figure 4.6: Hydraulic head response to simulated pumping tests in the new added well P6. Solid red, dotted and dashed black curves correspond to the simulated drawdowns using respectively the true conductivity, the hydraulic conductivity map obtained from hydraulic tomography and the hydraulic conductivity map obtained from the hydraulic tomography conditioned by flowmeter analysis data.*

Figure 4.6 compares different drawdowns obtained on 5 boreholes in response to a pumping test in the new added prediction well P6. The drawdowns were simulated by using different hydraulic conductivity fields; the curves represented by solid red lines correspond to simulated drawdowns using true hydraulic conductivity; the curves represented by dotted black lines correspond to simulated drawdowns using inverted hydraulic conductivity obtained from hydraulic tomography using other pumping tests observation data (Figure 4.5a); the curves represented by dashed black lines correspond to simulated drawdowns using inverted hydraulic conductivity obtained from hydraulic tomography using other pumping tests observation data and conditioned by flowmeter data (Figure 4.5e). The results clearly show that the dashed lines (HT + flowmeter data) are closer to the solid red lines (true drawdown) compared to the dotted lines (classical HT). Such observation confirms that incorporating flowmeter data in the hydraulic tomography leads to better K estimates.

We also show a scatter plot of true hydraulic conductivity and estimated hydraulic conductivity in Figure 4.7. Each scatter plot has a linear model of data fitting represented by a red dashed line with a linear regression expression and a coefficient of determination. The solid line is the first bisector line

of  $y=x$ . Figure 4.7a shows the result of using pumping tests and an exponential covariance model. Figure 4.7b presents the result of hydraulic conductivity comparison based on flowmeter interpretation. The small bias toward high absolute values of hydraulic conductivities indicates that the effective hydraulic conductivity is overestimated by the interpolation of flowmeter profiles. When the interpreted hydraulic conductivity distribution from flowmeter is used as initial guess for the inversion, we observe that the characterization of hydraulic conductivity becomes considerably better (compare Figure 4.7c to Figure 4.7a). The incorporation of multiscale heterogeneity with the nested covariance model generates a different representation, but the hydraulic conductivity estimates is considerably improved as well (Figure 4.7d). This demonstrates the importance of integrating flowmeter data.

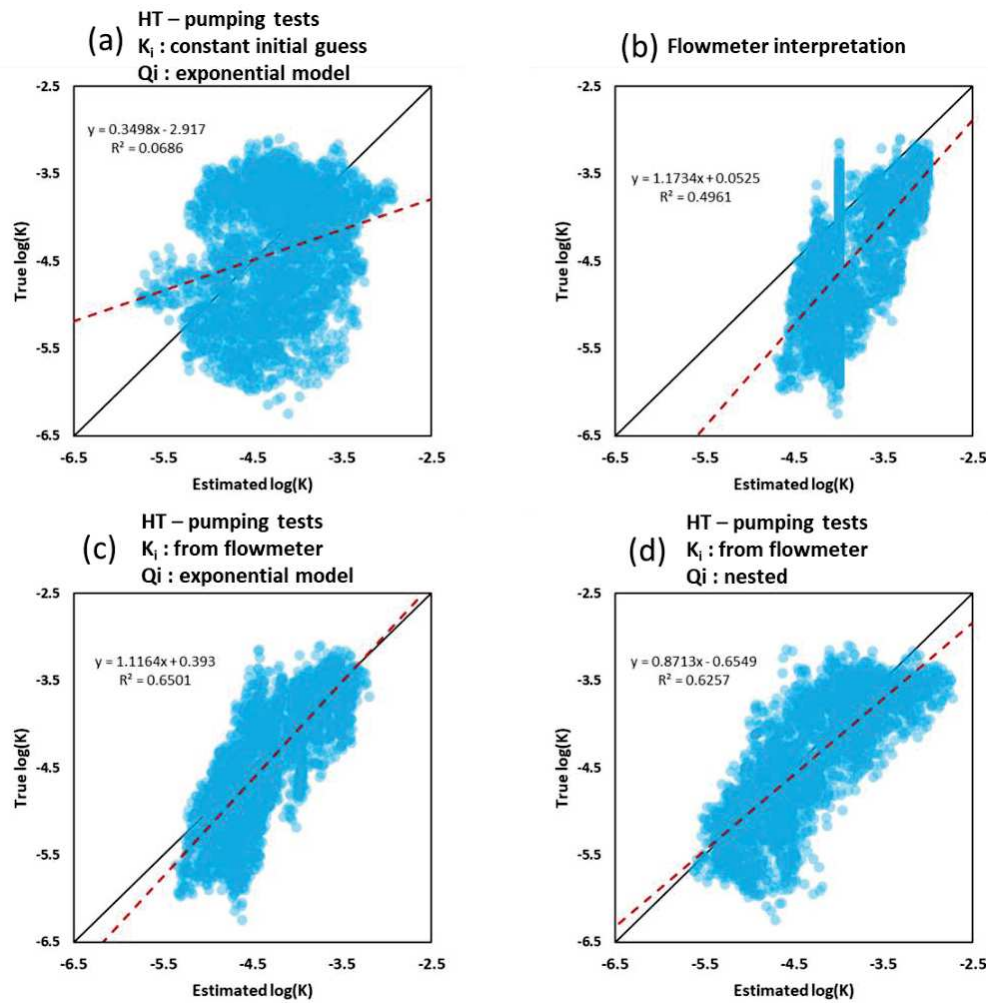


**Figure 4.7:** Two-dimensional validation case – scatterplots of true hydraulic conductivity versus estimated hydraulic conductivity for the different cases of the two-dimensional synthetic case. b) scatter plot of true  $K$  versus interpreted  $K$  from flowmeter. a, c and d are scatter plots of true  $K$  versus inverted  $K$  using different prior models.

## 4.5 Application

In this section, the approach is applied to an experimental field site on the basis of real field data. The experimental site is located in Southern France, 20 km northeast of Montpellier (Figure 4.8a). The site's aquifer is composed of mollusc shells of late Burdigalian. The deposit is a dune system constructed during Miocene's tidal currents. Within the experimental site, 13 vertical wells were drilled in a square of 50 m by 50 m in which full-diameter cores were obtained in borehole P6, P8 and P12 (Figure 4.8b). The wells have a depth of 30m and are fully-penetrating wells, since they crosscut the whole late Burdigalian, down to the roof of the mid Burdigalian which presents a very low permeability. The hydraulic conductivity measured using 330 one-inch diameter cores plugged from the full-diameter cores spans four orders of magnitude ( $10^{-8}$  to  $10^{-4}$ ). The preliminary analysis of hydrodynamic response to pumping test and slug tests (Wang et al., 2019) showed a pretty high lateral heterogeneity of the hydraulic conductivity field. Besides, both the well logs and laboratory measurements on cores, showed that the spatial distribution of the hydraulic conductivity field is constrained by a multilayered system (Figure 4.8c).

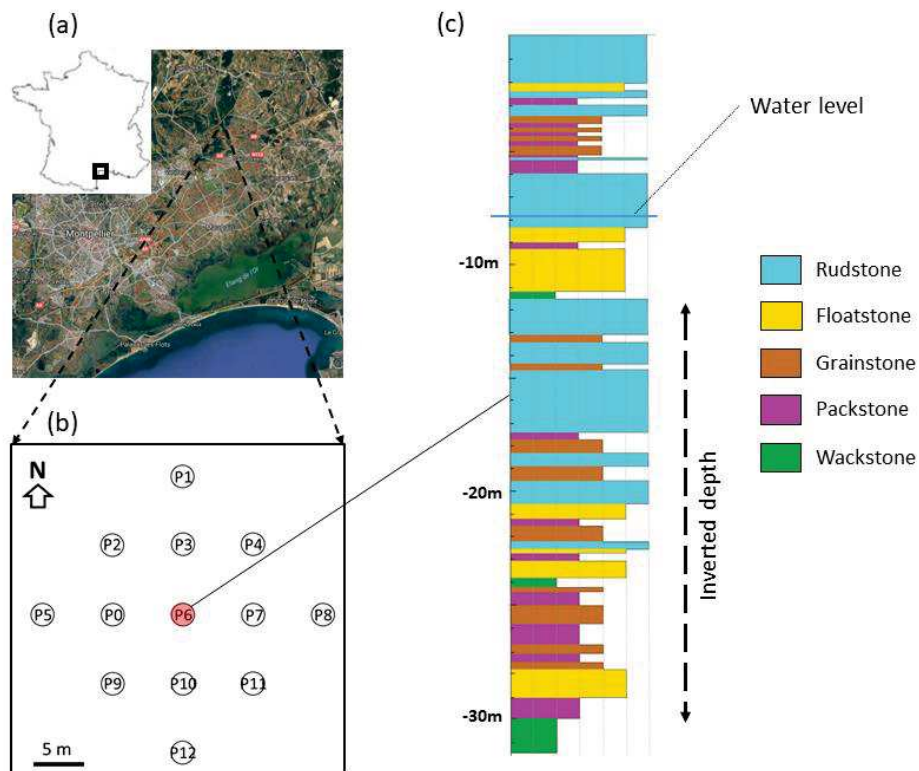


**Figure 4.8:** Experimental site composed of a multilayered system. a) geo-localization map, b) well pattern, c) log of P6 obtained from the core analysis.

### 4.5.1 Flowmeter implementation and analysis

A series of spinner flowmeter tests are performed in the experimental site. The flowmeter tests are performed in each well. As described in the methodology, the flow log is obtained in a well subject to a pumping where the pump is positioned close to the surface. We also point out that the pump needs to remain under water and, depending on the generated drawdown, the investigated depth will be limited. To maximize the investigated depth, a small pumping flow rate was used. A series of flowmeter sweeps are performed inside a PVC with static water in order to realize the tool calibration of spin-velocity conversion. The log of flow rate can be obtained by taking into consideration the well diameter changes along the depth. An example of flowmeter measurements and interpretation for hydraulic conductivity distribution may be found in the Appendix (Figure S3).

Considering that the total pumping flow rate comes under the pump, we can estimate the hydraulic conductivity log of the well as a function of the flow rate contribution of the different layers, once the effective hydraulic conductivity of the investigated depth of the aquifer is determined.

With the estimated hydraulic conductivity logs from the different wells, we fill the remaining space between them by interpolation, assuming that the distribution of the hydraulic properties in layers is continuous and correlated. A 3D hydraulic conductivity field is obtained.

### 4.5.2 Pumping tests data

13 pumping tests were performed in our experimental site during summer 2016. During each test, the transient responses are measured in all the wells for all the tests. The pumping tests were long enough to reach a pseudo-steady state response. We randomly choose 5 cross hole pumping tests to use as observations for the following application. Different times from early and middle parts of the response were sampled and used as the HT observations. We didn't sample from late time to avoid any instability that may come from the biased modelling of the uncertain regional heterogeneity and boundary conditions. From the well test analysis, the estimated effective permeability and specific storage of the test site are  $K_{\text{eff}} = 1.34\text{e-}4 \text{ m.s}^{-1}$  and  $S_s = 2.65\text{e-}5 \text{ m}^{-1}$ , which are used in the inversions.

### 4.5.3 Hydraulic tomography

The dimensions of the inverted domain are length=50 m, width=50 m and height=20 m; the dimensions of the buffer area are length=200 m, width=200 m and height=20 m. The outer boundaries are set to constant hydraulic head  $h_0=25 \text{ m}$  while the upper and lower boundaries (top and bottom) are set to no flow condition. The initial condition is set to a constant hydraulic head  $h_0=25 \text{ m}$  in the whole domain. A covariance matrix is constructed using the hydraulic conductivity field. In fact, a nested

covariance function for multiscale heterogeneity is used in order to perform the inversion. It allows to incorporate geological information to constrain the results (Zha et al. 2017). The nested covariance matrix constructed based on flowmeter data interpolation can be found in Figure S5 in Appendix. The statistical parameter used for the generating the covariance is provided in Table S2. Different facies are determined and, in each facies, a correlation is defined. The main objective is not to perfectly reproduce the drawdown responses, but to obtain a more realistic hydraulic property distribution with a good fitting of the observed drawdowns. The initial guess is constructed from flowmeter interpreted hydraulic conductivity field. A similar interpolation method as adopted in the synthetic inversion is used to interpolate the flowmeter data. The covariance matrix is built accordingly to flowmeter results; layers information is prioritized. The covariance is a result of a sum of different covariance matrices, one defines the layers, another represents the variance and correlation length inside each layer and the last one defines the variance and the correlation length of the whole domain.

For the experimental field case, we performed two inversion runs, the first one by a classical hydraulic tomography approach and we used only observation from the pumping tests, while in the second run, flowmeter interpretations were used to initialize the parameter and the covariance matrix. Figure 4.7 shows the inverted hydraulic conductivity for both cases; Figure 4.7a corresponds to the inverted hydraulic conductivity field with classical hydraulic tomography while Figure 4.7b corresponds to the inverted hydraulic conductivity field with hydraulic tomography conditioned by flowmeter data; Figures 4.7c and 4.7d are scatter plots of observations (hydraulic head measurements) data fitting obtained using respectively results from Figure 4.7a and 4.7b.

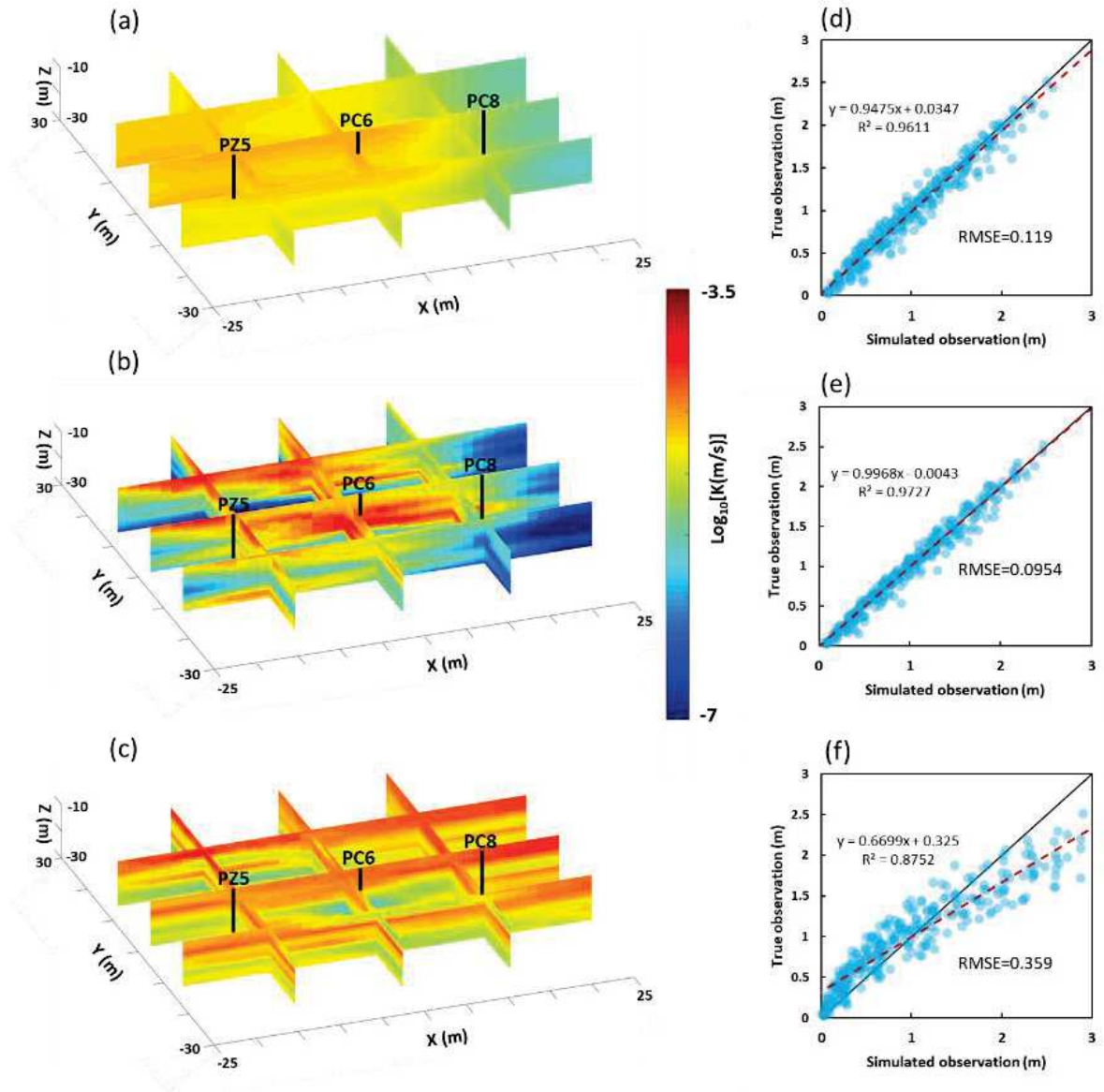


*Figure 4.9: Inverted hydraulic conductivity map and observation data fitting results from hydraulic tomography of real-case experimental site. a) inverted hydraulic conductivity map obtained from classical HT, b) inverted hydraulic conductivity map obtained from HT conditioned by flowmeter data, c) hydraulic conductivity map obtained from flowmeter interpretation, d) data fitting for classical HT results, e) data fitting for HT conditioned by flowmeter data, f) data fitting for flowmeter interpretation.*

## 4.6 Discussion

Incorporating flowmeter data into hydraulic tomography allows to obtain a better K estimate in the synthetic validation cases. For the 2D validation case, the results (see Figure 4.3) show that initializing the parameter and the covariance matrix with flowmeter interpretation data provides better K estimates. The initial parameter value can play an important role on converging to a different K estimate solution. Such an effect can be observed on the inverted hydraulic conductivity when flowmeter

estimate was used to initialize the parameter (Figure 4.3c). On the other hand, the initial covariance matrix can also contain layers' information by correlating the cells that belong to the same layer. However, the correlation constraint can be strong on the K estimate especially when the covariance remains unchanged and equal to the initial (Figure 4.3e). The covariance of unknown parameter can be updated to derive the residual covariance, the continuous updating of residual covariance allows to correctly address the uncertainty and enhance convergence of the inverse solution (Zha et al. 2018) which can be confirmed with the results in Figure 4.3f.

The approach of integrating flowmeter data was also tested using synthetic case in three dimensions and results (see Figure 4.5) are in total agreement with the 2D case observations. For this case, we also showed the quality of the result by simulating drawdown curves in a prediction well (which was not included in observation wells) using the inverted hydraulic conductivity field and compared them with the true observed drawdown (see Figure 4.6). It clearly shows how flowmeter data adds a non-redundant vertical profile information and, thus, enhance considerably the K estimates. In the present study, we focused on reconstructing K distributions by keeping  $S_s$  as a constant. Although previous studies have shown that the selection of  $S_s$  value may impact the K estimates (Castagna et al., 2011; Zhao et al., 2021), our interpretation of field site single-hole and cross-hole pumping tests did not indicate a strong variation of  $S_s$ . For this reason, we think the treatment is reasonable. However, in the future, we attempt to perform a full inversion to simultaneously estimate the spatial distribution of both K and  $S_s$ . These would require more pumping test data points to be sampled and used in the inversion as the inclusion of  $S_s$  distribution would double the number of unknown parameters, which increases drastically the underdetermined-ness of the inversion problem.

Figure 4.9 summarizes the results of the approach applied to a real field case. The two inverted hydraulic conductivity fields are totally different from each other while their data fitting are quite similar. K estimates obtained from HT conditioned by flowmeter data exhibits a multilayered system with more geological realism comparing to K estimates obtained from classical HT without any additional profile information. The same layering system has been observed in other measurements (core analysis, logs, permeameter measurements, etc.).

The data fitting in both inversions is relatively similar (RMSE = 0.0912 for HT using pumping tests data and RMSE = 0.0874 for HT using pumping tests and flowmeter data). However, the prediction of transient drawdowns becomes significantly better using K estimate obtained with the incorporation of flux measurements data. For further validation, we sampled hydraulic conductivity values from inversion results and we compared them to some available permeameter measurements at the same locations. Within the 13 wells available in the experimental site, three (PC6, PC8 and PC12) were cored. Cores allowed to obtain a permeability log from laboratory permeameter measurements along the wells. Figure 4.8 shows a comparison of extracted conductivity from THT results and laboratory permeability

measurements (converted into hydraulic conductivity using water density  $\rho=1000 \text{ kg m}^{-3}$ , water viscosity  $\mu=0.001 \text{ kg m}^{-1} \text{ s}^{-1}$  and gravity acceleration  $g=9.81 \text{ m s}^{-2}$ ) of plugs on the cored wells as well as the flowmeter interpreted hydraulic conductivity.

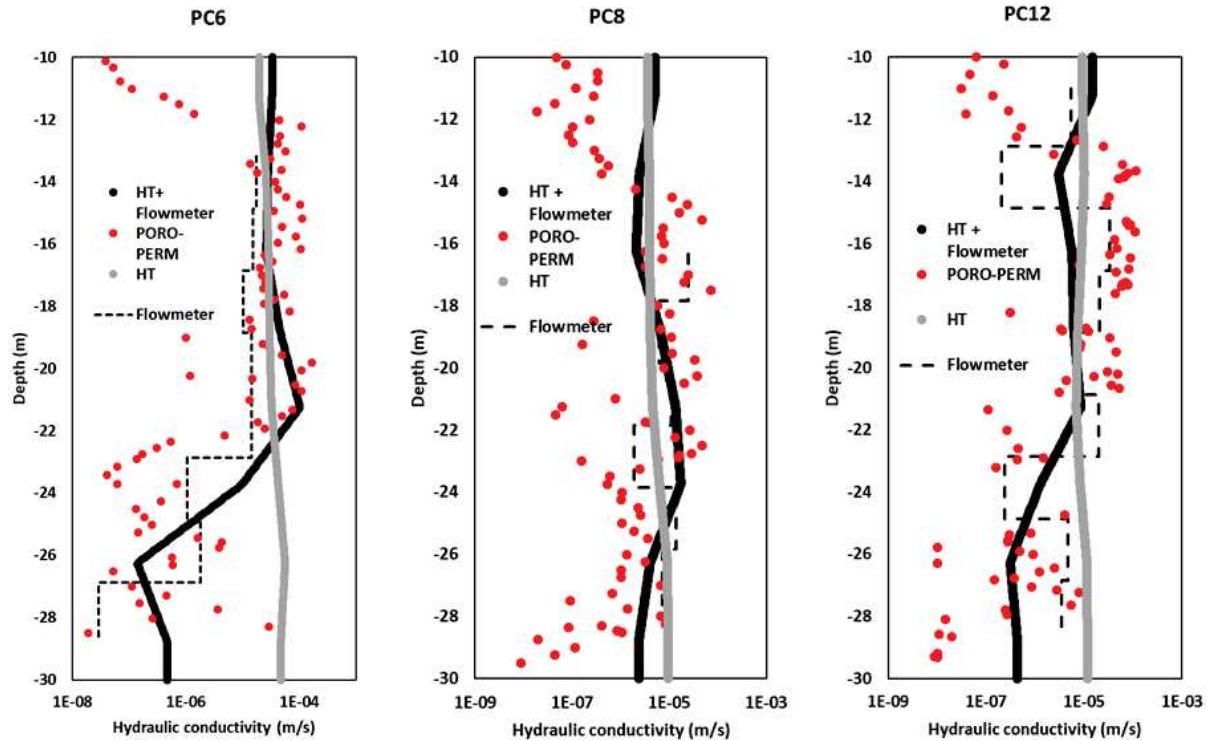


*Figure 4.10: Hydraulic conductivity profiles for wells PC6, PC8 and PC12 of the experimental site. Red dots are laboratory measurements. Grey solid line is extracted from THT results. Black solid line is extracted from THT integrating flowmeter analysis data results. Dashed line is from flowmeter interpretation.*

Figure 4.10 strengthens the fact that flowmeter data enhance HT results, especially in the vertical profiles of the hydraulic conductivity estimates. Flowmeter conditioning data allows the K estimate to get closer to the measured permeability from the plugs of the cored wells. Hydraulic conductivity profiles in the wells obtained from transient hydraulic tomography (Figure 4.10, grey solid line), show that normal pumping tests do not contain vertical information about the aquifer's hydraulic properties; the hydraulic conductivity profiles are similar to a result of a 2D THT extruded into the third dimension (depth averaged values).

Our work is in agreement with other previous works in terms of how flux measurements enhance hydraulic tomography results. The work of Li et al. (2008) showed that inverting both steady state hydraulic head measurements and flux measurements data leads to better hydraulic conductivity estimates. They used both data in the inverse process as conditioning observations. However, in this work, only transient hydraulic head measurements are used to condition the inversion and flowmeter tests data are used to initialize the prior inputs of the inversion. Our results show that incorporating

flowmeter data in the initial parameter and the prior covariance matrix may be sufficient to enhance considerably the K estimates. Zha et al. (2014) and Tso et al. (2016) also worked on combining flux measurements with pumping tests data. Zha et al. (2014) inverted synthetic case in 2D by using normal pumping tests and used lateral fluxes as an additional data to strengthen the result and Tso et al. (2016) extended it to 3D by using the same observation datasets. They both showed that flux data improves estimates resolution of HT analysis. The difference between the two studies is the dimension and the fact that Zha et al. (2014) used it to characterize a discrete fracture network while Tso et al. (2016) investigated a porous media instead. However, both studies were not tested on any real case study.

## 4.7 Summary and conclusions

In this study, we performed a transient hydraulic tomography of cross-hole pumping tests by integrating flowmeter data in prior inputs on an experimental site and managed a 3D imaging of the aquifer system that was coherent with geological observations and existing permeability measurements. We used flowmeter data as source of the vertical information additional to pumping tests that provides the lateral information. In order to incorporate the vertical data into hydraulic tomography, flowmeter tests are interpreted separately to obtain a prior K estimate which was used to initialize the parameter and the covariance matrix. While, the pumping tests observations were used to condition the inversion convergence process. Using different initial parameters and initial covariance matrices showed that the prior inputs of the inversion are important and can modify the result considerably. Also, the non-packer pumping tests do not contain vertical information: the inverted hydraulic conductivity using only pumping tests was generally constant along the vertical profile. The integration of vertical hydrogeological information obtained from flowmeter surveys and horizontal information from cross-hole pumping tests allow a 3D transient hydraulic tomographic (THT) characterization of sedimentary layered rocks. Flowmeter data are a non-redundant information and different data other than flowmeter could also be used to better define the variations of vertical hydraulic conductivity such as laboratory measurements on cored wells or classical logs that are able to be converted into relative conductivity profiles.

## References

- Berg, S. J., and W. A. Illman (2011), Three-dimensional transient hydraulic tomography in a highly heterogeneous glaciofluvial aquifer-aquitard system, *Water Resour. Res.*, 47, W10507, doi:10.1029/2011WR010616.
- Bohling, G. C., Zhan, X., Butler, J. J., and Zheng, L., Steady shape analysis of tomographic pumping tests for characterization of aquifer heterogeneities, *Water Resour. Res.*, 38(12), 1324, doi:10.1029/2001WR001176, 2002.
- Bohling, G. C., Butler Jr., J. J., Zhan, X., and Knoll, M. D. (2007), A field assessment of the value of steady shape hydraulic tomography for characterization of aquifer heterogeneities, *Water Resour. Res.*, 43, W05430, doi:10.1029/2006WR004932.
- Bohling, G.C. and Butler, J.J., Jr. (2010), Inherent Limitations of Hydraulic Tomography. *Groundwater*, 48: 809-824. <https://doi.org/10.1111/j.1745-6584.2010.00757.x>
- Brauchler, R., R. Hu, P. Dietrich, and M. Sauter (2011), A field assessment of high-resolution aquifer characterization based on hydraulic travel time and hydraulic attenuation tomography, *Water Resour. Res.*, 47, W03503, doi:10.1029/2010WR009635.
- Brauchler, R., R. Hu, L. Hu, S. Jimenez, P. Bayer, P. Dietrich, and T. Ptak (2013), Rapid field application of hydraulic tomography for resolving aquifer heterogeneity in unconsolidated sediments, *Water Resour. Res.*, 49, 2013–2024, doi:10.1002/wrcr.20181.
- Butler, J. J., McElwee, C. D., and Bohling, G. C. (1999), Pumping tests in networks of multilevel sampling wells: Motivation and methodology, *Water Resour. Res.*, 35(11), 3553–3560, doi:10.1029/1999WR900231.
- Cardiff, M., W. Barrash, P. K. Kitanidis, B. Malama, A. Revil, S. Straface, and E. Rizzo (2009), A potential-based inversion of unconfined steady-state hydraulic tomography, *Ground Water*, 47(2), 259–270, doi:10.1111/j.1745-6584.2008.00541.x
- Cardiff, M., Barrash, W., and Kitanidis, P. K. (2012), A field proof-of-concept of aquifer imaging using 3-D transient hydraulic tomography with modular, temporarily-emplaced equipment, *Water Resour. Res.*, 48, W05531, doi:10.1029/2011WR011704.
- Chen, J.S., S. Hubbard, and Y. Rubin. 2001. Estimating the hydraulic conductivity at the South Oyster Site from geo-physical tomographic data using Bayesian techniques based on the normal linear regression model. *Water Resources Research* 37, no. 6: 1603–1613
- Cooper, H. H., and Jacob, C. E. (1946), A generalized graphical method for evaluating formation constants and summarizing well-field history, *Eos Trans. AGU*, 27(4), 526–534, doi:10.1029/TR027i004p00526
- Day-Lewis, F.D., Johnson, C.D., Paillet, F.L. and Halford, K.J. (2011), A Computer Program for Flow-Log Analysis of Single Holes (FLASH). *Groundwater*, 49: 926-931. <https://doi.org/10.1111/j.1745-6584.2011.00798.x>
- De Clercq T., A. Jardani, P. Fischer, L. Thanberger, T.M. Vu, D. Pitaval, J.-M. Côme, P. Begassat. 2020. The use of electrical resistivity tomograms as a parameterization for the hydraulic characterization of a contaminated aquifer. *Journal of Hydrology* 587: 124986.
- Fienen, M.N., P.K. Kitanidis, D. Watson, and P. Jardine. 2004. An application of Bayesian inverse methods to vertical de-convolution of hydraulic conductivity in a heterogeneous aquifer at Oak Ridge National Laboratory. *Mathematical Geology* 36, no. 1: 101–126.

- Fischer P., Jardani A., Jourde H., Hydraulic tomography in coupled discrete-continuum concept to image hydraulic properties of a fractured and karstified aquifer (Lez aquifer, France) *Adv. Water Resour.*, 137 (2020), p. 103523, 10.1016/j.advwatres.2020.103523
- Gottlieb, J., and P. Dietrich. 1995. Identification of the permeability distribution in soil by hydraulic tomography. *Inverse Problems* 11, no. 2: 353–360.
- Hubbard S.S., Rubin Y. (2005) Introduction to Hydrogeophysics. In: Rubin Y., Hubbard S.S. (eds) *Hydrogeophysics*. Water Science and Technology Library, vol 50. Springer, Dordrecht. [https://doi.org/10.1007/1-4020-3102-5\\_1](https://doi.org/10.1007/1-4020-3102-5_1)
- Illman, W.A., X. Liu, and A. Craig. 2007. Steady-state hydraulic tomography in a laboratory aquifer with deterministic heterogeneity: Multi-method and multiscale validation of hydraulic conductivity tomograms, *Journal of Hydrology* 341, no. 3–4: 222–234
- Illman, W. A., Zhu, J., Craig, A. J., and Yin, D. (2010), Comparison of aquifer characterization approaches through steady state groundwater model validation: A controlled laboratory sandbox study, *Water Resour. Res.*, 46, W04502, doi:10.1029/2009WR007745.
- Javandel, I., and P.A. Witherspoon. 1969. A method of analyzing transient fluid flow in multilayered aquifer. *Water Resources Research* 5, no. 4: 856–869.
- Kabala, Z. J. (1994), Measuring distributions of hydraulic conductivity and specific storativity by the double flowmeter test, *Water Resour. Res.*, 30(3), 685–690, doi:10.1029/93WR03104
- Kitanidis, P.K. 1995. Quasi-linear geostatistical theory for inversion. *Water Resources Research* 31, no. 10: 2411–2419.
- Kitanidis, P. K., and Lee, J. (2014), Principal Component Geostatistical Approach for large dimensional inverse problems, *Water Resour. Res.*, 50, 5428–5443, doi:10.1002/2013WR014630.
- Klepikova, M. V., Le Borgne, T., Bour, O., and de Dreuzy, J.-R. (2013), Inverse modeling of flow tomography experiments in fractured media, *Water Resour. Res.*, 49, 7255–7265, doi:10.1002/2013WR013722.
- Li, W., Englert, A., Cirpka, O.A. and Vereecken, H. (2008), Three-Dimensional Geostatistical Inversion of Flowmeter and Pumping Test Data. *Groundwater*, 46: 193-201. <https://doi.org/10.1111/j.1745-6584.2007.00419.x>
- Liu, S., T.-C. J. Yeh, and R. Gardiner (2002), Effectiveness of hydraulic tomography: Sandbox experiments, *Water Resour. Res.*, 38(4), 1034, doi:10.1029/2001WR000338
- Liu, X., Illman, W. A., Craig, A. J., Zhu, J., and Yeh, T.-C. J. (2007), Laboratory sandbox validation of transient hydraulic tomography, *Water Resour. Res.*, 43, W05404, doi:10.1029/2006WR005144.
- Mao, D., T.-C. J. Yeh, L. Wan, C.-H. Lee, K.-C. Hsu, J.-C. Wen, and W. Lu (2013a), Cross-correlation analysis and information content of observed heads during pumping in unconfined aquifers, *Water Resour. Res.*, 49, 713–731, doi:10.1002/wrcr.20066.
- Mao, D., T.-C. J. Yeh, L. Wan, K.-C. Hsu, C.-H. Lee, and J.-C. Wen (2013b), Necessary conditions for inverse modeling of flow through variably saturated porous media, *Adv. Water Resour.*, 52, 50–61, doi:10.1016/j.advwatres.2012.08.001.

- Molz, F. J., Morin, R. H., Hess, A. E., Melville, J. G., and Güven, O. (1989), The Impeller Meter for measuring aquifer permeability variations: Evaluation and comparison with other tests, *Water Resour. Res.*, 25( 7), 1677– 1683, doi:10.1029/WR025i007p01677.
- Molz, F.J., G.K. Boman, S.C. Young, and W.R. Waldrop. 1994. Borehole flowmeters: Field application and data analysis. *Journal of Hydrology* 163, no. 4: 347–371.
- Paillet, F. L. (1998), Flow modeling and permeability estimation using borehole flow logs in heterogeneous fractured formations, *Water Resour. Res.*, 34( 5), 997– 1010, doi:10.1029/98WR00268.
- Paillet, F.L. and Reese, R.S. (2000), Integrating Borehole Logs and Aquifer Tests in Aquifer Characterization. *Groundwater*, 38: 713-725. <https://doi.org/10.1111/j.1745-6584.2000.tb02707.x>
- Paul Constantine (2021). Random Field Simulation (<https://www.mathworks.com/matlabcentral/fileexchange/27613-random-field-simulation>), MATLAB Central File Exchange. Retrieved July 19, 2021.
- Räss, L., Kolyukhin, D., Minakov, A. (2019). Efficient parallel random field generator for large 3-D geophysical problems. *Computers & Geosciences* 131, 158-169
- Rehfeldt, K. R., J. M. Boggs, and L. W. Gelhar (1992), Field study of dispersion in a heterogeneous aquifer: 3. Geostatistical analysis of hydraulic conductivity, *Water Resour. Res.*, 28(12), 3309–3324, doi:10.1029/92WR01758.
- Roubinet D., Irving J., Day-Lewis F.D., Development of a new semi-analytical model for cross-borehole flow experiments in fractured media *Adv. Water Res.*, 76 (2015), pp. 97-108, 10.1016/j.advwatres.2014.12.002
- Soueid Ahmed, A., Zhou, J. Jardani, A., Revil, A., Dupont, J.P., Image-guided inversion in steady-state hydraulic tomography *Adv. Water Resour.*, 82 (2015), pp. 83-97, 10.1016/j.advwatres.2015.04.001.
- Tamayo-Mas, M. Bianchi, M. Mansour Impact of model complexity and multi-scale data integration on the estimation of hydrogeological parameters in a dual-porosity aquifer *Hydrogeol. J.*, 26 (6) (2018), pp. 1917-1933, 10.1007/s10040-018-1745-y
- Theis, C. V. (1935), The relation between the lowering of the Piezometric surface and the rate and duration of discharge of a well using ground-water storage, *Eos Trans. AGU*, 16( 2), 519– 524, doi:10.1029/TR016i002p00519.
- Tso, M., C.-H., Zha, Y., J. Yeh, T.-C., and Wen, J.-C. (2016), The relative importance of head, flux, and prior information in hydraulic tomography analysis, *Water Resour. Res.*, 52, 3– 20, doi:10.1002/2015WR017191.
- Wang, X., Jourde, H., Aliouache, M., Massonnat, G., Characterization of horizontal transmissivity anisotropy using cross-hole slug tests, *J. Hydrol.*, 564 (2018), pp. 89-98, 10.1016/j.jhydrol.2018.06.068
- Wen, J.-C., Chen, J.-L., Yeh, T.-C.J., Wang, Y.-L., Huang, S.-Y., Tian, Z. and Yu, C.-Y. (2020), Redundant and Nonredundant Information for Model Calibration or Hydraulic Tomography. *Groundwater*, 58: 79-92. <https://doi.org/10.1111/gwat.12879>
- Williams, J., and F. Paillet (2002), Using flowmeter pulse tests to define hydraulic connections in the subsurface: A fractured shale example, *J. Hydrol.*, 265, 100–117.

- Yeh, T.-C., Mas-Pla, J., Williams, T. M., and McCarthy, J. F. (1995), Observation and Three-Dimensional Simulation of Chloride Plumes in a Sandy Aquifer Under Forced-Gradient Conditions, *Water Resour. Res.*, 31( 9), 2141– 2157, doi:10.1029/95WR01947.
- Yeh, T.-C., M. Jin, and S. Hanna, An iterative stochastic inverse method: Conditional effective transmissivity and hydraulic head fields, *Water Resour. Res.*, 32(1), 85-92, 1996
- Yeh, T.-C. J., and Liu, S. (2000), Hydraulic tomography: Development of a new aquifer test method, *Water Resour. Res.*, 36( 8), 2095– 2105, doi:10.1029/2000WR900114.
- Yeh, T.-C. J., D. Mao, L. Wan, C.-H. Lee, J.-C. Wen, and K.-C. Hsu (2011), Well Definedness, Scale Consistency, and Resolution Issues in Groundwater Model Parameter Identification, *Dep. of Hydrol. and Water Resour.*, Univ. of Ariz., Tucson.
- Yeh, T.-C. J., R. Khaleel, and K. C. Carroll (2015a), *Flow Through Heterogeneous Geologic Media*, Cambridge Univ. Press, Cambridge, U. K.
- Yeh, T.-C. J., D. Mao, L. Wan, C.-H. Lee, J.-C. Wen, and K.-C. Hsu (2015b), Well definedness, scale consistency, and resolution issues in groundwater model parameter identification, *Water Sci. Eng.*, 8(3), 175–194, doi:10.1016/j.wse.2015.08.002.
- Zha, Y., T.-C. J. Yeh, D. Mao, J. Yang, and W. Lu (2014), Usefulness of flux measurements during hydraulic tomographic survey for mapping hydraulic conductivity distribution in a fractured medium, *Adv. Water Resour.*, 71, 162–176, doi:10.1016/j.advwatres.2014.06.008.
- Zha, Y., Yeh, T.-C.J., Illman, W.A., Tanaka, T., Bruines, P., Onoe, H., Saegusa, H., Mao, D., Takeuchi, S. and Wen, J.-C. (2016), An Application of Hydraulic Tomography to a Large-Scale Fractured Granite Site, Mizunami, Japan. *Groundwater*, 54: 793-804. <https://doi.org/10.1111/gwat.12421>
- Zha, Y., Yeh, T.-C. J., Illman, W. A., Onoe, H., Mok, C. M. W., Wen, J.-C., Huang, S.-Y., and Wang, W. (2017), Incorporating geologic information into hydraulic tomography: A general framework based on geostatistical approach, *Water Resour. Res.*, 53, 2850– 2876, doi:10.1002/2016WR019185.
- Zha, Y., Yeh, T.-C. J., Illman, W. A., Zeng, W., Zhang, Y., Sun, F., et al. (2018). A reduced-order successive linear estimator for geostatistical inversion and its application in hydraulic tomography. *Water Resources Research*, 54, 1616– 1632. <https://doi.org/10.1002/2017WR021884>
- Zhao,Z.,Illman,W.A.,Berg,S.J.,2016.On the importance of geological data for hydraulic tomography analysis: laboratory sandbox study. *J.Hydrol.*<https://doi.org/10.1016/j.jhydrol.2016.08.061>
- Zhao, Z., and W. A. Illman (2017), On the Importance of Geological Data for Three-dimensional Steady-State Hydraulic Tomography Analysis at a Highly Heterogeneous Aquifer-Aquitard System. *J. Hydrol.*, 544, 640– 657
- Zheng, C. and Gorelick, S.M. (2003), Analysis of Solute Transport in Flow Fields Influenced by Preferential Flowpaths at the Decimeter Scale. *Groundwater*, 41: 142-155. <https://doi.org/10.1111/j.1745-6584.2003.tb02578.x>
- Zhu, J., and T.-C. J. Yeh (2006), Analysis of hydraulic tomography using temporal moments of drawdown recovery data, *Water Resour. Res.*, 42, W02403, doi:10.1029/2005WR004309
- Zhu, J., and Yeh, T.-C. J. (2005), Characterization of aquifer heterogeneity using transient hydraulic tomography, *Water Resour. Res.*, 41, W07028, doi:10.1029/2004WR003790.

Zlotnik, V.A., and B.R. Zurbuchen. 2003. Estimation of hydraulic conductivity from borehole flowmeter tests considering head losses. *Journal of Hydrology* 281, no. 1–2: 115–128.

<sup>[1]</sup> COMSOL Multiphysics® v. 5.6. [www.comsol.com](http://www.comsol.com). COMSOL AB, Stockholm, Sweden.

## Appendix

### Supplementary material for chapter 4

**Table S1.** Model and parameters used in random field generation

Parameter	2D case	3D case
Model	Exponential	Exponential
Standard deviation	1.5	1.5
Correlation length in x direction	100	100
Correlation length in y direction	5	100
Correlation length in z direction	-	10

**Table S2:** Model and parameters used to construct one covariance of the total nested covariance matrix.

parameter	value
Correlation function	exponential
Standard deviation	1
Correlation length in x direction $L_x$	20
Correlation length in y direction $L_y$	20
Correlation length in z direction $L_z$	5

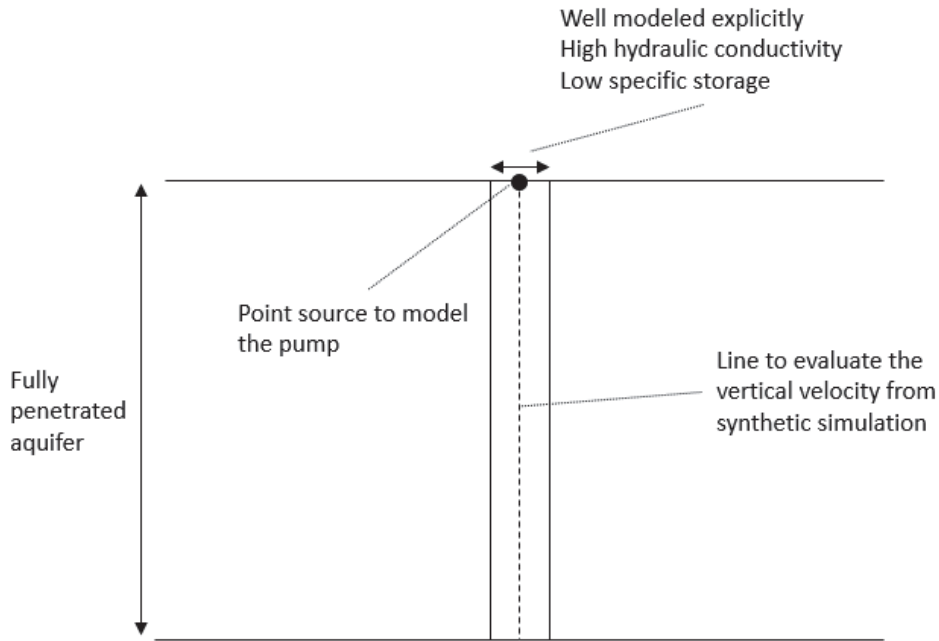


Figure S1. Illustration of flowmeter data simulation.

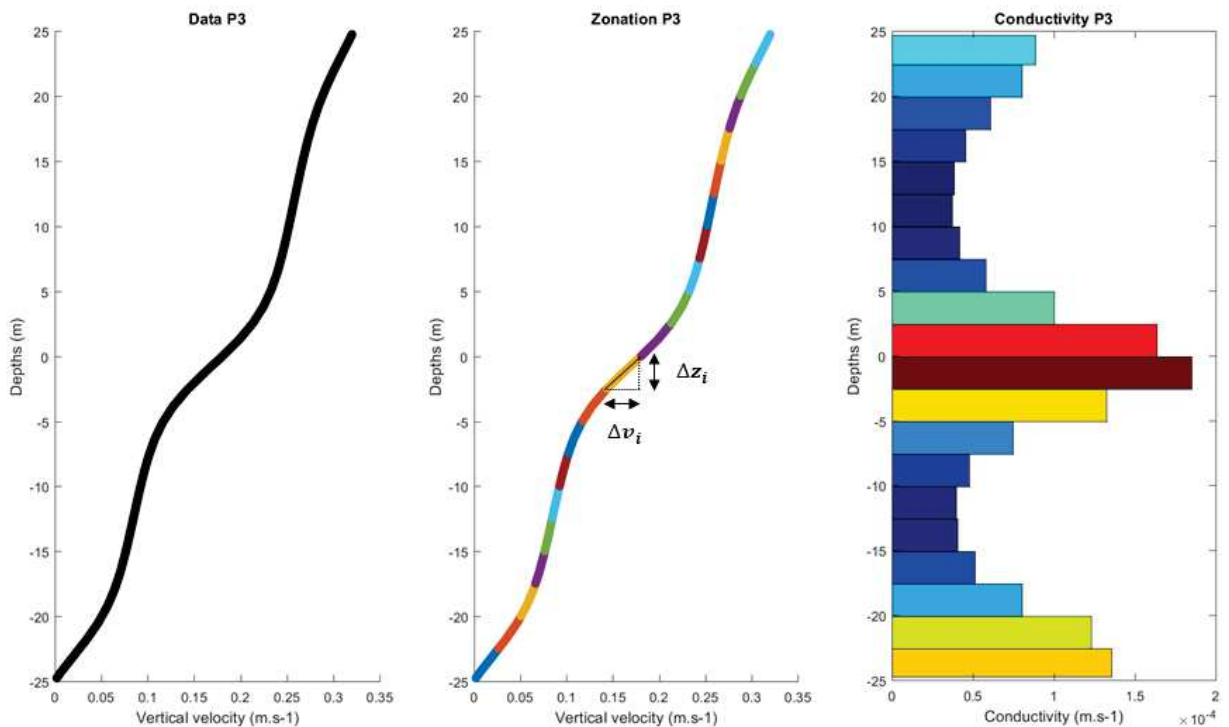


Figure S2. An illustration of flowmeter interpretation. (a) Simulated vertical velocity representing flowmeter measurements; (b) Zonation of data in vertical direction. and (c) Interpreted hydraulic conductivity distribution.

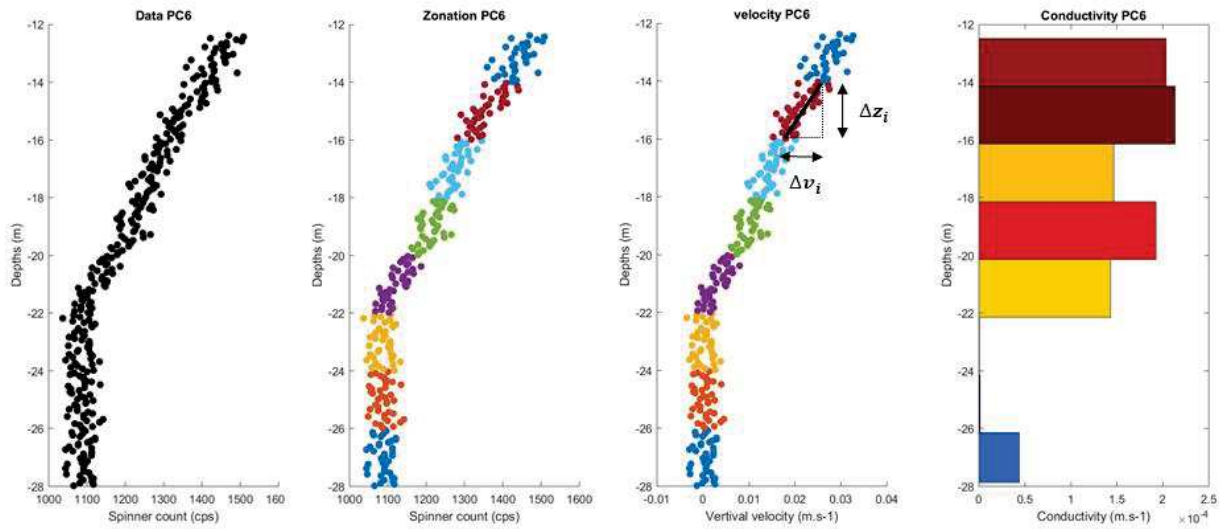


Figure S3. Example of interpretation of flowmeter data obtained from the test site.

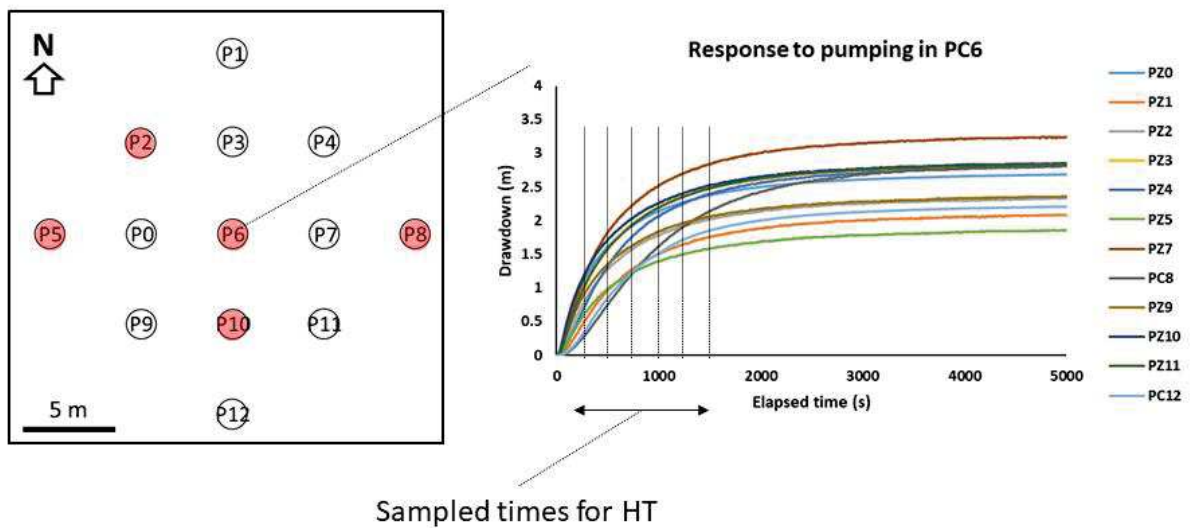
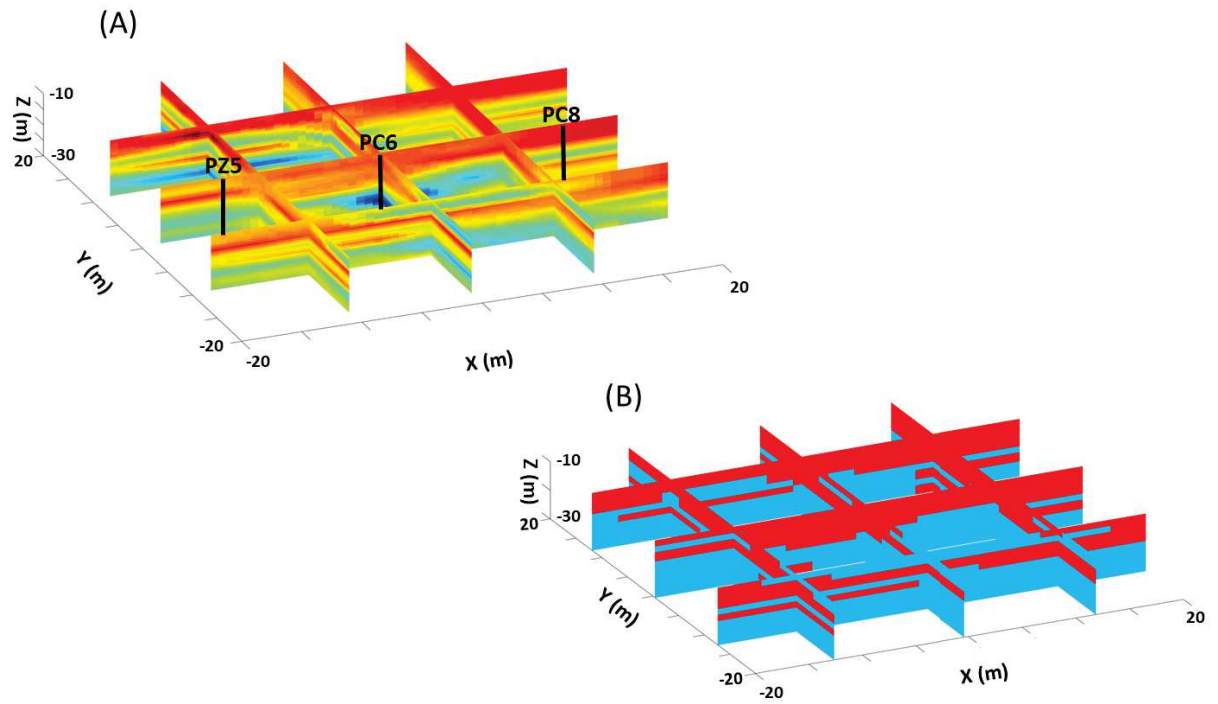
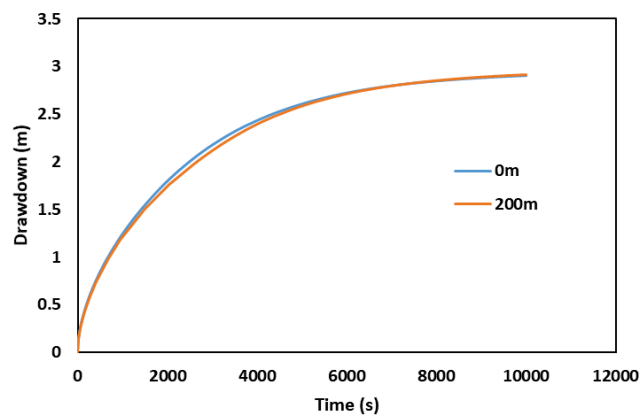


Figure S4. Sampling of drawdown data for real field HT



**Figure S5.** Interpolated hydraulic conductivity field from flowmeter data analyses (A) and the constructed facies (B)



**Figure S6.** Comparison of modeled drawdown with zero and non-zero initial hydraulic head assumed in the model domain.

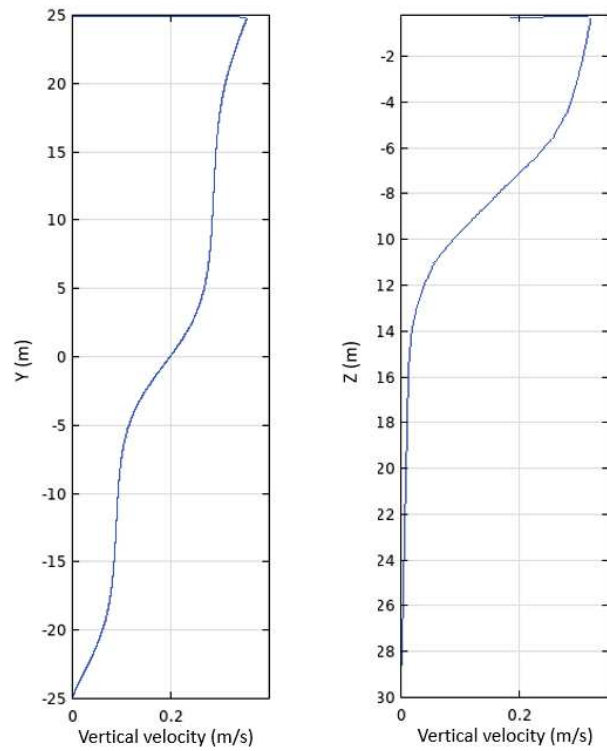
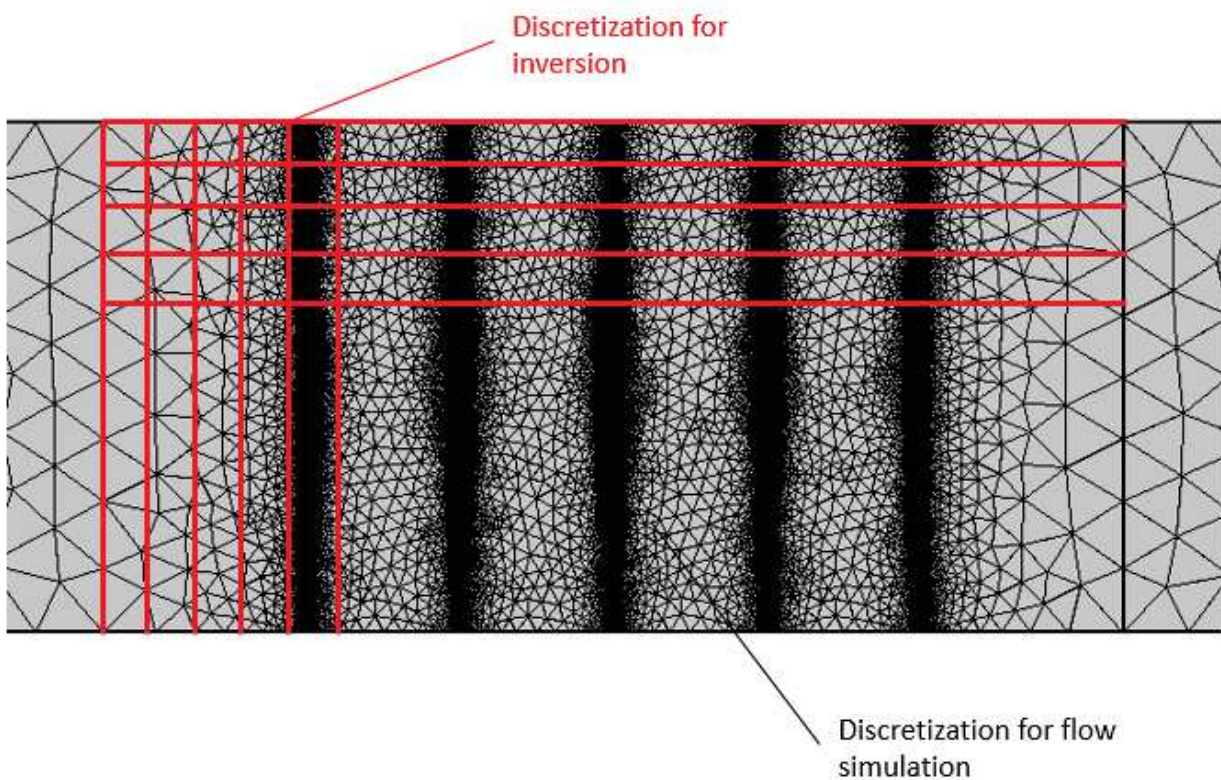


**Figure S7.** Example of simulated flowmeter measurements (vertical velocity) for the (left) 2D and (right) 3D synthetic cases.

A)



B)

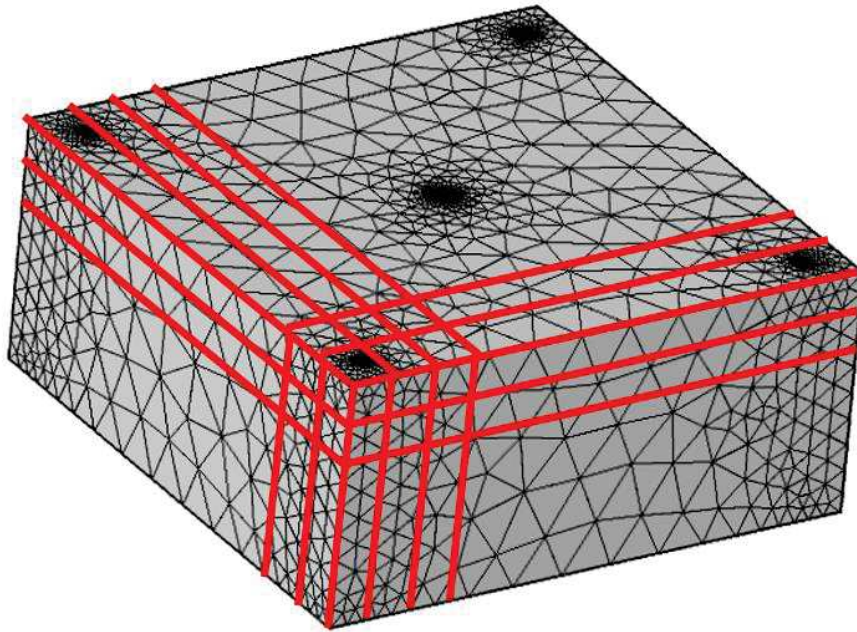


**Figure S8.** Mesh of inverted domain used during flow simulation (finite element) and hydraulic tomography (structured mesh) for (A) two-dimensional and (B) three dimensional cases.

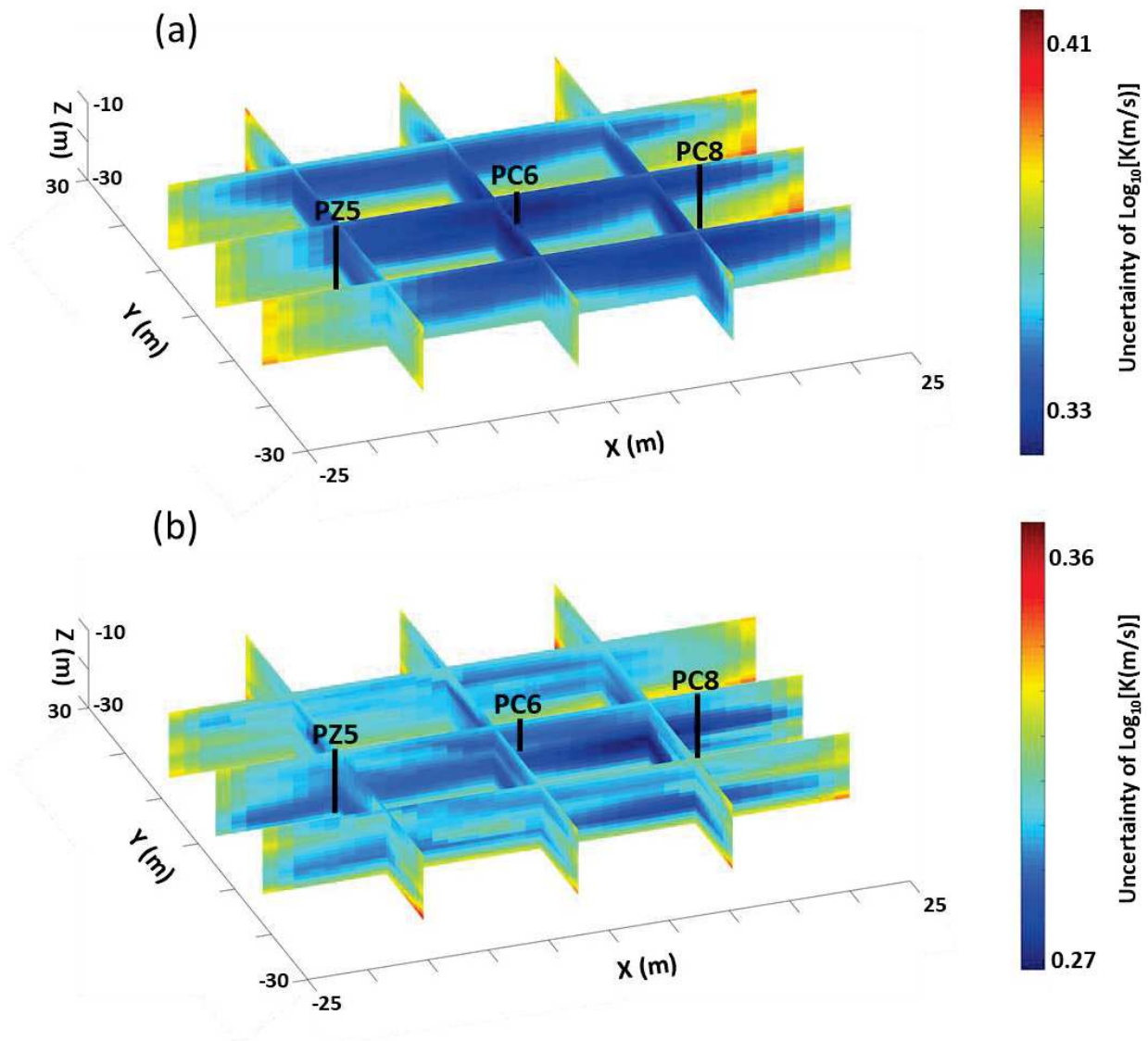


**Figure S9:** Uncertainty analyses of the estimated hydraulic conductivity for the real field case. A) Uncertainty of  $K$  estimate from hydraulic tomography. B) Uncertainty of  $K$  estimate from hydraulic tomography using a nested covariance constructed using flowmeter analyses data.

## CHAPTER 5

**Résumé :** Le passage de données synthétiques à des données réelles pour l'application de ces techniques d'inversion est souvent accompagné d'instabilités numériques généralement traitées au moyen d'approches d'inversion spécifiques (considération d'une zone tampon dans les modèles, non-considération des données acquises pour des temps longs). Ces techniques d'inversion sont également assujetties à des problématiques d'équifinalité puisque plusieurs solutions permettent parfois de simuler correctement les données hydrauliques (solution non unique). Dans le présent travail de doctorat, nous avons proposé une approche permettant de limiter ces instabilités, sans pour autant éliminer les données à l'origine de celles-ci. L'inversion des réponses hydrodynamiques transitoires présentait une forte instabilité lorsque les données pour des temps longs étaient prises en compte. Afin de limiter ces instabilités, différentes approches ont été utilisées, celles-ci ayant par ailleurs permis de montrer que les réponses hydrauliques sur les temps longs étaient contrôlées par les conditions aux limites du système mais également par la présence d'hétérogénéités à plus grande échelle (échelle régionale). Fort de ce constat, des investigations complémentaires ont permis de proposer une méthode d'inversion stable sur le plan numérique et permettant d'apprécier les propriétés hydrauliques associées aux hétérogénéités à l'échelle régionale.



5. HYDRAULIC TOMOGRAPHY CONSIDERING  
REGIONAL HETEROGENEITIES THROUGH LATE TIME  
PUMPING TESTS DATA



## HYDRAULIC TOMOGRAPHY CONSIDERING REGIONAL HETEROGENEITIES THROUGH LATE TIME PUMPING TESTS DATA

Mohammed Aliouache<sup>a,\*</sup>, Xiaoguang Wang<sup>b</sup>, Pierre Fischer<sup>a</sup>, Gerard Massonnat<sup>c</sup>, Herve Jourde<sup>a</sup>

<sup>a</sup> *Laboratoires Hydrosiences Montpellier, UMR 5151 CNRS-UM-IRD, Montpellier, France, 34000*

<sup>b</sup> *Chengdu University of Technology, Sichuan, China, 610059*

<sup>c</sup> *CSTJF-PAU Total Energies, Avenue Larribau, Pau, France, 64000*

\*Correspondence: [mohammed.aliouache@umontpellier.fr](mailto:mohammed.aliouache@umontpellier.fr)

### Highlights

1. We investigate inversion instability issues from ill-posed forward model
2. We propose a multi-grid framework for stabilizing the inverse problem
3. The approach is tested on a real field application

## 5.1 Abstract

Hydraulic tomography (HT) has been proved as an effective approach for estimating heterogeneous aquifer properties (e.g., hydraulic conductivity and storativity) in the last decade. The technique is highly performant in synthetic studies, but, the transition from synthetic models to real field applications often exhibits numerical instabilities. The inversion techniques can also suffer from non-uniqueness of the estimates since several solutions might correctly mimic the observed hydraulic data. In this work, we investigate the origin of the instabilities observed when trying to perform HT using real field drawdown data; this study focuses on drawdown transient data acquired on an experimental site that show a strong inversion instability if a simple forward model is used. We firstly identify the cause of these instabilities. We then use different approaches, where one is proposed, in order to regain inverse model stability, which also allows to estimate different hydraulic property fields at local and regional scales. Results show that ill-posed models can lead into inversion instability while different approaches that limit these instabilities may lead into different estimates. The study also shows that the late time hydraulic responses are strongly linked to the boundary conditions and thus to the regional heterogeneity. Accordingly, the use on these late-time data in inversion might require a larger dimension of the inverted domain, so that it is recommended to position the boundary conditions of the forward model far away from the wells. Also, the use of the proposed technique might provide a performant tool to obtain a satisfying fitting of observation, but also to assess both the site scale heterogeneity and the surrounding variabilities.

## 5.2 Introduction

Understanding the underground hydrodynamics due to subsurface heterogeneities has always been challenging. Through the last decades, new approaches to identify spatial heterogeneities in aquifers have been developed (Dagan 1993; Yeh et al. 1985; Clifton and Neuman 1982; Ahmed and Marsily 1992; Kitanidis 1995; Yeh et al. 1996). Hydraulic tomography (HT) is an aquifer characterization approach coupling a set of punctual responses to an inversion framework (Gottlieb and Dietrich, 1995, Kitanidis 1995, Renshaw, 1996, Yeh and Liu 2000, Vasco et al. 2000, Yeh et al. 1996) in order to spatially identify hydraulic properties of geological media, such as hydraulic conductivity and specific storage. Several applications of HT are available in the literature: some used steady state observations, others were extended to transient data to estimate both hydraulic conductivity and specific storage (Zhu and Yeh, 2005), also, HT were conducted on sandbox experiments data (Yeh and Liu 2000, Illman et al. 2007) Even though computers and CPUs become more and more powerful, HT calculations can be time consuming. To overpass such a burden, methods have been developed to decrease inversion calculation time by decreasing the number of forward model runs needed (e.g. Kitanidis and Lee, 2014;

Zha et al. 2018). For instance, the adjoint state method computes the sensitivity matrix with a number of forward simulations proportional to the number of observations instead of the number of inverted parameters. A limited amount of observations can, however, increase the number of solutions of property distribution that fits those data (Chavent, 1979; Mao et al., 2013).

Most of HT works use a simplified forward model to reduce the simulation time and are mainly led using synthetic studies (Yeh and Liu 2000, Yeh and Zhang 1996, Zhu and Yeh 2005, Hao et al. 2008, Cardiff and Barrash 2011, Sun et al. 2013, Bohling et al. 2002, Bohling and Butler 2010). In synthetic studies, the model and its boundary conditions are fully controlled. Many authors also worked at laboratory scale using sandbox experiments data (Liu and Yeh 2002, Sharmeen et al. 2012, Illman et al. 2010, Liu and Kitanidis 2011, Xiang et al. 2009, Yin and Illman 2009, Liu et al. 2007). Sandbox experiments allow us to obtain observation that are results from real hydrodynamic behavior. However, lab scale experiments remain easier to control and easier to model compared to aquifers that are associated to unknown heterogeneities and boundary conditions.

HT was also applied to real field cases to characterize aquifer's hydraulic properties (Zhao and Illman 2017, Wen et al. 2020, Bohling et al. 2007, Zha et al. 2017, Cardiff et al. 2012, Zha et al. 2016, Berg and Illman 2011, Zha et al. 2018). And, some studies showed that infusing different levels of geological information into HT considerably helps obtaining higher quality of aquifer characterization and may reduce the number of solutions (Zha et al., 2016, 2017). However, real field applications are often limited on information about boundary conditions and regional heterogeneities. This lack of information can lead into an ill-posed forward model which can induce inversion instability. Bohling et al. (2002) stated that boundary conditions will always be miss-specified to some extent and such misspecification have a significant effect on the estimated conductivities. Authors have Approached the forward model differently: use of a simple domain with boundary conditions (Zha et al. 2018, Berg and Illman 2011, Wen et al. 2020), use of an additional buffer zone to push the boundary conditions away from the wells, use of a bigger domain (Zhao and Illman 2017) with adaptive mesh (Zha et al. 2016). Also, performing pumping tests with small flow rate decreases the impact of the regional area on the drawdown responses (Cardiff et al. 2012). Moreover, most HT applications just avoid using the late time drawdown observations because they are the most sensitive to boundary conditions (Berg and Illman, 2011; Zha et al. 2016; Aliouache et al. 2021).

Yeh et al. (2015) emphasized the discussion about the instabilities of inverse problems in relation with scale, resolution and non-uniqueness of solutions. They also showed the importance of the boundary conditions in the forward modelling. Only few papers investigated the influence of boundary conditions on inverse modelling approaches. Sun et al. (2013) presented inversions results where they showed that a wrong boundary condition led into overestimation or underestimation of the hydraulic conductivity in the zone close to that boundary. Jiao and Zhang (2014), and Zhang, (2014) used an

approach that considers the boundary conditions also as unknowns in inverse modelling. More recently, Daranond et al. (2020) showed that HT results can identify the impermeable boundaries with a low transmissivity zone. Liu et al. (2020) showed the potential of HT on identifying the boundary conditions: they confirmed that an impermeable boundary can be identified by a low transmissivity zone and that a constant head boundary condition can be identified by a high transmissivity zone.

In this study, we investigate the inversion instability that can be caused by the lack of information about the regional area surrounding the experimental site. We focus on a real case dataset consisting of drawdown responses to pumping tests that showed a strong instability when using a simple forward model during transient HT. We firstly identify the cause of this instability. We then test different existing approaches that consider different forward model set up such as a) using a simple buffer area between the domain of interest and the boundary conditions or b) avoiding late time observations which are highly impacted by the regional area and boundaries. Then, we perform a multi-resolution HT to try to characterize the regional surroundings. Finally, we compare the different inverted transmissivity fields and discuss the results.

### 5.3 Methodology

Our main objective is to estimate a 2D depth averaged transmissivity field that mimics the drawdown data obtained during pumping in the confined aquifer of an experimental site. The experimental site is located in Southern France, 20 km northeast of Montpellier. It has 13 vertical wells drilled within a square of 30 m by 30 m. The wells have an average depth of 30m where they penetrate the upper Burdigalian which is permeable and reach the roof of the mid Burdigalian that exhibits a very low permeability. 13 cross-hole pumping tests in the wells were performed and the observation data showed a steady shape behavior in their hydraulic pumping test responses (Figure 5.1.c). The term steady shape is used to designate a condition in which drawdown is continuing to change with time while the hydraulic gradient over time remains constant (Bohling et al. 2002).

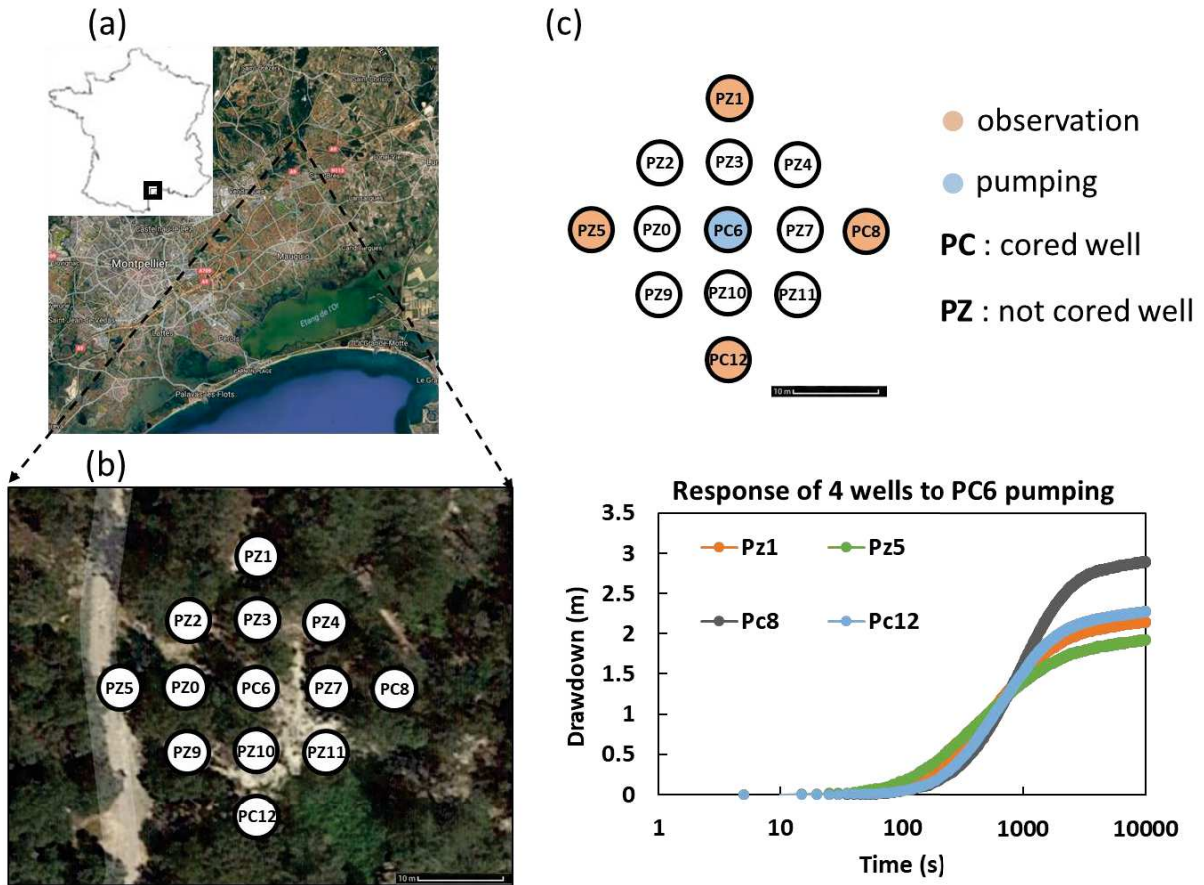


*Figure 5.1: Presentation of the experimental site. a) geo-localization of the site, b) well pattern, c) example of the hydrodynamics of the site through a response to a pumping test in P6.*

### 5.3.1 Groundwater flow equations

We solve the two-dimensional fluid flow continuity equation for a confined, saturated and heterogeneous porous media. The flow equation is solved in the time domain:

$$S_s \frac{\partial h}{\partial t} + \nabla(-K\nabla h) = Q_p,$$

with

$$h|_{t=0} = h_0, h|_{\varphi} = h_0,$$

where  $\nabla$  is the gradient operator,  $S_s$  is the specific storage which is assumed homogeneous in this study,  $h$  is the hydraulic head,  $K$  the hydraulic conductivity,  $Q_p$  the source term and  $h_0$  is the initial hydraulic head which remains constant at the boundary conditions  $\varphi$ .

### 5.3.2 Forward model description

The forward problem consists in solving the groundwater flow equation in a large 2D domain that represents a top-down view of the hydraulic property field of the aquifer. The fluid flow continuity equation for a confined, saturated and heterogeneous porous media is solved in the time domain:

$$S_s \frac{\partial h}{\partial t} + \nabla(-K\nabla h) = Q_p, \quad (1)$$

with

$$h|_{t=0} = h_0, h|_{\varphi} = h_0, \quad (2)$$

where  $\nabla$  is the gradient operator,  $S_s$  is the specific storage which is assumed homogeneous in this study,  $h$  is the hydraulic head,  $K$  the hydraulic conductivity,  $Q_p$  the source term and  $h_0$  is the initial hydraulic head which remains constant at the boundary conditions  $\varphi$ .

In the middle of the domain the different wells of the experimental site are built as points. Around this central zone a buffer zone is setup in order to move the boundaries of the model away from the wells area.

### 5.3.3 Inverse model description

Hydraulic tomography is applied in this study to characterize transmissivity field of an aquifer using the SLE deterministic inversion approach (J. Yeh 1996). Inverse modeling discretizes the modeled domain into a field of  $n$  elements (in this case T values) which are initially given a prior unconditional mean and correlated by a covariance matrix  $\mathbf{Q}$ . The initial hydraulic parameters are then iteratively updated conditioned by  $m$  observed drawdown responses in a vector  $\mathbf{y}$ . SLE estimates an updated solution for each element as follows:

$$s_{i+1} = s_i + \omega_i^T (\mathbf{y} - \mathbf{H}(s_i))$$

where  $i$  is the iteration index;  $\mathbf{s}$  is the hydraulic parameter vector of  $n \times 1$  elements;  $\mathbf{H}(\cdot)$  refers to the forward problem used to simulate drawdown data using the current hydraulic parameter.  $\omega$  which denotes inversion weights, it has a size of  $m \times n$  and contains the current step perturbation to add to the solution. The coefficient matrix  $\omega$  is estimated by solving the following equation:

$$[E_i^{yy} + \theta \text{diag}(E_i^{yy})] \omega_i = E_i^{sy}$$

Where  $\theta$  is a dynamic stability multiplier.  $E_i^{yy}$  ( $m \times m$ ) and  $E_i^{sy}$  ( $m \times n$ ) are, respectively, the conditional covariance of observation data and the residual cross-covariance between parameter and data. The SLE can exhibit an instability while solving the equation system that determines  $\omega$ . Hence, a stabilizer term is usually added to ensure the equation system stability.  $E_i^{yy}$  and  $E_i^{sy}$  are obtained from the following first order approximation (Yeh and Liu, 2000):

$$E_i^{yy} = J_i Q_i J_i^T$$

$$E_i^{sy} = J_i Q_i$$

Where  $J$  is a sensitivity matrix estimated using the current parameter. The Jacobian matrix calculation is the most time consuming part in a deterministic inversion.

At  $i=0$ ,  $Q$  is the unconditional covariance matrix of parameters vector  $s$  constructed from a variogram function based on a prior variance and correlation lengths (see inputs parameters subsection). The residual covariance after each step is defined as follows (Yeh and Liu, 2000):

$$Q_{i+1} = Q_i - \omega_i^T E_i^{sy}$$

At any iteration step, the flow equation in a model in order to simulate drawdown data at the same location than the observed ones. The sensitivity matrix calculation requires several forward problem runs: to obtain the current sensitivity matrix, it requires usually  $n$  runs of the forward model where  $n$  corresponds the size of parameters vector  $s$ .

### 5.3.4 Model setup and input parameters

Different cross hole pumping test were performed on the experimental site. For this study, we randomly used the responses to 5 of them while the rest was used as data for validation. For each pumping test we sample precise times to use as observation data accordingly to the purpose of the inversion and what is wanted to be shown. For each pumping test, continuous drawdown measurement in the observation wells were obtained. The initial transmissivity guess used in all inversions is  $\log[T_{\text{initial}}(m^2 \cdot s^{-1})] = -4$ ; the storage coefficient for all inversions is  $\log(S) = -3.5$  and the storage remains unchanged and assumed homogeneous. The values are chosen because the interpretation of the hydraulic tests showed similar effective parameters. For the simple initial inversion case, the model domain only consists on a square of 40 m by 40 m covering the wells and discretized with a regular squared grid of size  $L1=2m$  and a buffer area of 300 m by 300 m extending to the boundaries defined

by a transmissivity  $T_{\text{buffer}}=10^{-4}$  ( $\text{m}^2.\text{s}^{-1}$ ) and a storage  $S_{\text{buffer}}= 10^{-3.5}$ . For the multi-scale HT cases, the domain is divided radially into 3 subdomains. The first one, a square of 40 m by 40 m covering all the available wells in the experimental site, is discretized with a grid size  $L1=2$  m. The second subdomain is a squared ring 100 m by 100 m surrounding the first square which was discretized with a grid size  $L2=10$  m. The third subdomain 300 m by 300 m is the rest of the domain extending until the boundaries and it is discretized into only 8 elements defining eight main directions for a potential recharge to the system.

The covariance model follows an exponential law defined by:

$$Q(i, j) = Q(j, i) = \sigma \left[ \exp\left(-\left(\frac{|x_i - x_j|}{L_x} + \frac{|y_i - y_j|}{L_y}\right)\right) \right]$$

where  $\sigma$  is the variance,  $\mathbf{x}$  and  $\mathbf{y}$  are the coordinates of the middle of each grid element,  $L_x$  is the correlation length in x direction and  $L_y$  is the correlation length in y direction. Usually, an estimation of the covariance parameters can be obtained from the field and prior observations/interpretations. Although, Liu et al. (2000) concluded that, in many cases, these covariance parameters have minor impact on T estimate. For this study we use these following initial values for the variance and the correlation scales:  $\sigma = 2$ ;  $L_x=10$  m;  $L_y=10$  m.

Table 5.1 presents a summary of inputs for different inversions: the sampled times, the number of observations and if the multilevel grid refinement was used. In the first inversion, we attempted to achieve a HT using constant effective hydraulic properties for the buffer zone and responses were sampled from early and late times. In the second inversion, we run a HT using constant effective hydraulic properties for the buffer zone and responses were sampled from early times only. In the third inversion, we run a similar HT as in inversion 1 but effective hydraulic properties of the buffer zone are included in the inverted unknowns. In inversion 4, we discretize the buffer so the number of inverted unknowns are increased; responses were sampled from early and late times. For inversions 1-4, we used observations sampled from a single pumping test in P6 while in inversion 5, we added more observation data from 4 other pumping tests (P2, P5, P6, P8 and P10). The proposed method is firstly applied to a synthetic case.

**Table 5.1:** Summary of inversions input data

parameter	Inversion 1	Inversion 2	Inversion 3	Inversion 4	Inversion 5
Sampled times (s)	[200 500 800 1000 2000 4000]	[200 500 800 1000]	[200 500 800 1000 2000 4000]	[200 500 800 1000 2000 4000 6000 10000]	[200 500 800 1000 2000 4000 6000 10000 15000]

Multilevel local grid refinement	No	No	No	Yes	Yes
Number of pumping tests	1	1	1	1	5
Total number of observations	72	48	72	96	540

## 5.4 Results and discussion

### 5.4.1 Inversion using a buffer zone (Inversion 1, 2 and 3)

#### 5.4.1.1 Use of a buffer area to reduce the effect of the boundary conditions

We here attempt to invert the transmissivity field around the wells assuming that the transmissivity in the buffer zone is constant and fixed to a value interpreted by the pumping test as the effective transmissivity of the site. The model is as follows: a square covering the wells and discretized with a uniform squared grid. A bigger square around the first one will play the role of the buffer zone and takes a constant transmissivity value that was interpreted from single wells pumping tests  $T_{\text{buffer}}=10^{-4} \text{ m}^2.\text{s}^{-1}$ . At the edge of the buffer domain a constant head boundary condition is defined as equal to the initial head in the domain  $h=25\text{m}$ . Only one set of measured responses to one pumping test in P6 is used as the conditioning data. The sampled measurements cover the whole drawdown curve, from early to late times. The results (Figure 5.2.a) show the inverted transmissivity map and a scatter plot of the simulated observation versus the true observation (Figure 5.2.b). We firstly report that the inversion during this case showed an instability and had difficulties to converge to a better solution. It may be due to a conflict when fitting early and late time observation data and a strong constraint from the buffer with its fixed hydraulic properties. The inversion tries to fit the early time observation points by adjusting the hydraulic property of the cells surrounding the wells. These cells manifest an important sensitivity to the early time of the pumping test observation. However, it shows a lower sensitivity to the late time observation. Simulated drawdown responses using the inverted transmissivity map follow an infinite reservoir behavior: they present a straight line at the late time part and no flattened behavior was observed. The scatter plot showed a total misfit between simulations and observations. Also, the inverted transmissivity map shows a strong discontinuity between the wells area and the buffer zone which classified the result as unrealistic.

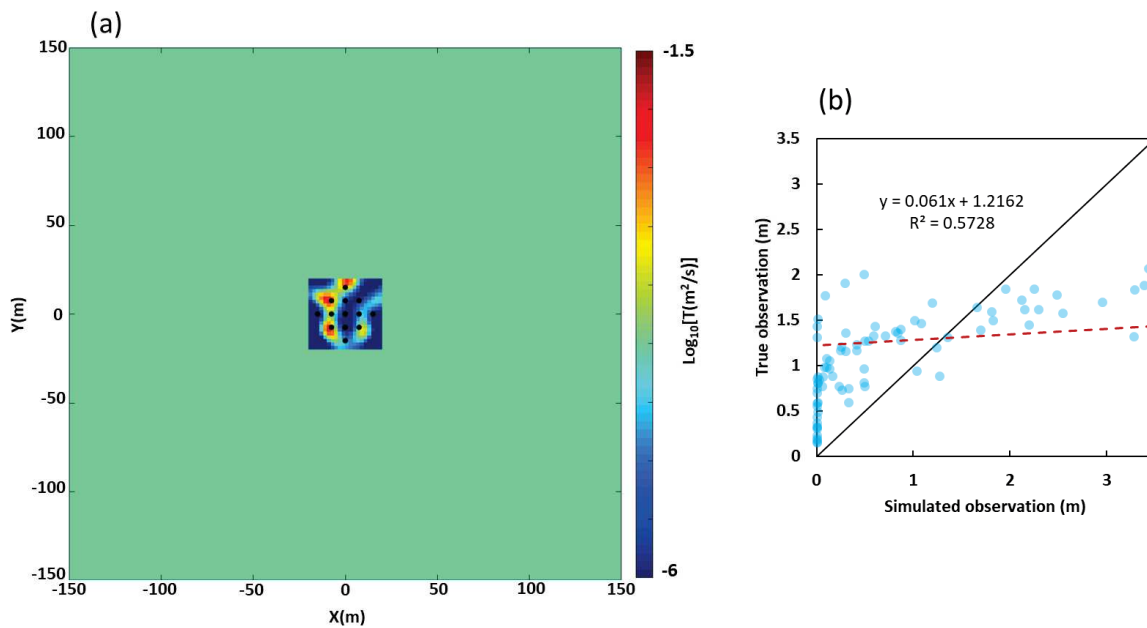


**Figure 5.2:** Inversion results using a fixed constant hydraulic transmissivity for the buffer domain; conditioning measurements cover early and late times of the drawdown curves. a) Inverted  $\text{Log}_{10}$  Transmissivity map. b) A scatter plot of simulated versus true observation data.

#### 5.4.1.2 Use of early part of drawdown curve only

Taking into consideration results from the previous inversion, it is obvious that late time responses are hard to fit because of the flattening of the drawdown curve (Figure 5.1c) that our model did not allow to capture. In this next inversion, we try to confirm that the late time observations strongly affect the inversion stability and cause such poor fitting. Everything is set up similar as the previous inversion, however, only the early time of the drawdown curves is used; no point is sampled from the flattened part of the drawdown curve. The results (Figure 5.3.a) show the inverted transmissivity map and a scatter plot of the simulated observation versus the true observation (Figure 5.3.b). Results from this case confirmed that, without using late time observations, the inversion became stable and converged to a solution that fits the data. Also, we notice that, as in the previous case, the boundary between the inverted area and the buffer area is sharp and discontinuous.

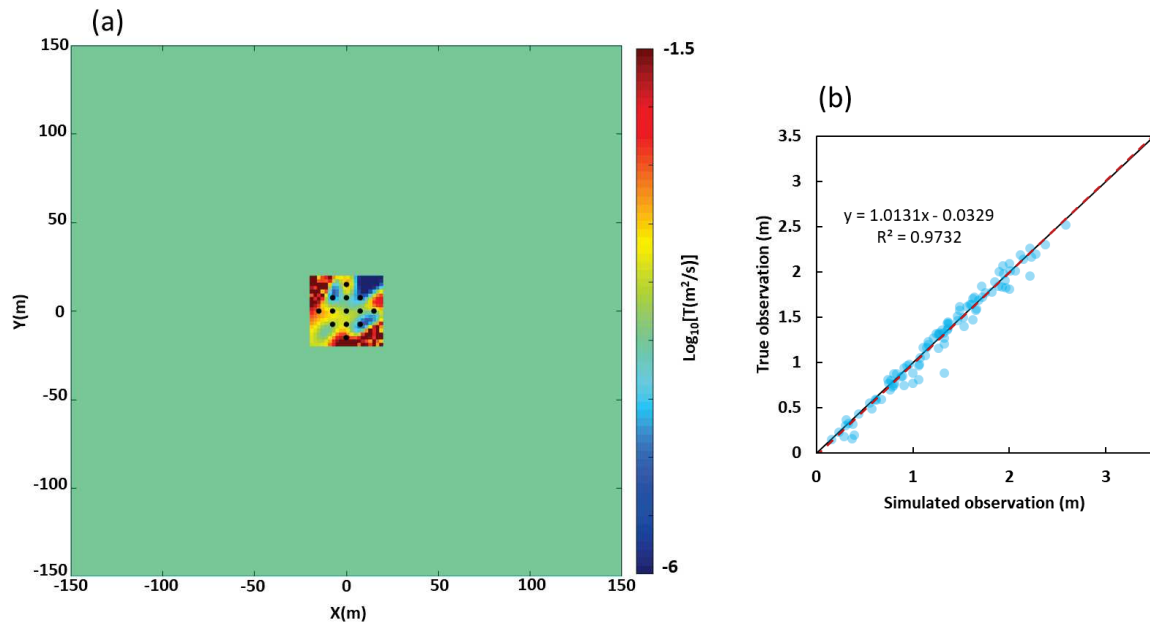


*Figure 5.3: Inversion results using a fixed constant hydraulic transmissivity for the buffer domain; no conditioning measurements were sampled in the flattened part at late times. a) contour plot of the inverted  $\log_{10}(\text{Transmissivity})$  map. b) scatter plot of simulated versus true observation data.*

#### 5.4.1.3 Hydraulic property of the buffer area is added as an unknown to HT

The buffer domain properties may have an impact on the inverted hydraulic transmissivities and may explain the instability of the inversion when the late time observations are included. Hence, in the following inversion, the transmissivity of the buffer area is considered unknown and is added to the inverted parameter vector. The whole buffer zone was represented by a homogeneous value. The sampled observation points cover the whole drawdown curve, from early to late times. The results (Figure 5.4.a) show the inverted transmissivity map and a scatter plot of the simulated observation versus the true observation (Figure 5.4.b).

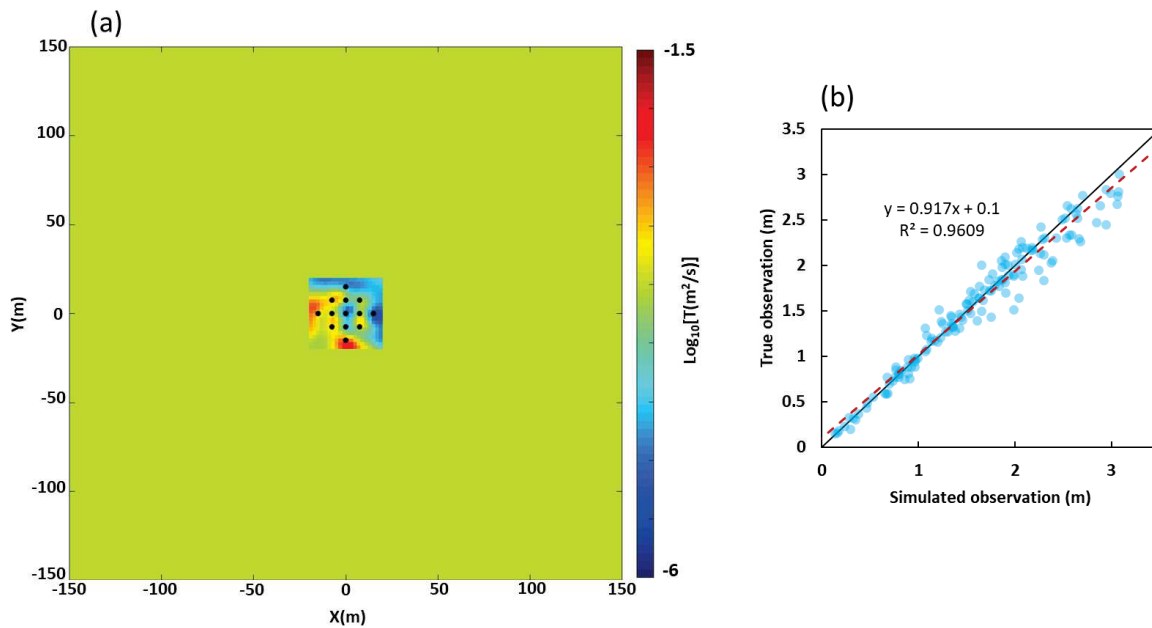


**Figure 5.4:** Inversion results using an unknown hydraulic transmissivity value for the buffer domain; conditioning measurements cover early and late times of the drawdown curves. a) Contour plot of the inverted  $\log_{10}(\text{Transmissivity})$  map. b) scatter plot of simulated versus true observation data.

This inversion was more stable than the first one and the inverted hydraulic transmissivity map between the wells shows a better spatial distribution. However, the contrast between the transmissivities around the wells and the buffer zone remains unrealistic and could be improved. The results show that the buffer zone transmissivity value has an important effect on the stability of HT and impacts the late time responses. In this HT, the simulated drawdowns started to show a flattened drawdown behavior at late times, as it is observed on real responses.

#### 5.4.2 Multi-level grid inversion (Inversion 4 and 5)

In order to obtain a smooth map of transmissivities that better reproduces the behavior of the true experimental site, the discretized inversion domain surrounding the wells was expanded. Although, the discretization in-between the wells need to be keep fine to not loose resolution. However, discretizing a bigger domain quickly increased the number of inverted unknowns and the inversion computation time. In order to overcome such a burden, we choose to use a multi-level grid refinement: the zone covering the wells remained at a very fine discretization while the buffer zone was radially divided into two distinct zones (see Figure 5.5.a). A squared ring surrounding the wells domain had a discretization which was coarser than the one around the wells. The remaining buffer zone was discretized using a very coarse grid. The covariance matrix model was adapted and extended to the whole domain as shown in Figure 5.5.b.

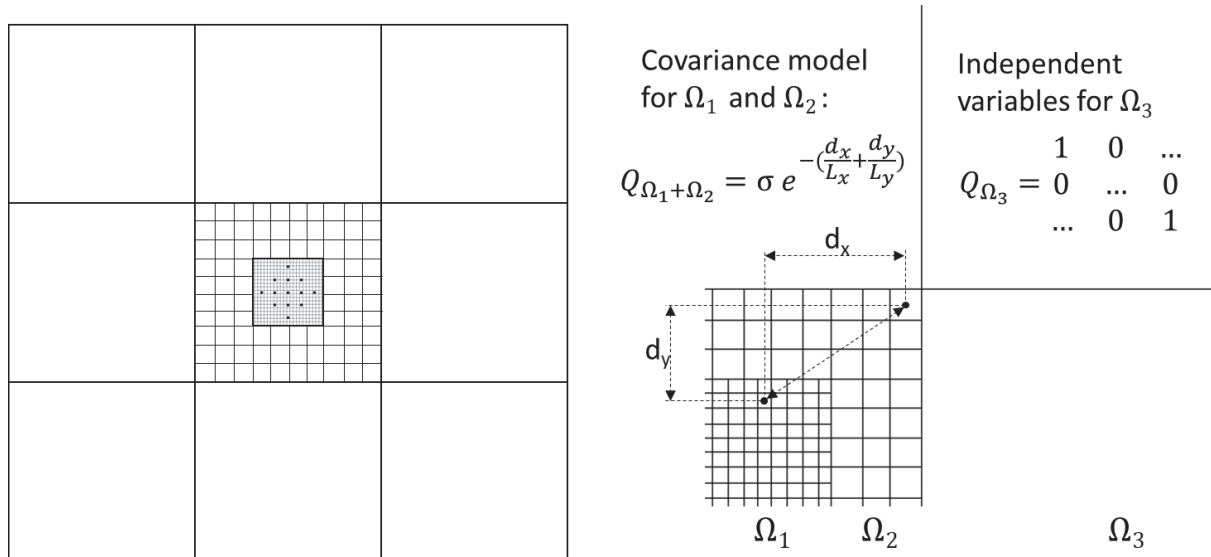


**Figure 5.5:** a) Inverted domain used in the HT and distribution of the multigrid refinement cells. b) Equivalent covariance model used for HT; the covariance model is used in domains  $\Omega_1$  and  $\Omega_2$  while the cells in  $\Omega_3$  are not correlated.

#### 5.4.2.1 Synthetic case

In order to show that the inverted transmissivity in the buffer area can have a physical meaning even though no observations were collected in that area, a simplified synthetic case is used. We created a model with 5 wells localized in a square of 25 m by 25 m and a hydraulic transmissivity field map that is larger than the wells area (Figure 5.6.a). We firstly simulated cross-hole pumping tests in the 5 wells and their responses that will be used in the inversion. Figure 5.6 shows the result of the hydraulic tomography using two grid levels: one in which the buffer area is only discretized into 8 zones surrounding the wells (the inverted hydraulic transmissivity is shown in Figure 5.6.b) and one which is discretized into three grid levels as represented in Figure 5.5.a (the inverted hydraulic transmissivity is shown in Figure 5.6.c). In general, the results clearly show a good reproduction of the true hydraulic transmissivity field even in the buffer area.

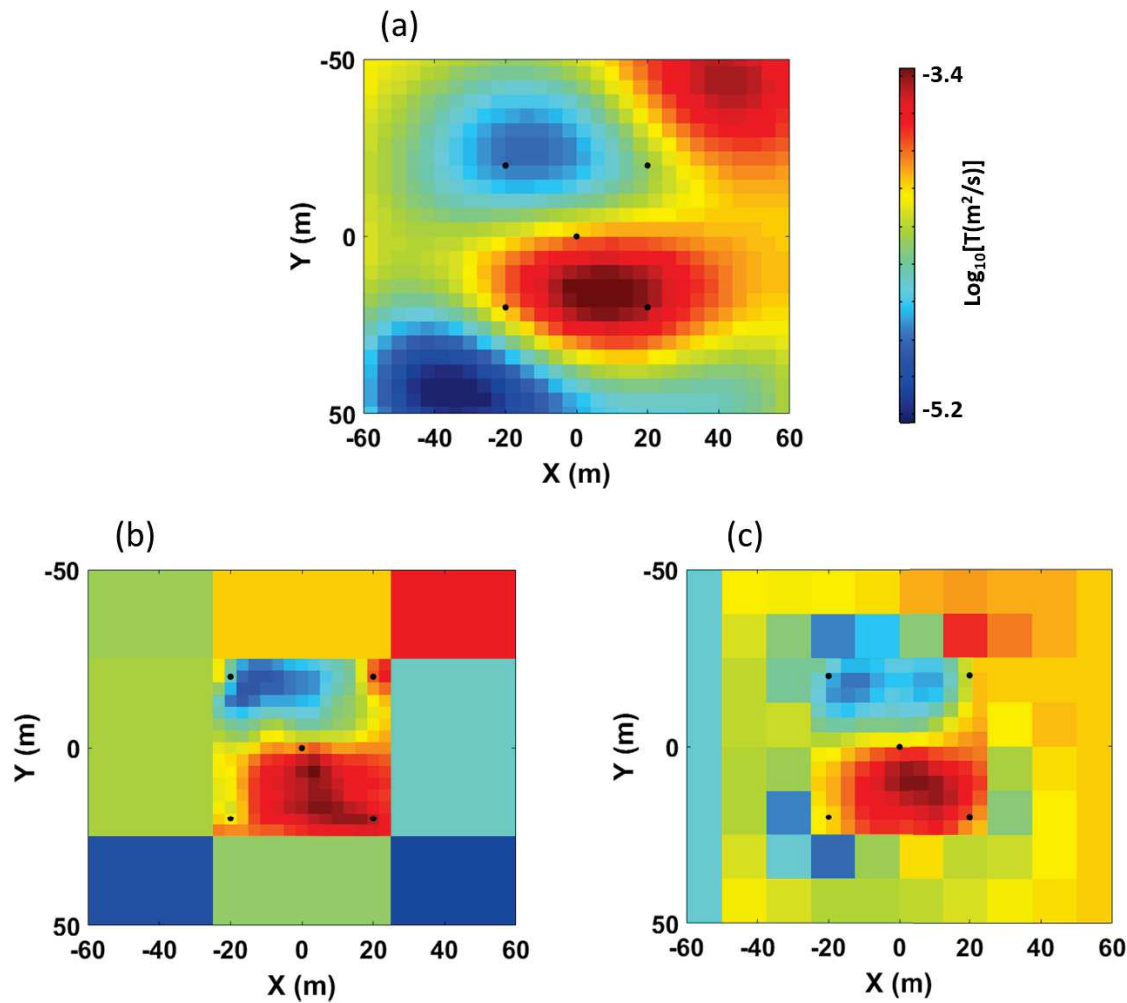


**Figure 5.6:** Synthetic case results: inversion using a multiscale local grid refinement. a) True hydraulic transmissivity field. b) Inverted hydraulic transmissivity field using 2 grid levels. c) Inverted hydraulic transmissivity field using 3 grid levels.

The inverted hydraulic transmissivity using 3 grid discretization levels shows a better transition and a better resolution than the inverted hydraulic transmissivity using 2 grid discretization levels. Multiple levels could be used to have a smoother transition between different levels.

#### 5.4.2.2 Application to real field data

The inversion with the multi-level grid refinement approach was then applied to the experimental site data. The distribution of the unknown grid cells of the inverted domain for the HT is summarized in Figure 5.6.a, Figure 5.6.b shows the covariance model used for matrix Q.

The model is as follows: a square covering the wells and discretized with a fine grid for high resolution. A transition domain surrounding the first one is discretized with a normal grid, coarser than the previous one. The remaining buffer is discretized with a very coarse grid (divided into 8 big regions) (see Figure 5.6.a). All the cells transmissivities were considered unknowns and could be updated during

inversion. At the edge of the buffer domain a constant head boundary condition was defined, which is equal to the initial head of the domain  $h=25\text{m}$ . The sampled observation drawdowns cover early and late times (see Table 5.1). The results (Figure 5.7.a) show a plot of the inverted hydraulic transmissivity map and a scatter plot of the simulated observation versus the true observation (Figure 5.7.b).

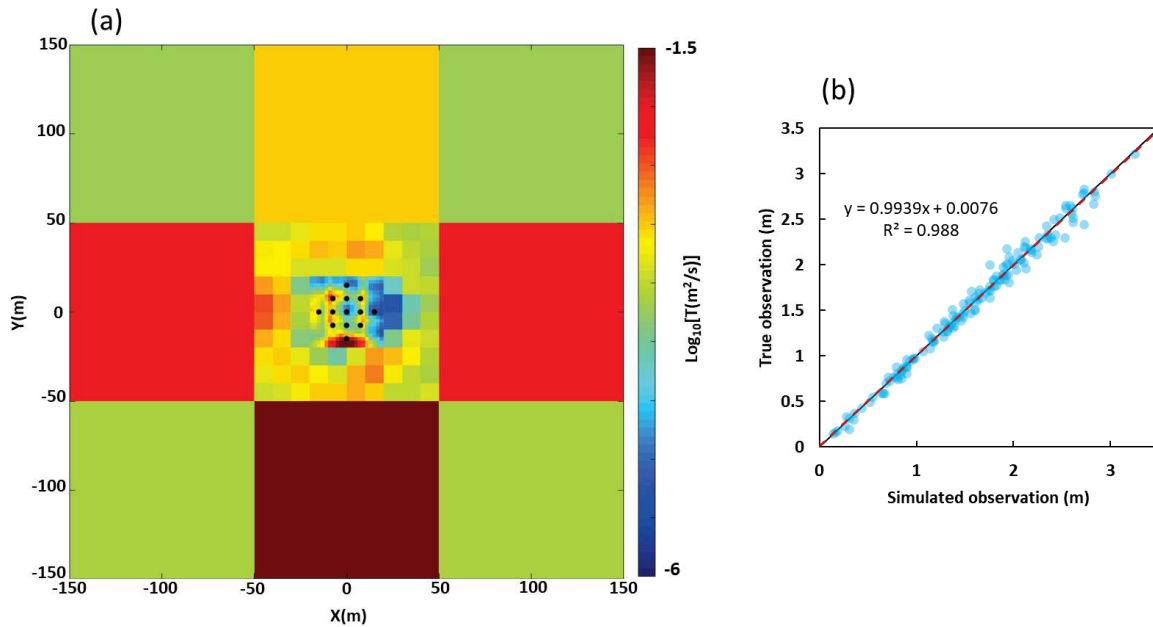


**Figure 5.7:** Inversion results using multilevel local grid refinement approach for one cross hole pumping test; conditioning measurements cover early and late times. a) contour plot of the inverted  $\log_{10}$ (hydraulic transmissivity) map. b) scatter plot of simulated versus true observation.

The inversion is stable and provides a good data fitting. All the responses of both early and late times are well reproduced and the simulations highlight the flattened part (Figure 5.1.c) as seen in true observations. The results also show a high variability in the inverted values of transmissivity in the 8 big regions; the 4 regions that are directly connected to the middle domain have been modified compared to the initial values while the 4 other regions remain almost unchanged and equal to the initial values. This is probably due to the fact that the 4 big cells adjacent to the middle domain are more sensitive than the 4 remaining cells. Figure 5.8 shows a plot of the normalized sensitivity of the different cells of the inverted domain during a pumping test in P6 before inversion. The sensitivity plot confirms the fact that the 4 regional cells connected to the middle domain have a higher sensitivity, which explains why they have been updated during inversion.

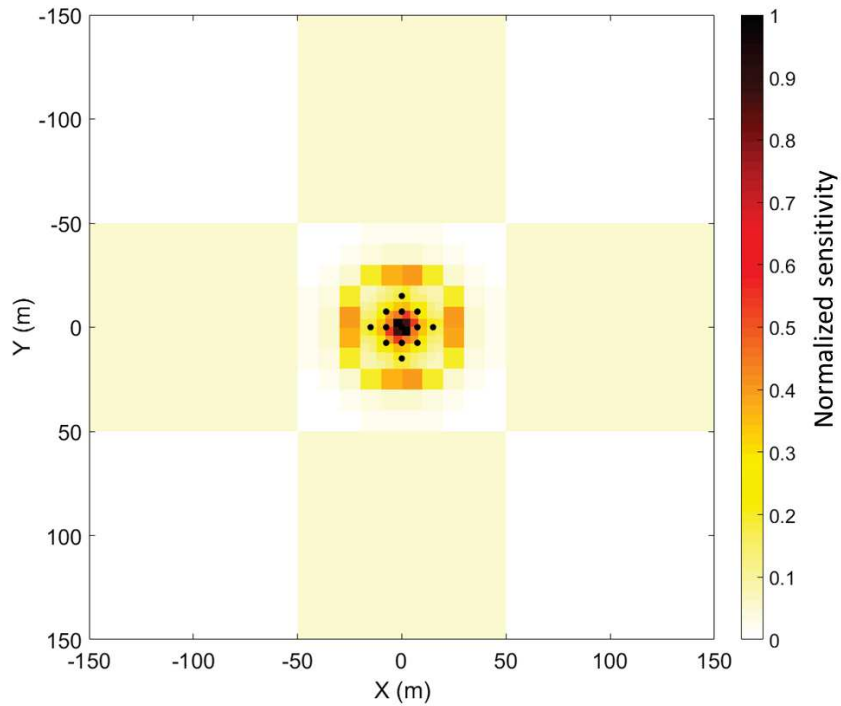


**Figure 5.8:** Plot of the normalized sensitivity of the different cells in the inverted domain for the pumping test in P6.

4 more cross-hole pumping tests data were added. The model remains similar to the previous inversion. Five sets of observations responding to five different pumping tests were given as the conditioning data. The sampled data cover early and late times of the drawdown curve. The results show the inverted hydraulic transmissivity map (Figure 5.9.a) and a scatter plot of the simulated observation versus the true observation (Figure 5.9.b). This test also allows to confirm that the stability is not lost when using several cross-hole pumping tests simultaneously.

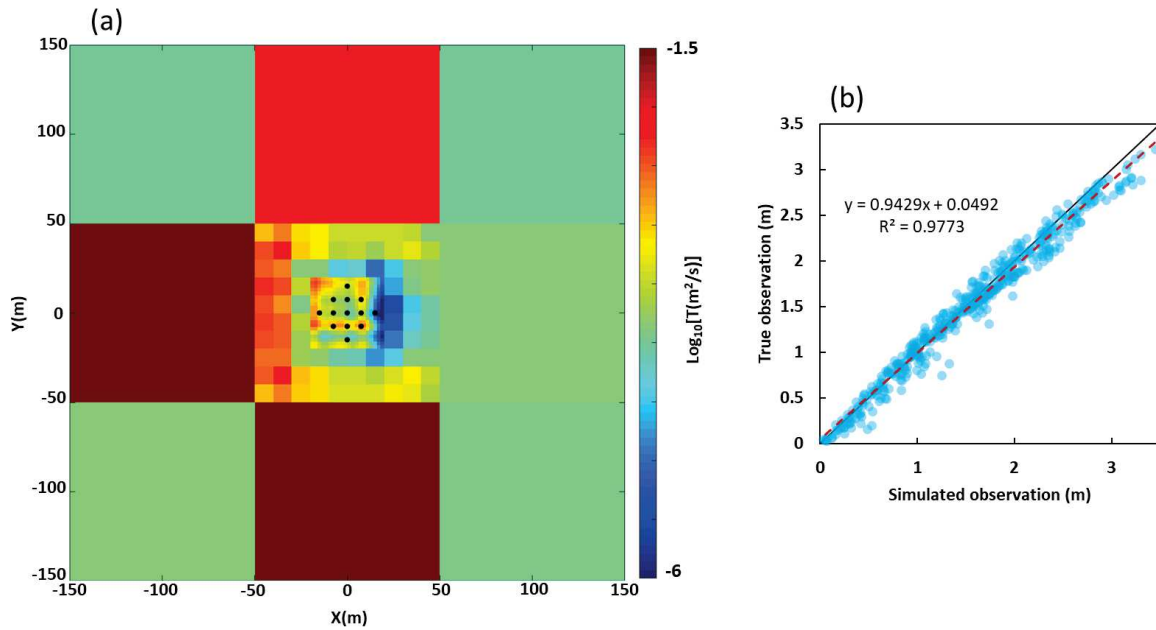


**Figure 5.9:** Inversion results using multilevel local grid refinement approach for one cross hole pumping test; conditioning measurements cover early and late times. a) plot of the inverted  $\log_{10}$ (hydraulic transmissivity) map. b) scatter plot of simulated versus true observation.

The inverted hydraulic transmissivities have been updated in order to fit more data. The data fitting remains good. The transmissivity field estimate looks improved in the buffer area when using more data. Furthermore, we notice that both of the multi-level grid inversions manage to detect a high transmissivity zone west of the experimental site.

### 5.4.2.3 Prediction

In the next step, we attempt to validate the inverted hydraulic transmissivity field generated in the previous inversion, by predicting drawdowns in different wells for a pumping test not used in the inversion as conditioning data and comparing them to the true observed drawdowns. Figure 5.10 shows a comparison between the real drawdowns and the simulated drawdowns responses to a pumping in well PZ3, using the inverted hydraulic transmissivity field obtained from the previous inversion.

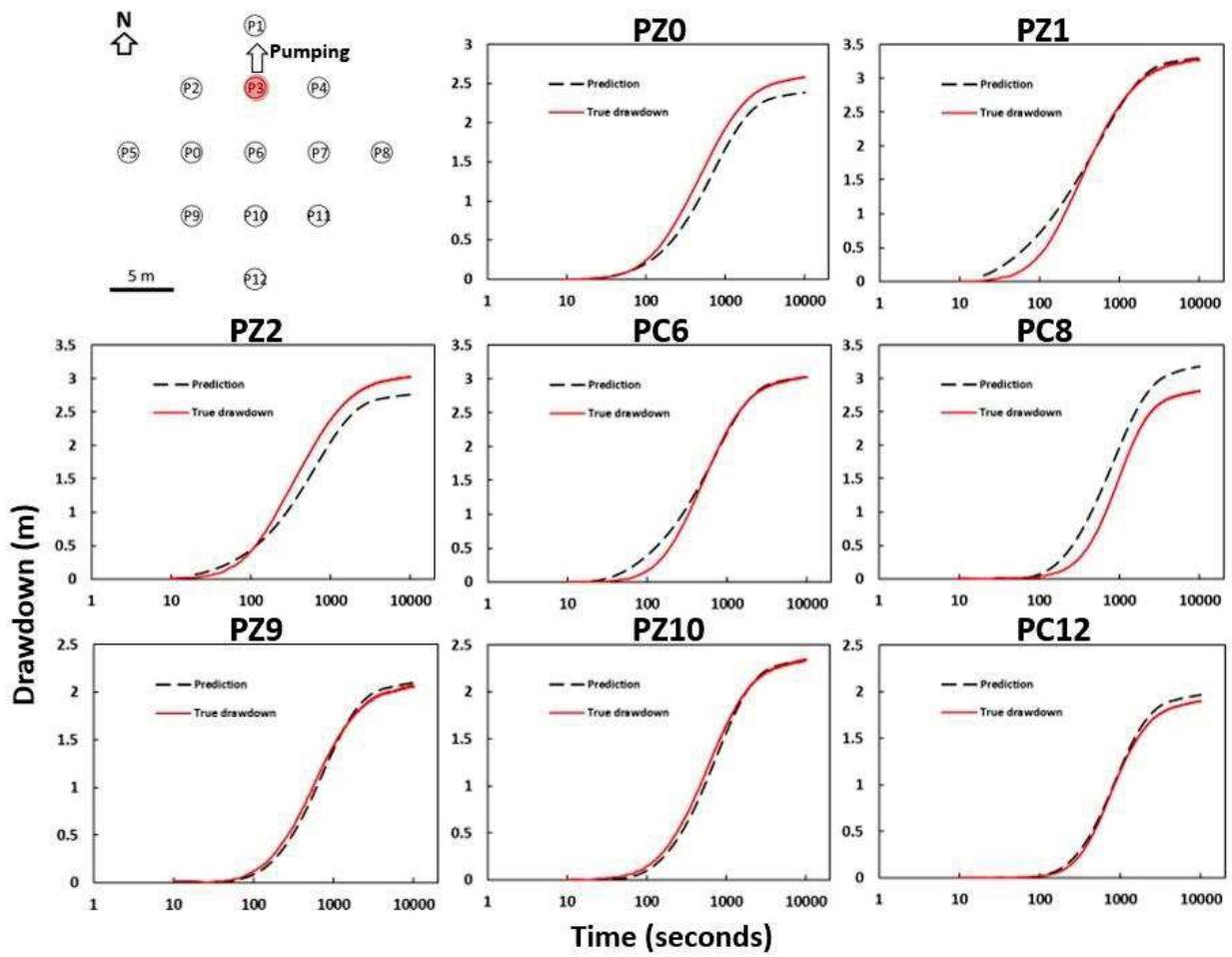


*Figure 5.10: Prediction of drawdowns at different wells (black dashed line) using the inverted hydraulic transmissivity field from inversion 5 and its comparison to real observed drawdowns (red line). Pumping at PZ3.*

We also predict drawdowns response to pumping in PZ7 and PZ9 and sample observations at different times (200, 500, 800, 1000, 2000, 4000) to cover the curve and scatter plot the true observations versus the predicted observations (see Figure 5.11) to show the accuracy of the inverted hydraulic transmissivity map for predicting new pumping.

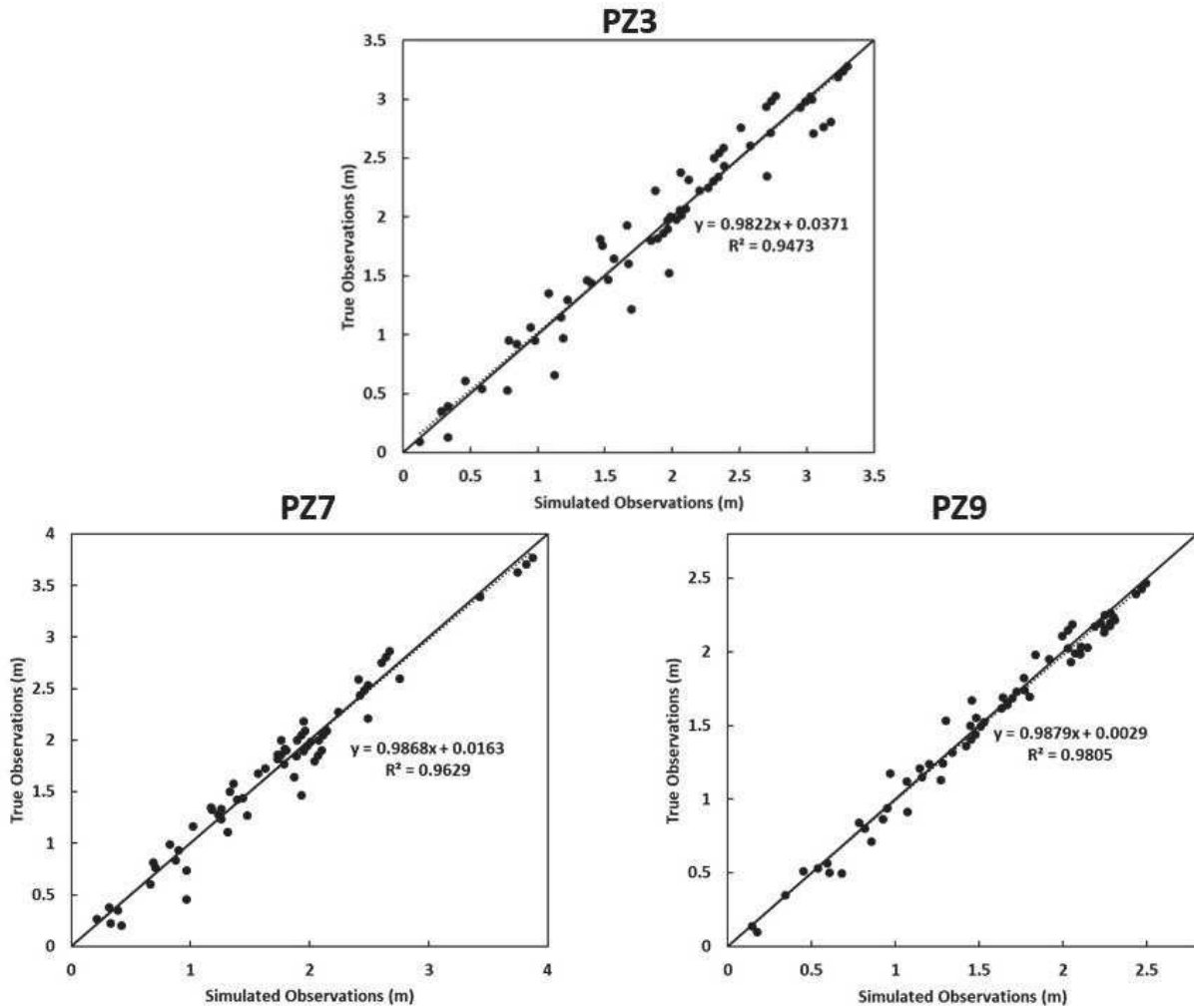


*Figure 5.11: True versus predicted observations for three different pumping tests (PZ3, PZ7 and PZ9). Dashed lines represent the linear regression of the scatter, solid lines represent 1:1 lines*

### 5.4.3 Comparison of different solutions

Figure 5.12 summarizes the different solutions obtained from the different inversion cases and a plot of the simulated drawdown in PZ3 while pumping in P6 for each case to show the late time behavior. The transmissivity fields are zoomed in to the middle domain in order to see the details in the surroundings of the wells area.

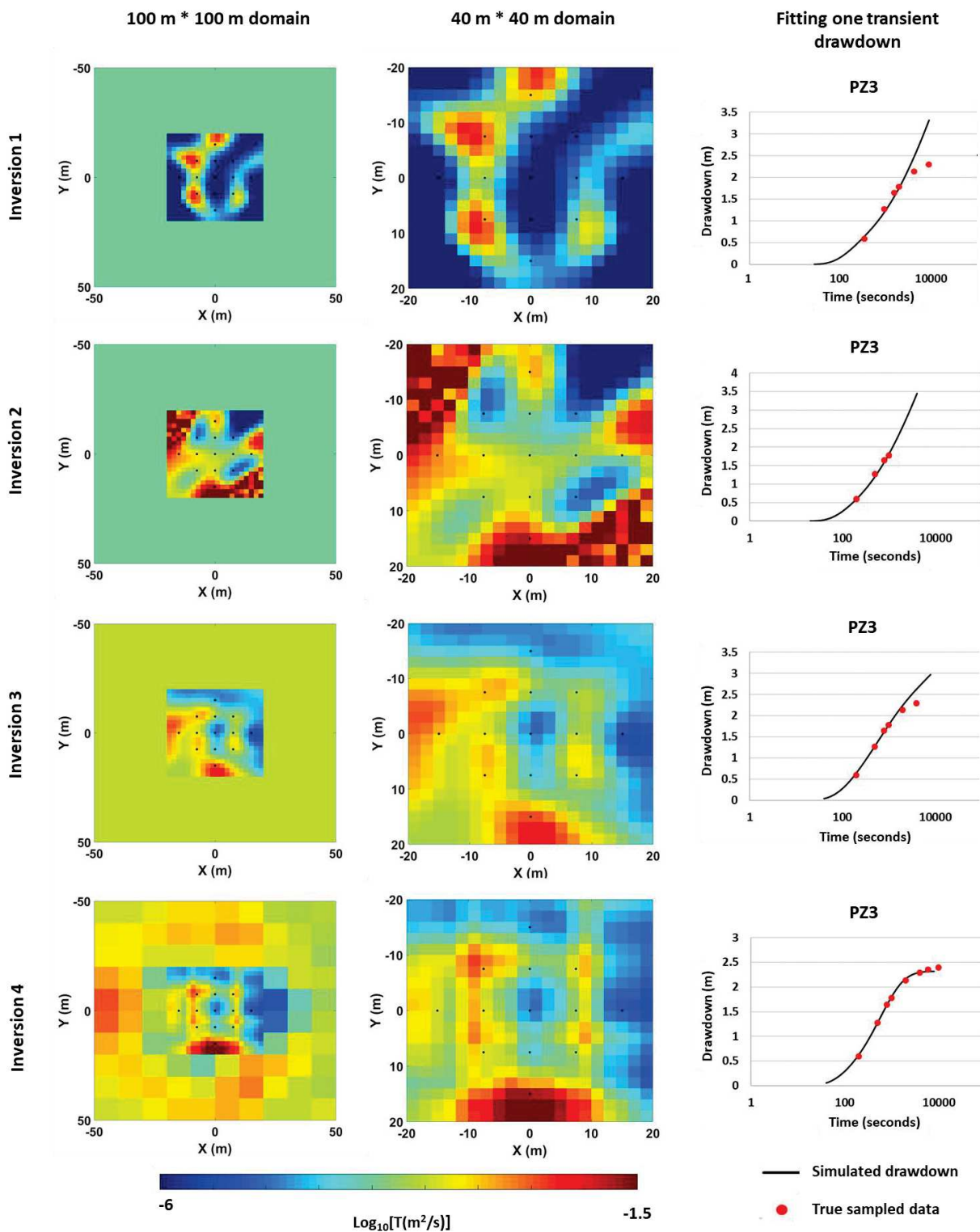


Figure 5.12: Comparison of different inverted transmissivity fields and their potential to fit the observed drawdowns and delineate the late time behavior.

We clearly notice that different inversions set ups lead into a different transmissivity estimate. In inversion 1, the fact that using a constant transmissivity value for the buffer area can create a conflict between early and late time observation which can result in an instable solution. Results of inversion 2

show that removing late time data can in fact stabilize the inverse system, however, the result might be considerably biased. Comparing results of inversions 3 and 4 can conclude that using a buffer area in which hydraulic properties are considered also unknowns can be a good low-cost option for inverse model stabilization. However, the multi-level grid used in inversion 4 allows to obtain a transmissivity field estimate with the best transient drawdown data fitting especially during late times.

## 5.5 Summary and conclusions

In this study, 2D hydraulic tomography was performed on an experimental site with both synthetic and experimental drawdown data. Experimental drawdown curves measured at the site showed a flattened part at late times. The goal of the HT was to perform a spatial characterization of the confined aquifer in order to simulate our site hydraulic behavior with a 2D depth averaged model. One possible interpretation of the flattened part in the drawdown curves can be the existence of a high permeable buffer recharging the site. However, we show that using a homogeneous transmissivity value for the whole buffer area does not allow for a good drawdowns fitting and the inverted hydraulic transmissivity maps better reproduce the hydrodynamics of the system. In order to fit the late time responses and enhance our model, the buffer zone was also discretized and its hydraulic transmissivity inverted. By pushing the boundary conditions very far away from the wells, discretizing the whole domain with a same resolution as in-between the wells quickly arises unbearable inversion times. Thus, a multi-level grid refinement was used to greatly decrease the calculation time. The main observations from our results are:

- Real data often induce strong instability during HT because of a lack of information about the regional surroundings of the wells and the aquifer boundaries. Using different inversion approaches to solve the instability issue might lead into different inverted solutions.
- The use of early time drawdown responses alone or the use of a buffer area stabilizes the convergence of the inversion, however the reproduction of the whole drawdown curve cannot be achieved.
- Inverting the flattened part of the drawdowns curve with a homogeneous hydraulic property buffer area generates instability. The hydraulic tomography requires a forward problem that needs to be realistic toward the real aquifer, otherwise, considerable instability and absence of convergence might appear and the aquifer characterization becomes hard to achieve.
- In a 2D model, the buffer area impacts the pumping test responses mainly at the late times by modifying their behavior from an infinite reservoir response to a finite reservoir with a recharge boundary response. Allowing the buffer properties to be updated through iterations solves the instability issue.

- The multilevel local grid refinement allows to achieve the 2D depth averaged characterization of the real aquifer considering both early and late times of the drawdown curves. The obtained hydraulic transmissivity map allows to fit the observed drawdowns and better mimics the hydraulic behavior of the aquifer. Also, the results are satisfactory and the calculation time cost is optimized.

## References

- Ahmed, S., and De Marsily, G. (1993), Cokriged estimation of aquifer transmissivity as an indirect solution of the inverse problem: A practical approach, *Water Resour. Res.*, 29(2), 521– 530, doi:10.1029/92WR00226.
- Aliouache, M., Wang, X., Fischer, P., Massonnat, G., & Jourde, H. (2021). An inverse approach integrating flowmeter and pumping test data for three-dimensional aquifer characterization. *Journal of Hydrology*, 126939.
- Berg, S. J., and W. A. Illman (2011), *Three-dimensional transient hydraulic tomography in a highly heterogeneous glaciofluvial aquifer-aquitard system*, *Water Resour. Res.*, 47, W10507, doi: 10.1029/2011WR010616.
- Berg, S. J., and W. A. Illman (2011), Three-dimensional transient hydraulic tomography in a highly heterogeneous glaciofluvial aquifer-aquitard system, *Water Resour. Res.*, 47, W10507, doi:10.1029/2011WR010616.
- Berg, S.J. and Illman, W.A. (2015), Comparison of Hydraulic Tomography with Traditional Methods at a Highly Heterogeneous Site. *Groundwater*, 53: 71-89. <https://doi.org/10.1111/gwat.12159>
- Bohling, G. C., Butler Jr., J. J., Zhan, X., and Knoll, M. D. (2007), A field assessment of the value of steady shape hydraulic tomography for characterization of aquifer heterogeneities, *Water Resour. Res.*, 43, W05430, doi:10.1029/2006WR004932.
- Bohling, G. C., Butler Jr., J. J., Zhan, X., and Knoll, M. D. (2007), A field assessment of the value of steady shape hydraulic tomography for characterization of aquifer heterogeneities, *Water Resour. Res.*, 43, W05430, doi:10.1029/2006WR004932.
- Bohling, G. C., Zhan, X., Butler, J. J., and Zheng, L., Steady shape analysis of tomographic pumping tests for characterization of aquifer heterogeneities, *Water Resour. Res.*, 38( 12), 1324, doi:10.1029/2001WR001176, 2002.
- Bohling, G. C., Zhan, X., Butler, J. J., and Zheng, L., Steady shape analysis of tomographic pumping tests for characterization of aquifer heterogeneities, *Water Resour. Res.*, 38( 12), 1324, doi:10.1029/2001WR001176, 2002.
- Bohling, G.C. and Butler, J.J., Jr. (2010), Inherent Limitations of Hydraulic Tomography. *Groundwater*, 48: 809-824. <https://doi.org/10.1111/j.1745-6584.2010.00757.x>
- Bohling, G.C. and Butler, J.J., Jr. (2010), Inherent Limitations of Hydraulic Tomography. *Groundwater*, 48: 809-824. <https://doi.org/10.1111/j.1745-6584.2010.00757.x>
- Cardiff, M., and Barrash, W. (2011), 3-D transient hydraulic tomography in unconfined aquifers with fast drainage response, *Water Resour. Res.*, 47, W12518, doi:10.1029/2010WR010367.
- Cardiff, M., and Barrash, W. (2011), 3-D transient hydraulic tomography in unconfined aquifers with fast drainage response, *Water Resour. Res.*, 47, W12518, doi:[10.1029/2010WR010367](https://doi.org/10.1029/2010WR010367).
- Cardiff, M., Barrash, W., and Kitanidis, P. K. (2012), A field proof-of-concept of aquifer imaging using 3-D transient hydraulic tomography with modular, temporarily-emplaced equipment, *Water Resour. Res.*, 48, W05531, doi:10.1029/2011WR011704.
- Cardiff, M., Barrash, W., and Kitanidis, P. K. (2012), A field proof-of-concept of aquifer imaging using 3-D transient hydraulic tomography with modular, temporarily-emplaced equipment, *Water Resour. Res.*, 48, W05531, doi:10.1029/2011WR011704.

- Cardiff, M., Barrash, W., and Kitanidis, P. K. (2012), A field proof-of-concept of aquifer imaging using 3-D transient hydraulic tomography with modular, temporarily-emplaced equipment, *Water Resour. Res.*, 48, W05531, doi:10.1029/2011WR011704.
- Chavent, G., About the stability of the optimal control solution of inverse problems, in *Inverse and Improperly Posed Problems in Differential Equations*, edited by G. Anger, pp. 45-58, Akademie-Verlag, Berlin, 1979a.
- Clifton, P. M., and Neuman, S. P. (1982), Effects of kriging and inverse modeling on conditional simulation of the Avra Valley Aquifer in southern Arizona, *Water Resour. Res.*, 18(4), 1215–1234, doi:10.1029/WR018i004p01215.
- Dagan, G. Higher-order correction of effective permeability of heterogeneous isotropic formations of lognormal conductivity distribution. *Transp Porous Med* 12, 279–290 (1993). <https://doi.org/10.1007/BF00624462>
- Daranond, K., Yeh, T. C. J., Hao, Y., Wen, J. C., & Wang, W. (2020). Identification of groundwater basin shape and boundary using hydraulic tomography. *Journal of Hydrology*, 588, 125099.
- Gottlieb, J., & Dietrich, P. (1995). Identification of the permeability distribution in soil by hydraulic tomography. *Inverse Problems*, 11(2), 353.
- Hao, Y., Yeh, T.-C.J., Xiang, J., Illman, W.A., Ando, K., Hsu, K.-C. and Lee, C.-H. (2008), Hydraulic Tomography for Detecting Fracture Zone Connectivity. *Groundwater*, 46: 183-192. <https://doi.org/10.1111/j.1745-6584.2007.00388.x>
- Hao, Y., Yeh, T.-C.J., Xiang, J., Illman, W.A., Ando, K., Hsu, K.-C. and Lee, C.-H. (2008), Hydraulic Tomography for Detecting Fracture Zone Connectivity. *Groundwater*, 46: 183-192. <https://doi.org/10.1111/j.1745-6584.2007.00388.x>
- Illman, W. A., Liu, X., Takeuchi, S., Yeh, T.-C. J., Ando, K., and Saegusa, H. (2009), Hydraulic tomography in fractured granite: Mizunami Underground Research site, Japan, *Water Resour. Res.*, 45, W01406, doi:10.1029/2007WR006715.
- Illman, W. A., Zhu, J., Craig, A. J., and Yin, D. (2010), Comparison of aquifer characterization approaches through steady state groundwater model validation: A controlled laboratory sandbox study, *Water Resour. Res.*, 46, W04502, doi:10.1029/2009WR007745.
- Illman, W.A., X. Liu, and A. Craig. 2007. Steady-state hydraulic tomography in a laboratory aquifer with deterministic heterogeneity: Multi-method and multiscale validation of hydraulic conductivity tomograms, *Journal of Hydrology* 341, no. 3–4: 222–234
- Jiao, J., & Zhang, Y. (2014). Two-dimensional physical-based inversion of confined and unconfined aquifers under unknown boundary conditions. *Advances in water resources*, 65, 43-57. Doi: <https://doi.org/10.1016/j.advwatres.2013.10.011>
- Kitanidis, P. K., and Lee, J. (2014), Principal Component Geostatistical Approach for large dimensional inverse problems, *Water Resour. Res.*, 50, 5428–5443, doi:10.1002/2013WR014630.
- Kitanidis, P. K. (1995), Quasi-Linear Geostatistical Theory for Inversing, *Water Resour. Res.*, 31(10), 2411–2419, doi:10.1029/95WR01945.

- Liu, F., Yeh, T.-C. J., Wang, Y.-L., Song, X., Lei, X., Wen, J.-C., et al. (2020). Potential of hydraulic tomography in identifying boundary conditions of groundwater basins. *Water Resources Research*, 56, e2020WR028331. <https://doi.org/10.1029/2020WR028331>
- Liu, S., T.-C. J. Yeh, and R. Gardiner (2002), Effectiveness of hydraulic tomography: Sandbox experiments, *Water Resour. Res.*, 38(4), 1034, doi:10.1029/2001WR000338
- Liu, X., and Kitanidis, P. K. (2011), Large-scale inverse modeling with an application in hydraulic tomography, *Water Resour. Res.*, 47, W02501, doi:10.1029/2010WR009144.
- Liu, X., Illman, W. A., Craig, A. J., Zhu, J., and Yeh, T.-C. J. (2007), Laboratory sandbox validation of transient hydraulic tomography, *Water Resour. Res.*, 43, W05404, doi:[10.1029/2006WR005144](https://doi.org/10.1029/2006WR005144).
- Liu, X., Illman, W. A., Craig, A. J., Zhu, J., and Yeh, T.-C. J. (2007), Laboratory sandbox validation of transient hydraulic tomography, *Water Resour. Res.*, 43, W05404, doi:10.1029/2006WR005144.
- Mao, D., T.-C. J. Yeh, L. Wan, C.-H. Lee, K.-C. Hsu, J.-C. Wen, and W. Lu (2013a), Cross-correlation analysis and information content of observed heads during pumping in unconfined aquifers, *Water Resour. Res.*, 49, 713–731, doi:10.1002/wrcr.20066.
- Mao, D., T.-C. J. Yeh, L. Wan, K.-C. Hsu, C.-H. Lee, and J.-C. Wen (2013b), Necessary conditions for inverse modeling of flow through variably saturated porous media, *Adv. Water Resour.*, 52, 50–61, doi:10.1016/j.advwatres.2012.08.001.
- Renshaw, C. E. (1996). Estimation of fracture zone geometry from steady-state hydraulic head data using iterative sequential cokriging. *Geophysical research letters*, 23(19), 2685-2688.
- Ronayne, M. J., Gorelick, S. M., and Caers, J. (2008), *Identifying discrete geologic structures that produce anomalous hydraulic response: An inverse modeling approach*, *Water Resour. Res.*, 44, W08426, doi:10.1029/2007WR006635.
- Sharmeen, R., Illman, W. A., Berg, S. J., Yeh, T.-C. J., Park, Y.-J., Sudicky, E. A., and Ando, K. (2012), Transient hydraulic tomography in a fractured dolostone: Laboratory rock block experiments, *Water Resour. Res.*, 48, W10532, doi:10.1029/2012WR012216.
- Sun, N. Z. (2013). *Inverse problems in groundwater modeling* (Vol. 6). Springer Science & Business Media.
- Vasco, D. W., Keers, H., and Karasaki, K. (2000), Estimation of reservoir properties using transient pressure data: An asymptotic approach, *Water Resour. Res.*, 36( 12), 3447– 3465, doi:10.1029/2000WR900179.
- Wen, J.-C., Chen, J.-L., Yeh, T.-C.J., Wang, Y.-L., Huang, S.-Y., Tian, Z. and Yu, C.-Y. (2020), Redundant and Nonredundant Information for Model Calibration or Hydraulic Tomography. *Groundwater*, 58: 79-92. <https://doi.org/10.1111/gwat.12879>
- Wen, J.-C., Chen, J.-L., Yeh, T.-C.J., Wang, Y.-L., Huang, S.-Y., Tian, Z. and Yu, C.-Y. (2020), Redundant and Nonredundant Information for Model Calibration or Hydraulic Tomography. *Groundwater*, 58: 79-92. <https://doi.org/10.1111/gwat.12879>
- Xiang, J., Yeh, T.-C. J., Lee, C.-H., Hsu, K.-C., and Wen, J.-C. (2009), A simultaneous successive linear estimator and a guide for hydraulic tomography analysis, *Water Resour. Res.*, 45, W02432, doi:10.1029/2008WR007180.

- Xiang, J., Yeh, T.-C. J., Lee, C.-H., Hsu, K.-C., and Wen, J.-C. (2009), A simultaneous successive linear estimator and a guide for hydraulic tomography analysis, *Water Resour. Res.*, 45, W02432, doi:10.1029/2008WR007180.
- Yeh, T.-C. J., and Liu, S. (2000), Hydraulic tomography: Development of a new aquifer test method, *Water Resour. Res.*, 36(8), 2095– 2105, doi:10.1029/2000WR900114.
- Yeh, T.-C. J., and Zhang, J. (1996), A Geostatistical Inverse Method for Variably Saturated Flow in the Vadose Zone, *Water Resour. Res.*, 32( 9), 2757– 2766, doi:10.1029/96WR01497.
- Yeh, T.-C. J., D. Mao, L. Wan, C.-H. Lee, J.-C. Wen, and K.-C. Hsu (2015b), Well definedness, scale consistency, and resolution issues in groundwater model parameter identification, *Water Sci. Eng.*, 8(3), 175–194, doi:10.1016/j.wse.2015.08.002.
- Yeh, T.-C. J., M. Jin, and S. Hanna (1996), An iterative stochastic inverse method: Conditional effective transmissivity and hydraulic head fields, *Water Resour. Res.*, 32(1), 85– 92, doi:10.1029/95WR02869.
- Yeh, T.-C. J., and Liu, S. (2000), Hydraulic tomography: Development of a new aquifer test method, *Water Resour. Res.*, 36( 8), 2095– 2105, doi:10.1029/2000WR900114.
- Yeh, T.-C. J., Gelhar, L. W., and Gutjahr, A. L. (1985), Stochastic Analysis of Unsaturated Flow in Heterogeneous Soils: 2. Statistically Anisotropic Media With Variable  $\alpha$ , *Water Resour. Res.*, 21( 4), 457– 464, doi:10.1029/WR021i004p00457.
- Yin, D., and Illman, W. A. (2009), Hydraulic tomography using temporal moments of drawdown recovery data: A laboratory sandbox study, *Water Resour. Res.*, 45, W01502, doi:10.1029/2007WR006623.
- Yin, D., and Illman, W. A. (2009), Hydraulic tomography using temporal moments of drawdown recovery data: A laboratory sandbox study, *Water Resour. Res.*, 45, W01502, doi:[10.1029/2007WR006623](https://doi.org/10.1029/2007WR006623).
- Zha, Y., Yeh, T.-C. J., Illman, W. A., Onoe, H., Mok, C. M. W., Wen, J.-C., Huang, S.-Y., and Wang, W. (2017), Incorporating geologic information into hydraulic tomography: A general framework based on geostatistical approach, *Water Resour. Res.*, 53, 2850– 2876, doi:[10.1002/2016WR019185](https://doi.org/10.1002/2016WR019185).
- Zha, Y., Yeh, T.-C. J., Illman, W. A., Zeng, W., Zhang, Y., Sun, F., et al. (2018). A reduced-order successive linear estimator for geostatistical inversion and its application in hydraulic tomography. *Water Resources Research*, 54, 1616– 1632. <https://doi.org/10.1002/2017WR021884>
- Zha, Y., Yeh, T.-C. J., Illman, W. A., Onoe, H., Mok, C. M. W., Wen, J.-C., Huang, S.-Y., and Wang, W. (2017), Incorporating geologic information into hydraulic tomography: A general framework based on geostatistical approach, *Water Resour. Res.*, 53, 2850– 2876, doi:10.1002/2016WR019185.
- Zha, Y., Yeh, T.-C.J., Illman, W.A., Tanaka, T., Bruines, P., Onoe, H., Saegusa, H., Mao, D., Takeuchi, S. and Wen, J.-C. (2016), An Application of Hydraulic Tomography to a Large-Scale Fractured Granite Site, Mizunami, Japan. *Groundwater*, 54: 793-804. <https://doi.org/10.1111/gwat.12421>
- Zhang, Y. Nonlinear Inversion of an Unconfined Aquifer: Simultaneous Estimation of Heterogeneous Hydraulic Conductivities, Recharge Rates, and Boundary Conditions. *Transp Porous Med* 102, 275–299 (2014). <https://doi.org/10.1007/s11242-014-0275-x>
- Zhao, Z., and W. A. Illman (2017), On the Importance of Geological Data for Three-dimensional Steady-State Hydraulic Tomography Analysis at a Highly Heterogeneous Aquifer-Aquitard System. *J. Hydrol.*, 544, 640– 657

Zhao, Z., Illman, W.A., Berg, S.J., 2016. On the importance of geological data for hydraulic tomography analysis: laboratory sandbox study. *J. Hydrol.* <https://doi.org/10.1016/j.jhydrol.2016.08.061>

Zhu, J., and Yeh, T.-C. J. (2005), Characterization of aquifer heterogeneity using transient hydraulic tomography, *Water Resour. Res.*, 41, W07028, doi:[10.1029/2004WR003790](https://doi.org/10.1029/2004WR003790).



## CONCLUSION

A methodology to characterizing the permeability field in a sedimentary context, based on i) carrying out hydraulic tomography and constructing models at the scale of the investigated area and ii) considering geological, geophysical, petrophysical and hydraulic data, acquired at different scales, has been proposed. After presenting the different types of heterogeneity potentially present in geological reservoirs depending on the deposit environment (siliciclastic or carbonate) and the processes likely to modify these heterogeneities on the geological time scale, their potential influence on underground flows was discussed with regard to the experimental site located in a coastal sedimentary context (shell limestones) and used as a support for the proposed methodology.

A review of the various hydraulic techniques that characterize the heterogeneity and anisotropy of geological reservoirs was then proposed before showing how the integration of data (pumping tests data and flowmeter surveys) in the interpretation of hydraulic tomography allows to lead to a rapid and low-cost characterization of the permeability field in 3D.

An approach to limit the instabilities associated with inversions showed that the hydraulic responses at late times might be strongly affected by the boundary conditions of the system and also by the presence of strong heterogeneities on a larger scale (regional scale). Based on this observation,

---

additional investigations allowed to propose a numerically stable inversion technique that assess the hydraulic properties associated with heterogeneities on a larger scale.

Based on this work, different perspectives can already be considered:

- As the integration of different data measured at different scales is relevant, it is recommended to continue this process by integrating more datasets in the inversions in order to build a model in line with the different data and which presents a better realism geological.
- Investigations relating to the discretization of heterogeneities, and therefore to taking into account models of facies and sedimentary structures according to their deposition environment, should be continued for the 3D characterization of the hydrodynamic properties of the medium. The main objective is to obtain fields of hydraulic properties which present structures similar to sedimentary structures.
- It will also be relevant to further investigate the horizontal anisotropy of the properties of geological reservoirs, in order to propose new approaches which, based on synthetic validation models, improve the estimation of hydrodynamic properties (for example, permeability tensors estimated using different combinations of hydraulic responses can act as constraints on the permeability field estimated by inverse methods).
- With the abundance of data, artificial intelligence can be a promising avenue for the analysis and interpretation of responses. Indeed, there are some experimental sites that have been the subject of multiple tests and interpretations. These sites are often well understood and their hydraulic properties are well estimated. It would be very interesting to propose techniques, based on well-understood site learning models, which can improve the estimation of hydraulic properties at sites with less data.

University of Montpellier

2021

